2012

SPECTRUM SENSING AND COOPERATION IN COGNITIVE-OFDM BASED WIRELESS COMMUNICATIONS NETWORKS

Alghamdi, Owayed A

http://hdl.handle.net/10026.1/1090

http://dx.doi.org/10.24382/4559
University of Plymouth

Copyright Statement

SPECTRUM SENSING AND COOPERATION IN COGNITIVE-OFDM BASED WIRELESS COMMUNICATIONS NETWORKS

By

OWAYED A ALGHAMDI

A PhD thesis submitted to the University of Plymouth

in partial fulfilment for the degree of

DOCTOR OF PHILOSOPHY

Mobile Communications and Networks Research Group

Electrical, Communications and Electronic Engineering

July 2012

To my parents, my wife, my sons and daughter.

Spectrum Sensing and Cooperation in Cognitive-OFDM Based Wireless Communications Networks

Owayed Abdullah Alghamdi

Abstract

The world has witnessed the development of many wireless systems and applications. In addition to the large number of existing devices, such development of new and advanced wireless systems increases rapidly the demand for more radio spectrum. The radio spectrum is a limited natural resource; however, it has been observed that it is not efficiently utilized. Consequently, different dynamic spectrum access techniques have been proposed as solutions for such an inefficient use of the spectrum. Cognitive Radio (CR) is a promising intelligent technology that can identify the unoccupied portions of spectrum and opportunistically uses those portions with satisfyingly high capacity and low interference to the primary users (i.e., licensed users). The CR can be distinguished from the classical radio systems mainly by its awareness about its surrounding radio frequency environment. The spectrum sensing task is the main key for such awareness. Due to many advantages, Orthogonal Frequency Division Multiplexing system (OFDM) has been proposed as a potential candidate for the CR's physical layer. Additionally, the Fast Fourier Transform (FFT) in an OFDM receiver supports the performance of a wide band spectrum analysis. Multitaper spectrum estimation method (MTM) is a non-coherent promising spectrum sensing technique. It tolerates problems related to bad biasing and large variance of power estimates.

This thesis focuses, generally, on the local, multi antenna based, and global cooperative spectrum sensing techniques at physical layer in OFDM-based CR systems. It starts with an investigation on the performance of using MTM and MTM with singular value decomposition in CR networks using simulation. The Optimal MTM parameters are then found. The optimal MTM based detector theoretical formulae are derived. Different optimal and suboptimal multi antenna based spectrum sensing techniques are proposed to improve the local spectrum sensing performance. Finally, a new concept of cooperative spectrum sensing is introduced, and new strategies are proposed to optimize the hard cooperative spectrum sensing in CR networks.

The MTM performance is controlled by the half time bandwidth product and number of tapers. In this thesis, such parameters have been optimized using Monte Carlo simulation. The binary hypothesis test, here, is developed to ensure that the effect of choosing optimum MTM parameters is based upon performance evaluation. The results show how these optimal parameters give the highest performance with minimum complexity when MTM is used locally at CR.

The optimal MTM based detector has been derived using Neyman-Pearson criterion. That includes probabilities of detection, false alarm and misses detection approximate derivations in different wireless environments. The threshold and number of sensed samples controlling is based on this theoretical work.

In order to improve the local spectrum sensing performance at each CR, in the CR network, multi antenna spectrum sensing techniques are proposed using MTM and MTM with singular value decomposition in this thesis. The statistical theoretical formulae of the proposed techniques are derived including the different probabilities.

The proposed techniques include optimal, that requires prior information about the primary user signal, and two suboptimal multi antenna spectrum sensing techniques having similar performances with different computation complexity; these do not need prior information about the primary user signalling. The work here includes derivations for the periodogram multi antenna case.

Finally, in hard cooperative spectrum sensing, the cooperation optimization is necessary to improve the overall performance, and/or minimize the number of data to be sent to the main CR-base station. In this thesis, a new optimization method based on optimizing the number of locally sensed samples at each CR is proposed with two different strategies. Furthermore, the different factors that affect the hard cooperative spectrum sensing optimization are investigated and analysed and a new cooperation scheme in spectrum sensing, the master node, is proposed.

Contents

List of Figures

List of Tables

Abbreviations

ADC	Analog to Digital Converter
AF	Amplify and Forward Protocol
AOR	Angle of Arrival
AWGN	Additive White Gaussian Noise
BS	Base Station
CAF	Cyclic Autocorrelation Function
CC	Control Channel
CHF	Characteristic Function
CP	Cyclic Prefix
CPE	Consumer Premise Equipments
CR	Cognitive Radio
CR-BS	Cognitive Radio-Base Station
CSD	Cyclic Spectral Density
CSI	Channel State Identification
CSS	Cooperative Spectrum Sensing
DAC	Digital to Analog Converter
dB	Decibel
D	Decision Statistic
DPSS	Discrete Prolate Slepian Sequences
DSA	Dynamic Spectrum Access
DySPAN	Dynamic Spectrum Access Networks
ED	Energy Detector
FB	Filter Bank
FCC	Federal Communications Commission
FFT	Fast Fourier Transform
FH	Frequency Hoping
FPGA	Field Programmable Gate Array
FT	Fourier Transform
GLRT	General Likelihood Ratio Test
HCSS	Hard Cooperative Spectrum Sensing
HF	High Frequency
HyperLAN	High Performance Radio Local Area Network
IEEE	Institute of Electrical and Electronics Engineers
IFFT	Inverse Fast Fourier Transform
ISI	Inter Symbol Interference
ITU	International Telecommunication Union
ITU-R	International Telecommunication Union-Radio Sector
LC	Linear Combiner
LO	Local Oscillator
LRT	Likelihood Ratio Test
LTE	Long Term Evolution
MAC	Medium Access Control
MF	Matched Filter
MIMO	Multi Input Multi output
ML	Maximum Likelihood
MSCSS	SCSS with Multi Measurements
MTM	Multitaper Spectrum Estimation Method
MTM-SVD	Multitaper Spectrum Estimation -Singular Value Decomposition
NC	Non Contiguous
NTIA	National Telecommunications and Information Administration

OFCOM	Office of Communications
OFDM	Orthogonal Frequency Division Multiplexing
OFDMA	Orthogonal Frequency Division Multiplexing Access
OSA	Opportunistic Spectrum Access
PDF	Probability Density Function
PE	Periodogram
PHY	Physical
PMP	Point to Multi Point
POMPD	Partially Observable Markov Decision Process
PR	Primary
PSD	Power Spectral Density
PSK	Phase Shift Keying
PU	Primary User
QAM	Quadrature Amplitude Modulation
QoS	Quality of Services
QPSK	Quadrature Phase Shift Keying
RF	Radio Frequency
ROC	Receiver Operating Characteristic
RX	Receiver
SCSS	Soft Cooperative Spectrum Sensing
SD	Sequential Detection
SDR	Software Defined Radio
SHF	Spectra High Frequency
SIMO	Single Input Multi output
SLC	Square Low Combining
SNR	Signal to Noise Ratio
SR	Software Rdaio
SS	Spread Spectrum
STBC	Space Time Block Codes
STC	Space Time Coding
STTC	Space Time Trellis Codes
SU	Secondary User
SVD	Singular Value Decomposition
TDMA	Time Division Multiplexing Access
TH	Time hoping
Tx	Transmitter
UHF	Ultra High Frequency
UMTS	Universal Mobile Telecommunications System
UWB	Ultra Wide Band
VHF	Very High Frequency
WLAN	Wireless Local Area Network
WMAN	Wireless Metropolitan Area Network
WRAN	Wireless Regional Area Network
WRC-12	World Radio Communications Conference 2012
WSS	Wide Sense Stationary

List of Symbols and Operators

T_{Int}	Interference Temperature
T_{Limit}	Upper interference limit
P_{Int}	Interference power to the PR receiver
P_r	The received CR power at the PR receiver
BW	Signal Bandwidth
k_b	Boltzmann's constant ($k_b = 1.38 \times 10^{-23}$ Joule/Kelvin)
ΔST	Sensing time duration in CR
ΔTT	Transmission time duration in CR
$\mathcal{H}_0$	Null hypothesis
$\mathcal{H}_1$	Alternative hypothesis
D	Decision statistic
$s(l)$	PR transmitted signal at the lth time sample
$x(l)$	PR received signal at CR receiver at the lth time sample
$w(l)$	AWGN at the CR reviver at the lth time sample
σ_w^2	Noise power
$p(D;\mathcal{H}_0)$	Probability density function of decision statistic when $\mathcal{H}_0$ is valid
$p(D;\mathcal{H}_1)$	Probability density function of decision statistic when $\mathcal{H}_1$ is valid
γ	Decision threshold
P_d	Probability of detection
P_f	Probability of false alarm
P_m	Probability of miss detection
$E[.]$	The expectation mean
$Var(.)$	The variance
$Q(.)$	The complementary cumulative distribution function
$LRT\ (D)$	The likelihood ratio test of decision statistic D
$GLRT\ (D)$	The general likelihood test of decision statistic D
$\hat{\sigma}^2{}_w$	The estimated noise power
d'	The deflection coefficient
d	The mean difference between two Gaussian distributions
D_{ED}	Decision statistic of the energy detector
L	The number of samples (i.e., number of OFDM blocks used in sensing)
$\lvert . \rvert^2$	The absolute value square
$(.)^{\mathfrak{h}}$	Hermitian transportation
$(.)^{\mathrm{T}}$	Vector transpose
E_s	The QPSK symbol energy
σ_s^2	The power of Gaussian PR signal
P_d^{ED}	Probability of detection of energy detector
P_f^{ED}	Probability of false alarm of energy detector
P_m^{ED}	Probability of miss detection of energy detector
f_i	The ith frequency bin of FFT
N	The FFT size
t	The tth sample from the N FFT samples
Σ	The sum operator
$(*)$	The conjugate operator
D_{MF}	Decision statistic of the matched filter
P_d^{MF}	Probability of detection of matched filter
P_f^{MF}	Probability of false alarm of matched filter
P_m^{MF}	Probability of miss detection of matched filter

$R_s(l_1, l_2)$	The autocorrelation of s between times l_1 and l_2
$A_x^{\varepsilon}(\tau)$	The cyclic autocorrelation function
j	$\sqrt{-1}$
G	The total cooperative CR users
g	g out of total G is the fusion rule
T_s	The QPSK symbol duration
T_{os}	The OFDM symbol duration
N_{CP}	The length of the cyclic prefix
Δf_{os}	The OFDM subcarriers frequency spacing
Φ_{sub}	The PSD of OFDM subcarrier
NW	The half time bandwidth product
$\Delta f = 2W$	Frequency resolution in MTM
N_{tapers}	Total number of generated tapers
K	Total number of used tapers
$v_{(t,k)}(N, W)$	The tth sample of the kth taper
$\lambda_k(N, W)$	The eigenvalue of the kth taper
$Y_k(f_i)$	The eigenspectrum at f_i produced from using the kth taper
$S_{MTM}(f_i)$	The power spectral density at f_i when MTM is used
$S_{PE}(f_i)$	The power spectral density at f_i when PE is used
$\boldsymbol{A}(f_i)$	The spatiotemporal matrix at f_i
$\boldsymbol{\sigma}(f_i)$	The singular values matrix at f_i
$N_{\Delta f}$	Number of subbands with width Δf in MTM
N_W	Number of subbands with width W in MTM
$x_t(l)$	The tth FFT sample that from the lth OFDM block received at the CR
$s_t(l)$	The PR t^{th} IFFT sample that from the lth OFDM block
$w_t(l)$	The Gaussian t^{th} FFT sample that from the lth OFDM block at CR Rx
$D_{MTM}(f_i)$	Decision statistic of the MTM at f_i
com_{MTM}	Computational complexity of MTM
com_{PE}	Computational complexity of PE
$\alpha_k(f_i)$	The kth taper decision coefficient
ρ_{ij}	Correlation coefficient between the ith and j^{th} tapers
$P_d^{MTM}(f_i)$	Probability of detection of MTM at f_i
$P_f^{MTM}(f_i)$	Probability of false alarm of MTM at f_i
$P_m^{MTM}(f_i)$	Probability of miss detection of MTM at f_i
L_{dB}	Number of sensed samples in decibel
h_p	Channel impulse response of path p
P	Total number of resolvable paths
$H(f_i)$	Discrete frequency response of the channel at f_i
$P_d^{PE}(f_i)$	Probability of detection of PE at f_i
$P_f^{PE}(f_i)$	Probability of false alarm of PE at f_i
$P_m^{PE}(f_i)$	Probability of miss detection of PE at f_i
P_d^{AC}	Probability of detection of Auto Correlation OFDM technique
P_f^{AC}	Probability of false alarm of Auto Correlation OFDM technique
η_l	Threshold in Auto Correlation OFDM technique
P_d^{SD}	Probability of detection of global sequential detection OFDM technique

P_f^{SD}	Probability of false alarm of global sequential detection OFDM technique
η_{SD}	Threshold in global sequential detection OFDM technique
f_c	Carrier frequency
λ	Wave length
M	Total number of antennas used in sensing at CR Rx
M	The mth antenna branch at CR Rx
$x_{t,m}(l)$	The tth FFT sample that from the lth OFDM block received at the CR from the mth antenna branch
$w_{t,m}(l)$	The Gaussian t^{th} FFT sample that from the lth OFDM block at the CR from the mth antenna branch
$Y_{k,m}(f_i)$	The eigenspectrum at f_i produced from the m^{th}antenna using the kth taper at CR Rx
$D_{MTM}^m(f_i)$	Decision statistic of the MTM at f_i using the m^{th}antenna
$S_{MTM}^m(f_i)$	The power spectral density at f_i of the MTM using the m^{th}antenna
$D_{PE}^m(f_i)$	The power spectral density at f_i of the PE using the m^{th}antenna
$\boldsymbol{r}^m(f_i)$	Complex eigenspectrums row vector in LMS
$\boldsymbol{c}^m(f_i)$	Complex eigenspectrums column vector in LMS
$S_{LMS}(f_i)$	The power spectral density at f_i using LMS
$D_{LMS}(f_i)$	Decision statistic of LMS at f_i
V	Total number of singular values used in LMS
$P_d^{LMS}(f_i)$	Probability of detection of LMS at f_i
$P_f^{LMS}(f_i)$	Probability of false alarm of LMS at f_i
$D_{MTM-SLC}$	Decision statistic of the MTM-SLC
D_{MTM-LC}	Decision statistic of the MTM-LC
D_{PE}	Decision statistic of the PE
D_{PE-SLC}	Decision statistic of the MTM-SLC
D_{PE-LC}	Decision statistic of the MTM-LC
$P_d^{MTM-SLC}$	Probability of detection of MTM-SLC
$P_d^{MTM-SLC}$	Probability of false alarm of MTM-SLC
P_d^{MTM-LC}	Probability of detection of MTM-LC
P_d^{MTM-LC}	Probability of false alarm of MTM-LC
P_d^{PE-SLC}	Probability of detection of MTM-SLC
P_d^{PE-SLC}	Probability of false alarm of MTM-SLC
P_d^{PE-LC}	Probability of detection of MTM-LC
P_d^{PE-LC}	Probability of false alarm of MTM-LC
β	Variance factor
$L^{MTM-SLC}$	Number of sensed OFDM blocks in MTM-SLC
L^{MTM-LC}	Number of sensed OFDM blocks in MTM-LC
L^{PE-SLC}	Number of sensed OFDM blocks in PE-SLC
L^{PE-LC}	Number of sensed OFDM blocks in PE-LC
$h_{p,m}$	Channel impulse response between the PR Tx and CR's m^{th} branch for path p

$H_m(f_i)$	Discrete frequency response of the channel between the PR Tx and CR's m^{th} branch
com_{LMS}	Computational complexity of LMS
com_{SVD}	Computational complexity of SVD
$com_{MTM-SLC}$	Computational complexity of MTM-SLC
com_{MTM-LC}	Computational complexity of MTM-LC
com_{PE-SLC}	Computational complexity of PE-SLC
com_{PE-LC}	Computational complexity of PE-LC
b_r	Binary digits {0,1}
$D_{COP}(f_i)$	Cooperative decision statistic at f_i
$Q_d(f_i)$	Joint/global probability of detection at f_i
$Q_f(f_i)$	Joint/global probability of false alarm at f_i
$Q_m(f_i)$	Joint/global probability of miss detection at f_i
$Q_{error}(f_i)$	Total error probability of the cooperative spectrum sensing at f_i
$g_{optimal}$	The optimal fusion rule
L'	The optimal number of sensed samples

Acknowledgements

Foremost, I would like to thank my supervision team, Dr Mohammed Zaki Ahmed and Dr Mosa Ali Abu Rgheff. Their continuous support, guidance, and encouragement were invaluable to me in completing this research.

Many thanks go to the Saudi Arabian government, and the Ministry of Interior, in particular, for their financial and administration support. Without such support, this work would not have been a success.

I wish to thank my last colleagues at the mobile communications research group, Dr Ghassan Abdalla, and Dr Fan Wu. Working with them has been most enjoyable; I have shared with them countless technical discussions and meetings and I wish all of them the very best in their lives. Many thanks also go to the administration staff at the faculty for their priceless help and support. Special thanks go to Mrs Carole Watson and Mrs Lucy Cheetham who have supported me unreservedly.

My special thanks go to my father for his continuous encouragement, support, and prayer. I am well aware that the attainment of my PhD was one of his most treasured dreams. I would also like to thank my brothers Nasser and Abdulmajeed, and all my sisters for their encouragement and understanding.

Last but no means least, I would like to thank my wife for her patience and encouragement. You shared my moments of anguish during my PhD and were ever present at my side through the good times and the bad, providing hope and motivation. Many thanks too to my sons Abdullah and Nasser; I must have seemed to be a busy father during this period, but I am sure as you grow older you will appreciate the reasons behind this. As for you, my little daughter Juri, you have just given the family yet another thing to celebrate by joining us at this special time in our lives. We shall all remember these monumentally life-changing events forever.

Author's Declaration

At no time during the registration for the degree of Doctor of Philosophy has author been registered for any other University award.

About the Author

Owayed A. Alghamdi was born in Saudi Arabia on 22 January, 1977 and received B.Sc. and M.Sc. degrees in Electrical Engineering with a Communications major from King Saud University, Riyadh, Saudi Arabia, in 2000 and 2007. From February 2000 to May 2000 he worked as a distributed electrical engineer in the Saudi Consolidate Electric Company, central region, Riyadh. From May 2000 to September 2000 he worked as a communications engineer in an advanced electronic company. Since 2001, he has worked with the Ministry of Interior (MOI) of Saudi Arabia as a telecommunication engineer, where he has gained theoretical and practical experience in different kinds of telecommunications until he was appointed as the head of the spectrum management section - General Directorate of Telecommunication (GDOT) - for the MOI, where he was awarded a PhD scholarship to obtain his PhD from the University of Plymouth. He has been a member of a number of Saudi government groups as part of numerous study associations and working parties and he attended the Conference Preparatory Meeting 2007 (CPM-2007) and the World Radio Communications Conference 2007 (WRC-2007) held by the international telecommunication union (ITU) in 2007. He has also been a member of several Arabic Gulf Radio Spectrum groups.

Currently, he is a Ph.D. candidate in the Department of Electrical and Electronic Engineering at the University of Plymouth, Plymouth, UK. His research interests include statistical signal processing, detection and estimation theories, wireless communications and networking, cognitive radio, and cooperative communications. He is a student member of the IEEE and IET and refereed technical papers in the Annual IEEE International Symposium on Personal, Indoor and Mobile Radio Communications (PIMRC 2010), The IEEE International Conference on Communication Systems (IEEE ICCS 2010), and the IEEE Wireless

Advanced conference (WiAd 2011). He has published many papers during his MSc and PhD studies and has been nominated as chairman of the Saudi student club in Plymouth in 2011 and 2012.

Publications:

[1] O. A. Alghamdi and M. A. Abu-Rgheff, "Performance evaluation of cognitive radio spectrum sensing using multitaper-singular value decomposition," in *Proc. 4th IEEE International Conference on Cognitive Radio Oriented Wireless Networks & Communications (CROWNCOM'09)*, 2009, pp. 1-6.

[2] O. A. Alghamdi, M. A. Abu-Rgheff and M. Z. Ahmed, "MTM Parameters Optimization for 64-FFT Cognitive Radio Spectrum Sensing using Monte Carlo Simulation," in *Proc. The Second International Conference on Emerging Network Intelligence (EMERGING 2010)*, 2010, pp. 107-113.

[3] O. A. Alghamdi, M. A. Abu-Rgheff and M. Z. Ahmed, "Probabilities of Detection and False Alarm in MTM- Based Spectrum Sensing for Cognitive Radio Systems," in *Proc. The Second International Conference on Emerging Network Intelligence (EMERGING 2010)*, 2010, pp. 114-119.

[4] O. A. Alghamdi, M. Z. Ahmed and M. A. Abu-Rgheff, "Probabilities of detection and false alarm in multitaper based spectrum sensing for cognitive radio systems in AWGN," in *Proc. 12th IEEE International Conference on Communication Systems (ICCS'10)*, 2010, pp. 579-584.

[5] O. A. Alghamdi and M. A. Abu-Rgheff, "Local MTM-SVD based spectrum sensing in SIMO OFDM cognitive radio under bandwidth constraint," in *Proc. 5th IEEE International Conference on Cognitive Radio Oriented Wireless Networks & Communications (CROWNCOM'10)*, 2010, pp. 1-6.

[6] O. A. Alghamdi and M. Z. Ahmed, "Optimal and Suboptimal Multi Antenna Spectrum Sensing Techniques with Master Node Cooperation for Cognitive Radio Systems," *Journal of Communications (JCM),* vol. 6, pp. 512-523, 2011.

[7] O. A. Alghamdi and M. Z. Ahmed, "New optimization method for cooperative spectrum sensing in cognitive radio networks," in *Proc. 7th IEEE Wireless Advanced Conference (WiAd 2011)*, 2011, pp. 54-59.

Word count of the main body of thesis: 52,691

Signed……

Date……

Chapter 1: Introduction

1.1 Motivations

1.1.1 Radio Spectrum

Radio Spectrum refers to the existing, natural medium that is used in different wireless communication systems and services: mobile, fixed, satellite-based, and low-power device communications systems (ultra wideband, sensors etc.). Most of the existing wireless communications operate on frequencies that lie within the frequency band of (3MHz-30GHz), including High Frequency (HF/3-30MHz), Very High Frequency (VHF/30-300MHz), Ultra High Frequency (UHF/300MHz-3GHz), and Spectra High Frequency (SHF/3-30GHz), due to their different propagation phenomena.

Since radio spectrum is a limited natural resource, spectrum management, monitoring, and controlling issues are important missions in the wireless communication world nationally and globally. Nationally, most countries have their own regulatory/authority agencies. Such agencies are supported by the respective governments, and are connected to the regional/international agencies that are responsible for the usage of the spectrum. These agencies are responsible for the categories listed below.

1.1.1.1 Management of the Spectrum Use in the Country

This mission includes allocating a given frequency band for a specific service (i.e., allocating the band between f_1 and f_2 MHz for Mobile/Fixed services, for Military/Civil/commercial sectors or shared between them) under restricted conditions; and assigning a frequency channel for a specific radio station under specific conditions. Furthermore, spectrum management includes creating the rules and the policies required

for the efficient use of the national spectrum. The output from this task consists of an allocation chart that contains all the radio spectrum subbands with their allocated services and sectors, and comprises a complete database for the whole radio spectrum bands and all the related licenses.

1.1.1.2 Monitoring of the Spectrum Use in the Country

As a part of national policies, specific spectrum frequencies have been assigned to be used by specific radio stations. These frequencies sometimes need to be monitored to ensure that their use is under the required technical conditions of the station's license (centre frequency, bandwidth, transmission power, coverage area/location, etc). In addition to such administrative procedures, the monitoring task requires technical tools to analyze the spectrum and detect the location of the stations that might cause unwanted harmful interferences to other licensed stations.

For example, the national spectrum in the United States is managed by two bodies. The Federal Communications Commission (FCC) is responsible for civil uses of the spectrum [8], whereas the National Telecommunications and Information Administration (NTIA) is responsible for federal use of the spectrum [9].

In The UK, the Office of Communications (OFCOM) is the regulatory body that is responsible for the spectrum management [10]. Figure 1.1 shows the radio spectrum allocation chart of the UK [11]. From the allocation chart, it is shown how the radio spectrum band is divided into subbands, which are allocated to different services. These subbands might be allocated for military use, civil use, or shared by both of them. The band (440-450MHz), is allocated for the mobile, radio location, and fixed services for military use. The chart shows the degrees of importance of the spectrum's allocating process, and gives some idea of the congestion of the services in certain spectrum subbands.

1.1.1.3 Management of the Spectrum Use Globally

Globally, the International Telecommunication Union (ITU) [12], which is the leading United Nations agency for information and communication technology issues, plays an important role in the international management of the radio spectrum via the Radio Sector (ITU-R) [13]. One of the ITU-R's important objectives is to ensure that all radio communications systems operate in an interference-free manner [13]. This is achieved by creating and implementing radio regulations and regional agreements, and the efficient updating of these systems via the procedures of the world radio communications conferences, along with the related regional conferences and study groups' meetings.

The ITU-R aims at the efficient and the economical use of the radio spectrum that is used by all radio communications services (for more information about ITU-R regulations of frequencies allocation, refer to Article 5 [14]). Satellite services cover areas larger than the other services, and span many countries. Thus the allocation of the satellite services' spectrum has to be agreed via the ITU-R [15].

1.1.2 Radio Spectrum Classifications

Radio spectrum bands are classified into licensed and unlicensed bands. The radio device needs a license from the spectrum authority to operate in a specific licensed band. Receiving the license is based on the availability of the free frequencies, satisfying the technical operation conditions, and paying the spectrum usage fees. The fees formula depends on different factors, such the bandwidth, the location of use, and antenna

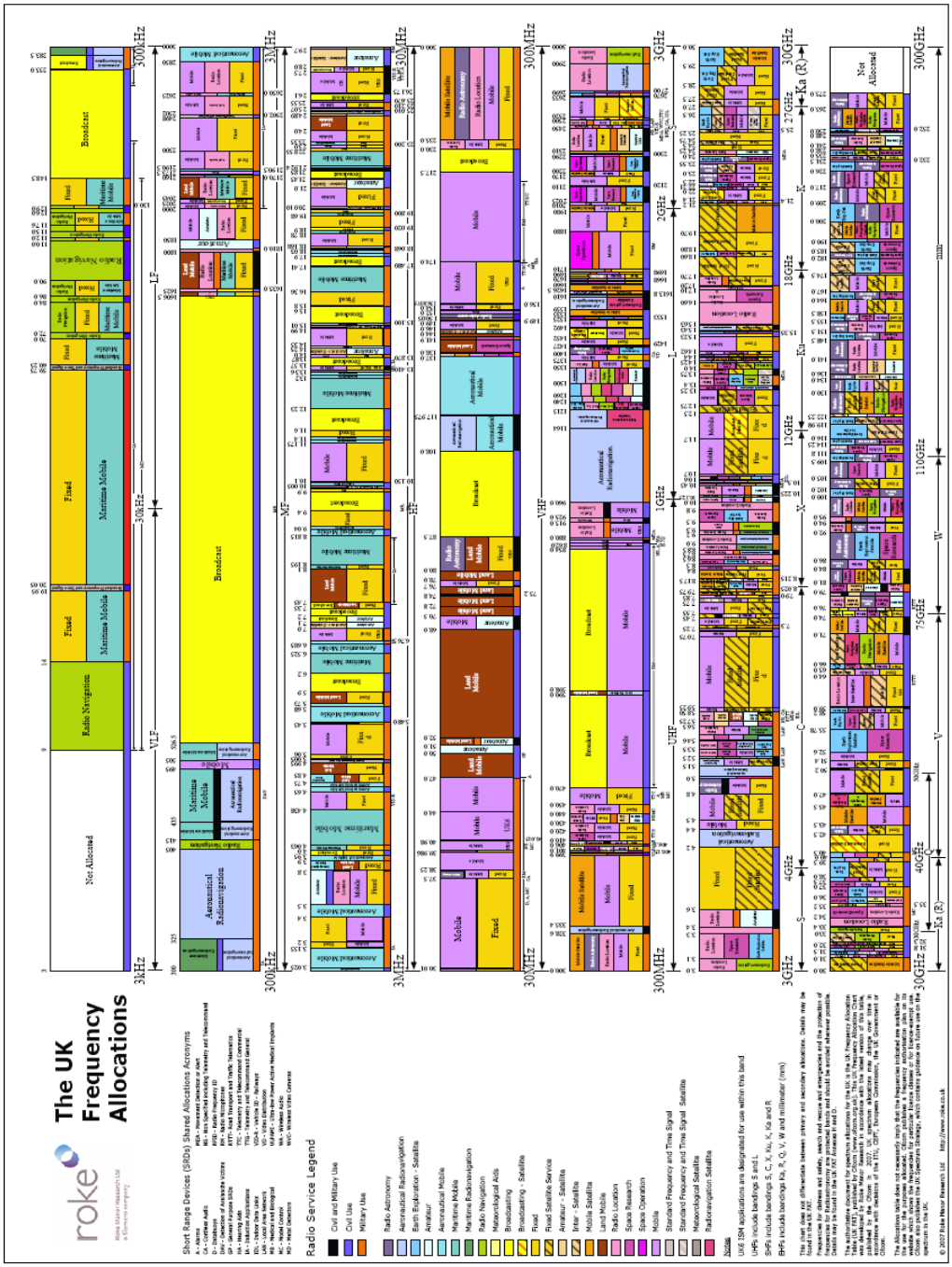

Figure 1.1 The United Kingdom's radio spectrum allocation chart.

parameters, and is different from country to country. The radios that have licenses to operate in the licensed bands are designed to work in such bands.

The spectrum authority must protect these radios from the interferences that might be caused by other coexisting radio systems. Some radio devices don't need a license from the spectrum authority to operate in the certain bands, and consequentially the use of such bands is free. These free bands' radio devices are designed according to specific standards and operational requirements in order to protect the coexisting radio systems from interference. Such free bands are well known as unlicensed bands.

In the UK, the unlicensed band (2.450-2.520 GHz) is allocated to the short range, wireless local area networks (WLANs), and Bluetooth applications [16]. The free band (5.850-5.925GHz) is allocated to the high performance radio local area networks (HyperLANs) services, and short-range applications [16]. In the USA, the unlicensed band (2.4-2.4835 GHz) is allocated to Bluetooth, 802.11b, and 802.11g WLANs services. The unlicensed band (5.15-5.25GHz) is allocated to the indoor systems and the 802.11a WLANs services [15].

1.1.3 Radio Spectrum Scarcity and Underutilization

It is clear that spectrum management and monitoring are very complicated, and at the same time important tasks. They also need great amounts of efforts and financial budgets both nationally and internationally. In parallel with this, the radio spectrum allocation charts show that different subbands have been crowded and there will be no more available subbands for the future wireless services and applications. With the continuing increase in wireless technologies and applications, there is an increasing demand for more spectrum bands, which are a limited resource in nature. The allocations and assignments of frequency bands for new wireless services are constrained by the available airwaves, and it is a vital problem, growing day by day.

In addition, recent measurements show that the radio spectrum at a specified geographical location and a specific time is inefficiently used. A study conducted by the

QinetiQ Proprietary for the OFCOM shows that a large amount of the spectrum is inefficiently used, as is shown in Figure 1.2 (the blue area) [17]. The FCC has found variations in the utilization of the licensed spectrum ranging from 15% to 85% [18].

In the previous part of this chapter, the spectrum management, monitoring, and the related national /international rules and policies have been reviewed. The spectrum scarcity and underutilization issues are discussed as well. Before we start focusing on the concept of cognitive radio (CR) systems, different technical terms related to the system technology will be reviewed.

1.1.4 Dynamic Spectrum Access (DSA)

Dynamic Spectrum Access (DSA) is a term used in newer concepts and techniques in the spectrum management rules and policies. The current rules and policies are fixed and can not provide efficient spectrum management requirements; DSA provides dynamic techniques, rules, or policies towards the spectrum reform. Based on the ideas which have been presented and discussed in the first Institute of Electrical and Electronics Engineers (IEEE) Symposium on the Dynamic Spectrum Access Networks (DySPAN); DSA is classified into three main models based on [19] as follows:

1.1.4.1 Dynamic Exclusive Use Model

The difference between this model and the other existing spectrum management rules and policies is that while the last is static, the dynamic exclusive model is more flexible. This model is divided into two sub models.

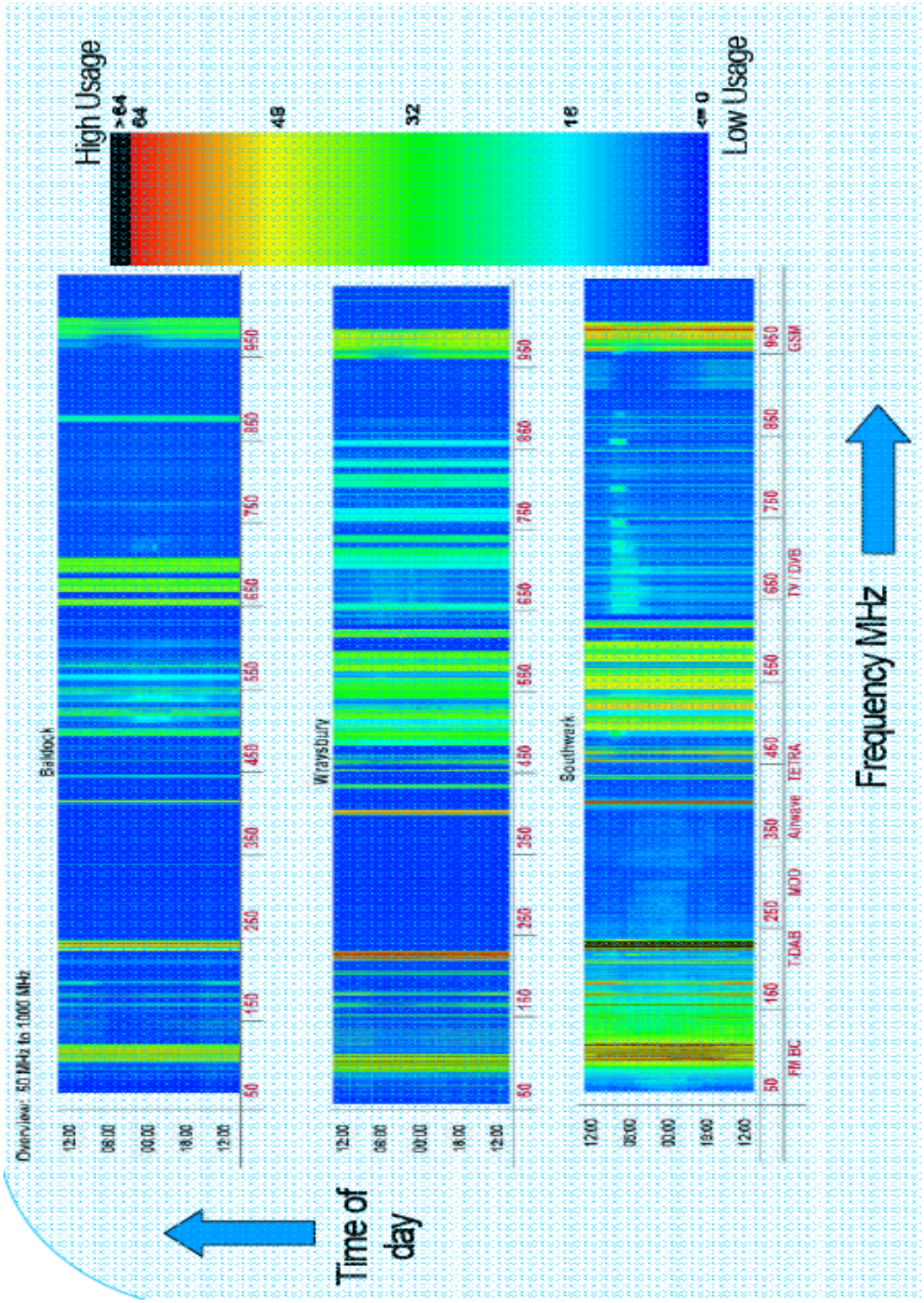

Figure 1.2 Measurements of the spectrum's usage in different locations.

The first is called as spectrum property right [20]. In this sub model, the flexibility comes from the authorization to the licensees to lease or sell their own unused licensed spectrum. The secondary market and economics have the main role towards spectrum reform in this sub model. The second sub model is known as 'Dynamic Spectrum Allocation' which was initiated by the European DriVE project [20]. In contrast to the static rules and policies of the spectrum allocation, this sub model allocates the spectrum in a specific location and at a specific time based on the different communications services' traffic statistical analysis.

1.1.4.2 Open Sharing Model

A spectrum can be shared by a number of different varieties of services in a specific area. The concept of sharing here means the ability of heterogeneous technologies to share the spectrum in a dynamic manner using specific frameworks or protocols and under the authority's assistance. Such a model is called as Spectrum Common' in [21], and [22], and the idea behind it is the success and the innovation of the unlicensed band wireless services (e.g,WLANs). An example of such model is the spectrum common centralized model which has been proposed in [23], where there were two services providers, one user, and a spectrum policy server in the same area. A spectrum policy server aims to control the spectrum allocation between the service providers and the user under a competition framework.

1.1.4.3 Hierarchical Access Model

This model classifies the spectrum users into two main classes: primary users (PRs) (i.e., licensed users), and secondary users (SUs). It allows the two users' classes to access the spectrum in a hierarchical manner where the PR must be protected from the interference that might be caused by the SUs. SU can access the spectrum in two ways.

The first is the spectrum underlay, where SU is allowed to access wide band spectrum by spreading its signal with very low transmitted power below the PR user signal noise floor. The PR will be protected and the SU will be able to access the spectrum. An example of this approach is the Ultra Wide Band (UWB) [24]. The second method is spectrum overlay; the target of this type of spectrum access is to exploit the available unused part of spectrum (white bands) in a specific time and location without causing interference to the PR user. This is mainly an idea which was initiated by Mitola in 1999 [25]. The approach of exploiting the white spectrum in the spectrum overlay access way is termed Opportunistic Spectrum Access (OSA) in the NeXT generation program, which is being investigated by the Defense Advanced Research Projects Agency [19].

1.1.5 Cognitive Radio

CR, a term first coined by Joseph Mitola in 1999 [25], addresses the problem of spectrum utilization by opportunistically accessing portions of the spectrum that are unused using techniques such as spectrum sensing, being aware of the operational environment dynamically and autonomously and adjusting their radio operating parameters accordingly. The long-term vision of this concept is the demand-based spectrum allocation to improve the relative spectral efficiency.

1.2 State-of-the-Art

In the previous sections and subsections within this chapter, a number of concepts, rules, definitions and real facts about radio spectrum have been reviewed. Theses facts and concepts have motivated a huge number of national and international organizations (academic, industrial, or even political) to deal with spectrum scarcity. This scarcity lead finally to a new CR technology, enabling an efficient use of the spectrum and

providing communications anywhere and at any time [26]. In the remainder of this chapter, we review general CR's technical issues - enough to give the reader a general and clear picture of the main aims and objectives of this thesis. More and deeper technical details will be found within the chapters subsequent to Chapter 1.

An OFDM based communication system is a promising candidate for CR technology as a PHY layer [27]. The high data rate and the robustness against the wireless channel impairments are main advantages of the OFDM system. Furthermore, the flexibility of the OFDM is another valuable feature. An OFDM-based CR system is able to deactivate a number of subcarriers that lie within the PR's frequency subband and activate those that lie in the vacant subbands for communications. The Fast Fourier Transform (FFT) process in the OFDM–based CR receiver supports the spectral analysis in a wide band. Additionally, the development of OFDM-based CR systems, allows CR to communicate with other existing OFDM-based wireless systems,which permits interoperability [28]. A number of OFDM-based wireless communications standards widely used. An IEEE802.11 (a/g), which is called Wireless Local Area Networks (WLAN), and IEEE 802.16, which is called Wireless Metropolitan Area Networks(WMAN) or WiMAX, are examples.

Basically, a CR system can be distinguished from the classical communications systems by its spectrum awareness. CR must be aware about its surrounding Radio Frequency (RF) environment. Of course, such awareness allows CR to define the radio spectrum portions that are being unoccupied by their own PRs. Spectrum sensing is a technique that can be done by CR to achieve full awareness about radio spectrum. In CR's cycle, spectrum sensing is a main function. After performing this function, CR would have gained a number of radio spectrum portions that would be free to be used. The remaining steps in the CR's cycle would then be to define the best channels to be

used and then adapt its transmission parameters to achieve the highest performance. Details about CR and OFDM- based CR technical issues can be found in Chapter 2.

1.2.1 The Importance of Spectrum Sensing in CR Systems

Spectrum sensing is a key functional factor in CR systems. In order to make a decision with a low probability of mistakes or a high probability of accuracy, CR must be supported by a high performance spectrum sensing technique. Generally, correct decisions when the PR user is not using the spectrum portion under sensing will increase the capacity of the CR networks. Furthermore, this would improve the spectrum efficiency by exploiting the unoccupied spectrum portions opportunistically. An error in the decision about the availability of PR user signal in a spectrum portion, when it is being used, causes harmful interference to the PR network. Thus, spectrum sensing in CR has been given more attention and interest from research groups at various universities and industrial institutions. In IEEE the term ‘‘cognitive radio spectrum sensing’’ has been included in 2011 journals and conference paper titles from the first mention of CR to the present day (updated on 30-09-2011). In the Google search machine, the same term has 267000 results (updated on 30-09-2011).

Spectrum sensing as a technique has existed in the past and thus many classic spectrum sensing techniques have been suggested and modified to be used as local spectrum sensing techniques, per CR, in the CR network. These techniques are classified into different types based on different assumptions and requirements, as can be seen in Chapter 2.

CR spectrum sensing techniques with a high probability of detection and a fixed probability of false alarm at low signal-to-noise ratio (SNR) is the main objective of CR applications. The sensing over wide parts of the radio spectrum is another objective. This has lead experts to search for more accurate spectrum sensing techniques that are

robust enough when faced with the main classical problems in spectrum estimation methods, the spectral leakage and the large variance in the estimated spectrum. It is preferable for CR not be supported by prior information about the PR's signalling. However, this might pose technical challenges and performance degradation, as can be seen later within Chapter 5.

1.2.2 The Importance of Using MTM as a Spectrum Sensing Technique for CR

Multitaper spectrum estimation method (MTM) was proposed in 1982 by Thomson [29]. MTM uses an optimal bank of band pass filters (known as tapers or windows). These orthonromal tapers are called Discrete Prolate Slepian Sequences (DPSS) [30]. MTM produces a single spectrum estimate with minimum spectral leakage and good variance. The spectrum estimation in MTM is an approximation of the optimal estimate; the maximum likelihood (ML) [31, 32]. One advantage for MTM compared to ML is the fact that it has lower computation complexity.

Since the first development of MTM in 1982, this advanced method has been widely used in many applications. In addition to the power spectrum estimation in signal processing and communications applications, MTM is used in neurosciences [33, 34], geophysics [35-38], and sonar [39]. Furthermore, MTM has been given more study via a number of recent PhD dissertations as in [40-43]. In 2005, Haykin suggested MTM as an efficient spectrum sensing technique in CR [26]. Singular Value Decomposition (SVD) process, was added to MTM in geophysics applications, and was called MTM-SVD [44, 45]. MTM-SVD used to correlate the information about signal using different DPSS and from different locations. MTM-SVD then is suggested by Haykin to produce near optimal power spectrum estimate for spectrum sensing in CR systems [26].

1.2.3 The Importance of Using Multi Antenna Based Spectrum Sensing in CR Systems

In order to improve the spatial diversity, classical wireless communications use multi antenna at transmitter (Tx) or receiver (Rx) or both. Such diversity improvement increases the system data rate and capacity. The reason behind this is that as the distance between antennas is chosen properly there will be a high probability of receiving independent fading through these different antennas. Therefore, the fading effects will be mitigated. Similarly, CR needs to mitigate the channel fading problems too. Thus, using multi antenna systems in CR is highly likely in the future, and many researches and publications have, in their literature, considered multi antenna issues in CR systems.

Fortunately, using multi antenna in CR supports both tasks of communication, and spectrum sensing. Spectrum sensing performance in CR can be improved using single input at the PR's Tx and multi output at the CR's Rx (SIMO). Considerable work has been done in spectrum sensing in SIMO CR systems, as can bee seen later in Chapters 2 and 5.

1.2.4 The Importance of Cooperative Spectrum Sensing (CSS) in CR Systems

In the absence of any information about the PR's signalling and in the presence of the CR user in a bad location with respect to PR's Tx, there would be a high probability of CR making mistakes in its decisions about the vacancy of PR's spectrum portion under sensing. The reason behind this is that CR might not be able to detect the PR's signal due to multipath fading or shadowing (known as 'hidden problem'). Therefore, CSS among a number of CR users in the CR network improves the overall probability of detection [46].

There are two main types of CSS. In the first, each CR forwards its real measurements to a main CR base station (CR-BS) that fuses all collected measurements

and declares the final decision to the CR network, as in [47]. This type of cooperation is called Soft Cooperative Spectrum Sensing (SCSS). In the second one, each CR detects the PR's signal locally and sends binary digits presenting the states of the PR's spectrum portion under sensing to CR-BS, which applies logical fusion rule to declare the final decision as in [48]. This is called Hard Cooperative Spectrum Sensing (HCSS). SCSS requires huge feedback overhead, which requires wide bandwidth to send the real measurements to CR-BS; this is the main disadvantages of using SCSS when compared to HCSS. For this reason, the HCSS will be considered in this thesis.

1.2.5 The Importance of HCSS Optimization in CR Systems

As the number of CR users in the CR network increases, huge numbers of binary digits must be sent to CR-BS. Such huge numbers also increase the overhead feedback. Thus, a number of optimization methods have been proposed in this literature to minimize the number of binary digits in HCSS as in [49, 50]. Another optimization problem is the negative effect of using the binary digits that are produced from CR users with low SNR. Therefore, a number of optimization methods have also been proposed to improve the overall (or global) probability of detection [51, 52]. However, HCSS optimization is still an open issue in CR HCSS, and requires more work towards the most optimal cooperation. Additionally, all optimization methods have been examined on energy detector (ED) only.

1.3 Aims and Objectives

The information that has been provided above in subsection 1.2 determined the main objectives of this thesis. The main aim initially is the undertake a performance evaluation of MTM-SVD, and then to define the practical challenges of this method for CR applications. Optimal parameters of using MTM in CR's spectrum sensing are the

next target. An optimal MTM-based detector development is necessary for CR spectrum sensing and the applications that are mentioned earlier in this chapter. Developing optimal and suboptimal multi antenna based spectrum sensing techniques to improve the performance of spectrum sensing in SIMO CR's systems is also a primary objective. A new, effective concept for CSS and HCSS optimization are two further vital issues. So proposing a new concept of CSS and a new optimization method are likewise key targets here. Thus, my main objectives in this thesis can be summarized as follows:

- Since the MTM-SVD performance as a CR spectrum sensing technique has not been evaluated other than during some theoretical work, a simulation program is built to evaluate this method in OFDM-based CR. The simulation results indicate the method is powerful. However, practical implementation of this technique is found to be difficult in CR systems. The reasons behind this is that PR's signal measurements from different CR users using different DPSS (or tapers) must be sent via control channel to CR-BS. Thus, MTM-SVD is classified as SCSS with multi measurements (MSCSS). This requires huge control channel bandwidth, and will slow the spectrum sensing due to complexity. Additionally, it is found that the MTM-only technique requires the development of an optimal MTM-based detector to be used practically in CR's applications in either of the other mentioned applications.
- The last point leads me into building a simulation model to optimize the MTM parameters so that they may be optimally used in OFDM-based CR systems. Time bandwidth product and number of DPSS (or tapers) are the main parameters, which control the performance of the MTM it self. They control the amount of spectral leakage outside the band and the variance of estimate. Therefore, this point has been investigated and a simulation model

is proposed using the Monte Carlo method to evaluate the effects of these parameters and determines the optimal parameters.

- Using MTM in CR systems requires the development of the optimal detector that allows the designer to calibrate the threshold in order to achieve the highest probability of detection, or the lowest miss detection probability at fixed false alarm in different wireless environments using the Neyman-Pearson criterion. In this thesis, the optimal detector is developed and closed theoretical expressions are derived theoretically including:
  - Decision statistics' Probability Density Functions (PDFs) for the different hypothesis.
  - Probability of false alarm.
  - Probability of detection.
  - Probability of miss detection.
  - Number of required sensed samples to achieve a specific performance.
  - The chosen threshold to achieve a specific performance.

  Simulation programes are written to evaluate the performance in Additive White Gaussian Noise (AWGN), Rayleigh flat fading, and multipath fading environments. The theoretical results match the analytical results well. The MTM-based spectrum sensing technique has the highest performance level compared to both classical and recently-proposed spectrum sensing techniques.
- Supporting CR systems by a multi antenna system improves both communications and spectrum sensing. A review of the available multi antenna based spectrum sensing technique is the first task here. Based on this, one optimal and two suboptimal multi antenna based spectrum sensing

techniques are proposed using MTM. Theoretical expressions for the different probabilities are derived. The simulation and analytical results include performance evaluation in AWGN, Rayleigh flat fading, and multipath fading environments. Comparison between the proposed techniques and the ED based multi antenna based spectrum sensing techniques shows how the proposed ones outperform those that are ED based.

- A review study of the CSS, in general, is provided here. A new effective concept of cooperation is one of the objectives of this part. Thus, a new cooperation concept is proposed and defined. Then, a concentrated study will focus on HCSS. Due to the importance of HCSS optimization in cooperation, I aim to take all existing optimization methods to the most optimal point. Therefore, an optimization method with two different strategies is proposed in this part of the thesis.

1.4 Thesis Organization

A full introduction that gives a clear picture about the main subject and aims of this thesis has now been provided. The rest of this thesis is divided into a number of chapters that proceed to describe all the work up to the point where all objectives are achieved. These chapters can be summarized as follows:

Chapter 2 provides a full revision of the concepts and definitions of a CR system. It also includes the main challenges that face practical implementation of CR. Spectrum sensing techniques and cooperation will be reviewed in detail, as they are the main challenges in CR systems. An OFDM-based CR system as a good candidate at the PHY layer will be reviewed as well, including, the first IEEE CR wireless standard; IEEE802.22.

Chapter 3 gives a technically detailed study of MTM, and MTM-SVD. Simulation results for OFDM-based CR spectrum sensing that uses the MTM-SVD is shown in this chapter.

Chapter 4 provides the work behind developing an optimal MTM based detector for CR's spectrum sensing. It mainly includes two optimization targets. The first is to develop a simulation model that takes into account the effect of MTM parameters on the performance, and then determine the optimal MTM parameters. The second is to provide statistical theoretical derivations for the different PDFs and probabilities. This theoretical derivation facilitates the designing of the optimal MTM detector using the Neyman-Pearson criterion, and will be useful in a number applications. Simulation and analytical results are provided in different wireless environments. A comparison to different techniques is included.

Chapter 5 exploits the benefits of using multi antenna in CR systems and proposes one optimal and two suboptimal spectrum sensing techniques using MTM, and MTM-SVD. Statistical and theoretical works are derived for the proposed techniques and for energy detector (ED) too. The study here includes simulation and analytical results in different wireless environments.

Chapter 6 investigates the CSS in CR's systems and the challenges of implementing such cooperation. A new concept of cooperation, the master node, is proposed in this chapter. An optimization method for HCSS is proposed. ED and MTM are examined under different assumptions to review the proposed method.

Finally, chapter 7 concludes the thesis and defines some future work and issues. Figure 1.3 shows the thesis structure, including the contributions.

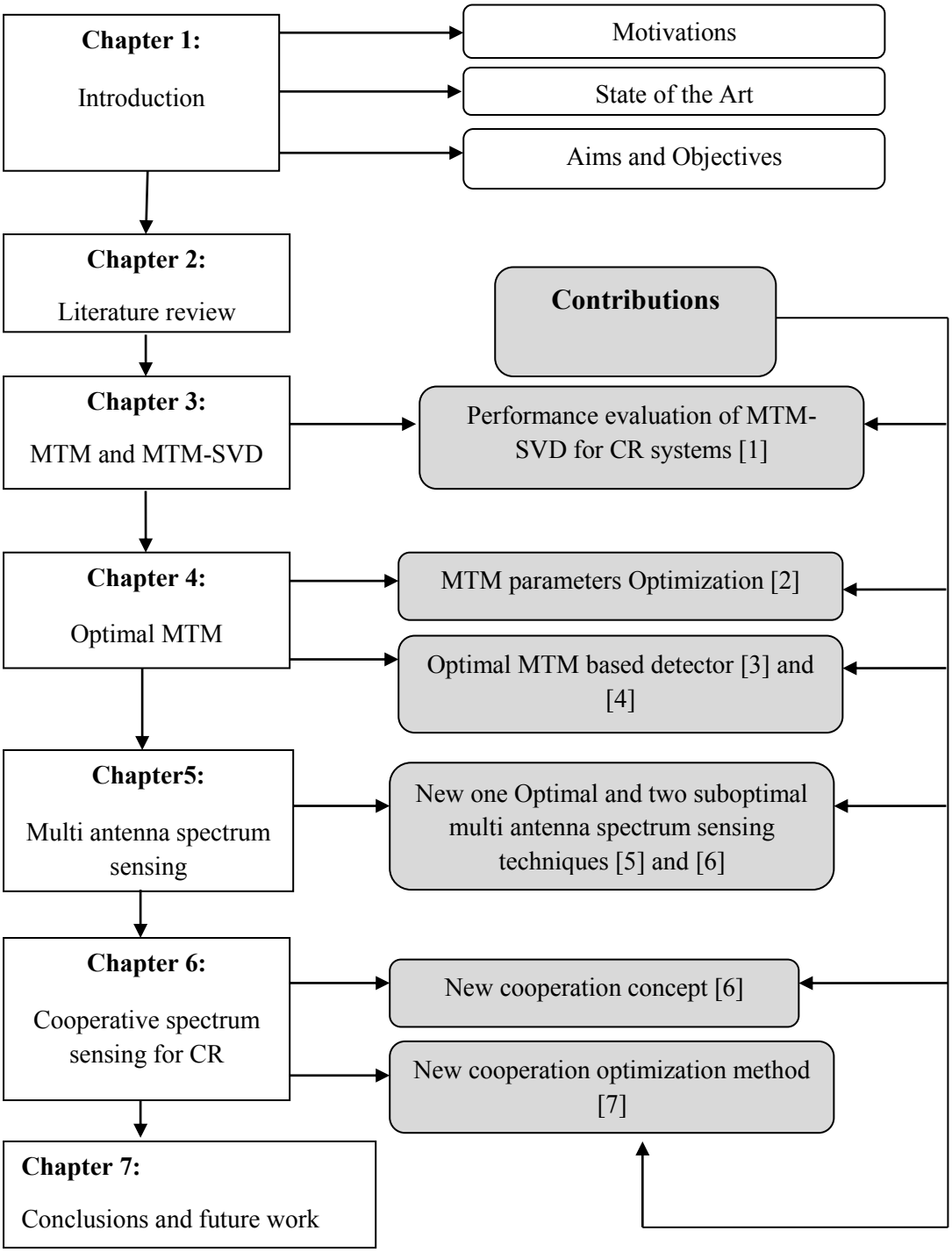

Figure 1.3 Thesis structure.

Chapter 2: Literature Review

2.1 Introduction

Before focusing on CR deep technical issues, an extensive revision study about the CR evolution, definitions, and functions will be provided in this chapter. Relevant names to CR such as, Software Radio (SR) or Software- Defined Radio (SDR), and interference temperature will also be outlined. To achieve more of a technical understanding about CR as communication system that is different from the classical radios, the CR cycle is an important issue to discuss.

Since it is the only technical way of allowing CR to define the vacant portions of spectrum that are not being used by their licensed PR users, spectrum sensing is a main function in the CR cycle. The spectrum sensing concepts, challenges, and techniques will be reviewed and discussed as shall be seen later within this chapter.

The analytical work of spectrum sensing from detection theory perspective will be covered, including, the problem formulation, the different probabilities, and the performance evaluation.

Different spectrum sensing techniques that exist in the wide literature will be explored. This includes the MTM method as it is the main chosen spectrum sensing technique in this thesis. The concept of cooperative spectrum sensing in CR will be reviewed as well. This includes the local spectrum sensing cooperation using multi antenna and the global cooperation among number of CRs. The output from the spectrum sensing function, as the spectrum resource from the PHY layer needs to be analyzed and managed in order to efficiently use such resources. This issue will be given some attention by the end of spectrum sensing issues in this chapter.

The OFDM as a promising physical layer candidate for CR will be investigated, including the advantages and reasons behind nominating OFDM transceivers for CR

systems, the transceiver structure of OFDM-based CR, the relevant IEEE wireless standards to IEEE802.22, and the OFDM –based spectrum sensing techniques.

2.2 Cognitive Radio Evolution and Basic Issues

Since the first introduction of cognitive radio in 1999, different national/international sectors and academic/industry research centres have been interested and focused on this type of radio. The ITU has considered the problem of the scarcity of spectrums via the Radio Communications Sector (ITU-R) [53], and has allocated a new agenda item to consider cognitive radio in the next World Radio Communications Conference 2012 (WRC-12); agenda 1.19 [54]. The IEEE 802.22 working group is developing a standard for cognitive wireless regional area networks (WRAN), which will be used in the unused television channels, and the standard's draft has been released [55, 56].

In the next subsections we review the main concepts and functions of cognitive radio to raise awareness about the challenges that would face the implementation of such radio systems.

2.2.1 Software Defined Radio (SDR)

The concept of the Software Radio (SR) or Software-Defined Radio (SDR) is not new, it has been known as one of the radio systems design and engineering revolution stages [57, 58]. This type of radio is different from the traditional one as [59, 60]: 1. it is able to cover larger frequency ranges than the traditional through using wide band antennas, advanced filters, and high speed analog to digital (ADCs) and digital to analog converters (DACs) at the radio frequency (RF) front end. 2. Its main basedband processing functions such as modulation/demodulation, coding/decoding processing can be controlled via software programmed on a reconfigurable unit as the field

programmable gate array (FPGA). The main defined objectives of developing SDR were, firstly, to decrease the radio system's costs by developing an SDR that is able to be programmed to work in different frequency ranges using different modulations and transmit powers, and, secondly, to develop radio systems that able are to improve the provided services for both military and civil sectors [58]. A new objective for SDR now is to support the implementation of CRs. The physical components of a CR will be SDR components that will support the *reconfigurability* [26] feature of the CR as can be seen in the next subsection.

The SDR is defined by the ITU–R as [53]: *"Software-defined radio (SDR), is a radio in which the RF operating parameters including, but not limited to, frequency range, modulation type, or output power can be set or altered by software, and/or the technique by which this is achieved.*" The CR is defined as an intelligent version of the SDR, where the intelligence in CR comes from its ability to know about its surrounding environment, adapt its transmission/receiving parameters, and learn from its mistakes. Figure 2.1 shows the main difference between the three classes of radios (modified from [61]).

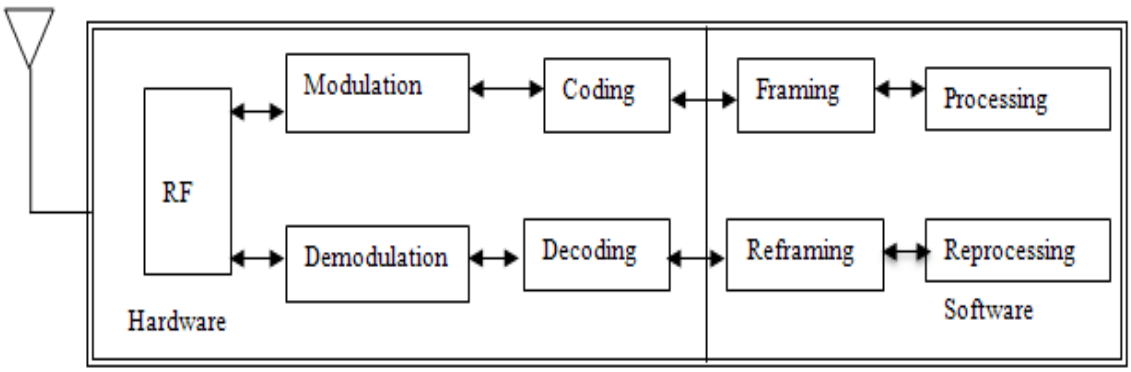

(a) Traditional Radio.

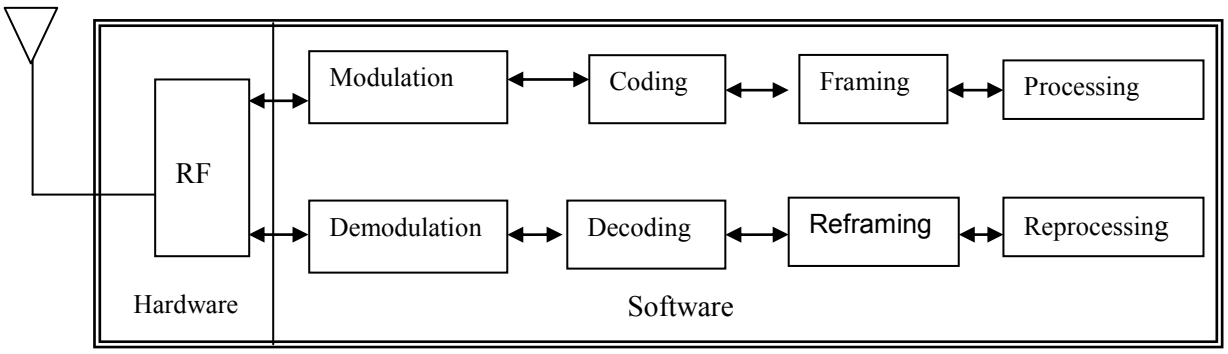

(b) Software Radio.

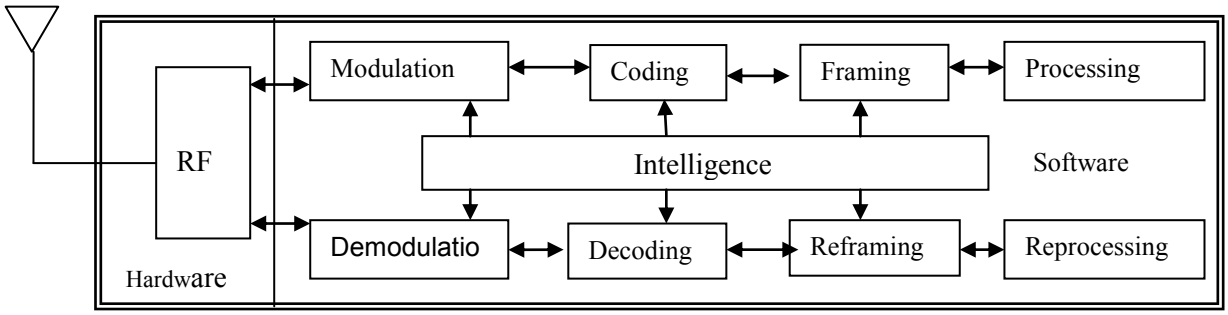

(c) Cognitive Radio.

Figure 2.1 Traditional, Software Defined, and Cognitive Radios.

2.2.2 Cognitive Radio Definitions

CR is an intelligent radio system able to be aware of its surrounding RF environment by using advanced sensing techniques to decide whether there are unoccupied spectrum portions (holes) available; it then changes its transmitting parameters (modulation type, transmission power, bandwidth, carrier frequency) to opportunistically exploit the unused spectrum band. The definition above is called the *capability* [26] of CR, which is one of the main features of CR. Thus, the capability here means the ability to be aware, adaptive, reliable, efficient, intelligent, and learnable [26]. The learnable word is the ability that CR makes current decision based on the last decisions and the prediction from the history and the mistakes toward effective use of

the spectrum holes. Another main feature of CR, is the *reconfigurability* [26], which can be achieved by using the SDR as a physical unit for CR. This would allow CR to cover a wide band range in tasks of sensing and communications. Furthermore, as the CR decides which carrier frequency, bandwidth, transmitted power, modulation scheme that will be used in communications to adaptively use the free spectrum toward a given Quality of Services (QoS) achievement, the transmission parameters can be simply modified by tuning the software. Based on these definitions, the main objectives of CR's development are defined, based on [26], as follow:

1. To improve the spectrum efficiency by opportunistically exploiting the unused spectrum portions (holes) at a specific time and location as shown in Figure 2.2.
2. To provide reliable communications at any time, and any place.

These reliable communications are expected to provide different wireless services such as voice, data, and video[62].

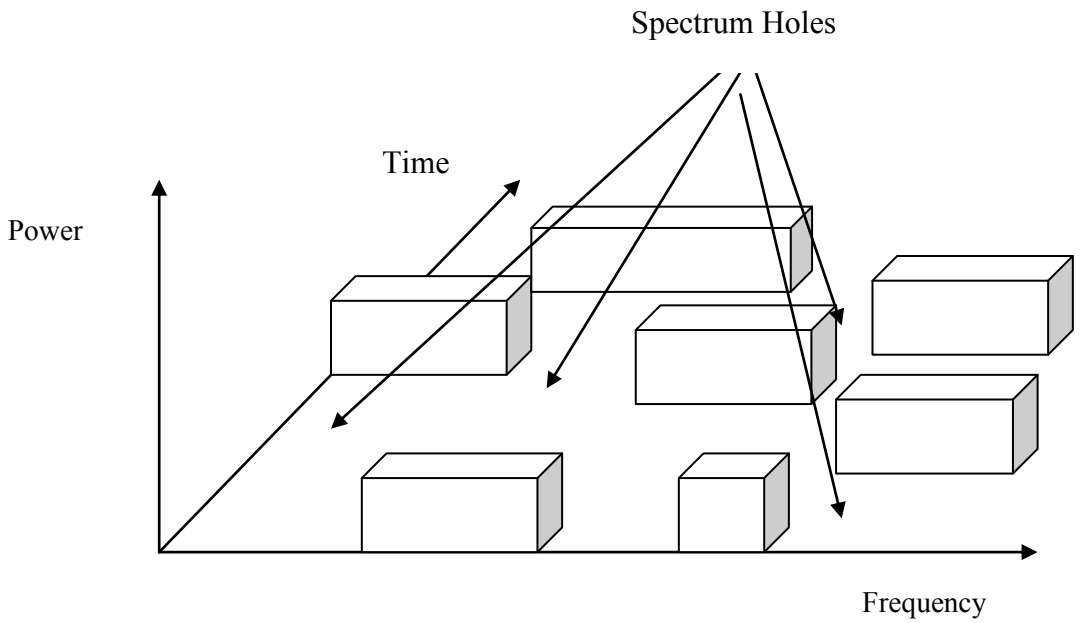

Figure 2.2 The unoccupied spectrum portions (holes) at specific geographical location.

The spectrum holes here have three dimensions: the time, the frequency, and the geographical location. The *spectrum hole* is found by locating specific times or geographical locations not being used by the PR user; it can be used opportunistically at these times and locations by CR users. More descriptions of spectrum holes can be found in section 2.4.1.

As CR scans a wide range of spectrum and defines the spectrum holes and adaptively uses them without interfering to the PRs, a more efficient use of spectrum can be achieved and more bandwidth is made available for different wireless services. Therefore, the applications of CR are classified into three categories based on [63], as follow:

a. Military applications: Using CR in military wireless communications systems provides more dynamic use of the spectrum that would support the military, by exploiting the underutilized spectrum portions at any time and location. Therefore, in addition to the secure communications; the military will be able to have adaptive and continues communications anywhere [64].
b. Public Safety: The infrastructure-based communications systems are not robust when disasters or terrorist attacks happen. Therefore, public safety in emergency situations needs to use a system that can detect the spectrum holes and operate in different frequencies, transmission schemes, and bandwidths. Additionally, public safety will be able to contact other different communication systems (i.e., interoperability) when CR is used.
c. Commercial and civil sector: more spectrum bandwidths will be available at any time, and any location when CR is used. This would increase the wireless communication networks that provide different services, such as voice, data, video, and images for different sectors. Additionally, such an intelligent system

alleviates the complicated tasks within the spectrum management in national and international agencies.

Before we start focusing on more technical issues in the CR's cycle, an important and relevant definition is provided in section 2.2.3 for the Interference Temperature.

2.2.3 Interference Temperature

The conventional way of controlling the interference is based on the transmitter [26, 60, 61]. The power of the transmitter is adjusted to cover a specific distance from the transmitter. This provides control over the transmitted power in order to protect other communications systems from interference. However, transmitter power controlling is a challenge in wireless mobile communications due to the variable location with time. In particular, the location variability changes the distance between the transmitter and receiver, which makes controlling the transmitter power [63]. Thus, the FCC has proposed a model to control the interference at the receiver, which is called the Interference Temperature [18]. Interference temperature defines a measure for the noise, and interfere powers within frequency bandwidth at a specific receiver, as a temperature, and can be written as [65]:

$$T_{Int} = \frac{P_{Int}}{k_b BW}, \tag{2.1}$$

where P_{Int} is the interference power in Watts, k_b is Boltzmann's constant ($k_b = 1.38 \times 10^{-23}$ Joule/Kelvin) and BW is the bandwidth in Hertz. The interference temperature's unit is Kelvins. The interference temperature's maximum limit defines the upper limit where the receiver can operate well. The interference temperature at the PR receiver is given by [65]:

$$T_{Int} + \frac{P_r}{kBW} \leq \quad T_{Limit} \tag{2.2}$$

where P_r, is the received CR power at the PR receiver.

Based on interference temperature definition, the CR should measure the interference temperature and, based on this reading, adapt its transmitted power where the interference temperature does not exceed a pre-defined tolerance limit in (2.2).

2.3 Cognitive Radio Cycle

The CR is able to make discoveries about its surrounding RF environment by sensing and detecting the spectrum holes that have been left unoccupied by their licensed users. In the same task, the CR estimates the interference temperature of the surrounding RF environment in order to keep its transmitted power under the tolerated limit. In addition to the task of sensing and detecting holes, the receiver is responsible for the channel estimation. The channel state estimation (is known as channel state identification (CSI)) here is between a CR receiver and another CR transmitter. Using semi blind training [66], as an efficient method for CSI at the CR receiver has been proposed in [26]. The transmitter adapts its transmission parameters based on the received information from the receiver, and has two targets: to optimize the use of the available holes, and not to interfere with the PR. In [26], the author identified the *Feedback Channel* as a necessary connection tool to exchange the information between the CR transmitter and the receiver in the same terminal. The procedures discussed in this section as a summary represent the cycle of CR in one terminal, and are called CR cycle [26, 60, 64]. Figure 2.3 shows the CR cycle.

Based on the figure, it is clear that the main difference between CR's cycle and the traditional radio cycle is the spectrum sensing and its relevant missions in CR. It can be called the backbone of the CR's cycle. Spectrum sensing is performed at the physical layer, and can be managed through different upper layers as Medium Access Control layer (MAC) in centralized CR network. CR's main functions are based on spectrum sensing and it is relevant tasks, which are divided into [63, 67]:

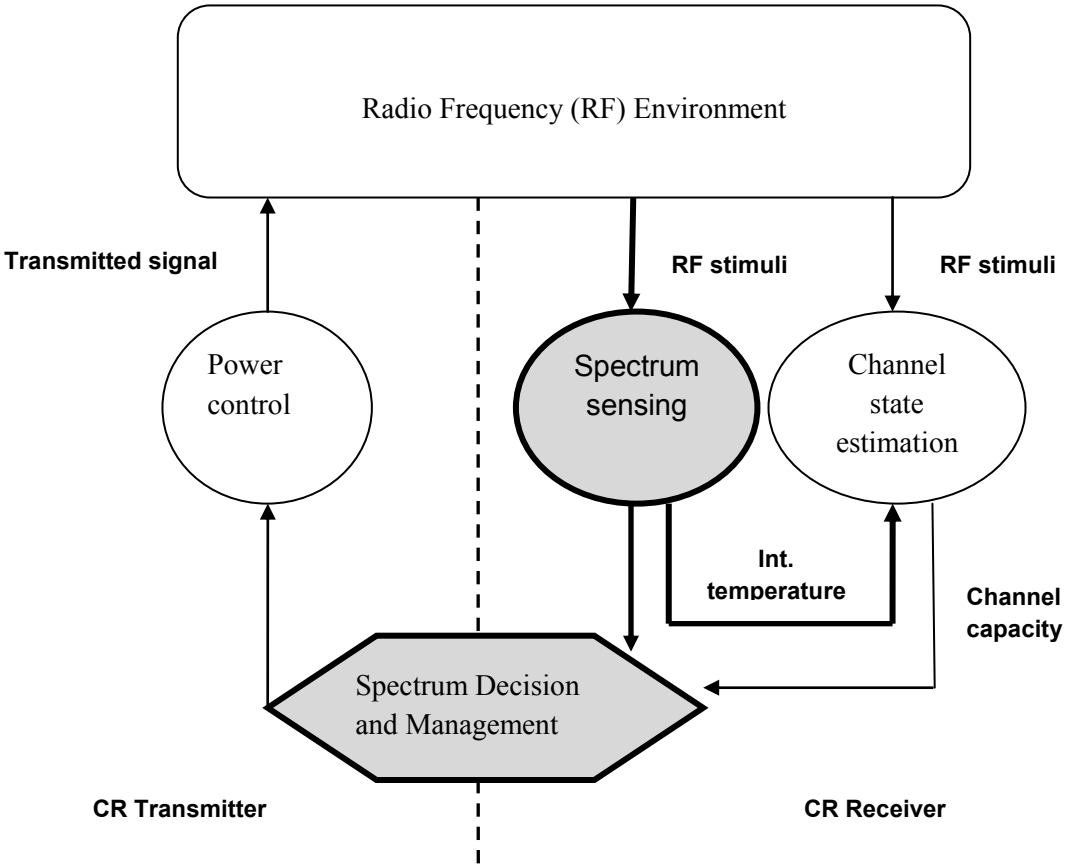

Figure 2.3 Cognitive radio cycle.

a. Spectrum sensing.

b. Spectrum resource analysis.

c. Spectrum resource management.

d. Spectrum resource dynamic sharing and dynamic allocation.

The different CR functions relevant to spectrum sensing functions will be reviewed in section 2.4.

2.4 Cognitive Radio Functions and Missions

As has been discussed in the CR's cycle in section 2.3, the spectrum sensing and its relevant tasks are main challenges in CR development, and it mainly distinguishes CR communications from traditional wireless communications. Before we start

focusing on spectrum sensing technical issues, which are the main objectives of this thesis; a number of concepts that define CR architecture will be covered in this section. As has been fully known, CR uses the licensed band of a PR user, when it is not being used (CR can use unlicensed bands as well). CR uses this temporarily unoccupied licensed band with two constraints: Protecting PR from interference; and optimizing using this unoccupied licensed band. Note that a CR user is known as a secondary user (SU) and PR is well known as a primary user (PU). In this thesis the CR user is likewise represented as SU and PR is represented as PU.

Figure 2.4 shows an example of CR centralized network architecture. There are two CR networks, CR1 (in green), and CR2 (in red), sharing a frequency band that has already been licensed to PR network. As it is assumed that this network is centralized, each CR network here has a main base station (BS): CR1-BS, and CR2-BS. Such BS coordinates the dynamic access of CR users to the available resources. In PR network, CR1 and CR2 users do not have any right to access the PR's frequency band unless they detect that the PR is away from the band and this can be known via spectrum sensing. On the other hand, PR users have the full right to access their licensed frequency band without disturbance from the CR users. As it is a centralised network, PR users can access their license band by coordinating with PR base station PR-BS. Note that; Figure 2.4 here shows a representative diagram of a possible case. However, in some cases the CR, and/ or PR networks can be distributed networks, called Ad Hoc networks, where there is no infrastructure that allows using a BS as a network coordinator.

The CR communication concept in the centralized CR network simply starts with performing local spectrum sensing at each CR, then the CR-BS collects enough information resulting from local spectrum sensing, combines the received information about the spectrum, then finally announces the final decision that describes how to use the licensed band opportunistically between different CR users, who reconfigure their

transmitters to adaptively use the free band. When there is more than one CR network sharing the opportunistic access to PR's licensed band; the *spectrum broker* [68] has been proposed to coordinate such access between different CR networks (e.g., CR1 and CR2 in Figure 2.4) [63]. Thus, no huge quantity of feedback information needs to be gathered at the CR node in the Ad Hoc CR network except when cooperative spectrum sensing is performed [67, 69]. Furthermore, each CR in the Ad Hoc network should exchange information about its spectrum sensing result with its neighbours to prevent collision in the network [70].

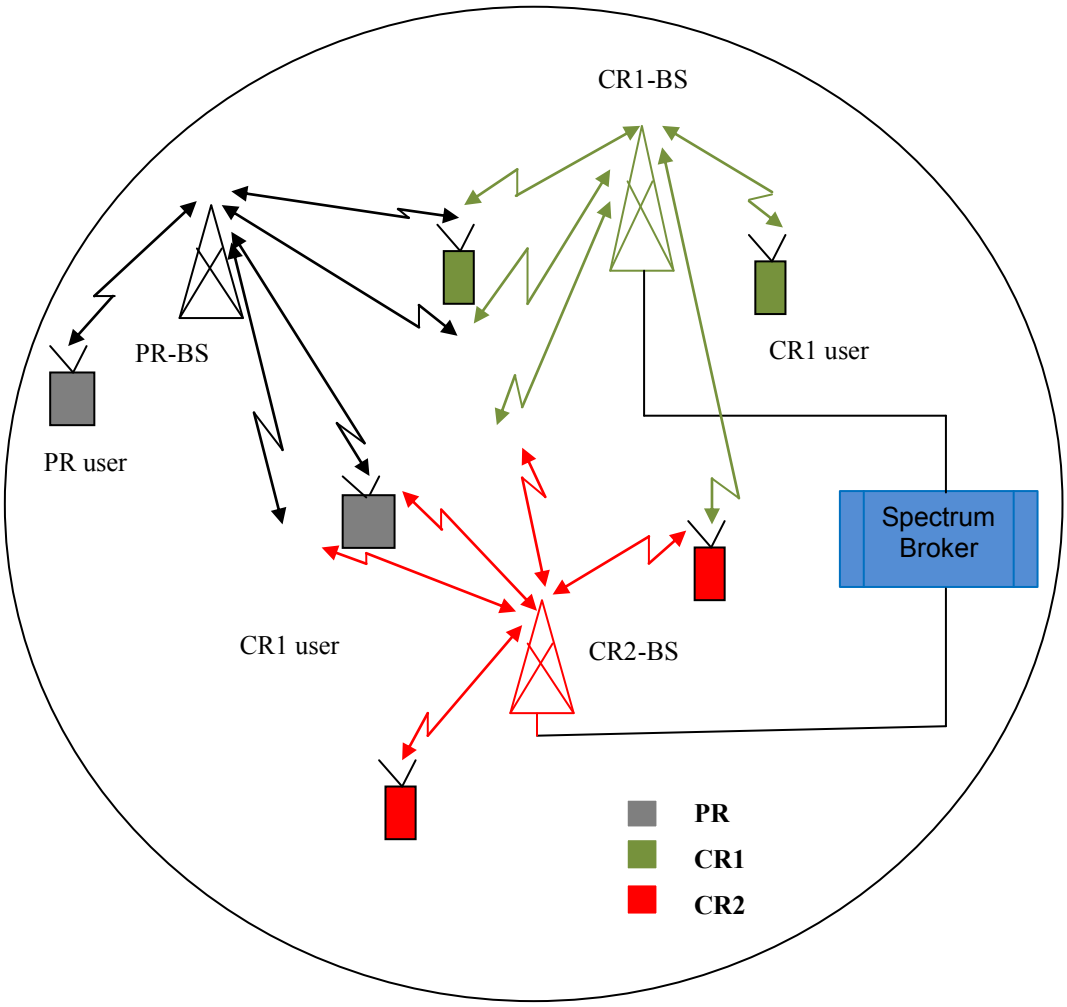

Figure 2.4 Centralized CR architecture.

In distributed CR architecture, there will be no BS that organizes the final spectrum sensing result announcement, and the opportunistic spectrum access. Most of the spectrum sensing and management functions will be performed at each CR independently in the CR Ad Hoc network [69], including spectrum sensing and analysis, final decision, and then transmitter reconfiguration to adaptively use the free band.

An overview of the possible spectrum sensing and access scenarios have been given in this section based on the architecture concept. Such scenarios give the reader a clear picture about the operation procedures in CR network from spectrum sensing prospect at the PHY layer per each CR until spectrum sharing at the upper layers. However, each mission of these procedures is a challenge in itself. In the next sub sections, more technical details will be provided starting from spectrum sensing techniques.

2.4.1 Spectrum Sensing

Spectrum sensing in CR is the technical way that allows scanning of the surrounding RF environment and defines the *spectrum holes* that can be used opportunistically by CR. Very simply, CR asks spectrum sensing techniques to define the free spectrum portions so as to be adaptively used. However, this simple question introduces different technical aspects and challenges in CR communication systems.

Basically, the spectrum sensing in the CRs is classified into: 1. The detection of the power leakage that is being emitted from local oscillator (LO) of PR Rx that has been receiving data from the primary transmitter [71]; and 2. The detection of the PR Tx transmitted signal. Recent researches have focused on the PR Tx transmitted signal detection due to the difficulty of the first kind of spectrum sensing, and the weakness of such emitted signals from the PR Rx [60, 72]. Thus, this thesis focuses on PR Tx signal sensing issues.

PR's transmitted signal can be sensed at the CR's Rx, in three mains ways. Firstly, by estimating the received energy over a frequency band and catching the PR's transmitted signal within this band; secondly, by correlating some parameters, which are statistically periodic and priori known at the CR Rx with the received signal, or, finally, by coherently detecting the PR's signal by the CR Rx, which requires full knowledge about the PR's signalling. More details about the CR spectrum sensing techniques will be found in section 2.4.2.

What is a *spectrum hole* in the context of spectrum sensing? *Spectrum hole* has been defined in [26] as:

"*A band of frequencies that are not being used by the primary user of that band at a particular time in a particular geographic area*".

Based on this definition, the spectrum hole, which is a frequency dimension, depends on two other dimensions: time and geographical area. This means that the discovered vacant band in a specific time might not be vacant after a duration of time. Furthermore, the vacant frequency band in a specific area might not be vacant at another geographical area. In addition to frequency, time and geographical location, the PR's Tx beam direction is found as another dimension in defining *spectrum hole* [73]. The different codes in spread spectrum (SS) technologies are also dimensions in defining a spectrum hole as [73]. The azimuth and elevation angles of the PR's beam and the location of PR Tx, are useful for CR communications when they are prior known to the CR user [73]. Prior knowledge of these parameters to the CR user would allow it to use the PR's frequency band without causing interference. This can be achieved by changing the beam direction of CR Tx [73]. CR can share a PR that is based on SS technologies of the same frequency band and at the same time and same area. However, such opportunistic use requires CR to have full knowledge about the SS codes such as

frequency hopping (FH), and time hopping (TH) that are used by PR in order to keep their transmission orthogonal, which ultimately protects PR from interference [73]. Such knowledge would increase the complexity of the spectrum sensing task in CR in such cases. Additionally, the applications of such techniques are limited.

Figure 2.5 shows a representative diagram where CR and PR networks are located in different areas and the frequency f_{PR} that is already licensed to be used by PR which can be used in the other regions at any time. CR here can use the licensed spectrum without interfering with the PR. Figure 2.6 shows a representative diagram where CR is located in the same transmission area of PR, and cannot use the frequency f_{PR} except when PR is not active. This means that CR can use the frequency f_{PR} when PR is not using it, this can be known based on the spectrum sensing task. CR senses f_{PR} and decides if it is vacant. Thus, in Figure 2.5, the geographical dimension plays the main role in the effective use of f_{PR}, and in Figure 2.6, the time plays the main role, since the PR does not use the f_{PR} the entire time.

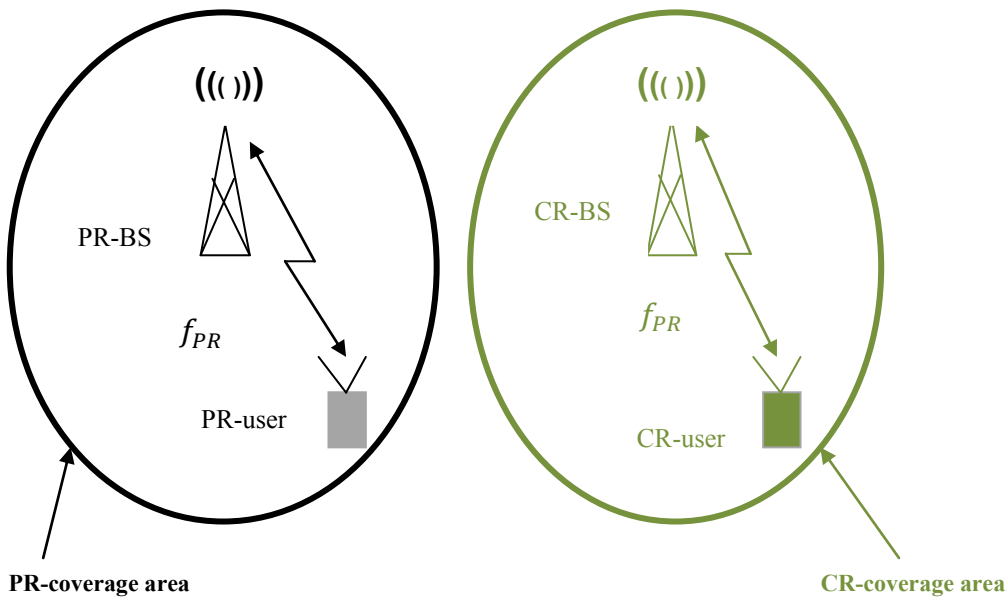

Figure 2.5 CR and PR in different areas.

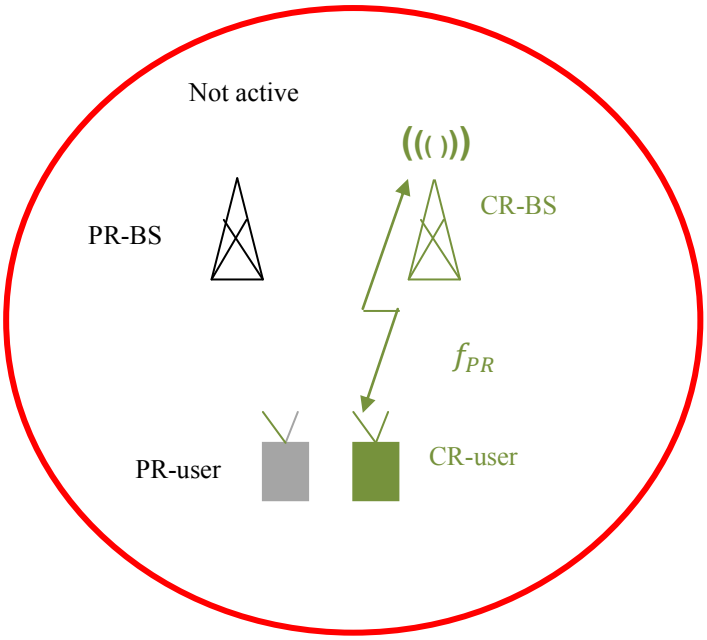

Figure 2.6 CR and PR are in the same area but PR is not active at a specific time duration.

The detected *spectrum hole* in Figure 2.6 is classified as a *temporal spectrum hole* [74]. In this category, the spectrum hole can be used by CR in time dimension until the PR user claims it again. The CR then has to leave this spectrum hole for its licensed user-otherwise CR cannot exploit this *spectrum hole*. Another classification of spectrum hole is called *spatial spectrum hole* [74]. Figure 2.7 [74] shows a representative diagram explaining such a *spectrum hole*. The coverage area of the PR Tx here is defined by R_{pp}, represents the radius of the transmission coverage of PR Tx. Assume that the PR Rx is located at the edge of this radius in the direction of the CR Tx as shown in the figure. At the same time, assume that the CR (which is supported by a receiver as well) is located at a distance R_{cp} from the PR Rx and in a direction outside the PR Tx transmission coverage area. It is clear that under these assumptions, the CR Rx will not be able to sense the transmitted signal from PR Tx, this is because the signal cannot reach the CR

Rx. In this case CR will detect no signal in the PR frequency band and the CR Tx therefore produces interference to the PR Rx when its transmission; R_{cc}, is greater than or equal to R_{cp}(i.e., $R_{cc} \geq R_{cp}$). Therefore, the problem can be summarized as: the CR user can not detect the PR Tx transmission because it is out of its transmitted coverage and can not be aware of the PR Rx that lies in its coverage. Using direction transmission is proposed in [75] to avoid interfering with the PR Rx in such cases. Using another CR node to relay the transmitted signal from CR Tx to CR Rx while avoiding interference with the PR is proposed in [76]. This problem is known as *receiver uncertainty* [60].

Figure 2.8 shows an illustration of the problem of shadowing in CR communications systems. Such a problem happens when the CR, which performs spectrum sensing and is named as CR Tx in the figure, is obstructed by an obstacle such as a building. In such a case the CR Tx is not able to detect (using its Rx) the PR Tx transmits in its licensed band due to the received signal with low SNR. Thus, CR Tx will interfere with the PR2 Rx when it transmits in the PR frequency band, as can be seen in the figure [60, 73]. Furthermore, the PR's transmitted signal that

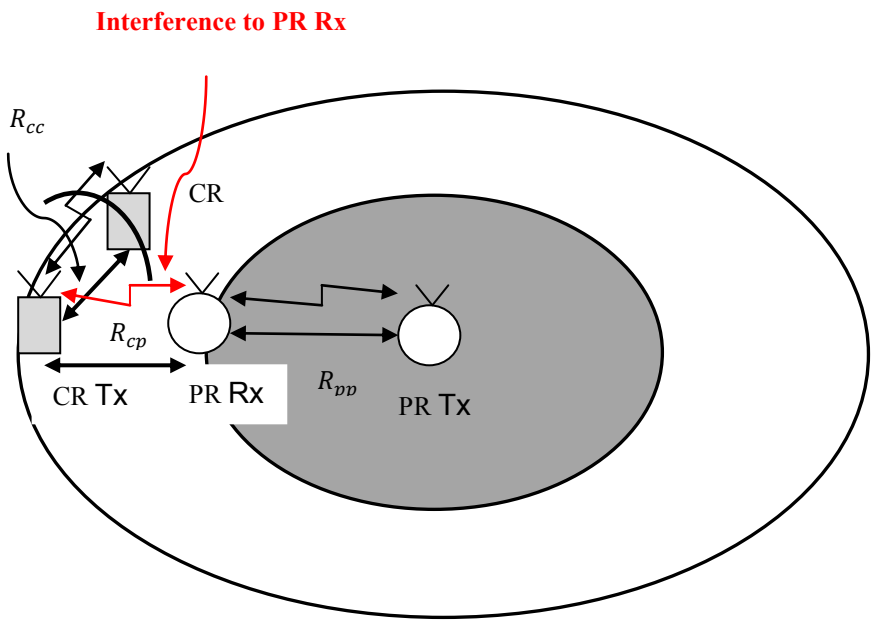

Figure 2.7 Illustration of spatial spectrum holes in CR systems (or receiver uncertainty).

is under sensing by the CR might be suffering from deep fading and this would affect the decision of the CR about the frequency band vacancy. These problems are called *hidden problems*, and are one of the challenges in CR spectrum sensing [77]. A spatial and multi CR users diversity have been exploited in order to improve the single CR spectrum sensing; and this is called 'Cooperative Spectrum Sensing' in the literature. There are a number of cooperative spectrum sensing methods and classifications to be discussed in section 2.4.2.

An overview of some definitions and concepts about spectrum sensing has been covered above. Spectrum sensing is a key functional factor in CR development, and many challenges meet the practical implementation of such intelligence technology. Let us refer back to the *spectrum hole* definition, as a singular noun. Or, alternatively, how CR can detect *spectrum holes*, which is a multiple noun. Hardware components in CR should be able to support different frequency ranges and wide band sensing. This ability has been defined as a main challenge in the CR spectrum sensing and transmission schemes [60, 73]. CR needs to have RF front end components that satisfy the sensing

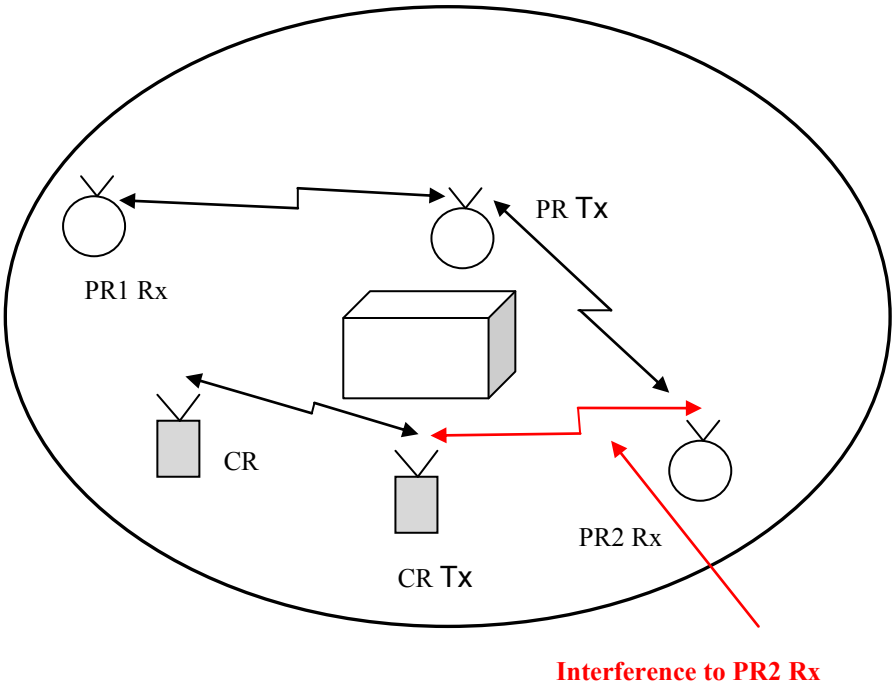

Figure 2.8 Illustration of shadowing problem.

and communication in different frequency ranges and in a wide aspect (i.e., large bandwidth). High speed with high resolution ADC/DACs, antennas and amplifiers for such purposes are the main hardware requirements in practical CR implementation [46].

A CR with only one radio architecture will not be able to sense and transmit at the same time [78]. This challenge has initiated two main ideas to solve the problem. An implementing of CR architecture with two radios would allow CR to sense and transmit at the same time [79, 80]. Another idea is to deal with the problem as an optimization problem, keeping one CR architecture for both sensing and transmission. As has been mentioned above, sensing and transmission at the same time cannot be done via one CR architecture. Such a conflict is handled by dividing the time slot between the two tasks using one CR architecture. Thus, CR can achieve high throughput, which improves the spectrum efficiency by an opportunistic usage of the spectrum for transmission by decreasing the sensing duration. This decrease in sensing time would decrease the sensing performance. Consequently, more interference will result in the PR's frequency band due to the error in the sensing result [73]. Therefore, different optimization methods have been proposed in the literature to minimize the amount of interference to the PR's frequency band with maximizing the CR's throughput under different assumptions, where the spectrum sensing was performed in a periodic manner [81-84]. A representative illustration of the trade-off between sensing time duration ΔST and transmission time duration ΔTT is shown in Figure 2.9. The time slot is divided into two tasks at: CR sensing, and transmission. The increase in the sensing time ΔST produces greater accuracy of the sensing performance. Accurate spectrum sensing means a low percentage of errors in the decision about the availability of the PR's frequency band under sensing. However, this low percentage in decision error is at the expense of the CR throughput, because the PR's frequency band will be used for a short duration of time by the CR. In order to satisfy a specific QoS, or in

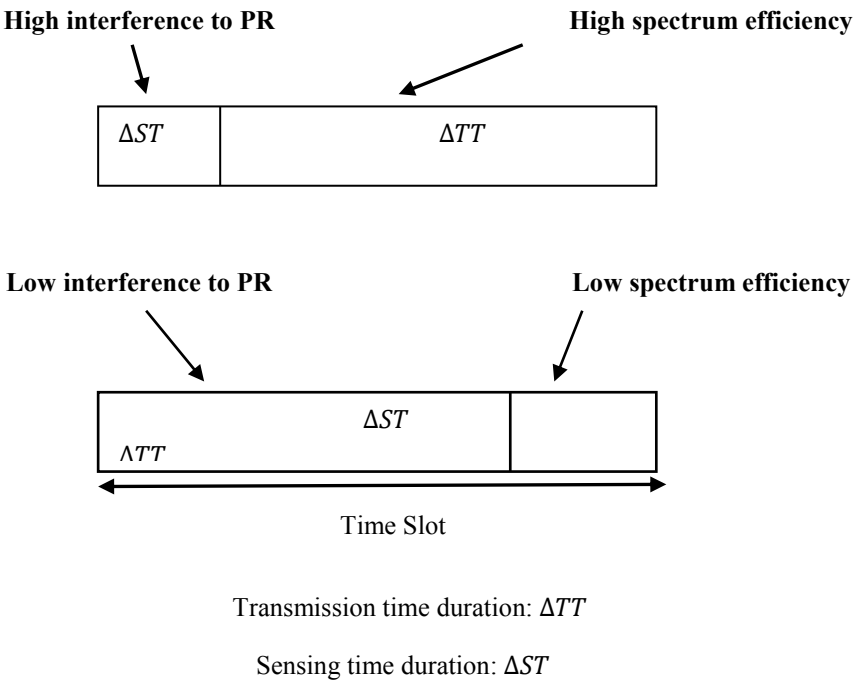

Figure 2.9 Tradeoff between sensing time and transmission time durations in CR systems.

another words to efficiently use the licensed frequency band, the CR might be forced to increase the ΔTT. Such increase is at the expense of producing more interference to the PR's frequency band.

The tolerance of this trade off problem also depends on the PR identity as well [73].When the PR's frequency band owner is a sector like public safety, the interference to such bands must be avoidable due to the sensitivity of these sectors [73]. Additionally, the availability of the public safety sector signal in its frequency is difficult to predict, and public safety might appear in the band any time. Therefore, interference avoidance is a apriority here via long and frequently sensing time duration This will keep the CR aware of the reappearance of a PR, which is in its own frequency band, and will increase the sensing accuracy in leaving the PR's frequency band any time that it becomes necessary [73]. Since the availability of the PR's signal in the TV channels does not change rapidly, the sensing time control is more flexible here. Generally, TV channels are active during the daytime. Thus, periodic spectrum sensing every one hour is proposed in the IEEE802.22 standard [55]. Additionally, the sensing time is defined

as 30 seconds to be performed by the CR user in the IEEE802.22 as well [85]. Furthermore, the PR's services sensitivity degree is lower in TV broadcasting services than when the PR is involved in public safety for example.

In this subsection, general definitions, technical issues, and challenges in CR spectrum sensing have been covered. The spectrum sensing technical background has been accumulated up to this point. However, the time is now due to go more deeply inside the spectrum sensing techniques themselves which are placed into different classifications and have different performances under different assumptions. The overall spectrum sensing performance is mainly controlled by the technique used for sensing at CR. Therefore, an overview of the spectrum sensing techniques that are available in the literature will be provided in the next subsection, including their performances, advantages, and disadvantages.

2.4.2 Spectrum Sensing Techniques

Spectrum sensing, as has been defined earlier in this chapter, is the technical method that can be used by CR to permit awareness of its surrounding RF environment. It is a main function in the CR's cycle. This technical method, represented by a physical device, employs an algorithm that allows CR to make decisions about the availability of the PR signal in a frequency band. The performance of such a device controls the following two main points:

1. The amount of the interference that might be introduced from the CR user into the PR user's frequency band when that frequency is being exploited by the CR user, based on a non-correct decision from spectrum sensing, while the PR's signal is available in the frequency band.
2. The throughput or the capacity of the CR network, which is called spectrum efficiency as well in CR systems. An error in the spectrum sensing decision

when the PR' s signal is not available in the frequency band will minimize the spectrum efficiency or CR network capacity, because the PR's frequency band is free to be used by CR but the CR decides that this is not the case.

Consequently, the local spectrum sensing technique at each CR in the CR network should be as accurate as possible to mitigate the above two main points. Before focusing on the different spectrum sensing techniques, a fact should be mentioned here again; most of the spectrum sensing techniques that are proposed in the literature for CR applications are not novel, but reintroduced from classical spectrum sensing techniques or detectors, which are already available in the signal processing and communication applications.

2.4.2.1 Problem Formulation of CR Spectrum Sensing Using Neyman Pearson Criteria

Generally, the spectrum sensing problem formulation can be classified as a signal detection problem of the variety found in communications systems. Fortunately, the signal processing in spectrum sensing is much simpler than that in demodulation processing [74]. However, there are still some types of spectrum sensing techniques requiring complex signal processing such those that apply coherent detection, as can be seen later in the next subsections.

The problem formulation in spectrum sensing techniques can be defined simply by the distinguishing process between two hypotheses. These hypotheses define the possible states of the PR's activity in the frequency band under sensing. One hypothesis indicates the presence of the PR's signal in the band; $\mathcal{H}_1$, which is called *alternative hypothesis*, and the other hypothesis, $\mathcal{H}_0$, which is called *null hypothesis*, indicates that the PR's signal is not present in the frequency band under sensing [86]. Thus, the spectrum sensing here is represented by decision statistic *D,* which produces

observations that describe the state of the frequency band under sensing, is it $\mathcal{H}_0$, or $\mathcal{H}_1$?. The input to the D, might be the PR's transmitted signal that's affected by channel or additive white Gaussian noise (AWGN) at the CR Rx, or random samples of the AWGN when there is no PR activity in the frequency band. The output from the decision is one of the hypotheses $\mathcal{H}_1$ or $\mathcal{H}_0$. Thus, the relation between the real states of the activity of the PR in a frequency band and D is based on probabilities, and the behaviour of the D is statistically affected by the states of the frequency band under sensing [86]. Figure 2.10 shows an illustration of spectrum sensing problem formulation in CR.

Assume that, the PR user transmits a signal $s(l)$, and the signal is corrupted by an AWGN at the CR Rx, $w(l) \sim \mathcal{CN}(0, \sigma_w^2)$, where l represents the time index. The D main function is to distinguish between the two hypotheses [87]:

$$\mathcal{H}_0: x(l) = w(l)$$

$$\mathcal{H}_1: x(l) = s(l) + w(l) \tag{2.3}$$

where $x(l)$ represents the received signal at CR Rx.

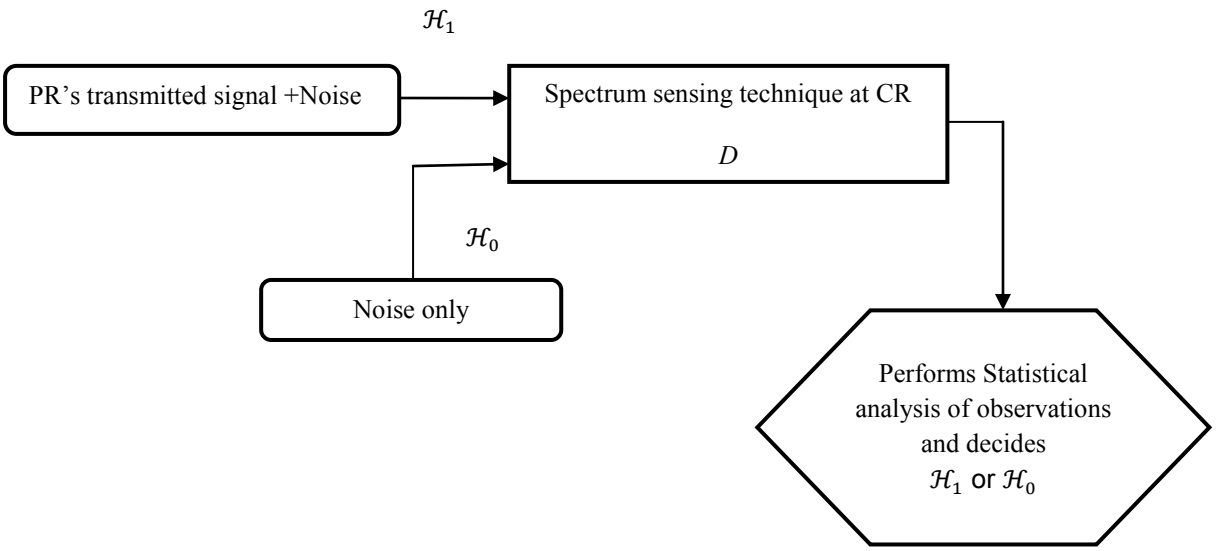

Figure 2.10 Illustration of spectrum sensing problem formulation in CR systems.

There are three well known hypothesis testing formulations; *Bayesian*, *minimax,* and *Neyman Pearson* hypothesis testing [86]. Generally, the D has probability of density function (PDF) for $\mathcal{H}_0$ state; $p(D;\mathcal{H}_0)$, and a another different PDF for $\mathcal{H}_1$; $p(D;\mathcal{H}_1)$. Note that D is different from one spectrum sensing technique to another. Therefore, each spectrum sensing technique type has different PDFs. The $p(D;\mathcal{H}_0)$, and $p(D;\mathcal{H}_1)$ should be defined for any spectrum sensing technique in order to optimize the performance. Prior knowledge of the probabilities of $\mathcal{H}_0$ and $\mathcal{H}_1$ occurrences are necessary in optimizing the performance using *Bayesian*, and *minimax criteria* [86]. This statistical prior information is not the case in CR spectrum sensing due to the lack of information about the PR's activities in a specific frequency band. Hence, *Neyman Pearson* criterion is widely used in optimizing the performance of spectrum sensing in CR systems [87].

When the $p(D;\mathcal{H}_0)$, and $p(D;\mathcal{H}_1)$ are known for any spectrum sensing technique, the optimal design can be obtained using *Neyman Pearson* criteria. The definitions of the D's PDFs for the different two hypotheses $\mathcal{H}_1$ and $\mathcal{H}_0$ include defining their means and variances. Figure 2.11 shows a representative example of such $p(D;\mathcal{H}_0)$ and $p(D;\mathcal{H}_1)$, which are Gaussian distributions here. The D is a statistical description of the used spectrum sensing technique that produces the observations. The resulting observations are then compared to a predefined threshold γ. Note that the threshold γ is chosen based on the noise variance in the signal strength-based spectrum sensing techniques (e.g., energy detector) for example. In the comparison, any observation is greater than or equal to γ, the hypothesis will be decided as $\mathcal{H}_1$ and this is indicated by ''yes'' region, or $R_{\mathcal{H}_1}$. In contrast, any observation is smaller than the γ, the hypothesis will be decided as $\mathcal{H}_0$, which is indicated by '' No '', or $R_{\mathcal{H}_0}$region. Note that as it is a statistical process here, there are two types of errors; *type I error* and *type II error* [87].

These types of errors are known as *false alarm* and *miss* respectively [87]. The observations decision can be defined as follows:

$$D \underset{\mathcal{H}_0}{\overset{\mathcal{H}_1}{\gtrless}} \gamma \tag{2.4}$$

Based on this, the possible four types of decisions are shown in Table 2.1. Thus, two possible decisions meet each state of the nature of the PR's activity in the frequency band under sensing. If the fact is, the PR is active in the licensed frequency band, and the CR spectrum sensing decides yes it is; the CR then makes the correct detection. Otherwise, CR misses the detection. In contrast, if the fact is, the PR user is silent in the licensed frequency band, and the CR spectrum sensing decides yes it is; the CR then makes the correct rejection. Otherwise, CR gives false alarm.

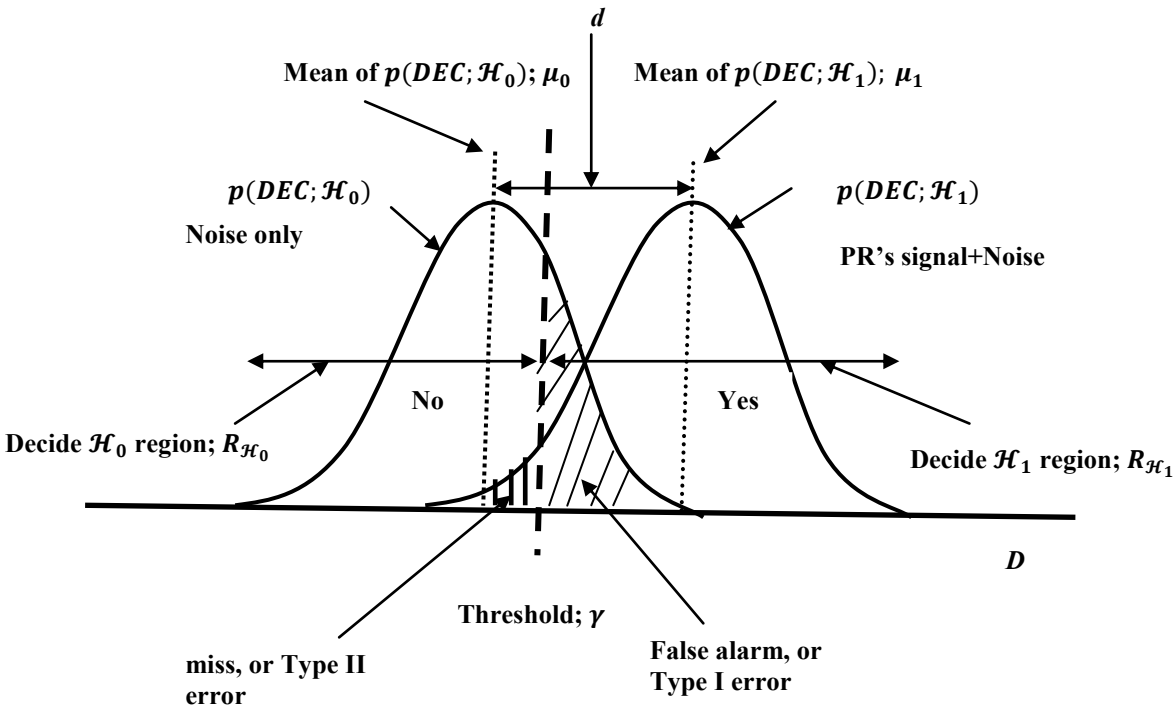

Figure 2.11 PDFs of the *D* and the design problem in typical spectrum sensing.

State of the nature	CR decision; Is it $\mathcal{H}_1$or $\mathcal{H}_0$?	
PR is active in the band; $\mathcal{H}_1$	**Yes**; correct detection	**No**; miss
PR is silent in the band; $\mathcal{H}_0$	**Yes**; correct rejection	**No**; false alarm

Table 2.1 The four possible decisions in CR spectrum sensing.

The spectrum sensing performance can be analyzed and optimized based on the different probabilities; probability of detection, false alarm, and miss detection. In the next subsections, all these probabilities will be reviewed referring to Figure 2.11 and Table 2.1.

2.4.2.1.1 Probability of Detection

The probability of detection, P_d, is defined as is the probability that the CR detector decides correctly the presence of the PR's signal. Therefore, this type of probability is related to the $p(D;\mathcal{H}_1)$, which represents the PR's signal plus noise case as shown in Figure 2.11. P_d can be defined as follows [87]:

$$P_d = Pr\{D > \gamma | \mathcal{H}_1\}$$

$$= \int_{\gamma}^{\infty} p(D;\mathcal{H}_1)\, dD \tag{2.5}$$

where Pr, represents the probability. It is clear that the P_d is the integration over $p(D;\mathcal{H}_1)$ from the threshold γ to infinity, or in another words, is the area under $p(D;\mathcal{H}_1)$ starting from the γ line, as shown in Figure 2.11. Since the $p(D;\mathcal{H}_1)$ is assumed as Gaussian distribution; P_d can be defined finally as follows [87]:

$$P_d = Q\left(\frac{\gamma - E[p(D;\mathcal{H}_1)]}{\sqrt{Var[p(D;\mathcal{H}_1)]}}\right) \tag{2.6}$$

where E and Var, are the mean and variance of the given distribution respectively. The term $Q(\xi)$ is the complementary cumulative distribution function, $Q(\xi)=\frac{1}{\sqrt{2\pi}}\int_{\xi}^{\infty} e^{-\frac{t^2}{2}}\, dt$;

it calculates the tail probability [87]. Note that the Gaussian distribution assumption here is valid as an approximation for the D in many CR spectrum sensing techniques based on the *central limit theorem* [88], as can be seen later in the next subsections.

2.4.2.1.2 Probability of False Alarm

The probability of false alarm, P_f, is defined as the probability that the CR detector decides by mistake the presence of the PR's signal. Therefore, this type of probability is related to the $p(D;\mathcal{H}_0)$, which represents the noise only case as shown in Figure 2.11. P_f can be defined as follows [87]:

$$P_f = Pr\{D > \gamma|\mathcal{H}_0\}$$

$$= \int_{\gamma}^{\infty} p(D;\mathcal{H}_0)\, dD \tag{2.7}$$

In this case, it is clear that the P_f is the integration over $p(D;\mathcal{H}_0)$ from the threshold γ to infinity, or in another words, is the area under $p(D;\mathcal{H}_0)$ starting from γ line as shown in Figure 2.11. The false alarm area is hashed in the figure. Following the same assumption in (2.6), P_f can be defined finally as follows:

$$P_f = Q\left(\frac{\gamma - E[p(D;\mathcal{H}_0)]}{\sqrt{Var[p(D;\mathcal{H}_0)]}}\right) \tag{2.8}$$

where E and Var, are the mean and variance of the given distribution respectively.

2.4.2.1.3 Probability of Miss Detection

The probability of miss detection, P_m, is defined as the probability that the CR detector decides by mistake the absence of the PR's signal. Therefore, this type of probability is related to the $p(D;\mathcal{H}_1)$, which represents the PR's signal plus noise case as shown in Figure 2.11 by the vertically hashed lines under $p(D;\mathcal{H}_1)$. P_m can be defined as follows [87]:

$$P_m = Pr\{D \leq \gamma|\mathcal{H}_1\}$$

$$= \int_{-\infty}^{\gamma} p(D;\mathcal{H}_1)\, dD \tag{2.9}$$

The case of P_m, is the complement of P_d case. The P_m is the integration over $p(D;\mathcal{H}_1)$ from the minus infinity to γ, or in another words, is the area under $p(D;\mathcal{H}_1)$ starting from minus infinity until γ line as shown in Figure 2.11. Therefore, P_m can be defined finally as follows[87]:

$$\begin{aligned} P_m &= 1 - P_d \\ &= 1 - Q\left(\frac{\gamma - E[p(D;\mathcal{H}_1)]}{\sqrt{Var[p(D;\mathcal{H}_1)]}}\right) \end{aligned} \tag{2.10}$$

2.4.2.1.4 The Importance of Deriving Probabilities Formulae

The different probabilities formulae for D with Gaussian distributions have been defined for both hypotheses $\mathcal{H}_0$, and $\mathcal{H}_1$. There are five main factors controlling the performance in such cases; the mean and variance for both $p(D;\mathcal{H}_0)$ and $p(D;\mathcal{H}_1)$ and the chosen threshold γ. These statistical factors should be derived for the different CR spectrum sensing techniques for design and optimization purposes. As such factors have been derived, the spectrum sensing technique can be analyzed and optimized by controlling the γ that will affect directly the resulting different probabilities. The statistical parameters, E, and Var of $p(D;\mathcal{H}_0)$ are defined based on the effect of the CR spectrum sensing technique on the noise statistic (i.e., the noise mean and variance). In contrast, the statistical parameters, E, and Var of $p(D;\mathcal{H}_1)$ are defined based on the effect of the spectrum sensing technique on the PR's signal plus noise statistic (i.e., the mean and the variance of PR's signal plus noise). Furthermore, the statistical parameters of $p(D;\mathcal{H}_1)$ are affected by multipath fading and shadowing environments.

Figure 2.12 shows a representative example of the relation between the P_d and P_f for three different techniques, which assumed to have been used for CR spectrum sensing under the same conditions of wireless environment. The relation plot between

P_d and P_f is well known as receiver operating characteristic (ROC) in signal detection theory. This example is not based on any real technique, but is just to give more understanding of the performance of spectrum sensing technique. Both P_f and P_d decrease together as γ increases, and they both increase with the decrease in γ. This type of relation can be represented in the opposite way by plotting P_m versusP_f. In this case, P_m increases with the increase in γ, and decreases with the decrease in γ. Therefore, the two types of errors false alarm and miss cannot be minimized together. The decrease in one of them increases the other one [87]. Thus, the *Neyman Pearson Theorem's* main objective is to maximize P_d (i.e., minimize P_m) at fixed $P_f = constant = \alpha$, for a decision statistic D, and can be written as follows [87]:

$$Maximize\ P_d\ subject\ to\ P_f = \alpha \tag{2.11}$$

The likelihood ratio test (LRT) decides that the hypothesis $\mathcal{H}_1$ is valid for any D when the condition in (2.12) [87] is satisfied.

$$LRT\ (D) = \frac{p(D;\mathcal{H}_1)}{p(D;\mathcal{H}_0)} > \gamma_{LRT} \tag{2.12}$$

where γ_{LRT}, is the threshold that satisfies (2.12).

The general likelihood ratio test (GLRT) is a well-known approach in signal detection theory [87]. It tolerates the detection problem blindly, when one or more of the parameters in the system model of (2.3) are unknown (e.g., σ_w^2) . Assume that the noise variance σ_w^2, is unknown to the CR; the GLRT has the following model [87]:

$$GLRT\ (D) = \frac{p\left(D;\ \hat{\sigma}^2{}_w; \mathcal{H}_1\right)}{p\left(D;\ \hat{\sigma}^2{}_w; \mathcal{H}_0\right)} > \gamma_{GLRT}$$

where $\hat{\sigma}^2{}_w$ is estimated using ML. The $p\left(D;\ \hat{\sigma}^2{}_w; \mathcal{H}_1\right)$, is maximized, then the $\hat{\sigma}^2{}_w$ is estimated for the $\mathcal{H}_1$ hypothesis and so on. The case can be extended for more unknown parameters such as the PR's power and the channel gain.

The ideal spectrum sensing technique, is that gives P_d=100% when P_f=0 [89]. Figure 2.12 shows also the P_d versus P_f curves for three different spectrum sensing techniques, A, B, and C, as an example. It is clear that technique C, outperforms B and A. This is because at any chosen point in the P_f axis, technique C gives higher P_d, or lower P_m. Note that again, the γ is controlled based on σ_w^2. The three curves can describe the effect of the change in SNR for a specific technique as well. In such an example, curve C (i.e., technique C) indicates that the SNR is higher than that in B and A curves.

Let us introduce a term that is used in signal detection theory to evaluate the detection performance: the *deflection coefficient* d' (is known as generalized SNR) [86].

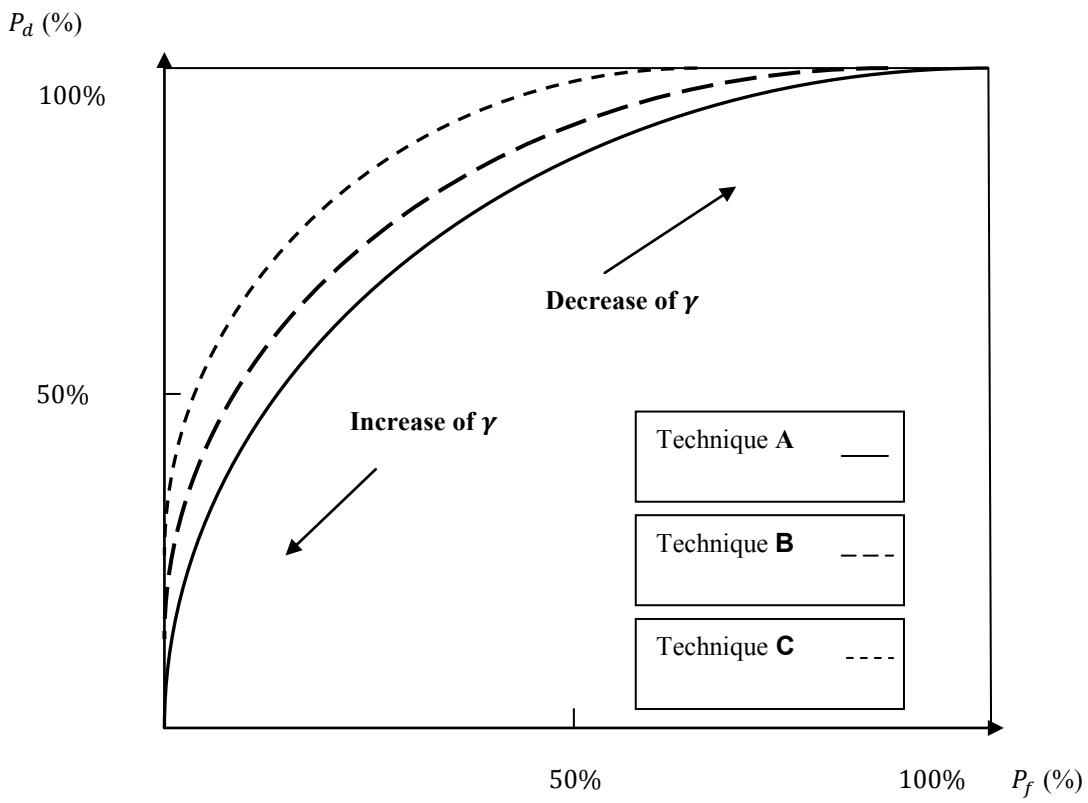

Figure 2.12 Representative example for ROC.

For any decision statistic D with PDFs; $p(D;\mathcal{H}_1)$, and $p(D;\mathcal{H}_0)$ for both hypotheses $\mathcal{H}_1$ and $\mathcal{H}_0$ respectively; the d' normalized to $Var[p(D;\mathcal{H}_0)]$, can be defined as follows [86]:

$$d' = \frac{d^2}{Var[p(D;\mathcal{H}_0)]} \tag{2.13}$$

where, $d = (E[p(D;\mathcal{H}_1)] - E[p(D;\mathcal{H}_0)])$, is the means distance difference.

The question now is how can d' be used in distinguishing the performance of techniques A, B, and C? Figure 2.13 shows a representative example of d for three different techniques, A, B, and C. It can be noted that in technique C's PDFs, the means distance difference d_C is larger than that in A and B techniques. Therefore, the *false alarm* and *miss errors* areas in technique C will be smaller than those in B and A. Hence, C outperforms B and A. The means distance difference of technique B d_B is larger than that in technique A. Hence, technique B outperforms A. In the same used technique, large d indicates that the PR's power, is higher than the noise power (i.e., σ_w^2), or, alternatively, high SNR. In the case when d is small, it means that the noise power is high, or low SNR. Generally, in a large d situation, the spectrum sensing technique can easily distinguish between the PR's signal plus noise case and the noise only case. In contrast, in a small d situation, it can not easily distinguish if it is PR's signal plus noise or noise only.

By the end of subsection 2.4.2 and the subsections within it, enough background about the spectrum sensing problem formulation in CR spectrum sensing will be accumulated. In the next subsections, different spectrum sensing techniques will be discussed.

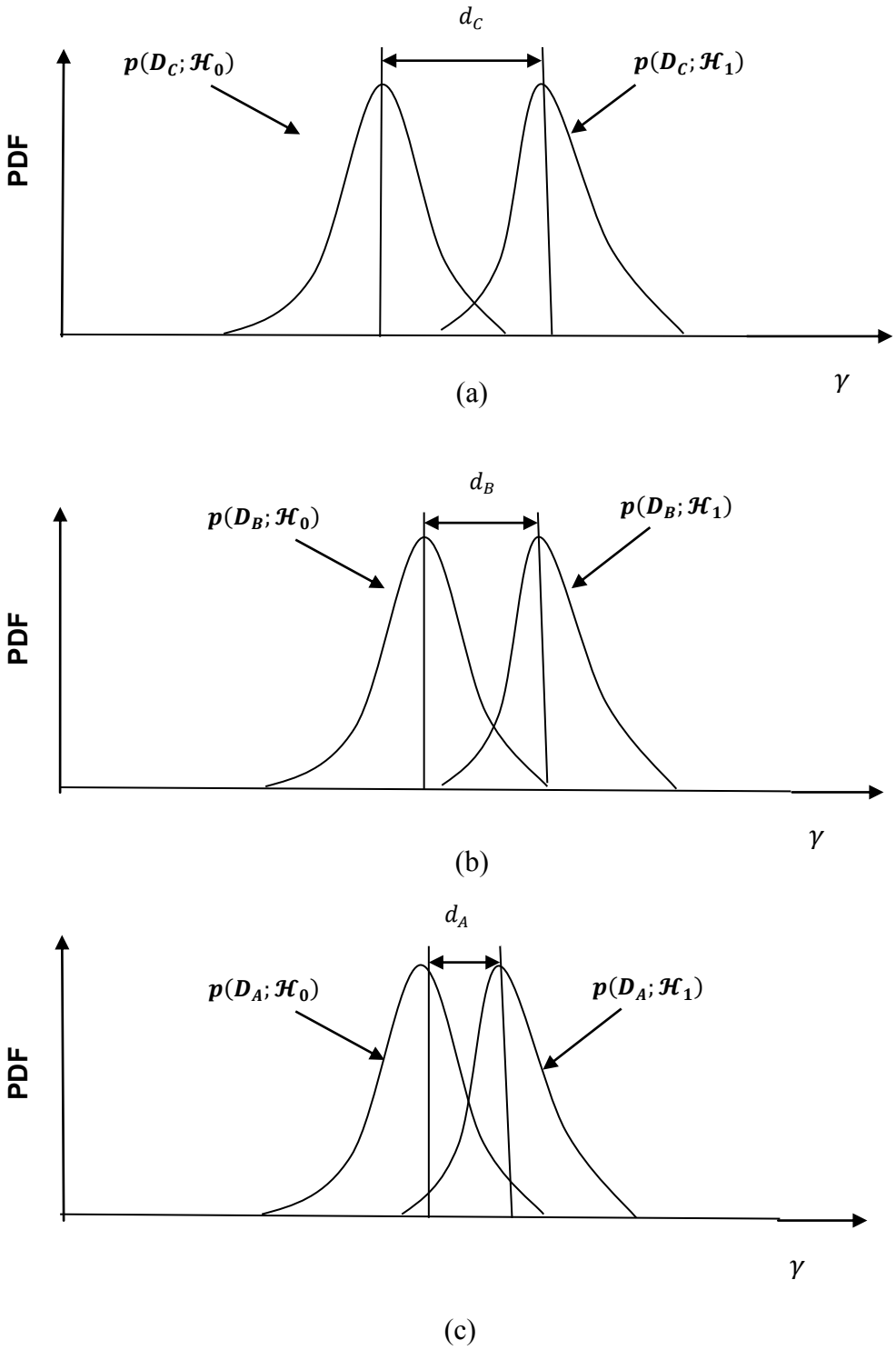

Figure 2.13 Representative examples for the means distance difference for A, B, and C techniques: (a) d_C for technique C (b) d_B for technique B (C) d_A for technique A, where $d_C > d_B > d_A$.

2.4.2.2 Energy Detector

The energy detector (ED) [90], is one of the most widely proposed spectrum sensing techniques in CR systems. It is, also, called as periodogram (PE) [91]. The main two reasons that helped the ED to become a common technique in CR spectrum sensing are [46, 63, 73, 92-94]:

a. Using ED in CR spectrum sensing does not require any prior information about the transmitted PR's signal, which is under sensing by CR.
b. The ED has noticeable low computational complexity.

The ED is a non-coherent method since it does not need information about the PR's signal type. It simply measures the energy in the received signal. Referring to the system model in (2.3), the decision statistic D about whether the PR's signal is present or absent is made by making the following test on the received signal at CR Rx, which is given by [47]:

$$D_{ED} \triangleq \sum_{l=1}^{L} |x(l)|^2 \underset{\mathcal{H}_0}{\overset{\mathcal{H}_1}{\gtrless}} \gamma \tag{2.14}$$

Thus, D_{ED}, is the summation of the energy of $x(l)$ over L samples using ED. In some works as in [51, 63, 95, 96], (2.14), is defined as the average of the energy of $x(l)$ over L samples, as the performance will be the same [47, 96]. Recalling (2.5), the probability of detection, P_d^{ED}, when ED is used is defined as follows [87]:

$$P_d^{ED} = Pr\{D_{ED} > \gamma | \mathcal{H}_1\} \tag{2.15}$$

Recalling (2.7), the probability of false alarm, P_f^{ED}, using ED, can be defined as follows:

$$P_f^{ED} = Pr\{D_{ED} > \gamma | \mathcal{H}_0\} \tag{2.16}$$

Note that the threshold here γ is controlled based on the noise variance (i.e., noise power) as has been mentioned earlier in the last subsection. The noise variance in the system model (2.3) is σ_w^2. The statistical characteristics of D_{ED}, are important now in defining the different probabilities. The D_{ED} in (2.14), is a sum of the square of L

Gaussian random variables. Therefore, the D_{ED} has a central Chi-square PDF, (χ^2), with L degrees of freedom when $\mathcal{H}_0$ is valid [87, 93]. Otherwise, D_{ED} has a non central Chi-square PDF with L degrees of freedom and non centrality parameter $\eta = \frac{E_s}{\sigma_w^2}$, which is the SNR, where E_s represents the energy of one sample of the PR's transmitted signal (i.e., $s(l)$ based on model (2.3)). Referring to the *central limit theorem* [88], the D_{ED}'s PDFs here can be approximated to be Gaussian distributions when L is large enough $L \geq 10$ [47]. Consequently, the mean E of D_{ED}, when $s(l)$ is assumed as a PR's modulated signal with energy $E_s = |s(l)|^2$, is written for both hypotheses as follows [47]:

$$E[D_{ED}] = \begin{cases} L\sigma_w^2 & \mathcal{H}_0 \\ L(E_s + \sigma_w^2) & \mathcal{H}_1 \end{cases} \tag{2.17}$$

and variance Var [47]

$$VAR(D_{ED}) = \begin{cases} 2L\sigma_w^4 & \mathcal{H}_0 \\ 2L\sigma_w^2(\sigma_w^2 + 2E_s) & \mathcal{H}_1 \end{cases} \tag{2.18}$$

The PR's signal in the case above might be a modulated signal such as quadrature phase shift keying (QPSK), for example. In some cases, the PR's signal samples have been tolerated as Gaussian random variables, $s(l) \sim \mathcal{CN}(0, \sigma_s^2)$, that are identical and independent from $w(l)$ [97-99]. This was for derivation only in CR spectrum sensing techniques [99]. The mean E in such cases is calculated as follows [97]:

$$E[D_{ED}] = \begin{cases} L\sigma_w^2 & \mathcal{H}_0 \\ L(\sigma_s^2 + \sigma_w^2) & \mathcal{H}_1 \end{cases} \tag{2.19}$$

and variance [97]

$$Var(D_{ED}) = \begin{cases} 2L\sigma_w^4 & \mathcal{H}_0 \\ 2L(\sigma_s^2 + \sigma_w^2)^2 & \mathcal{H}_1 \end{cases} \tag{2.20}$$

Using (2.17) and (2.18) into (2.6), (2.8), and (2.10) results in the different probabilities formulae P_d^{ED}, P_f^{ED}, and P_m^{ED} as follow [47]:

$$P_d^{ED} = Q\left(\frac{\gamma - L(E_s + \sigma_w^2)}{\sqrt{2L\sigma_w^2(\sigma_w^2 + 2E_s)}}\right) \tag{2.21}$$

$$P_f^{ED} = Q(\frac{\gamma - L\sigma_w^2}{\sqrt{(2L\sigma_w^4)}}) \tag{2.22}$$

and

$$P_m^{ED} = 1 - Q\left(\frac{\gamma - L(E_s + \sigma_w^2)}{\sqrt{2L\sigma_w^2(\sigma_w^2 + 2E_s)}}\right) \tag{2.23}$$

The probabilities formulae for the PR's signal that is assumed as a Gaussian noise can be written following the same steps by substituting (2.19), and (2.20) into (2.6), (2.8), and (2.10).

The ED can be performed in two ways: time domain and frequency domain. Figure 2.14 shows schematic diagrams for the two different ways of ED based spectrum sensing. In the time domain, the received PR's signal at the CR terminal is passed through a low pass filter to match to the bandwidth of interest under sensing that might be occupied or not occupied by PR's signal. Then, the signal is converted from analog to digital using ADC. After that, the digital samples are passed through a squarer device, and L samples integrator, which computes finally the energy over L samples. The resulting energy is then compared to the γ, and the availability of the PR's in the sensed bandwidth will be decided at this stage. In the frequency domain way, which is called PE, the signal is down converted from RF to baseband. Then, ADC is used to convert it to digital samples. The serial parallel S/P device is used before the signal samples are passed to the fast Fourier transform (FFT). The resulting samples through the FFT output bins represent signal samples in the frequency domain. The energy over each frequency bin $f_i = 0, 1,2 , \dots , N - 1$, can be computed using squarer and integrator over L samples as well, and the resulting energy represents the energy in the frequency bin f_i (i.e., channel f_i). Finally, the energy over each frequency bin will be compared to the γ, and

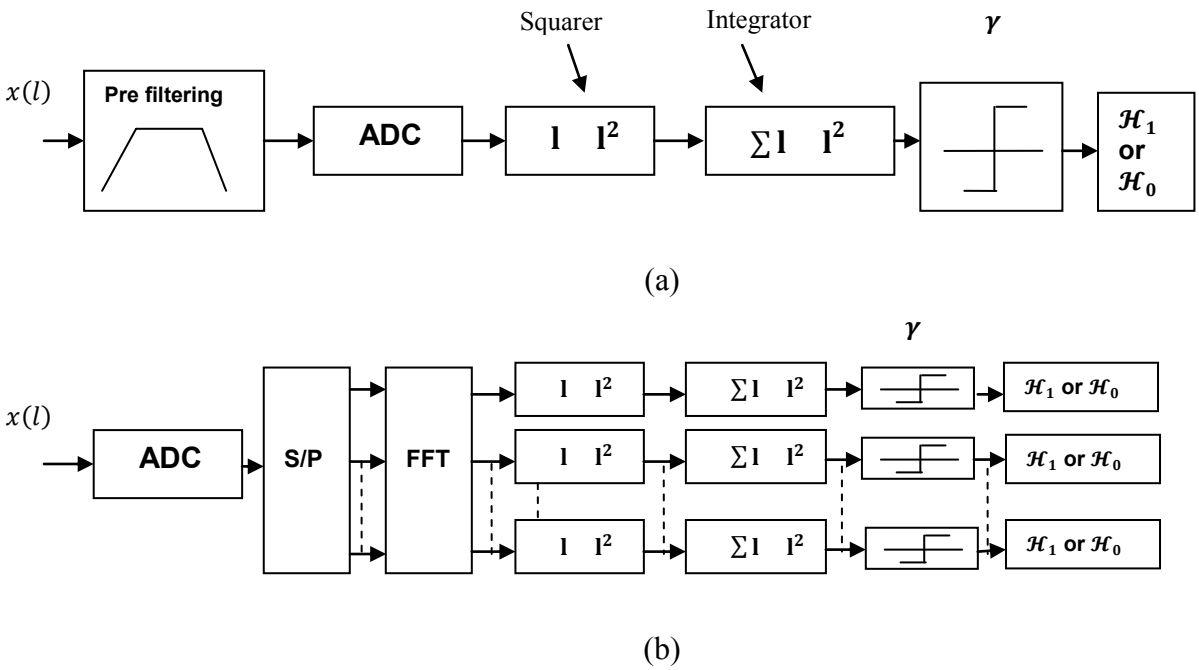

Figure 2.14 Schematic diagrams of ED based CR spectrum sensing (a) Time domain (b) Frequency domain based (i.e., periodogram(PE)).

the decision will be made for each frequency bin. Note that, the FFT size here is *N*, and the operations here might include cyclic prefix (CP) removal as can be seen in chapter 4.

In the PE case, statistical characteristics, and the probabilities formulae of $D_{ED}(f_i)$ (i.e., D_{ED} at every frequency bin f_i), are equal to the statistical characteristics and probabilities formulae in (2.19)-(2.23) [100]. In other words, the output from each frequency bin f_i is applied to a separate ED. Generally speaking, PE is one of the classical power spectrum estimation methods where the power spectral density (PSD) over a wide band can be estimated [91].

The ED based spectrum sensing technique performance in different wireless environments is investigated in [93]. The work included deriving probabilities formulae in AWGN, Rayleigh and Nakagami wireless channels. In multi band OFDM systems that need to coexist with indoor fixed services, it is found that the spectrum sensing of indoor fixed services signals using PE gives an acceptable percentage of false alarm and miss errors [101]. Using stochastic resonance before ED process in CR spectrum

sensing is proposed in [102]. Stochastic resonance amplifies the received PR's signal at CR Rx, which results in an increase in the SNR. ED is used to analyse measurement results to define the time periods occupancy in WLAN [103].

The main advantages of using ED in CR spectrum sensing, as mentioned earlier in this subsection, are simplicity, and no prior information about PR's is required at CR. However, the γ control is based on knowing priori the noise variance, σ_w^2, which needs estimation. Such noise variance estimation is subject to some error [104]. Furthermore, in low SNR conditions, CR was found not able to detect PR's signal when ED was used for spectrum sensing [104]. This was because in such low SNR, noise power is large compared to PR's signal power. The SNR level where ED cannot detect the PR's signal is called the SNR wall [105]. In order to minimize the noise power estimation error, the work in [106], proposed an adaptive method to estimate such power. This was based on using the multiple signal classification algorithm (MUSIC) for the isolating of the PR's signal and the noise subspaces. The forward energy based method is, also, used to adaptively estimate the noise power level as in [107].

Finally, when ED is used for spectrum sensing in frequency domain (i.e., PE) the spectral leakage of the power from frequency bin to the adjacent frequency bins(known as bad bias property) and the large variance of the estimated power are the main challenges [26]. The reason behind these problems is that PE uses single rectangular windowing of the received signal in the time domain. Therefore, there are two main significant disadvantages of using PE in CR spectrum sensing: it is not accurate at low SNR, and suffers it from the bad-bias and large variance of the estimated power.

2.4.2.3 Matched Filter

When the CR has prior information about the PR's signal, the optimal sensing algorithm is the matched filter (MF) [87]. MF coherently detects the PR's signal. In

such coherent detection, CR needs to know the centre frequency, bandwidth, used modulation and its order, pulse shape and packet format. Additionally, CR needs to know some types of patterns of the PR's signal such as the pilot, preambles and midambles that are used for synchronization and equalization purposes [63, 73]. The MF improves the performance of the CR spectrum sensing by maximizing the SNR of the received signal, and minimizing the required time for detection [104] due to coherent detection. However, in addition to the prior information that MF needs to know, using MF in CR spectrum sensing consumes more power due to the signal processing complexity, and requires a separate receiver for each type of PR's transmitted signal [63, 73]. Furthermore, the required number of samples for sensing increases as the SNR decreases [105].

Referring to the system model in (2.3), MF correlates coherently the received signal at the CR Rx, $x(l)$, with a priori known signal $s(l)$, and the decision statistic of MF, D_{MF}, can be defined as follows [108]:

$$D_{MF} \triangleq \sum_{l=1}^{L} x(l)s^{*}(l) \underset{\mathcal{H}_0}{\overset{\mathcal{H}_1}{\gtrless}} \gamma, \tag{2.24}$$

where $(*)$,is the conjugate operator. The D_{MF} has PDFs with Gaussian distribution for both hypotheses, and the mean E is defined as follows [108]:

$$E[D_{MF}] = \begin{cases} 0 & \mathcal{H}_0 \\ LE_s & \mathcal{H}_1 \end{cases} \tag{2.25}$$

and variance

$$Var(D_{MF}) = \begin{cases} LE_s\sigma_w^2 & \mathcal{H}_0 \\ LE_s\sigma_w^2 & \mathcal{H}_1 \end{cases} \tag{2.26}$$

the different probabilities formulae can be written as follow[108]:

$$P_d^{MF} = Q\left(\frac{\gamma - LE_s}{\sqrt{LE_s\sigma_w^2}}\right) \tag{2.27}$$

$$P_f^{MF} = Q\left(\frac{\gamma}{\sqrt{LE_s\sigma_w^2}}\right) \tag{2.28}$$

and

$$P_m^{MF} = 1 - Q\left(\frac{\gamma - LE_s}{\sqrt{LE_s\sigma_w^2}}\right) \tag{2.29}$$

2.4.2.4 Cyclostationary/Feature Method

In cyclostationary [109] spectrum sensing, CR user detector exploits the produced periodicity in the PR's signal due to the use of sine wave carriers, pulse trains, and CP in the modulation of the PR's signal. The cyclostationary term comes from the fact that the signal can be characterized by its statistics, such as mean and auto correlation, because they exhibit periodicity [73]. This method can distinguish between the PR's signal and noise, because the noise is a wide sense stationary (WSS) signal with no correlation, while the PR's signal under sensing is a modulated signal that has spectral correlation [110]. The method can distinguish between different PR signals as well [111].

Compared to MF, cyclostationary spectrum sensing requires partial information about the PR's signal. Therefore, it has a lower performance and complexity compared to MF. Compared to ED, it is better in term of performance but with higher complexity than ED. Cyclostationary spectrum sensing faces difficulties in distinguishing between the different OFDM signals (i.e., between different OFDM-based PR signals), due to their similarity [63]. Different signatures that can be impeded within the OFDM-based PR signals are proposed in [112, 113]. Furthermore, cyclostationary spectrum sensing performance is affected by the noise uncertainty, and frequency selective fading in low SNR [63], and needs a long time period to perform spectrum sensing [60].

The main philosophy of cyclostationary is to exploit the periodicity in the modulated signals. The means and autocorrelations of such modulated signals are periodic over fundamental time periods. Referring again to the system model in (2.3), the PR's transmitted signal $s(l)$ has a mean as $E[s(l)]$; after time period T_{ss}, the mean of $s(l +$

T_{ss}), is $E[s(l+T_{ss})] = E[s(l)]$. The autocorrelation between $s(l_1)$ and $s(l_2)$, where l_1 and l_1 are different time samples is equal to the autocorrelation between $s(l_1+T_{ss})$ and $s(l_{12}+T_{ss})$, and this can be written as [108],

$$R_s(l_1, l_2) = R_s(l_1 + T_{ss}, l_2 + T_{ss})$$

where R_s, represents the autocorrelation of s. In CR spectrum sensing using cyclostationary method, the received signal at the CR that has been defined in the system model of (2.3) is used again here. The calculation of the Cyclic Spectral Density (CSD) of the received signal at CR (i.e., $x(l)$ based on (2.3)) is given by [114]:

$$S(f,\alpha) = \sum_{\tau=-\infty}^{\infty} A_x^{\varepsilon}(\tau)\, e^{-j2\pi f\tau} \tag{2.30}$$

where $A_x^{\varepsilon}(\tau)$ is the cyclic autocorrelation function (CFA), and ε is the cyclic frequency. $A_x^{\varepsilon}(\tau)$ can be written as follows [114]:

$$A_x^{\varepsilon}(\tau) = E\left[x(l+\tau)x^*(l-\tau)e^{j2\pi\varepsilon l}\right] \tag{2.31}$$

When ε is equal to the fundamental frequencies of the PR's transmitted signal $s(l)$, CSD produces peak values in (2.30) and the decision is $\mathcal{H}_1$. Note that the fundamental frequencies, are $\frac{z}{T_{ss}}$, and hence the peaks appear at $\varepsilon = \frac{z}{T_{ss}}$,where z is an integer number. In the absence of the PR's signal, CSD does not produce peaks at ε, because the received signal at CR is noise only, which is WSS and does not exhibit periodicity, and then the decision will be $\mathcal{H}_0$. The different probabilities formulae of using cyclostationary in CR spectrum sensing have not been derived theoretically due to the mathematical intractable in such derivation [108]. The prior information that must be known when cyclostationary is being used for spectrum sensing is the ε, which is the multiple of the fundamental frequencies of the PR's signal (i.e., multiple of $\frac{1}{T_{ss}}$), where T_{ss} is the signal period. However, when there are different numbers of PR systems, which use different signal periods, the cyclostationary is required to know these

different time periods priori, that would increase the cyclostationary complexity as a CR spectrum sensing [74]. In fading environment, it is found that the cyclostationary method completely fails [115]. Furthermore, it is too sensitive to the sampling cyclic offset [116].

2.4.2.5 Multi Taper Spectrum Estimation Method (MTM)

A short introduction of the MTM [29], has been given in subsection 1.2.2. The given introduction was general with technical outlines about MTM rather than in depth analysis. Basically, MTM is a nonparametric spectrum estimation method that estimates the PSD in a wide band aspect. The task of MTM here is the same as that of PE in spectrum sensing, but with a better performance than any other power spectrum estimation method. The reason behind this, in simple words, is that MTM mitigates the well-known classical problems in spectrum estimation methods, which are called *bad bias* and *large variance* of estimate. The MTM strength was achieved by using an orthonormal family of tapers; DPSS [30]. Simon Haykin [26] suggested the use of MTM as an efficient spectrum sensing technique for CR in his famous paper about the CR [26]. In addition to the definitions, and the technical background of MTM, Chapters 3 and 4 of this thesis include a performance evaluation of MTM-SVD for CR spectrum sensing and challenges definitions, MTM parameters optimization for CR spectrum sensing and optimal MTM based detector design using Neyman Pearson criterion, to be used practically for CR.

To connect the discussed spectrum sensing techniques in the last subsections with the MTM spectrum sensing concept, we list the following notes:

a. MTM is an energy based spectrum sensing technique.

b. MTM is a wideband spectrum sensing technique.

c. MTM does not need any prior information about the PR's signal (i.e., non coherent nor partial coherent).

d. MTM needs to know the noise variance to control the threshold.

e. MTM minimizes the spectral leakage outside the band and improves the variance of estimate.

2.4.2.6 Filter Bank

The filter bank (FB) is proposed in [117] as a spectrum sensing technique to be used in multicarrier communication based CR systems [118]. FB estimates the power as well over wideband simultaneously like in PE, and MTM. In FB based spectrum sensing, a number of filters, which are modulated copies of the prototype filter are used to concentrate the energy within their sub bands as shown in Figure 2.15 [117]. The prototype filter is a low pass filter (LPF) representing the filter of the zeroth subband, and the others filters are band pass filters (BPF) that are shifted copies of the prototype filter at normalized frequency bins $f_i = 0, \frac{1}{N}, \frac{2}{n}, \dots, \frac{N-1}{N}$. After filtering the received samples at CR Rx using FB, the absolute square of the output from each FFT branch (i.e., frequency bin) represents the energy at that branch. The results in [117] included comparison between FB and MTM which indicated that the MTM is more efficient in the applications, where the spectrum estimations require smaller samples of the underlying process. FB required more samples to achieve the same performance that had been achieved by MTM.

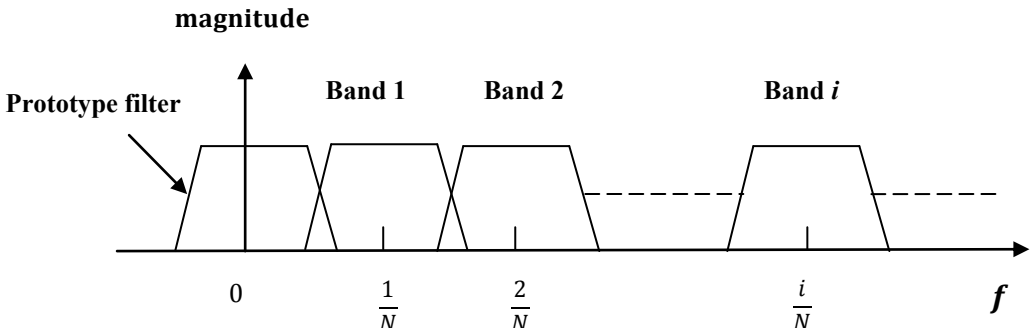

Figure 2.15 Filter bank concept representation.

2.4.3 Cooperative Spectrum Sensing

Subsections 2.4.2.2 to 2.4.2.6, explored different classical CR spectrum sensing techniques. These techniques can be called local spectrum sensing techniques at CR terminals/nodes. Each local spectrum sensing technique has its own requirements, advantages, and disadvantages. Thus, the technical philosophy of each type determines its advantages and disadvantages. A first stage in the engineering research of CR development was therefore about the local spectrum sensing technique itself. Numerous research publications about local spectrum sensing techniques have tried to take the CR spectrum sensing technique to their proposed techniques based on how they evaluate the advantages and disadvantages of the proposed techniques.

The performance of any spectrum sensing techniques is evaluated via the P_d, P_f, and P_m. For any chosen γ, when a specific spectrum sensing technique is used, there are probabilities pair (P_d, P_f), or (P_m, P_f) that meet the chosen γ. In terms of performance, the CR spectrum sensing techniques are comparable together based on these probabilities under the same conditions. Increasing P_d, or minimizing P_f locally at each CR has been attempted in the literature by proposing multi antenna based spectrum sensing techniques at the CR. Such techniques can be called *local cooperative spectrum sensing techniques*, due to the cooperation aspect of the decision between number of antennas at CR.

One of the main challenges that meets local spectrum sensing in CR is the *hidden problem* due to shadowing or multipath fading as discussed in subsection 2.4.2. Thus, when the resulting measurements and decisions of local spectrum sensing of CRs in the CR network are gathered and fused at CR-BS for example, it would improve the overall performance. In other words, the over all P_d will be increased, or the overall P_m will be decreased. Such a type of spectrum sensing is called the cooperative spectrum sensing [77].

In the next two subsections, the concept of *local cooperative* and *global cooperative spectrum sensing* will be reviewed. The found works in the literature will be explored to show the different technical issues and challenges of such cooperation scenarios.

2.4.3.1 Local Cooperative Spectrum Sensing (Multi Antenna)

In wireless communications, the main objective of using multi antenna at the receiver is to resolve the deep fading problems. Choosing suitable distances between the different antennas insures that the fading events are independent through the different antennas. Then one of the classical combining techniques is used to combine the different outputs from the different antennas [15]. Multi antenna in wireless communications allows an increase in the data rate and improves the spatial diversity. Thus, CR's user can use it for both communications and spectrum sensing. Figure 2.16 shows a representative diagram of multi antenna based spectrum sensing in CR. The CR is supported by number of antennas that are used for both communications and spectrum sensing. The PR's signal that is being transmitted from PR's Tx is received at the CR via a number of antennas. This type of channel can be represented as a single input at the primary PR's Tx and multi output antenna at the CR's Rx, which can be called single input multi output (SIMO).

Multi antenna spectrum sensing techniques and issues in CR's systems have been investigated in [99, 119-124]. Two main ED-based multi antenna spectrum sensing techniques, the linear coherent combining, and the selection processing are considered in [119]. In [120], each antenna is connected to an ED, where the PR's signal is decided to be present when more than one antenna decides this. In [121, 122], using ED-based square law combining (SLC) technique in OFDM-MIMO based CR, gave significant improvement in the performance compared to using single antenna. Generally, these

works depend on ED, which has a poor performance in low SNR; this is not practical in CR's applications. General likelihood ratio detectors (GLRDs) using multi antenna are derived from different assumptions in [123]. GLRD1 is derived assuming that only the channel gain is unknown, and is estimated using maximum likelihood (ML) estimation. Blind GLRD is derived when all signal variance, noise variance, and channel gain are unknown to the CR, requiring estimation of these parameters as well. GLRD is derived in [124], assuming that the PR user had three different signal sources. Deriving asymptotic performance of GLRDs at different assumptions can be found in [99]. We can say that even GLRDs in some cases do not need prior information about PR's signal, the channel and the noise, they depend on estimating, which degrades the performance significantly and requires high SNR to work.

Chapter 5 of this thesis proposes three different optimal and suboptimal multi antenna spectrum sensing techniques for CR. Simulation and analytical results under different conditions are included in the chapter. Furthermore, comparison to the mentioned multi antenna based spectrum sensing techniques is included as well.

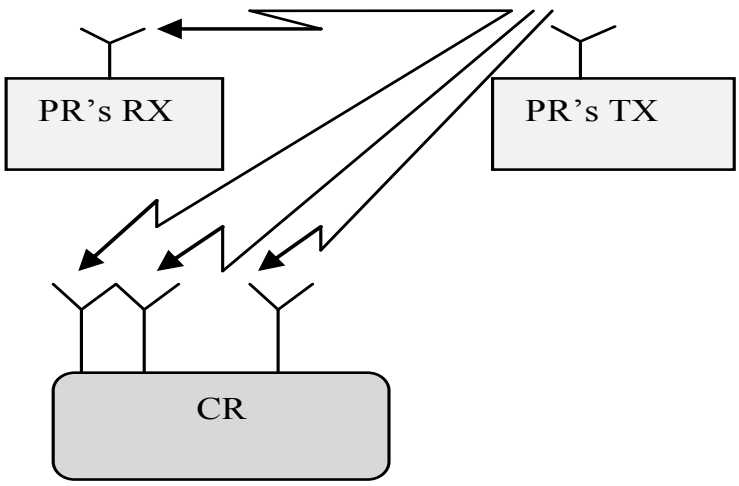

Figure 2.16 Multi antenna based spectrum sensing in CR's systems.

2.4.3.2 Global Cooperative Spectrum Sensing

Global cooperative spectrum sensing (global CSS) in CR's network, exploits the spatial diversity among a number of CRs in the CR network to mitigate the *hidden problem* in CR spectrum sensing. Thus, the measurements or the decisions that have been taken locally at the CRs will be sent and combined at CR-BS in the centralized based CR network, for example. Then, the final decision and channel allocation between the different CRs will be declared, which reconfigure their transmission/ receiving parameters in order to utilize the PR's vacant frequency band. CRs in the centralized architecture are required to perform sensing, sending of the results, and responding to the declaration from the CR-BS. In the CR architecture with no infrastructure, such as CR Ad Hoc network, each CR exchanges its locally sensed or decided measurements about the PR's transmitted signal with its neighbours. Unfortunately, this increases the tasks per CR in the CR Ad Hoc network. Furthermore, the complexity of the networking here required more solutions, because the CR Ad Hoc network is assumed to work in different licensed PR frequency bands, which require complicated protocols to avoid collisions between different CRs [70]. Figure 2.17 shows an illustration of the centralized and distributed cooperative spectrum sensing in CR [108]. It can be seen that the CRs in the CR Ad Hoc network perform the mission of CR-BS in terms of fusing the measurements and decisions in addition to the local spectrum sensing itself. Of course, this would lead to high complexity of the hardware and software processing at each CR, and a greater consumption of power.

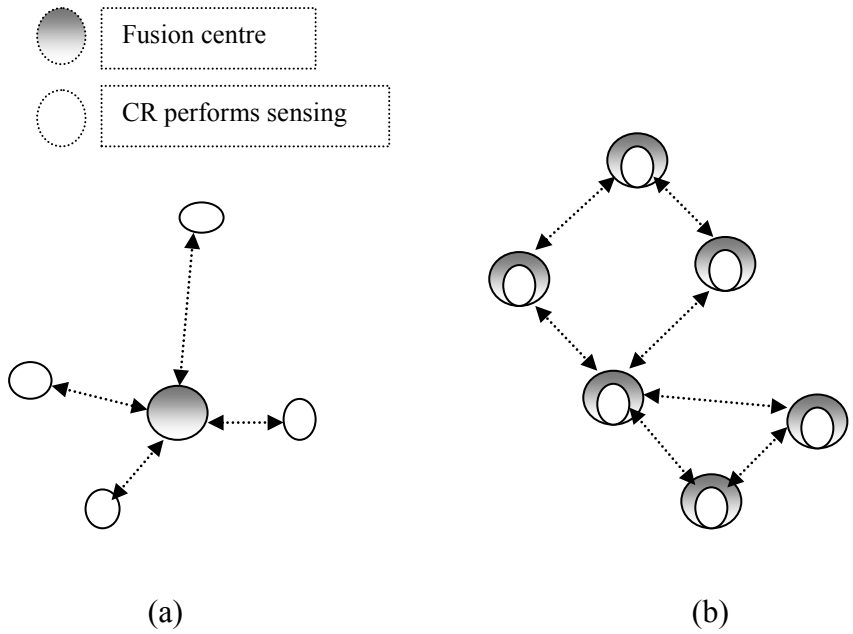

Figure 2.17 Illustration of the spectrum sensing cooperation in CR network: (a) centralized cooperation (b) distributed cooperation.

An example for the distributed CSS is the relay based technique that is proposed in [125]. In the CR network, two CRs cooperate sensing of PR's transmitted signal. Their sensed measurements about the PR's transmitted signal are passed to a common CR in the CR network based on amplify and forward protocol (AF) [126]. The access based between the two CRs and the common CR is assumed to be time division multiplexing access (TDMA). The time slots are divided as follow: the first slot is assigned to the first CR to forward the measurement to the common CR, while the second CR listens to the first CR's transmission. In the second slot, the second CR forwards what has been listened from the first CR to the common CR, and so on. The work is extended for a CR network with multi users as in [127]. The result shows how the cooperation increases the overall agility.

Until now, it has been understood that the CSS has the main advantage of mitigating the *hidden problem* in CR spectrum sensing. Cooperation in CSS results in an increase in the detection probability and decrease in the errors. Of course, this would lead to minimizing the interference to the PR's frequency band, and would improve the spectrum efficiency. The cooperation in CSS might be centralized or distributed, based

on the CR operation requirements. Some pictures of the difference between them have also been provided. Interesting questions are due now; the first: after PR's signal is sensed locally at the different CRs, what sort of the information should be sent to CR-BS or common CR in the CR network? Secondly, how can the CR-BS decide finally the occupancy of the PR's frequency band?. The answers of these two questions fall under two types of CSS: soft CSS (SCCS), and hard CSS (HCSS).

2.4.3.2.1 Soft Cooperative Spectrum Sensing (SCSS)

Figure 2.18 shows the possible scenario of CSS in centralized CR's network. It's clear that CSS includes three main stages. The first is sensing the PR's transmitted signal locally by different CRs in the CR's network. The second is sending the resultant information to the CR-BS. The third is fusing the gathered information at the CR-BS, where CR-BS finally declares the decision to the CRs. The type of information sent to the CR-BS and the final decision rule at CR-BS distinguish between SCSS and HCSS. In SCSS, the spectrum sensing process is done through the following steps:

a. Each CR performs local spectrum sensing independently from the others CRs.
b. The resulting measurements from local spectrum sensing, which are energy measurements, are then sent from the CRs to the CR-BS via control channel (CC).
c. CR-BS fuses the received measurements from the different CRs and declares the final decision.

This type of cooperation is called *data fusion* as well in [128]. The CC task is crucial here, since the spectrum sensing information and allocation are required to be sent via this channel.

Before starting to focus on SCSS, the reader can refer to the ED local spectrum sensing in subsection 2.4.2.2, since it is the main local spectrum sensing technique that has

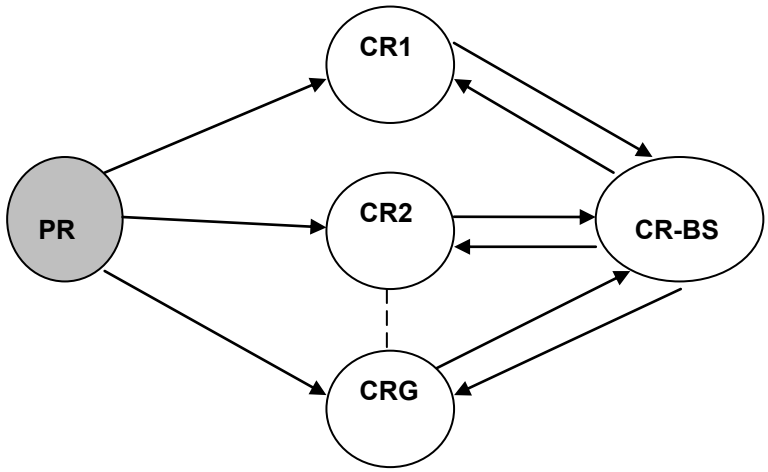

Figure 2.18 centralized CSS structure in CR.

been chosen in most CSS techniques. In ED based SCSS, the D_{ED} for each CR is sent to the CR-BS via CC (the decision statistic here does not mean complete the comparison in (2.14)). Of course, the channel between the PR and each CR, the noise at each CR, the CC between CRs and CR-BS and the noise at the CR-BS all have an effect on the performance. An optimal linear SCSS algorithm is proposed in [47], where the performance is optimized by linearly combining the individual CRs' local decision statistic D_{ED} at the CR-BS. The algorithm is based on giving weights for the different CRs depending on their local SNR. The CR with high SNR is given high weight and so on. In [129], the authors proposed an optimal SCSS based on *deflection coefficient* maximization criterion. The CSS performance using LRT-soft combination has been evaluated in [130]. It has been found that the SCSS scheme has a better performance in terms of probability than the "AND'' based HCSS. However, the main disadvantage of SCSS is that it needs huge bandwidth of the CC [47, 73, 128]. This is actually the main reason behind avoiding any focus on SCSS in this thesis.

An interesting and different SCSS method is MTM-SVD. In Geophysics applications, MTM-SVD has been used for signal detection and reconstruction in global temperature data over the past century [44]. The MTM-SVD methodology avoids most

of the weakness and limitation in the detection and reconstruction of spatiotemporal oscillatory signals immersed in colored noise [45]. Simon Haykin recommended this method to estimate the interference temperature exploiting the spatial variation in an RF environment [26]. In MTM-SVD, the energy of the transmitted PR's signal at the frequency bin can be estimated using a number of CRs that are located at different locations with respect to PR, and using a number of tapers (i.e., DPSS). Since this method is applied practically in Geophysics and only recommended by Simon Haykin to be used in CR spectrum sensing, and due to the strength of this method; chapter 3 of this thesis evaluates its practical use in CR systems using simulation, and defines the challenges and requirements that face using both MTM and MTM-SVD in CR's systems.

2.4.3.2.2 Hard Cooperative Spectrum Sensing (HCSS)

Referring back to step (b) in the SCSS steps, one can distinguish between the two CSS techniques at this point. At this point, each CR detects the availability of the PR's signal in the frequency band under sensing. The detection here means deciding if the PR's signal is available or not. Thus, if ED is used as in HCSS, each CR completes the comparison in (2.14). The output from the gth CR to the CR-BS in the CR's network is a binary digit as "1''represnting $\mathcal{H}_1$ hypothesis, or "0'' representing $\mathcal{H}_0$. Therefore, the gathered information at the CR-BS is binary digits and the fusion rule is based on one of the logic rules. This type of CSS is called as *decision fusion* [128]. The logic rule "AND'', is proposed as a fusion rule in the HCSS [130]. The CR-BS decides $\mathcal{H}_1$ only if all CRs decide $\mathcal{H}_1$ locally. Such a fusion rule decreases the interference probability to the PR's frequency band but at the expense of the spectrum efficiency. The "OR'' logic rule at the CR-BS is proposed for HCSS in [48], where the CR-BS declares that the PR's signal is present in the band under sensing when at least one CR decides the signal is present. Therefore, the interference possibility percentage can be increased in such a

fusion rule, but higher spectrum efficiency will be achieved. The “VOTING’’ logic rule [131], is one of the classical fusion rules that can be used in HCSS [47]. In this scheme, the CR-BS decides the presence of the PR’s signal in the frequency band under sensing, when more than one CR decides this.

The main advantage of HCSS over SCSS is that it does not need a huge bandwidth for CC; this supports the main objective of CR’ systems – namely, the more efficient use of the spectrum by using narrow band CC. Furthermore, the HCCS outperforms SCSS in term of probability when the total number of cooperated CR is large [77]. However, there are a number of optimization problems with HCSS, and have been given more attentions. The optimal fusion rule at the CR-BS has been investigated in [132]. It was found that the half “VOTING’’, is the optimal fusion rule when ED is used locally, and the total number of cooperative CRs was 10. The CC in their work was assumed to be free of error. The authors in [51], maximized the global probability of detection in “OR’’ and “AND’’ fusion rules by fixing the global false alarm probability and maximizes the local probability of detection. Optimal strategies to minimize the total error probability under Neyman Pearson, and Bayesian criterion have been considered in [133]. The CC is mostly assumed as free of error (i.e., perfect) in the publications about HCSS. In [95], the overall/global detection of HCSS is maximized where the overall false alarm is fixed by fusing the decisions from the CRs that have CC with low error only. This work has focused on improving the HCSS performance from the CC viewpoint.

Chapter 6 of this thesis investigates different optimization conditions and strategies in HCSS. Furthermore, it proposes a method that takes the HCSS optimization methods to their optimum performance. Simulation and analytical results included in this chapter show such conditions and the proposed method performance.

2.4.4 Spectrum Resource Analysis, Management, and Dynamic Sharing

After finishing the spectrum sensing in the PHY layer of the CR, the output of the sensing might be a number of frequency subbands. These sensed subbands might be allocated as licensed, unlicensed, or a mixture of both. The CR terminal should analyze the vacant subbands and decide which of them is or are the most suitable for use by its transmitter. This step is known as spectrum analysis or decision [60, 67]. In spectrum analysis, the sensed vacant frequency subbands usually have different characteristics, varying with time. The understanding of the vacant spectrum's characteristics by the CR terminal is an important task after the subbands have been sensed. In addition to the carrier frequency, bandwidth of each subband and the operating parameters of the PR user activity, there are a number of parameters that should be taken into account before the CR decides which subbands are going to be used. For example with [60, 67], in regards to the path loss factor, the vacant subbands might be in different frequency ranges. At the same transmission power, the transmission distance is decreased as the frequency is increased. Thus, when the CR increases its transmission power to overcome this problem it might cause harmful interference to the PR user. The difference in the interference level of the vacant subbands and the used modulation techniques causes changing in the error rate of the wireless channels. Furthermore, different link layer protocols are required by CR to deal with the different frequency subbands characteristics, which will result in different link layer delays [67].

Spectrum analysis/decision lies under the spectrum management function in CR systems. Spectrum management is defined by Simon Haykin as the connection between the output from the spectrum sensing step and the power control of the CR's transmitted signal [26]. The main objective of spectrum management here is to optimize the use of the detected vacant frequency subbands by choosing the suitable modulation scheme,

and to enhance reliable and seamless communication between CR users. Consequently, the spectrum management here aims to tolerate the problem when the required QoS cannot be satisfied by [26]: 1. Changing the modulation scheme, or 2. Changing the frequency subband. *Spectrum handoff* occurs when the subband that has been found vacant and is being used by CR, is reclaimed again by its licensed PR user [60, 67, 69, 70]. Therefore, CR must change its frequency subband to another vacant frequency subband, and this is called *spectrum mobility* [60, 67, 69, 70]. Another *spectrum handoff* type might occur when the transmission conditions of the vacant frequency subband, which is being used by CR, become worse due to time varying of the wireless channel. When CR moves from area to area, the vacant frequency subband might not be vacant any more due to the change in CR's location where the PR is active in the frequency subband and in the new location [60]. This type of transition process from one vacant frequency subband to another one might cause packet delay [63]. Reserving a number of frequency subbands (i.e., channels), to be used by the CR user in *spectrum handoff*, can minimize the performance degradation [134]. CR can use one of the reserved frequency subbands, when it is being forced to leave the current frequency subband. In [135], the sensing technique is supported by location estimation to overcome the performance degradation in *spectrum handoff*. Each CR sends the vacant frequency subbands information and its location to a main CR-BS. Thus, CR can be aware of the geographical locations of the vacant frequency subbands.

Joint sensing at the PHY layer and accessing at the MAC layer in CR systems, have been concentrated upon in this literature. The reason behind this is that CR can not sense the whole spectrum due to hardware and energy constraints. Moreover, it can not use all the vacant frequency subbands. Two main questions here are: which frequency subband can be sensed or accessed by CR with minimal interference to the PR transmission? When?. Such a problem is feasible in CR Ad Hoc networks, where there

is no CR-BS [136]. An analytical framework based on the theory of partially observable Markov decision process (POMPD) has been developed in [137]. A cross-layer based multi channel MAC protocols for CR Ad Hoc networks are proposed in [136]. The proposed protocols integrate the spectrum sensing at PHY with packet scheduling at MAC. Each CR is supported by two transceivers. The first one is for CC functions, and the second one is used for both sensing and communications. In [138], the authors considered the problem in a different way. When there are a number of available frequency subbands, and CR can sense and access one subband at time, then the question becomes how can CR choose a free and good subband very quickly? Their work is to optimize the sensing order in CR systems when there are number of frequency subbands available for sensing and accessing. This research shows how the spectrum sensing has more challenges at the upper layers as well.

In CR networks, after performing spectrum sensing tasks, there might be a number of licensed frequency subbands available to be used by CR users. The dynamic sharing problem of the available frequency subbands between PR and CR users, and between CR users themselves is analyzed using the well know mathematical approach, *game theory* [139]. Using game theory formulation in the dynamic sharing problem allows analyzing the PR and CR users' behaviours and actions to be game based. In *game theory*, the game consists of players, players' strategies, and players' payoff functions. This can be applied to dynamic sharing problem, where PR and CR users are players with different strategies and objectives. CR users share the licensed frequency subbands with the PR users and pay the PR users or service providers in dynamic sharing. This is called spectrum trading [140]. Based on the objectives of spectrum trading for both PR and CR users and their behaviours, the authors in [140] proposed three different pricing models; market-equilibrium, competitive, and cooperative pricing models. The problem of power and frequency subbands allocation and sharing among Ad Hoc CR users, via

developing an efficient MAC mechanism, is considered as game based in [141]. A distributed pricing approach is proposed for an efficient power and frequency subbands allocation.

2.5 Cognitive Radio Transceiver

In sections 2.2-2.4, an overview of the CR revolution, along with relevant definitions and concepts have been given. The CR cycle is reviewed as well, and then more technical details about spectrum sensing task and its related tasks are also provided. A good understanding about the CR's spectrum sensing issues and challenges at both PHY and MAC layers can thereby be achieved.

In this section, a general technical overview of the promised CR transceiver, the OFDM, will be provided. However, it should be taken into account that the main aims of this thesis are about CR spectrum sensing, and about both local and global cooperative spectrum sensing using multi antenna and multi CRs' diversities.

2.5.1 Why OFDM for Cognitive Radio Systems?

In CR PHY layer design, the spectrum flexibility of the transmitted signal is a main requirement. Such flexibility would allow CR to efficiently fill the frequency subbands of the PR users (i.e., spectrum holes), when they are not being used by their licensed PR users [27]. In OFDM-based CR systems, this is made possible by deactivating the OFDM subcarriers that lie within the PR users' frequency subbands [27]. Furthermore, the FFT process at the CR Rx can be used for wide spectrum analysis in the frequency domain. Based on [28], the main OFDM features that support practical implementation of CR systems, are defined as follow:

1. The FFT process, in CR Rx, allows monitoring the PR's activities in the frequency domain which supports spectrum sensing in OFDM-based CR systems.
2. Deactivation of the CR subcarriers that lie within the frequency subband of PR user makes the waveform shaping much easier which supports the efficient use of the spectrum in OFDM-based CR systems.
3. The OFDM parameters such as FFT size, subcarriers spacing and powers, modulation and coding types, and cyclic prefix (CP) length can be adapted for OFDM-based CR systems to meet different wireless environment conditions.
4. There are number of already developed and successful OFDM-based wireless standards; this makes the interoperability of OFDM-based CR with such standards much easier compared to other standards.
5. OFDM standard supports the multi user access in OFDM-based CR communications by assigning a number of subcarriers for groups of users as in OFDM access (OFDMA).
6. Multi antenna techniques are used in OFDM standards due to the simple required equalizers. Smart antennas can be also used in OFDM standards.

Figure 2.19 shows a representative diagram of the serial high data rate stream conversion to parallel with low rate sub streams in OFDM. In OFDM, the high data rate stream, which contains N serial symbols with symbol duration T_s for each symbol, is converted to N parallel substreams with low rate (N here represents IFFT/FFT size). The parallel low rate symbols have duration as T_{os}. The OFDM transmission can be described as follow: The serial input data samples to the OFDM transmitter are mapped first to phase shift keying (PSK) or quadrature amplitude modulation (QAM) arrays. The resultant mapped symbols are converted to parallel symbols with duration T_{os} each. Every symbol then is modulated onto the subcarrier using IFFT. The resultant

modulated symbols represent the so called OFDM symbol with duration T_{os}. The OFDM symbol duration here is equal to NT_s. The use of parallel conversion from high to low symbol rate on each OFDM subcarrier mitigates the inter symbol interference (ISI) problem, which is caused by multipath fading in high data rate transmission. The OFDM symbol duration is increased due to the increase in the duration of the parallel substreams. Therefore, the effect of time dispersion will be limited on some data symbols. Adding CP to the OFDM symbol eliminates the remaining effects of ISI. Such a feature results in a simple equalizer structure that can be used to equalize the received signal. Figure 2.20 shows the transmission and reception processes in an OFDM based system. The reception in OFDM is opposite to the OFDM transmission (e.g., using FFT and demodulator, etc.). The red blocks in the figure show how the CR Tx, responds to the results from the spectrum sensing, and deactivates subcarriers that lie in the PR frequency subbands. The CR Rx for both source and destination of a CR communication link must be aware of the activated/deactivated subcarriers.

In order to mitigate the ISI effect, the proper CP duration must be greater than the expected channel time delay that resulted from multi path fading. In OFDM, the CP insertion is achieved by copying the last N_{CP} out of N subcarriers in each OFDM symbol and inserting it at the beginning of that OFDM symbol. Thus, the new OFDM symbol length will be $N_{CP}+ N$ after this insertion, where N_{CP}, is the CP length. Therefore, the new OFDM symbol duration in time is $(N_{CP}+ N)\ T_s$.

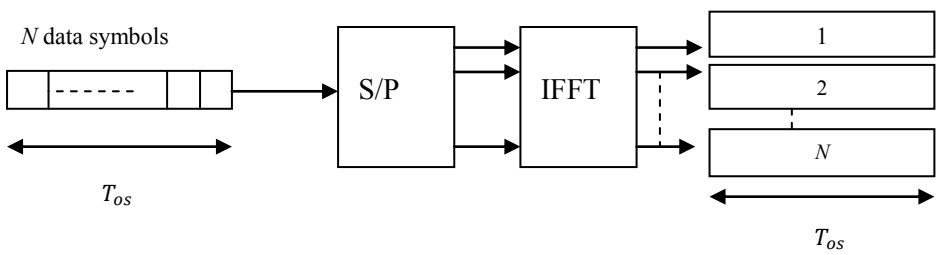

Figure 2.19 High data rate stream conversion to low rate substreams in OFDM.

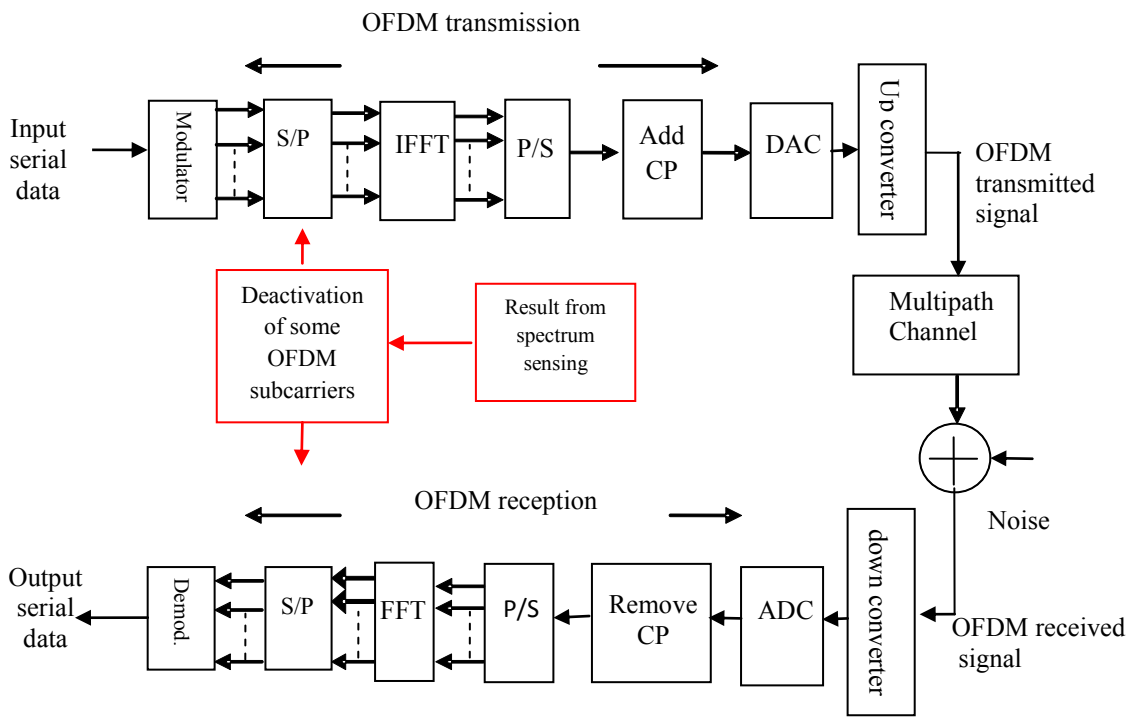

Figure 2.20 Transmission and reception in OFDM based system.

Figure 2.21 shows an OFDM signal consisting of 11 subcarriers. The subcarriers spacing, Δf_{os}, is the spectrum distance between two adjacent subcarriers. Mathematically, subcarriers spacing can be represented by the division of the total bandwidth BW over N subcarriers, or $\Delta f_{os} = \frac{BW}{N} = \frac{1}{T_{os}} = \frac{1}{NT_s}$. The modulated subscribers in OFDM signal are kept orthogonal as the subcarriers spacing, Δf_{os}, is kept equal to $\frac{1}{T_{os}}$.

Figure 2.22 shows an example of the deactivation and activation process of some subcarriers in OFDM-based CR. After performing spectrum sensing in an OFDM-based CR system, the subcarriers that lie within the frequency subband of PR user will be switched to zero in OFDM-based CR transmission, and hence CR can exploit the other remaining subcarriers for its transmission. The non-contiguously of subcarriers in OFDM-based CR system earned it another name: a non-contiguous (NC) OFDM system [142]. It is clear that the OFDM approach is very suitable for CR transmission in terms of spectrum flexibility.

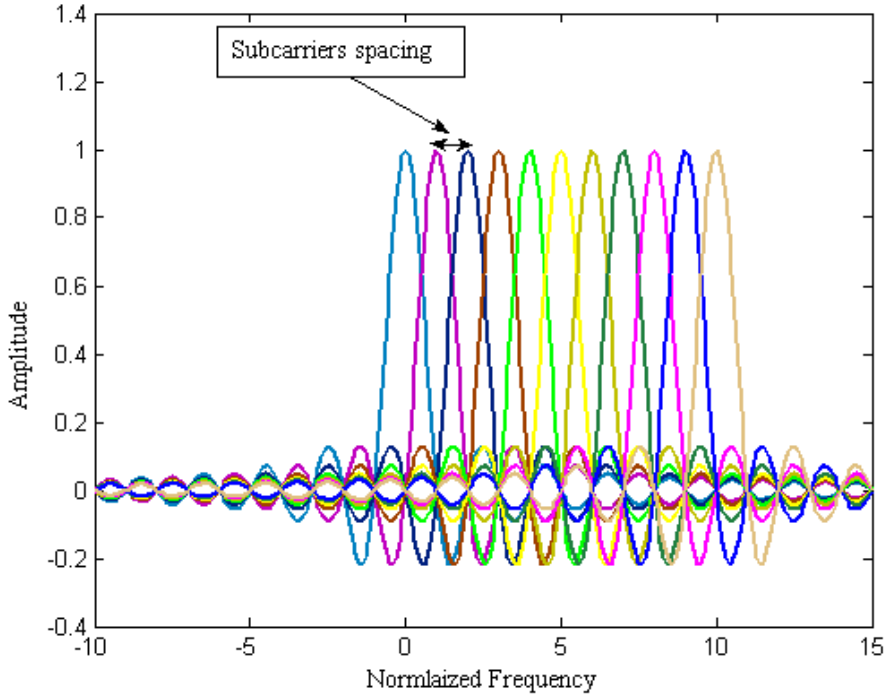

Figure 2.21 Number of 11 subcarriers in OFDM signal.

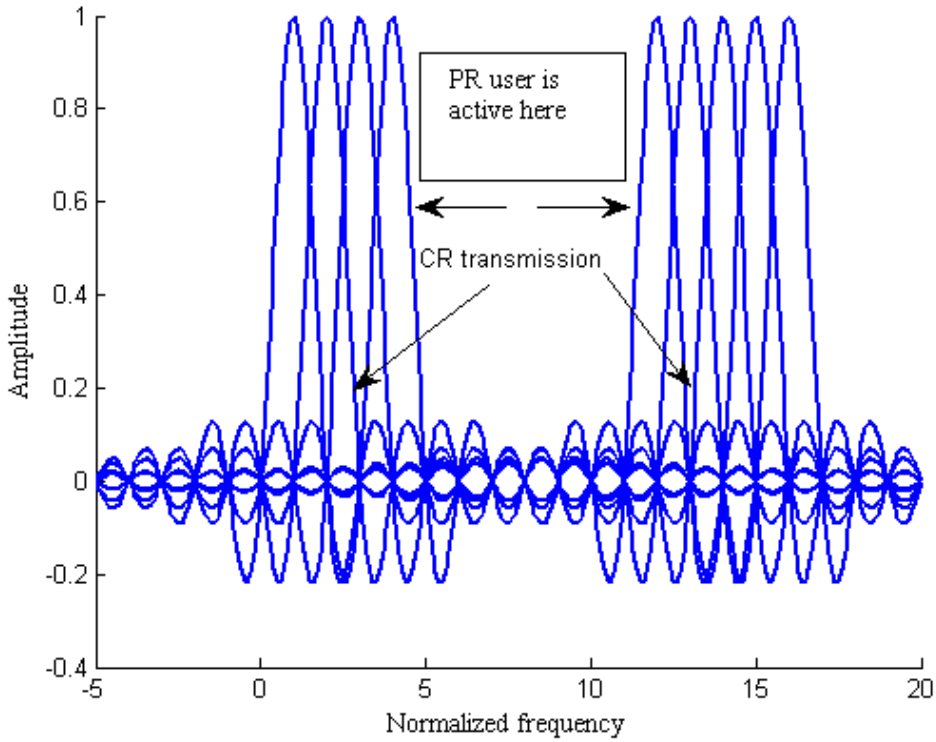

Figure 2.22 Subcarriers activation and deactivation in OFDM-based CR signal.

2.5.2 IEEE802.22 and the Other OFDM Based Wireless Standards

The IEEE 802.22 standard is the first OFDM based wireless standard that supports the CR concept. It provides high data rate services to rural geographical areas, exploiting the unused TV channels in the VHF/UHF frequency ranges [56]. IEEE 802.22 is also called wireless regional area network (WRAN), since it basically serves rural areas. The IEEE802.22 working group aims to develop an international standard for CR that operates in TV frequency ranges. The initial frequency range that is supported by IEEE802.22 is the North American frequency range 54-862 MHz. The frequency ranges of IEE802.22 is going to be extended to 41-910MHz frequency range to meet the international requirements [55]. Furthermore, the standard will be able to operate in different TV channel bandwidths, 6, 7, and 8MHz [55]

In IEEE802.22 network, there are a number of consumer premise equipments (CPEs) which are served by a main entity that can be called CR-BS in a specific cell. Therefore, this type of wireless air interface can be called point to multi point (PMP) air interface. The CR-BS here fully controls the access to the frequency subbands under restricted conditions to protect the PR and incumbent users from interference. It also controls the bandwidth, power, modulation, and coding of CPEs. The PR and incumbent users are referred to the TV broadcasting and wireless microphones. Moreover, the CR-BS controls the distributed spectrum sensing from different CPEs in the cell and makes a final decision on using the TV frequency subbands [55].

Figure 2.23 shows a comparison between the IEEE802.22 and the other IEEE802.xx standards in term of transmission distance, data rate, and frequency range [55, 56]. The IEEE802.15, IEEE802.11, and IEEE802.16 standards are known as the wireless personal area network (WPAN), WLAN, and wireless metropolitan area network (WMAN) respectively. The WMAN is also called as WiMAX.

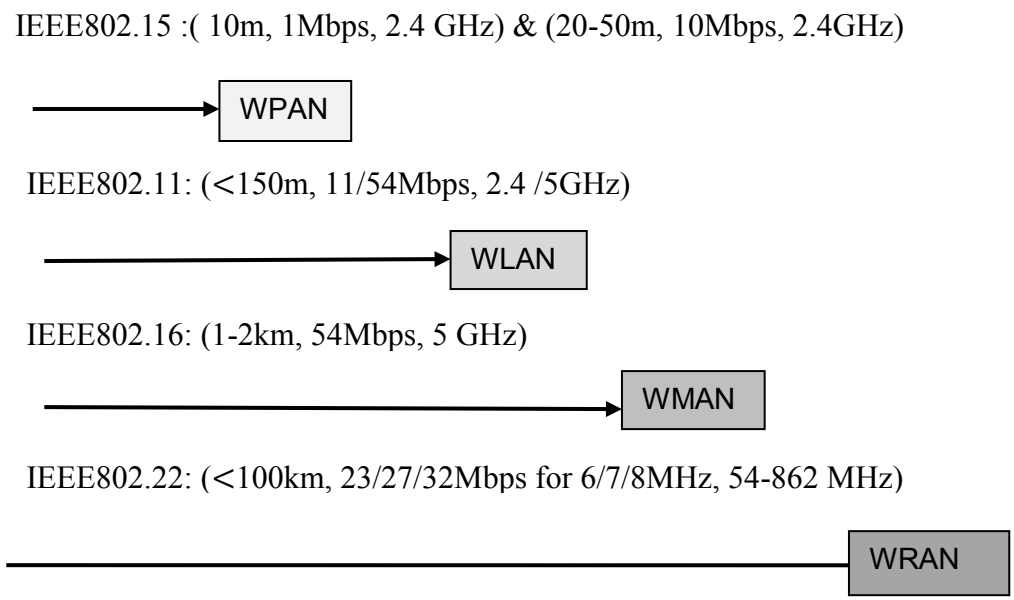

Figure 2.23 A comparison between IEEE802.22 and other IEEE802.xx standards in term of (transmission distance, data rate, frequency range).

The used spectrum sensing technique in IEEE802.22 as a technique name cannot be specified due to the IEEE802 rules. However, IEEE802.22 working group defines general requirements from the spectrum sensing technique that should be taken into account by manufacturers [143]. For example the preferred ranges of P_d and P_f for spectrum sensing technique are (90-95%), and (1-10%) respectively [143]. However, these ranges can not be generalized for all applications. In applications where the PR users are military or civil rescue, the P_d must be kept very high at very low P_f

2.5.3 Spectrum Sensing Techniques in OFDM-Based CR

Generally, all spectrum sensing techniques that have been investigated in sections 2.4.2.2-2.4.2.6 are useful in OFDM–based CR systems. Of course, spectrum sensing techniques have different performances and different requirements as to what has to be. For example, ED does not require knowledge about the PR's signal parameters, but it is not robust in low SNR conditions. Spectrum sensing techniques that exploit the CP correlation in OFDM signals are proposed in [144, 145]. In autocorrelation based

spectrum sensing techniques, the autocorrelation coefficients are not equal to zero at multiple integers of the OFDM symbol [144]. This due to the presence of the CP in the OFDM signals. Based on this, the authors have proposed a local spectrum sensing technique that exploits such CP correlation. Furthermore, the proposed SCSS scheme would collect the decision statistics that resulted when autocorrelation based techniques were used by the different CR users. The CR-BS receives the decision statistics one by one, applies the hypothesis test each time, and if the decision is not reliable, it asks for another decision statistic from another CR user. The proposed technique in [145], decides that the PR user is active in the frequency subband under sensing when the correlation between two different samples representing the same CP samples that are reflected form different paths, give a peak value. The main drawbacks of such techniques are that they require full knowledge about the CP parameters for different OFDM PR signals, and their use is limited to spectrum sensing of OFDM PR signals only and can not be used widely for different types of PR signals. Furthermore, such techniques perform spectrum sensing of OFDM signal and know the CP parameters and the frequency subband as well. Regarding performance, the autocorrelation based spectrum sensing technique and SD SCSS will be compared to MTM in Chapter 4.

2.6 Chapter Summary

In this chapter, a number of definitions and concepts that are related to the CR were presented. The CR's definition itself, the CR cycle, and the CR functions and missions have also been reviewed. The chapter then started to focus on the spectrum sensing task in CR as it is a key task in developing CR systems.

The spectrum sensing definition and its relevant concepts and challenges were given concentration. The spectrum sensing problem formulation using *Neyman Pearson* criterion was discussed. The discussion included the different probabilities formulae and

the performance evaluation. The different classical spectrum sensing techniques were reviewed. The cooperation in spectrum sensing was given attention in this chapter via technical discussions of the different local and global cooperation techniques. The spectrum management as an important task after the performing of spectrum sensing was then outlined.

The OFDM–based CR system was the final part of this chapter. A full revision of this good PHY layer candidate was provided. That included, it is advantages and drawbacks, and its structure. Moreover, the IEEE802.22 as the first OFDM-based CR standard was reviewed and compared to the other IEEE802.xx standards. Finally, spectrum sensing techniques in OFDM-based CR were reviewed.

Chapter 3: Performance evaluation of MTM-SVD spectrum sensing in CR systems

3.1 Introduction

This chapter focuses mainly on the MTM and MTM-SVD as efficient CR spectrum sensing techniques. The general reasons behind choosing MTM are provided in this chapter. Thereafter, a revision of the *bias-variance dilemma*, which is a main problem in the classical spectrum estimation methods, is provided to achieve deep technical understanding about this problem and its effect on CR spectrum sensing. The MTM concept, and features are then discussed. The MTM methodology in spectrum estimation is provided including the DPSS generation.

There has been an interested in using MTM-SVD for spectrum sensing in CR networks, which is classified in chapter 2 as MSCSS, from famous researchers such as Simon Haykin. However, the MTM-SVD practical implementation and performance evaluation for CR spectrum sensing had not been investigated and analyzed in their literature. In this chapter a performance evaluation of MTM-SVD CR spectrum sensing is provided, using a simulation. A *D* threshold control method is proposed, exploiting the different levels of power between adjacent frequency subbands. Additionally, the challenges and requirements of practical implementation of MTM, and MTM-SVD are identified. Solving such defined challenges and requirements is the main objective of chapter 4.

The main content of this chapter has been published in one paper that represents the chapter contribution. The published paper is:

O. A. Alghamdi and M. A. Abu-Rgheff, "Performance evaluation of cognitive radio spectrum sensing using multitaper-singular value decomposition," in *Proc.*

***4th IEEE International Conference on Cognitive Radio Oriented Wireless Networks and Communications (CROWNCOM '09)*, 2009, pp. 1-6.**

3.2 Our Chosen Spectrum Sensing Technique

As is known, spectrum sensing is a key task in the CR systems. It allows the CR to opportunistically use the idle frequency subbands (i.e., spectrum holes) that have been left unoccupied by the PR users. Therefore, developing an accurate spectrum sensing technique is a main aim of industry and academic research centres in the practical design of CR systems, with a view to protecting PR users from interference and maximizing the CR throughput. The possible interference to the PR frequency subband, when non robust spectrum sensing techniques are used in CR, may influence political decisions about allowing the use of CR in a country. This is because PR users might be sensitive to such interference. Military, police, intelligence, and other governmental bodies are examples of such users.

The RF environment surrounding the CR might consist of different PR users' signals and different frequency bands. The CR sensing algorithm should be able to deal with different PR signals without using any prior information about them. Accordingly, we exclude the prior information-based sensing algorithms from our research except for comparison issues. The chosen sensing algorithm should be based on the power spectrum estimation, and thus will support the sensing in the CR to deal with different PR signal levels and modulations in wide frequency bands (i.e., FFT based). Such based methods are classified as *nonparametric* methods, since they do not need to model the sensed signal itself [91]. The conventional *nonparametric* power spectrum estimation method is the PE [91] (or ED[90]). For finite time measurement samples, PE can be represented simply by squaring the absolute of the output of the analyser's FFT bins. PE has significant points of weakness, such as out-of-band leakage of the power and large

variance of power spectrum estimate [26]. At a low SNR, the PE will fail to detect the present of the PR user signal because it will not be able to distinguish between the PR user signal power and the background noise. Welch proposed a modified method of PE that depends on averaging the PE of number of overlapped data samples' segments [146]. However, the method still suffers from spectral leakage [147]. The MTM [29] *nonparametric* spectrum estimation method is the efficient spectrum sensing technique that accomplishes spectrum sensing with following main features [147]:

1. Accurate.
2. Effective.
3. Robust.
4. Feasible computational complexity.

A comparison between FB and MTM shows that the FB requires large numbers of sensed samples to achieve the same MTM performance in the same conditions [117]. Sections 3.3 and 3.4 discuss the spectral leakage and large variance of power estimates that classical spectrum estimation methods suffer from.

3.3 Spectral Leakage

The spectrum analyser/detector can take measurements of the signal power within a specific finite duration in a limited time for the signal, which is continuous. Practically, the digital signal processing (DSP) processor requires the signal to be observed only in discrete time intervals [148]. The FFT assumes that the signal repeats itself outside the measurement interval [148]. At the end of each signal measurement interval and the beginning of the next interval there will be discontinuity. Such discontinuity is not present in the original signal waveform and due to the sharpness between the two different measurements the spectrum at this point is spread out into the other frequencies causing spectral leakage. This is the source of the spectral leakage. Thus, in

spectral leakage concept, the energy that is assumed to be concentrated at a specific frequency leaks into other frequencies.

To understand the spectral leakage effect, let us consider the PSD of a single subcarrier in a multicarrier OFDM conventional system which is given by [118]:

$$\Phi_{sub} = |sinc(f - f_{sub})T_{os}|^2 \tag{3.1}$$

where $sinc(x) = \frac{\sin(\pi x)}{\pi x}$, and the subcarrier main lobe is concentrated around the normalized frequency, f_{sub} , and $T_{os} = 1$ is the normalized OFDM symbol/block duration. Figure 3.1 shows the PSD of OFDM subcarrier in decibels (dB). The energy of this subcarrier will leak into all adjacent subcarriers causing errors in the CR's decisions. This is due to the sharp discontinuity at the end of the time measurements (i.e., rectangular pulse) which has a *sinc* shape in the frequency domain.

The effect of the spectral leakage that might be caused is clear from Figure 3.1, where the first adjacent side lobe to the main lobe has about -13dB PSD. This amount of spectral leakage decreases with the increase in the spectral distance from the main lobe. Such spectral leakage will affect the CR decision, in spectrum sensing, about the signal measurements in the frequency subbands which are adjacent to the main lobe. Furthermore, the background noise energy from the whole spectrum will be added to the signal energy causing degradation to the SNR. Spectral leakage also makes it difficult to distinguish between different signals with different power spectrum levels [149]. Windowing is the classical technique employed to tolerate the problems of spectral leakage. Different windowing techniques have been proposed in the literature. In section 3.3, an overview of the windowing concept is provided. The section reviews three famous types of windows: rectangular, Hanning, and Hamming.

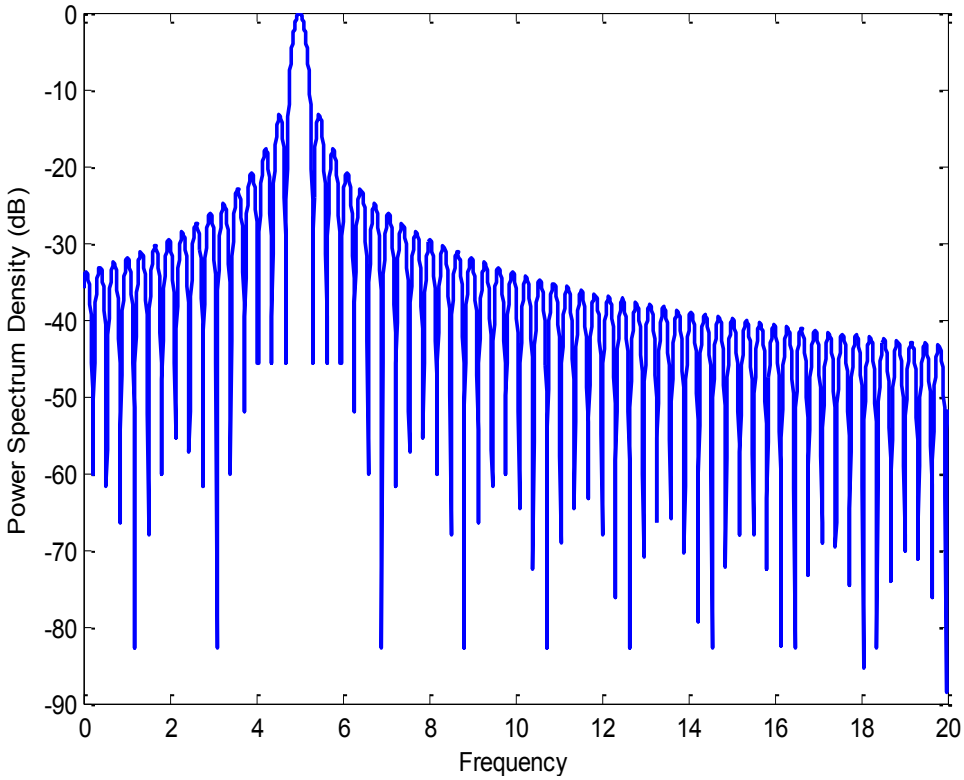

Figure 3.1 PSD in dB versus normalized frequency of a single OFDM subcarrier.

3.4 Windowing

It is clear that the problem of spectral leakage comes from the discontinuity at the end of the measurement time interval. The windowing is multiplying the time domain samples by a special type window which is capable minimizing the sharpness at the discontinue end by smoothly returning the signal to zero [148].

In the normal case the time samples are not multiplied by any type of window, or in another words, they are multiplied by one. The time samples multiplication by one is called rectangular windowing. This type of window is called a rectangular window. The problem with a rectangular window is that its spectral is a *sinc* function in the frequency domain that causes a significant leakage into the other frequency subbands. The PE spectrum estimation method uses rectangular windowing since the received signal samples at the analyzer/detector are multiplied by one. Different types of windows are

proposed to minimize the spectrum leakage, and to overcome the problems resulting from using rectangular windowing. The two well-known examples of such windows are Hanning and Hamming [148].

Figure 3.2 shows the magnitude response of different windows in the frequency domain. Hanning and Hamming windows try to overcome the problem of the spectral leakage that is produced from the rectangular window by minimizing the leakage outside the main lobe (i.e., attenuation reduction). However, this degrades the frequency resolution by making the main lobe much wider, as can be seen clearly from Figure 3.2. Another problem related to the power spectrum estimation is the large variance of estimate due to the single windowing. Classical windowing is based on multiplying the signal time samples by one taper/window. The drawback of this windowing is the loss of part of the information when the window smoothes the signal to zero. The power spectrum estimation of signal in multi carrier communication systems which are based on FFT is described as passing the signal in a bank of filters which they are band pass and narrow, and then measuring the output power at these filters [117, 118]. The prototype of this bank of filters is at the 0th subband band, and the remaining are shifted copies in the other subbands. As has been mentioned before, PE is the classical method of the *nonparametric* power spectrum estimation method, which can be represented by measuring the average power at the FFT frequency bins.

In conclusion, two main problems when dealing with the power spectrum estimation are: spectral leakage from a specific frequency into the other frequencies, and the variance of estimate caused by windowing using a single window/taper. The difficulty that is caused by these problems is called a *bias-variance dilemma* [26]. The 'bias' term refers to the energy's non concentration at a specific frequency. Therefore, the window with minimum spectral leakage is the window that has a good biasing property, and vice versa.

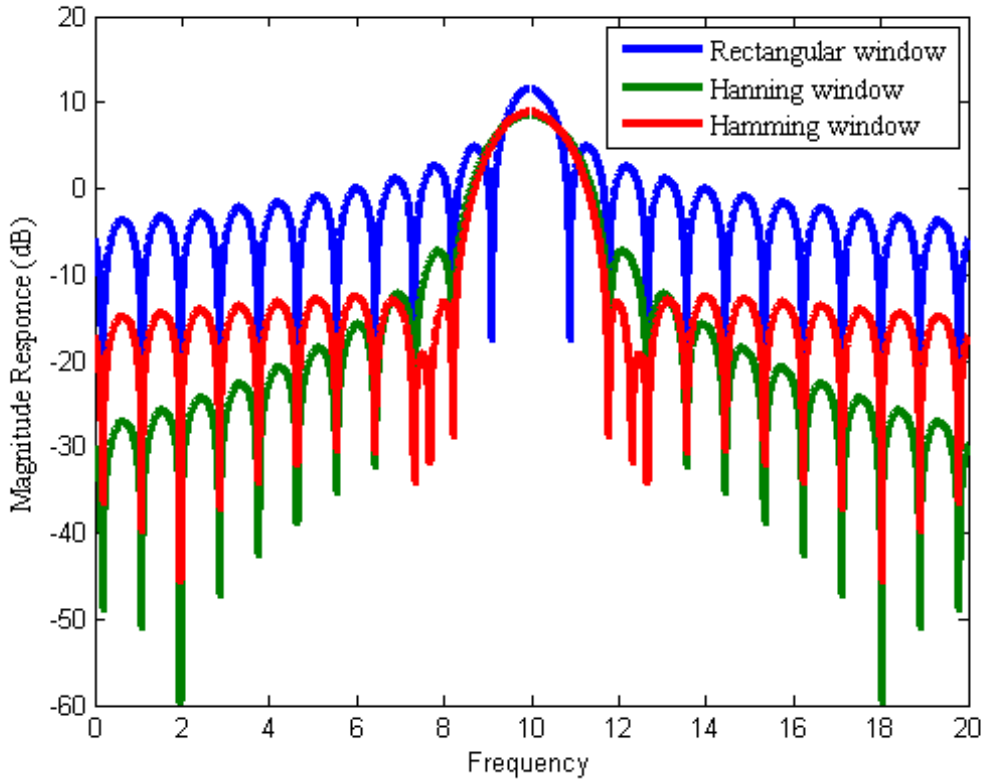

Figure 3.2 The magnitude response of rectangular, Hanning, and Hamming windows versus normalized frequency.

3.5 Multitaper Spectrum Estimation Method (MTM)

Thomson proposed using a bank of optimal band pass filters instead of rectangular windows; he called this method the multitaper spectrum estimation method (MTM) [29]. In MTM, the sampled data is multiplied by several leakage resistant tapers (i.e., windows) and this yields several tapered data samples from the original samples. By taking the FT of each of these tapered data samples, several eigenspectrums are produced, which can be combined to form a single spectrum estimate.

The MTM optimises the spectrum estimation in two ways: it minimizes the spectral leakage outside the band and it improves the variance of estimate by using number of

tapers. This technique is implemented using sequences of robust tapers, DPSS [30]. These sequences are reviewed and discussed in subsection 3.5.2.

In the literature, MTM-SVD is used for signal detection and reconstruction in global temperature data over the past century [44]. The MTM-SVD methodology avoids most of the weaknesses and limitations in the detection and reconstruction of spatiotemporal oscillatory signals immersed in coloured noise [45].

The advantages of using MTM in the spectrum analysis of high frequency seismograms are discussed in [37]. The MTM is used in the spectrum analysis of 16 bit seismic recorded data. The author has compared the performance of the MTM with different windowing techniques such as rectangular, Hanning, and 20% cosine. Although the MTM consumes more time in the spectrum analysis, it nevertheless overcomes the drawbacks in other methods.

Haykin in [26] suggested the use of MTM as an efficient method for spectrum sensing in CR. The author has described the requirements of accurate spectrum sensing and the spectrum estimation of the interference temperature using multiple-sensors, based on MTM-SVD. The MTM is applied to the TV bands spectrum analysis, and the performance is compared with the PE using real signal measurements [150]. The conclusions from the results are that MTM is fast enough to be used in real time, and there was a significant increase in the number of harvested channels with low false alarm probability. An FB for spectrum sensing in CR is proposed [117]. The performance of the suggested filter is compared to the MTM. It is found that the MTM is more efficient in the applications where the spectrum estimations require smaller samples of the underlying process.

ML methods provide an optimal estimate of the power spectrum. MTM technique is an approximation to the ML power spectrum estimates but at reduced computation [31, 32].

In subsection 3.5.1, the main features of MTM as an efficient CR spectrum sensing technique will be discussed.

3.5.1 MTM Features for Efficient Spectrum Sensing in CR

Based on subsection 2.4.2.5, Figure 3.3 shows the main notes that can be used to connect or compare MTM as a CR spectrum sensing technique to the other techniques that are mentioned in chapter 2.

The MTM can be combined with Loeve transform, which would allow CR to perform *time-frequency* analysis (TFA) providing cyclostationray property [147]. Furthermore, combing MTM with SVD or MTM-SVD enables CR to collect RF measurements from different locations. All these features and properties of MTM lead to developing an *integrated multifunction signal processor* [147]. Such a processor supports CR spectrum sensing in the three dimensions of frequency, time, and space [147].

The MTM produces power spectrum estimate in an *automatic* aspect compared to Welch's PE [147]. Furthermore, the way that MTM tolerates *bias-variance dilemma* can be controlled based on different parameters such as time bandwidth product and number of used tapers. Therefore, using MTM for CR spectrum sensing gives one an accurate, effective, robust, and feasible complex spectrum sensing technique.

3.5.2 Generation of the Discrete Prolate Slepian Sequences (DPSS)

DPSS [30], are a family of orthonormal tapers that have been proposed for use in MTM. DPSS concentrate the energy in the frequency interval $(-W, W)$, where $\Delta f = 2W$ is the frequency resolution, and maximize the rejection of the out-of-band energy. Denote the time-bandwidth product $2NW$, where N is the sequence's length. From [30], Slepian sequences are the real solution of (3.2):

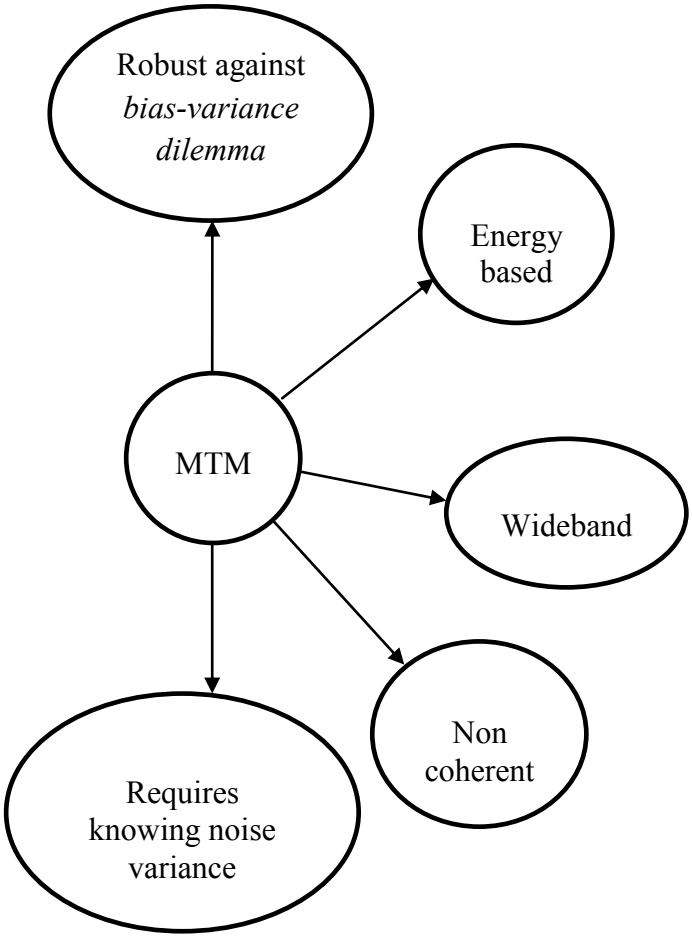

Figure 3.3 MTM's main distinguishing features compared to the other classical CR spectrum sensing techniques.

$$\sum_{t'=0}^{N-1} \frac{sin[2\pi W(t-t')]}{\pi(t-t')} v_{(t',k)}(N,W) = \lambda_k(N,W) v_{(t,k)}(N,W) \tag{3.2}$$

where $t = 0,1,2,\dots,N-1$, and both t and t', are time index. The eigenvalues $\lambda_k(N,W)$ in (3.2), are the eigenvalues of the $N \times N$ order matrix whose elements are given using (3.3) [30]:

$$\frac{sin[2\pi W(t-t')]}{\pi(t-t')},\ t,t' = 0,1,\dots,N-1 \tag{3.3}$$

Note that at $t = t'$, (3.3) is approximately equal to $2W$. The N elements of the corresponding eigenvectors for this matrix are in fact subsequences (tapers) of the DPSS. The total number of tapers produced, is $N_{tapers} = 2NW$. So from (3.2), and (3.3) we have the eigenvectors, $v_{(t,k)}(N,W); t = 0,1,2,\dots,N-1$, where k, represents the taper number. The eigenvalue, which is associated with k^{th} DPSS, is $\lambda_k(N,W)$. The total number of tapers that will be used in the estimation is K, with tapers own eigenvalues, $1 > \lambda_0(N,W) > \lambda_1(N,W) > \lambda_2(N,W) > \cdots > \lambda_{K-1}(N,W) > 0$.

For example let us consider a DPSS with tapers' length *N*=128, and half time bandwidth product *NW*=8. Therefore, $W=\frac{8}{128}= 0.0625$, these values are used in (3.2) and (3.3) to generate the different 16 DPSS. Figures 3.4 and 3.5 show the resulted first 4 out of 16 tapers in the time and frequency domains respectively.

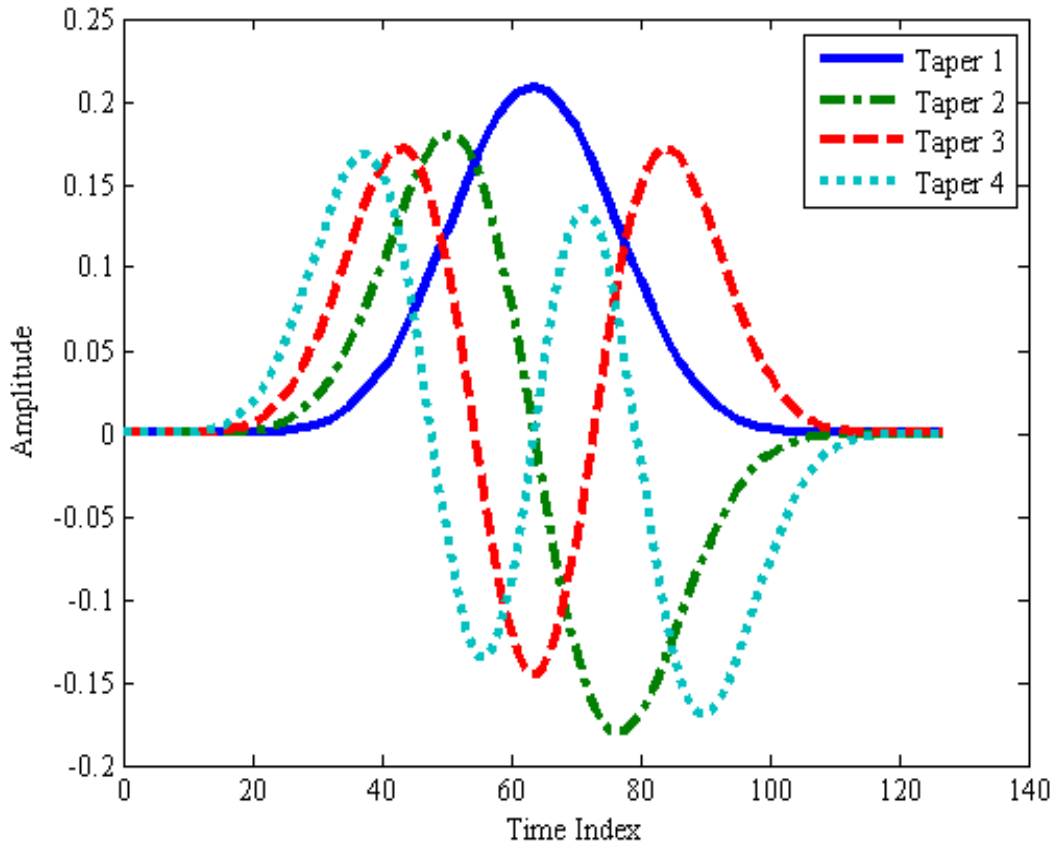

Figure 3.4 DPSS in time domain where *N*=128 and *NW*=8.

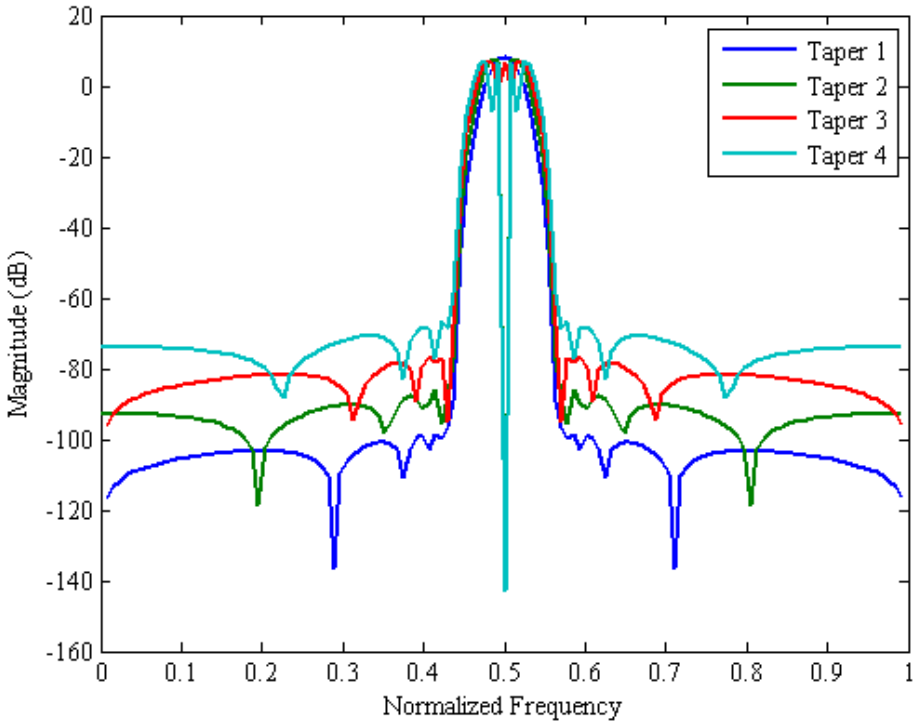

Figure 3.5 DPSS in frequency domain with N=128, and NW=8.

Power spectrum estimation using MTM improves the performance of the estimated power as follows: it improves the variance of estimate by using a number of orthogonal tapers; it minimizes the spectral leakage using a number of spectral leakage resisted tapers. In contrast to rectangular windowing, using DPSS in MTM returns the signal smoothly to zero in the time domain when it is being multiplied by the different DPSS. Furthermore, the signal information that was missed when the first taper is used will be recovered using the second taper, and so on. The DPSS has low spectral leakage, as can been seen clearly from Figure 3.5. For example, taper 1 has about -100 dB attenuation at the adjacent lobe of the main lobe.

3.5.3 Power Spectrum Estimation using MTM

Consider a finite time series $\{x_t; t = 0,1, \dots, N-1\}$ with discrete samples of a continuing time process that represent the PR's signal plus noise. Multiplying the

samples with different DPSS $v_{(t,k)}(N,W)$ (dot multiplication) represents convolution in the frequency domain.

The FFT of the product is taken to compute the energy concentrated in the bandwidth $(-W,W)$ and centred in a frequency f. Since there are K orthonormal tapers, then, there will be K different eigenspectrums produced from this process; this can be defined as [29]:

$$Y_k(f_i) = \sum_{t=0}^{N-1} v_{(t,k)}(N,W) x_t e^{-j2\pi f_i t} \tag{3.4}$$

where $v_{(t,k)}(N,W)$ is the DPSS which can be achieved using (3.2) and (3.3), and $f_i = 0, \frac{1}{N}, \frac{2}{N}, \dots, \frac{N-1}{N}$ are the normalized frequency bins. The first few eigenvalues are close to one. As the number of taper sequence increases towards the time bandwidth product, $2NW$, the eigenvalues decrease towards 0 indicating bad bias properties, and as it decreases away from the time bandwidth product towards 0, the eigenvalues increase towards 1 indicating good bias properties.

The spectrum estimate is given by the weighted sums of the first few eigenspectrums $Y_k(f_i)$ representing the largest eigenvalues $\lambda_k(N,W)$, which are produced from the first few K tapers, and is given by [29]:

$$S_{MTM}(f_i) = \frac{\sum_{k=0}^{K-1} \lambda_k(N,W) |Y_k(f_i)|^2}{\sum_{k=0}^{K-1} \lambda_k(N,W)} \tag{3.5}$$

In the conventional method of PE, the PSD, when the samples are taken at uniform time spacing is given by [91]:

$$S_{PE}(f_i) = \frac{1}{N} \left| \sum_{t=0}^{N-1} x_t e^{-j2\pi f_i t} \right|^2 \tag{3.6}$$

3.6 Estimating the PR's Power Using MTM-SVD

Consider a practical RF environment where both CR and PR nodes may exist together and let us assume there are G nodes of CR operating in the unused spectrum of PR RF environment. With MTM, each CR produces different eigenspectrums from the different used tapers and for different CR locations. The eigenspectrums, which are produced at different G CRs, are sent to a main CR-BS which uses them to formulate the spatio-temporal complex matrix $A(f_i)$ as [45]:

$$\boldsymbol{A}(f_i) = \begin{bmatrix} \rho_1 Y_0^{(1)}(f_i) & \rho_1 Y_1^{(1)}(f_i) & \dots & \rho_1 Y_{K-1}^{(1)}(f_i) \\ \rho_2 Y_0^{(2)}(f_i) & \rho_2 Y_1^{(2)}(f_i) & \cdots & \rho_2 Y_{K-1}^{(2)}(f_i) \\ \vdots & \vdots & \vdots & \vdots \\ \rho_G Y_0^{(G)}(f_i) & \rho_G Y_1^{(G)}(f_i) & & \rho_G Y_{K-1}^{(G)}(f_i) \end{bmatrix} \tag{3.7}$$

The complex matrix $\boldsymbol{A}\,(f_i) \in \mathbb{C}^{G\times K}$ in (3.7) has $G \times K$ order. Each row of $\boldsymbol{A}\,(f_i)$ is produced by a different CR node, and each column represents the eigenspectrum using a different taper. For example the element (2,1) of the matrix $\boldsymbol{A}\,(f_i)$, $(\alpha_2 Y_0^{(2)}(f_i))$, represents the eigenspectrum that has been resulted at the CR node number 2 using the first taper (i.e., k=0). The coefficients $\rho_1, \rho_2, \ldots, \rho_G$ represent spatially variable weights to adjust the relative position of the CR nodes from the PR TX.

The spatio-temporal complex matrix gives all possible eigenspectrums of different CR nodes. All these eigenspectrums can be decomposed into singular values via the singular value decomposition SVD method. This process can be applied to matrix $\boldsymbol{A}(f_i)$ in the matrices form shown in (3.8) [151]:

$$\boldsymbol{A}(f_i) = \boldsymbol{U}(f_i)\,\boldsymbol{\sigma}(f_i)\boldsymbol{V}(f_i)^{\mathfrak{h}} \tag{3.8}$$

where, $\boldsymbol{\sigma}(f_i) \in \mathbb{R}^{G\times K}$ is a diagonal real positive matrix consisting of singular values of matrix $\boldsymbol{A}$ at frequency bin f_i. If r = min $\{G, K\}$, there will be exactly r nonzero singular

values $\sigma_r(f_i)$. These singular values are represented by the r nonzero diagonal elements of the top left $r \times r$ block of $\boldsymbol{\sigma}(f_i)$, where $\sigma_1(f_i) \geq \sigma_2(f_i) \geq \cdots \geq \sigma_r(f_i) > 0$. Complex matrix $\boldsymbol{U}\ (f_i) \in \mathbb{C}^{G\times G}$ consists of the associated left vectors. Complex matrix $\boldsymbol{V}\ (f_i) \in \mathbb{C}^{K\times K}$ consists of the associated right vectors; the subscript $\mathfrak{h}$ denotes the Hermitian transportation. The eigenvalues of the matrix produced from $\boldsymbol{A}(f_i)^{\mathfrak{h}}\boldsymbol{A}(f_i)$ are $|\sigma_1(f_i)|^2 \geq |\sigma_2(f_i)|^2 \geq \ldots \geq |\sigma_r(f_i)|^2 > 0$. Equations (3.7) and (3.8) can be constructed at each bin of the frequency domain. This means that at each frequency bin, f_i, there will be r singular values. The square of the largest singular values at each frequency bin is proportional to the power at that bin.

The decision as to whether a given subband Δf_{sub} within the PR frequency subband is occupied or not is based on the statistics of the RF environment. The decision's computation is carried out into two scenarios: decision $de(f_i)$ in (3.9) on each frequency bin, at time *t*, is given by using the largest singular values as follows:

$$de(f_i) = \sum_{la=0}^{LA-1} |\sigma_{la}(f_i)|^2, \quad f_i = 0, \frac{1}{N}, \frac{2}{N}, \ldots, \frac{N-1}{N} \tag{3.9}$$

where LA, is the number of largest singular values of $A(f_i)$ at f_i. The decision on the subband Δf_{sub} is defined as:

$$D(\Delta f_{sub}) = \sum_{f_{sub}=f_{sub}^{start}}^{f_{sub}^{end}} de(f_{sub}) \tag{3.10}$$

where, f_{sub}^{start} is the first frequency bin in the subband Δf_{sub}, and f_{sub}^{end} is the last frequency in that subband. Basically, the subbands, which are under sensing, can be broadly classified into [26]:

1. Black subband, which is occupied by the PR user signal.

2. White subband, which is unoccupied by the PR user signal at a given location and time and consists mainly of noise. The threshold level can be defined as:

$$\gamma_{th} = \frac{D_{max} + D_{min}}{2} \tag{3.11}$$

where D_{max} and D_{min} are the maximum, and minimum decision values respectively in the four subbands in the system model shown in Figures 3.6 and 3.7. The subband Δf_{sub} is occupied by PR user signal, when the $D(\Delta f_{sub}) \geq \gamma_{th}$, and is unoccupied when $D(\Delta f_{sub}) < \gamma_{th}$.

3.6.1 System Model

The CR network in our model consists of a number, *G*, of CRs (transmitter/receiver) nodes/sensors, and one PR (transmitter/receiver) node transmitting in the subband between f_1 and f_2 as shown in Figures 3.6, and 3.7 respectively.

For each CR node, the DPSS is generated; the received samples of the PR's signal are multiplied by the DPSS and passed to the FFT to produce the eigenspectrums. The different eigenspectrums that have been achieved from different CR nodes are sent via CC to the main CR-BS. Then the Spatio-temporal complex matrix $\boldsymbol{A}(f_i)$ is constructed and the singular values are computed at each frequency bin of the base band signal.

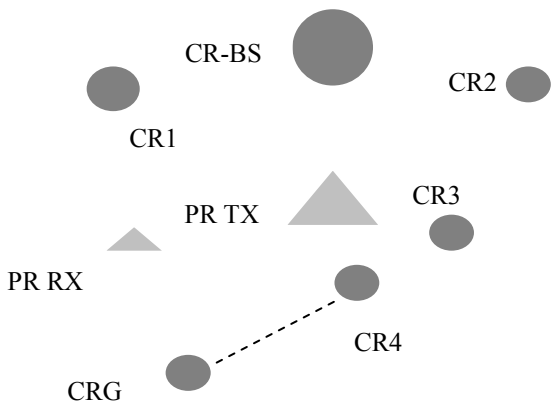

Figure 3.6 CR network model.

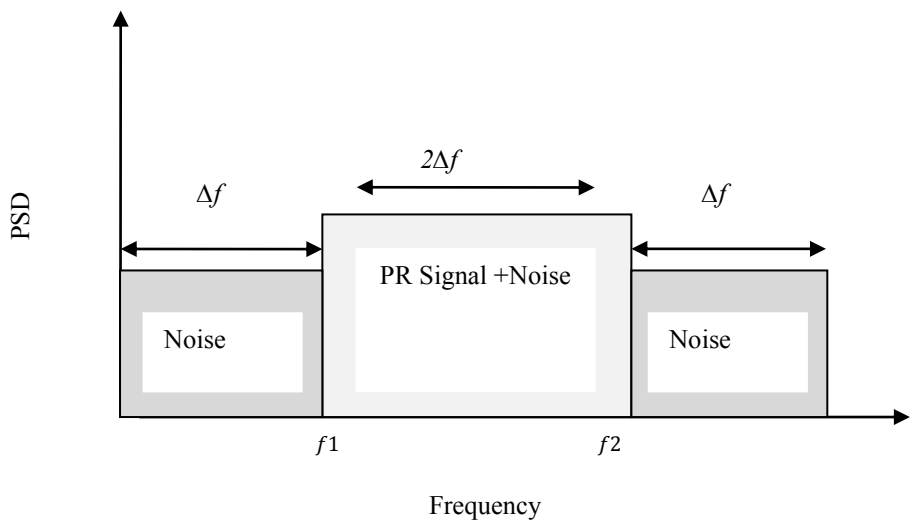

Figure 3.7 PR user's signal under spectrum sensing.

3.6.2 Simulation Results

In this section, the PSD across the bandwidth under scrutiny is estimated using MTM-SVD technique, and conclusions are drawn from the results. The power from a licensed PR user received by CR nodes at low SNR (SNR= -5 dB) is estimated using high-level software platform simulation. The eigenspectrums that resulted at each CR node are sent then to CR-BS via CC, which suffers from white Gaussian noise with variance, $\sigma_w^2 = 3.1623$. In the MTM method, the half time bandwidth product NW is assumed as 8, and the number of used tapers K is 4. The system model consists of a single PR Tx transmits to another PR Rx. In addition to the CR-BS, the CR system consists of 4, and 16 CR nodes. The whole band is divided mainly into four subbands as shown in Figure 3.7, and each with width, $\Delta f = 2W = 2\left(\frac{8}{64}\right) = 0.25$. The PR Tx is transmitting QPSK-IFFT signal with normalized energy to 1 over each IFFT subcarrier, using the subband between the frequencies $f_1 = 0.25$ to $f_2 = 0.75$, which has width a of $2\Delta f$. The PR Tx uses 64-IFFT (i.e., IFFT size is N=64) to generate its signal. The CR nodes also use 64-FFT to detect PR signal. The channel between each CR node and the

PR Tx is assumed as AWGN with zero mean and variance σ_w^2. The channel between each CR node and the CR-BS is also assumed as AWGN with zero mean and variance σ_w^2=3.1623. The two channels are independent and identically distributed. Note that, when we say SNR=-5 dB, it means the channel connects each CR node to the CR-BS (i.e., CC) has SNR=-5 dB, and also the channel between the PR Tx and each CR node has SNR=-5 dB. The weighting coefficients α_G are drawn from a uniformly distributed random source.

In this scenario, we estimate the performance of the MTM-SVD and we assume we have perfect knowledge of the exact distribution of the subbands of the whole band under scrutiny. We then compare our assumption of perfect knowledge of the usage of the spectrum with the results obtained from the MTM-SDV results. The decision statistics of the frequency bins of a specific Δf can be amalgamated together to represent the decision in that Δf as in reference [26]. Such a scenario might speed up the decision process. Each decision statistic is averaged over 10^4 simulation runs.

Figure 3.8 shows the subbands decision statistics using (3.9) and (3.10) at SNR $=$ 10, and -5 dB using 4 CR nodes. The calculated threshold at SNR $= 10$ dB is 0.1381 based on (3.11). Thus, the CR will detect optimally the presence of the PR user's signal in the band $f_1 = 0.25$ to $f_2 = 0.75$ as can be seen from the figure. At SNR $= -5$ dB, the calculated threshold is 3.9632, and there is a possibility of giving false alarm about the presence of the PR's signal between frequencies $f = 0.75$ to $f = 1$. Such a situation can be resolved by increasing the averaged samples of the decision statistics, and/or increasing the threshold level. We find that the mean of the decision statistics, in the subbands which contain only noise, decreases to zero with increasing averaged samples. This means that the decision statistics of random white Gaussian noise is random itself; therefore the mean of the squared singular values of random white Gaussian noise is also random.

Figure 3.9 shows the subbands decisions at SNR $= 10,$ and -5 dB, using 16 CR sensors. The decision at the subbands that is occupied by the PR user's signal is larger than the unoccupied ones. Therefore the threshold margin is large enough to give the correct decision. Under these conditions, the CR-BS is capable of deciding about the presence of the PR's signal with SNR as low as -5 dB. The threshold margin for the subbands decision at SNR $= -5$ dB is small compared to that used for the higher SNR. Increasing the number of CR nodes used in the simulation improves the decision between frequencies $f = 0.75\ to\ f = 1$. When 16 CR nodes are used, the calculated threshold at SNR $= 10$ and -5 dB are 0.4526, and 12.9283 respectively.

The performance of the MTM-SVD is compared with the performance of the conventional method of the PSD estimation, the PE, at low SNR when one CR node is used. Figure 3.10 shows the estimated PSD obtained using PE and the single bin decision when MTM-SVD is used with 16 CR nodes at SNR $= -5$ dB. The PSD using PE is averaged over 10^4 simulation runs as well.

Figure 3.10 shows a large variance and a bad biasing property of the PE that disturbs the estimated power which will produce an incorrect decision by CR-BS. The PE method is unable to distinguish between the noise and the PR signal unless the number of averaged samples is too large. Such a large number of samples needs much time to process the collected data. On the other hand, it is clear the MTM-SVD method resolves these problems, and improves the decision process.

Figure 3.11 shows the relation between the singular value square using 4, 8, and 16 CR nodes and the SNR and both in dB. It is clear that the decrease in the SNR causes an increase in the singular value square. The singular value square increases with the increase in the number of CR nodes as well. At SNR $= -20$ dB, singular value square is about 25 dB using 4 CR nodes, 27 dB using 8 CR nodes, and 30 for 16 CR nodes. At

SNR = 20 dB, singular value square is about −8 dB using 4 CR nodes, −5 dB using 8 CR nodes, and −3dB for 16 CR nodes.

Tables 3.1 and 3.2 show the probability of making the correct decision over the four subbands at various SNR using 4 and 16 CR nodes respectively. Each decision of the different four subbands is averaged over 1000 values, and then compared to the threshold. This decision test is repeated 100 times at each SNR. When 16 CR nodes are used, this yields a probability of 100% for the correct decision at SNR = 5 dB and higher. At SNR = 0dB, the probability of correct decision varies between 87% and 94%. However, at SNR below 0 dB, the decision becomes increasingly less reliable. On the other hand, when using 4 nodes, the decision becomes less reliable for SNR below 5 dB.

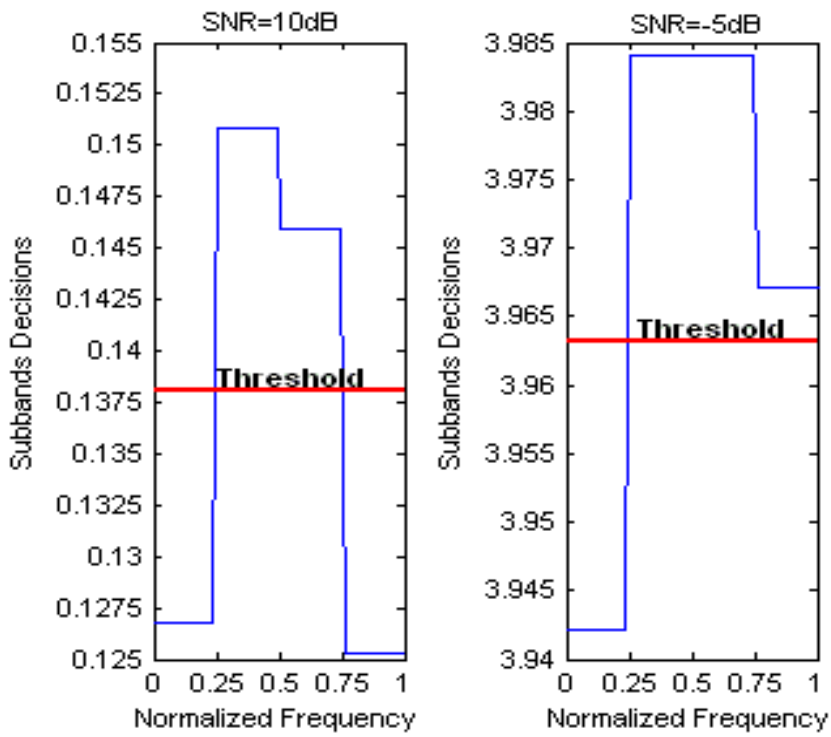

Figure 3.8 Subbands Decisions versus normalized frequency at SNR=10 and −5 dB using 4 CR sensors.

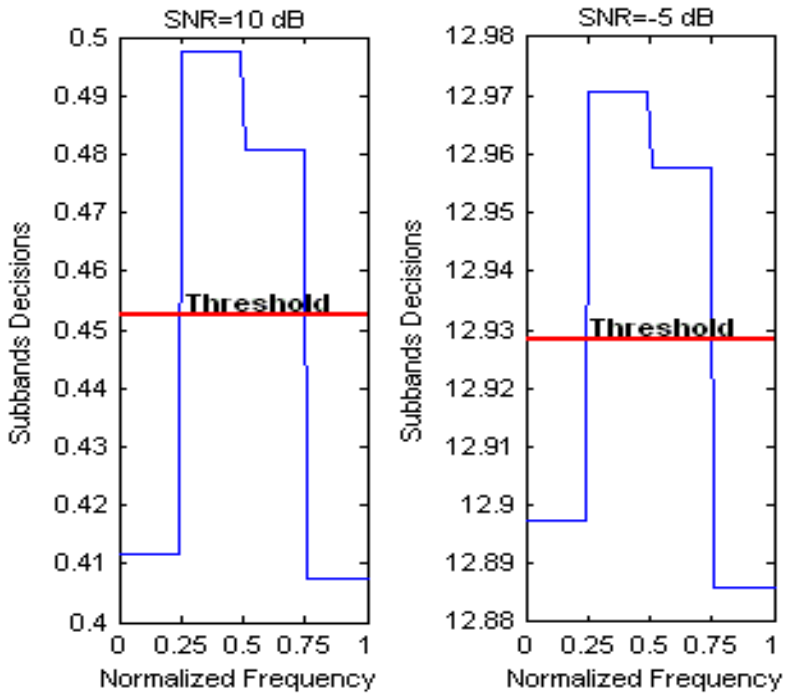

Figure 3.9 Subbands decisions versus normalized frequency at SNR= 10 and − 5 dB using 16 CR sensors.

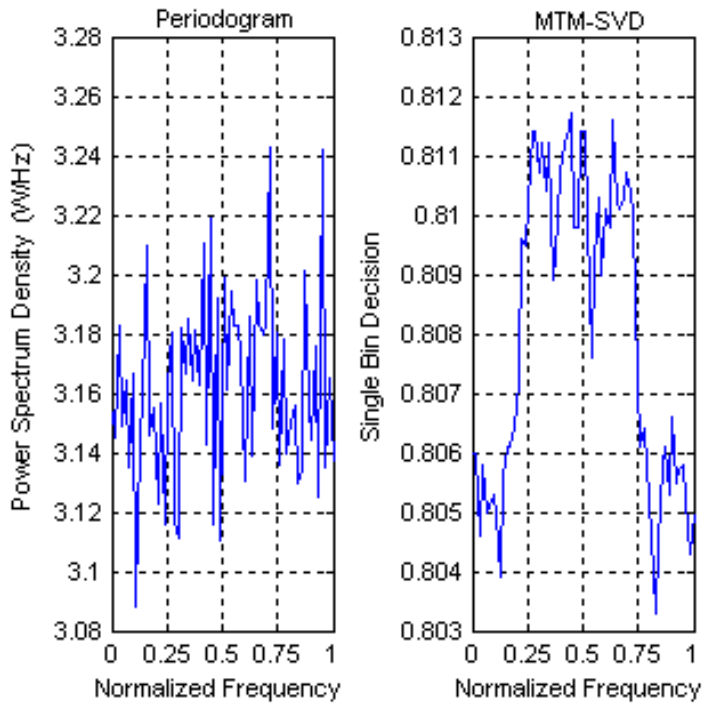

Figure 3.10 Comparison of the single bin decision results from the PE and the MTM-SVD using 16 CR sensors at SNR= −5 dB.

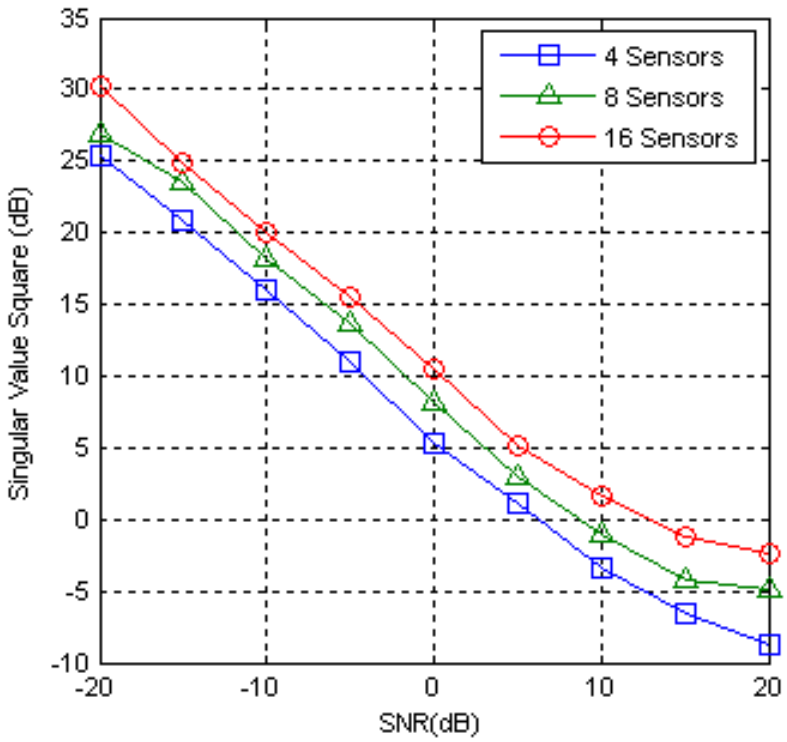

Figure 3.11 Singular value square using 4, 8, and 16 CR sensors versus SNR both in dB at f =30/64.

SNR(dB)	4 CR sensors			
	Subband -1	**Subband -2**	**Subband -3**	**Subband -4**
-10	75%	31%	34%	72%
-5	52%	64%	62%	53%
0	68%	81%	79%	64%
5	93%	98%	94%	96%
10	100%	100%	100%	100%

Table 3.1 Probability of MTM-SVD making the correct decision using 4 CR sensors at various SNR.

SNR(dB)	16 CR sensors			
	Subband -1	**Subband -2**	**Subband -3**	**Subband -4**
-10	41%	65%	64%	47%
-5	76%	50%	48%	73%
0	90%	94%	87%	89%
5	100%	100%	100%	100%
10	100%	100%	100%	100%

Table 3.2 Probability of MTM-SVD making the correct decision using 16 CR sensors at various SNR.

The probability of MTM-SVD making correct decision in the subbands 3, and 4 using 4 CR nodes and 8 tapers at SNR=5dB are found as 79 and 67% respectively. These values are lower than using 4 tapers that are shown in Table 3.1.

Figure 3.12 shows the threshold levels versus the SNR for 4 and 16 CR nodes schemes, using (3.10) that is averaged over 10^4 simulation runs. The increase in the CR nodes numbers produces an increase in the threshold level. As the SNR is increased, the difference between 4 and 16 CR nodes threshold becomes insignificant. In the higher SNR, the threshold levels decrease towards 0 and the difference in the 4 and the 16 CR nodes thresholds decreases as well.

Figures 3.13 and 3.14 show the probability of the correct decision at each frequency bin using 16 CR sensors at SNR=−5dB, threshold=0.807, and the averaged samples are 100 and 1000 respectively. The probability of the correct decision is around 50% for the 100 averaged samples scheme. When the averaged samples are increased to 1000, the probability of correct decision is also increased, especially in the subbands which contain only noise.

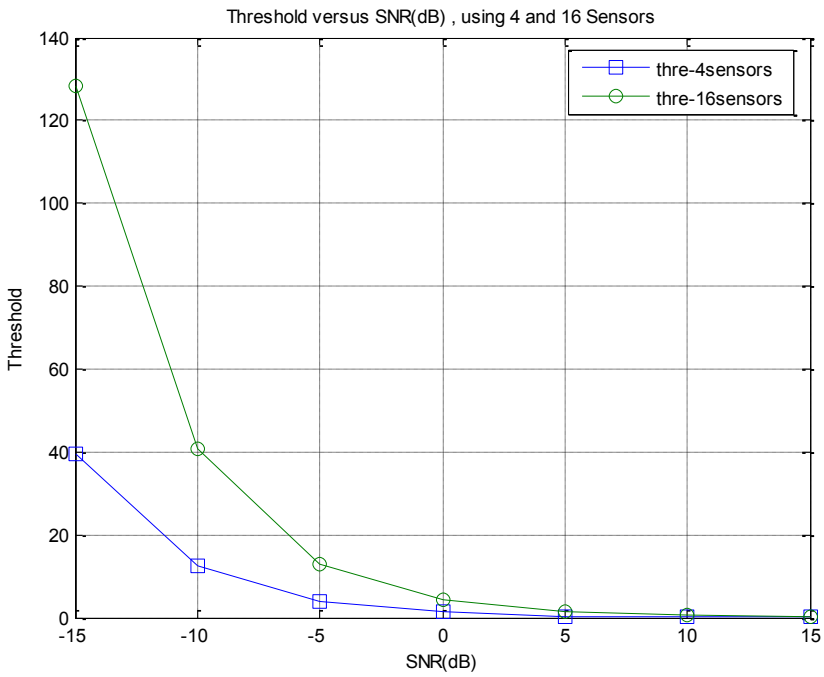

Figure 3.12 Threshold levels used in the simulation.

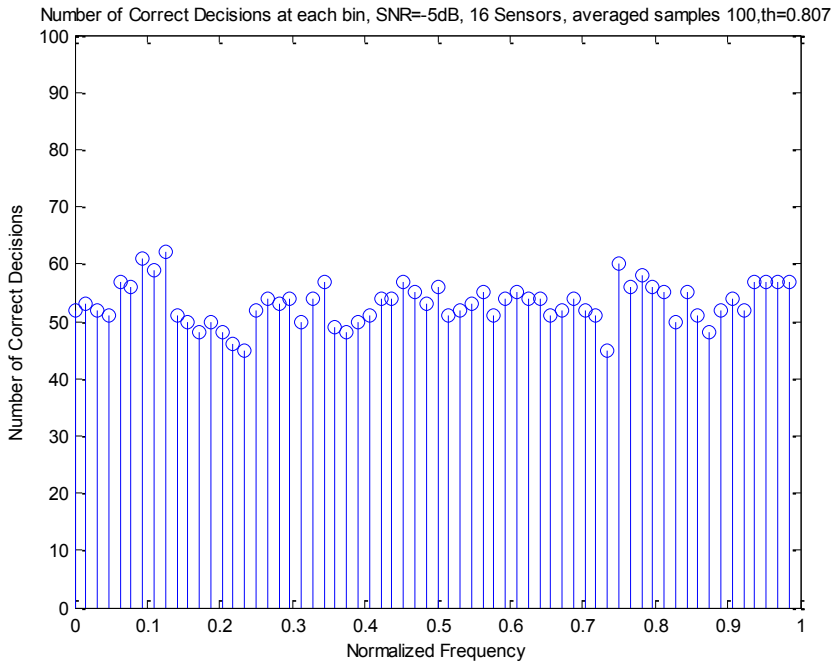

Figure 3.13 Probability of the correct decision at each frequnecy bin using 16 CR sensors and 100 averaged samples.

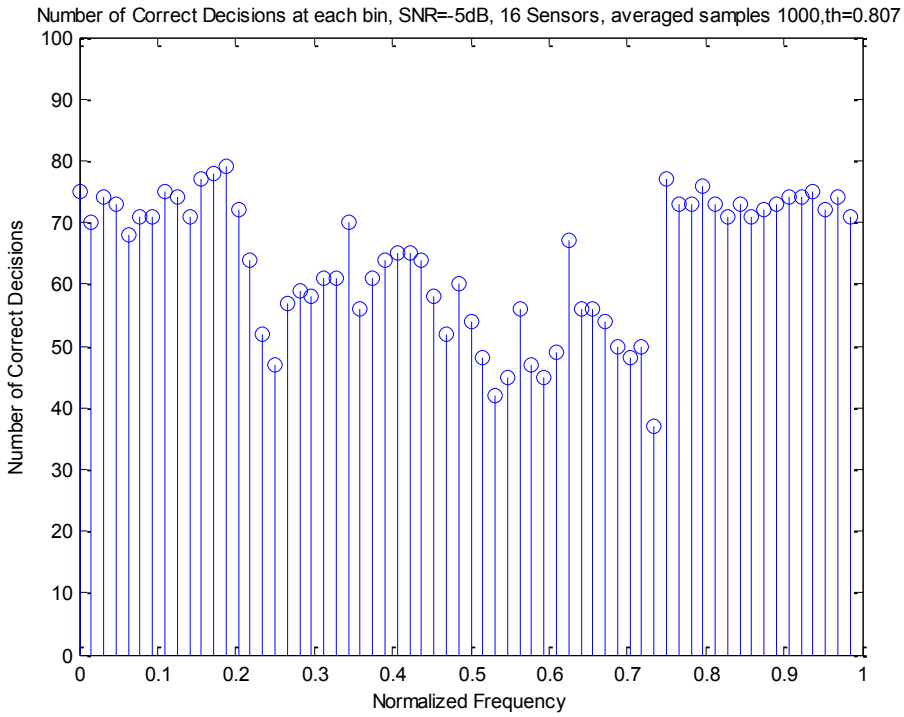

Figure 3.14 Probability of the correct decision at each frequnecy bin using 16 CR sensors and 1000 averaged samples.

3.6.3 Conclusion

In section 3.5, the MTM-SVD technique is investigated for CR spectrum sensing. The MTM-SVD power spectrum estimation's theoretical analysis is applied. MATLAB simulation codes are written for the MTM-SVD decision statistics using 4 and 16 CR nodes at various SNR values to find the capability of this technique. This has been published in [1].

Although the MTM-SVD scheme requires a lot of computation compared with the PE, the latter has a large variance and bad biasing at low SNR (i.e., SNR=−5dB). This would increase the possibility that the decision process might fail to detect the presence of the PR signal. This will result in an inefficient use of the spectrum or causes interference to the PR active users. The MTM-SVD has a better performance that allows the CR system to distinguish between PR signal and the background noise or low interference. The number of mathematical operations in one round simulation at each frequency bin is 2 for the PE, and 21 operations in the MTM using 4 tapers. The decision at each frequency bin needs 40 operations in the MTM-SVD, and the decisions at each subband needs 56 operations. The processing time in the decision of using 4 CR nodes and 4 tapers is about 2.56 times that used for the PE, and is about 3.63 times the PE in the 16 CR nodes and 4 tapers scheme.

The MTM-SVD performance functions across two parameters, namely: number of CR sensors and number of tapers used in the design of the CR system. Based on the results, the increase in the number of CR sensors improves the decision statistic and increases the threshold margin for low SNR. The number of tapers that used in the system is critical since using a large number of tapers may cause unwanted biasing properties to the spectrum estimates. The decision statistics for narrowband resolutions can be extended to the resolution of each subband in our model.

The next section provides a summary of chapter 3 including the auther's technical opinion of using MTM-SVD as a CR spectrum sensing technique, and the challenges of using MTM. The MTM challenges are then resolved in chapter 4.

3.7 Chapter Summary

In this chapter, the chosen spectrum sensing technique in CR, the MTM, was reviewed. This included what our chosen spectrum sensing technique shall be, and the reasons behind choosing the MTM. The spectral leakage and large variance of the power spectrum estimate were discussed since they are the main classical problems in spectrum estimation methods. Examples of different windows that tried to mitigate the spectral leakage are shown. The MTM was looked at in more detail and the following areas were explored:

- MTM definition and history.
- MTM features for CR spectrum sensing.
- MTM methodology including the DPSS generation.

The MTM-SVD had been given attention through the CR literature without any practical investigation of the method. This motivated the author to investigate this method using a simulation to explore the performance and the drawbacks. The method showed a promise performance compared to the PE. Based on the simulation results, the MTM-SVD can be classified as MSCSS since it needs multi measurements about each frequency bin to be sent to the CR-BS every sensing time. For example, when 8 tapers are used to generate the eigenspectrums in MTM, each CR must send 8 complex measurements of each frequency bin to the main CR-BS. This goes against the main objective of CR systems, since it requires huge bandwidth to exchange such measurements between CR users. Additionally, MTM-SVD has noticeable computation complexity that might slow the CR spectrum sensing decision. Therefore, the author

excluded the MTM-SVD as a SCSS from his research, and more concentration will be made on MTM.

Through the simulation results, two main technical requirements were defined, and can be listed as follow:

1. The performance of MTM or even MTM-SVD is affected and controlled by main two parameters:

   -The time bandwidth product NW

   -The number of used tapers K

2. Using MTM as a CR spectrum sensing technique requires developing the optimal detector based on Neyman Pearson criterion to optimize the performance and the threshold of MTM-Based CR spectrum sensing.

These two requirements defined the main objectives of chapter 4 as will be seen later.

Chapter 4: Optimal MTM based CR spectrum sensing

4.1 Introduction

As has been mentioned at the end of chapter 3, the MTM has two main parameters which must be optimized to be efficiently used in CR spectrum sensing. Such optimization supports the practical use of the MTM in the OFDM-based CR systems. Half time bandwidth product NW and the number of used tapers K are the parameters that affect the MTM performance as a CR spectrum sensing technique. Therefore, optimizing these parameters optimizes the performance and minimizes the complexity, as can be seen later within this chapter.

The MTM parameters are reviewed and discussed in order to understand their effects on the performance. The problem formulation and the system model of the optimization is developed in such a way that the parameters choosing effect on the spectral leakage and the variance can be taken into account. Based on this, a Monte Carlo simulation code is written to find the optimal MTM parameters.

The second important optimization target here is the optimal MTM detector design based on Neyman Pearson criterion. Subsection 2.4.2.1 shows how such a design is very important for the practical implementation of any spectrum sensing technique. The different probabilities formulae can be controlled via threshold and the number of sensed samples controlling. Then, the optimal performance can be achieved.

The optimal MTM based detector is developed in this chapter. This includes the PDFs derivation for the different hypotheses of the MTM decision statistic. The mean and variance for the different MTM decision statistic's hypotheses are derived within the PDF work. Different probabilities, the number of sensed samples, and the threshold formulae are then derived. Simulation codes are written to evaluate the system and

compare it to the theoretical works in AWGN, Rayleigh flat fading, and multipath fading wireless environments. A Comparison of MTM to the PE, and recently published spectrum sensing techniques for OFDM-based CR, are included in the results

The main content of this chapter has been published in three papers that represent the chapter contributions. The published papers are:

O. A. Alghamdi, M. A. Abu-Rgheff and M. Z. Ahmed, "MTM Parameters Optimization for 64-FFT Cognitive Radio Spectrum Sensing using Monte Carlo Simulation," in *Proc. The Second International Conference on Emerging Network Intelligence (EMERGING 2010)*, 2010, pp. 107-113.

O. A. Alghamdi, M. A. Abu-Rgheff and M. Z. Ahmed, "Probabilities of Detection and False Alarm in MTM- Based Spectrum Sensing for Cognitive Radio Systems," in *Proc. The Second International Conference on Emerging Network Intelligence (EMERGING 2010)*, 2010, pp. 114-119.

O. A. Alghamdi, M. Z. Ahmed and M. A. Abu-Rgheff, "Probabilities of detection and false alarm in multitaper based spectrum sensing for cognitive radio systems in AWGN," in *Proc. 12th IEEE International Conference on Communication Systems (ICCS'10)*, 2010, pp. 579-584.

4.2 MTM Parameters

The MTM parameters *NW*, and *K*, play an important role in controlling the MTM performance. They control the trade-off between bias and variance of the spectrum estimate. Additionally, the MTM complexity is affected by the different choices of such parameters as can be seen later within this chapter. However, such parameters were not given deep consideration in CR spectrum sensing, except for general recommendations and assumptions. In Haykin's work, the recommended range of *NW* is from 4 to 10, and

K from 10 to 16 tapers [147]. The NW is used as 4, and K as 3, 4, and 5 tapers for N=128, and 2048 in [117, 118]. In [152], a range of NW between 3 and 6 is preferred, and K=6 tapers is used where N=400.

All these works did not use a specific and justified NW and K, and were based on recommended ranges of such parameters. Based on these recommendations, it is clear that such parameters are still open issues, and have to be optimized towards achieving high performance and low complexity by determining a specific number of tapers. Note that the MTM parameters were originally the DPSS parameters that are now being used for MTM.

In this section, we investigate the optimization of MTM parameters in OFDM-based CR systems. The CR transceiver carries out 64-IFFT/FFT digital processing for both transmission and receiving operations. Consequently, the MTM processing in the spectrum sensing will not add additional hardware at the receiver except for taper sequences generation, multiplication and adding operations. The FFT size here is N=64, which is also the tapers length. Therefore, as a spectrum sensing technique for OFDM-based CR systems, the tapers length will have the FFT size of those CR systems. For example, IEEE 802.11(a/g) support 64-FFT (i.e., N=64), and IEEE 802.16 (d/e) support (128, 256, 512, 1024, 2048)-FFT (i.e., N=128, 256, 512, 1024, 2048) [28]. The N=64 case, is the main case under optimization in this chapter. The optimal MTM parameters of this case can be generalized then for the different FFT sizes that are used in the different OFDM based systems.

MTM tolerates the classical problems (i.e., bad bias and large variance of estimate) which occur in spectrum estimation by averaging over a number of orthonormal tapers (i.e., DPSS). The tapering sequences concentrate the energy within a bandwidth $\Delta f = 2W$, where $0 < W < 1/2$. The half time bandwidth product, NW, determines the bandwidth resolution for fixed length N. As the half time bandwidth product decreases,

the half bandwidth W decreases resulting in higher resolution in the spectrum sensing and vice versa. The main spectrum lobe of each taper is $2NW$ frequency bins (where the FFT- frequency bin spacing is $1/N$) [37]. Thus in OFDM-based CR applications with 64-FFT, the main band under sensing can be divided into a number of subbands based on the half time bandwidth product. For example using NW=2 means that there will be 16 subbands with $2W$ width each, and the main lobe is then 4 frequency bins out of the 64. Therefore in such applications, the useful half time bandwidth products should be 0.5, 1, 2, 4, 8, or 16, and 32 to concentrate the energy in one band, which is the whole band under sensing. Consequently, the higher edge of the half time bandwidth in 64-FFT case is NW=16.

Furthermore, the number of tapers in the higher resolution sensing is smaller than that found in the lower resolution since the total number of tapers is $N_{tapers} = 2NW$.

The eigenvalues $\lambda_k(N,W)$ of the first few tapers for the higher bandwidth resolution is much smaller than eigenvalues in the lower resolution, which implies that lower bandwidth resolution tapers have more energy concentration than tapers in the higher bandwidth resolution.

More concentration in the last paragraph means less spectral leakage. Asymptotically, the spectral leakage, 1-$\lambda_0(N,W)$, for a specific NW can be calculated using the largest eigenvalue, $\lambda_0(N,W)$, as follows [29]:

$$1 - \lambda_0(N,W) \approx 4\pi\sqrt{NW}e^{-2\pi NW} \tag{4.1}$$

Table 4.1 shows the spectral leakages of the first taper (i.e., that has $\lambda_0(N,W)$) for different NW values. The increase in NW causes significant decrease in the spectral leakage.

Furthermore, the first few eigenvalues of a specific time half bandwidth product are close to one. As the number of taper sequences increases, the eigenvalues decrease,

NW	1-$\lambda_0(N,W)$	1-$\lambda_0(N,W)$ in dB
2	6.1975×10^{-5}	-42.0778
4	3.0565×10^{-10}	-95.1477
8	5.2569×10^{-21}	-202.7927
16	1.0996×10^{-42}	-419.5877

Table 4.1 Spectral leakages of the first taper for different *NW* values.

indicating bad bias properties, and as number of tapers decreases, the eigenvalues increase towards 1, indicating good bias properties.

Figure 4.1 shows the subband divisions that are result from using different three half time bandwidth product values in MTM where $\Delta f\ in\ (a) < \Delta f\ in\ (b)\ < \Delta f\ in\ (c)$. It can be seen from the figure how the *NW* choice in MTM divides the subband under sensing (e.g., 64 frequency bins in 64-FFT) into a number of subbands with different $2W$. Table 4.2 shows the possible normalized tapers' *NW* values in the case of *N*=64. As has been said before, for a fixed *N* the increase in *NW* produces an increase in the bandwidth Δf, an increase in the total number of the resulted tapers and a decrease in the number of subband divisions.

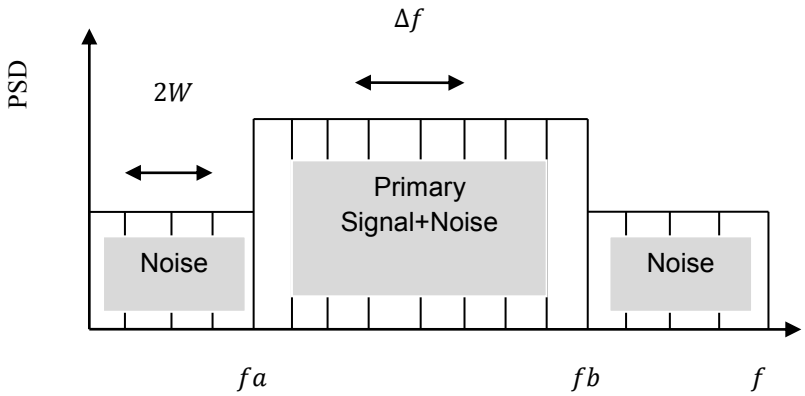

(a)

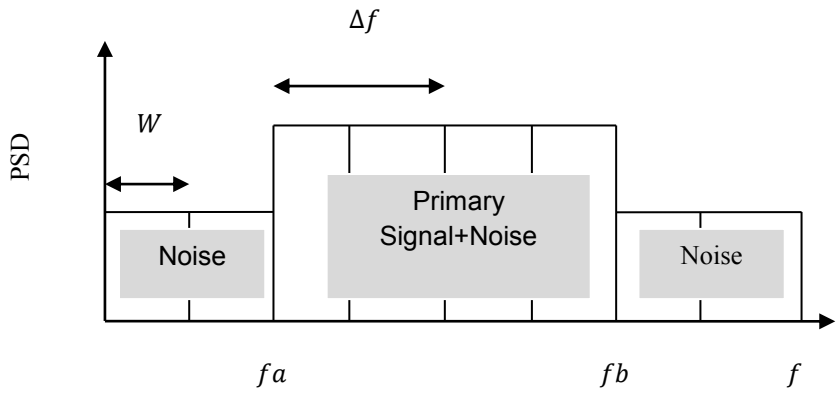

(b)

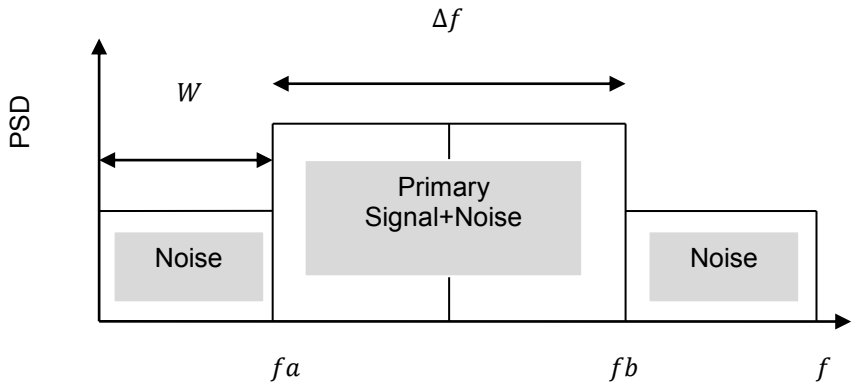

(c)

Figure 4.1 Representative examples of the subband divisions that are resulted from using different three half time bandwidth products in MTM, where $\Delta f\ in\ (a) < \Delta f\ in\ (b)\ < \Delta f\ in\ (c)$.

$\boldsymbol{NW}$	$\boldsymbol{W}$	$\boldsymbol{\Delta f}$	$\boldsymbol{N_{tapers}}$	$\boldsymbol{N_W}$	$\boldsymbol{N_{\Delta f}}$
0.5	0.0078	0.156	1	128	64
1	0.0156	0.03125	2	64	32
2	0.03125	0.0625	4	32	16
4	0.0625	0.125	8	16	8
8	0.125	0.250	16	8	4
16	0.250	0.500	32	4	2

Table 4.2 Different possible normalized tapers' half time bandwidth products used in MTM with their associated parameters for *N*=64.

Our work for choosing appropriate values of *NW* and *K* for MTM estimator uses two approaches. In the first approach, we compute the PSD using (3.5) to show that random choice of these values may generate a lot of leakage, causing an increase in false alarm probability during the estimation process. These results are presented in Figures 4.2 and 4.3. In the second approach, a Monte Carlo simulation is used to evaluate the probabilities of detection and false alarm for various values of *NW*, and *K* in 64-FFT based CR at SNR=−5dB, and then to find the optimal (*NW*, *K*).

In the following subsections, the MTM parameters' effects on PSD will be investigated to achieve more understanding of the problem, and then the MTM optimization process will be discussed under section 4.3.

4.2.1 Time Bandwidth Product Effect on MTM

Figure 4.2 shows the PR's PSD at CR Rx using MTM with *NW*=4 and 16 where the number of used tapers is *K*=5 and 25 respectively at AWGN channel with SNR=−15Db, and the number of averaged samples is 2500. The PSD estimation using MTM here is based on (3.5). Number of averaged samples is 2500; this means the power at each frequency bin is averaged over 2500 received samples. PR transmits OFDM-QPSK signal from normalized frequency $f_a = 16$ to $f_b = 48$ with power normalized to one over the whole band. Both PR and CR use 64-IFFT/FFT signal processing. The CR receiver implements MTM to estimate the PR's PSD using different *NW* and *K* parameters.

The ideal curve represents the levels of noise and noise added to PR signal. It can be clearly seen how much power spectral leakage there is outside the PR's signal band when using *NW*=16 and the number of tapers *K*=25. Such leakage of power will affect the decision outside the PR's band by introducing more false alarms. At the same time

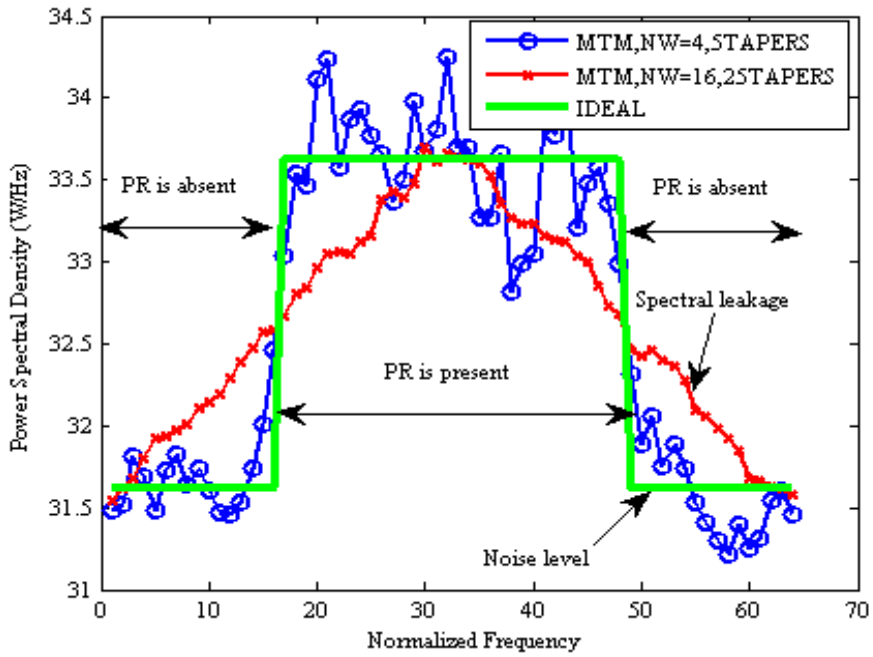

Figure 4.2 PSD using MTM with *NW*=4, and 16 and different values of *K* at AWGN with SNR=−15dB.

we can see how such leakage disappears when using *NW*=4 and the number of tapers as *K*=5. The reader should not be confused by the result here and the spectral leakage that has been shown in Table 3.1. Although the first taper of *NW*=16 has lower spectral leakage compared to that of *NW*=4, it uses large number of tapers, *K*=25, which produces more spectral leakage in this example. The reason behind this, in *NW*=16 case, is that the high orders tapers that have bad bias properties are included in the MTM.

4.2.2 Number of Used Tapers Effect on MTM

Figure 4.3 shows the PSD for the same system with *NW*=8 computed using (3.5). This figure clearly shows that using a small number of tapers, *K*=2, introduces large variance in the estimate due to the averaging over small number of tapers. At the same time using a large number of tapers, *K*=14, improves the variance, but at the expense of spectral leakage which is noticeable in this case. Using *K*=5 produces leakage that is between the previous two cases.

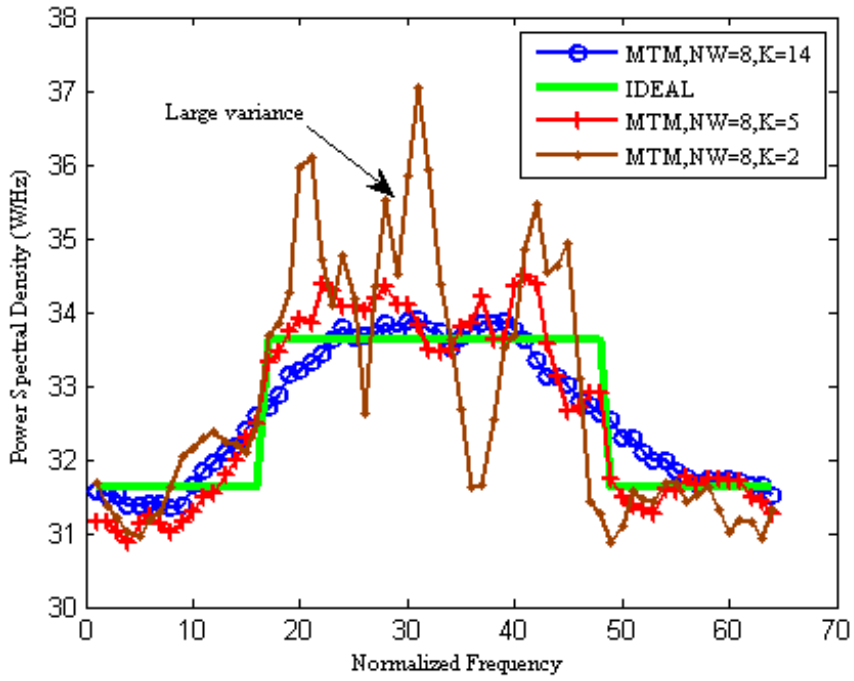

Figure 4.3 PSD using MTM with *NW*=8 and different values of *K* at AWGN with SNR=−15dB.

We may conclude from these two figures that an unwise choice of *NW* and *K* within the range suggested by Haykin and the others may have catastrophic results on false alarm and detection probability of the MTM estimator.

4.3 MTM Parameters Optimization

Figure 4.4 shows a representative diagram of the MTM parameters' optimization problem in 64-FFT based CR systems. In this case, *NW* axes values are *NW*=0.5, 1, 2, 4, 8, and 16. On the other side *K* axes values are *K*=1, 2, 3,…, 32. In regions R_1, and R_3, the half time bandwidth *NW* has higher resolution than the others two regions R_2, and R_4. At the same time R_1, and R_2 have a small number of tapers with good bias properties at the expense of higher variance when used in computing the PSD using (3.5). R_3 and R_4 regions have large number of tapers that improve the variance of the

spectrum estimate, but at the expense of larger spectral leakage. The recommended values of *NW*, and *K* ranges in the literature are shown in the figure. Although these ranges are useful in the CR spectrum sensing, they still need to be optimized to get the highest performance for 64-FFT CR systems. In addition to maximizing the performance, optimum parameters will contribute to reduce the MTM detector complexity.

The mathematical derivation of the optimal MTM parameters is intractable. Therefore, a Monte Carlo simulation program is used in this thesis to examine the effect of the different values of *NW* and *K* on the spectral leakage outside the PR's subband and the MTM detector decision statistic. Consequently the binary hypothesis at each frequency bin will be used to evaluate MTM detector performance.

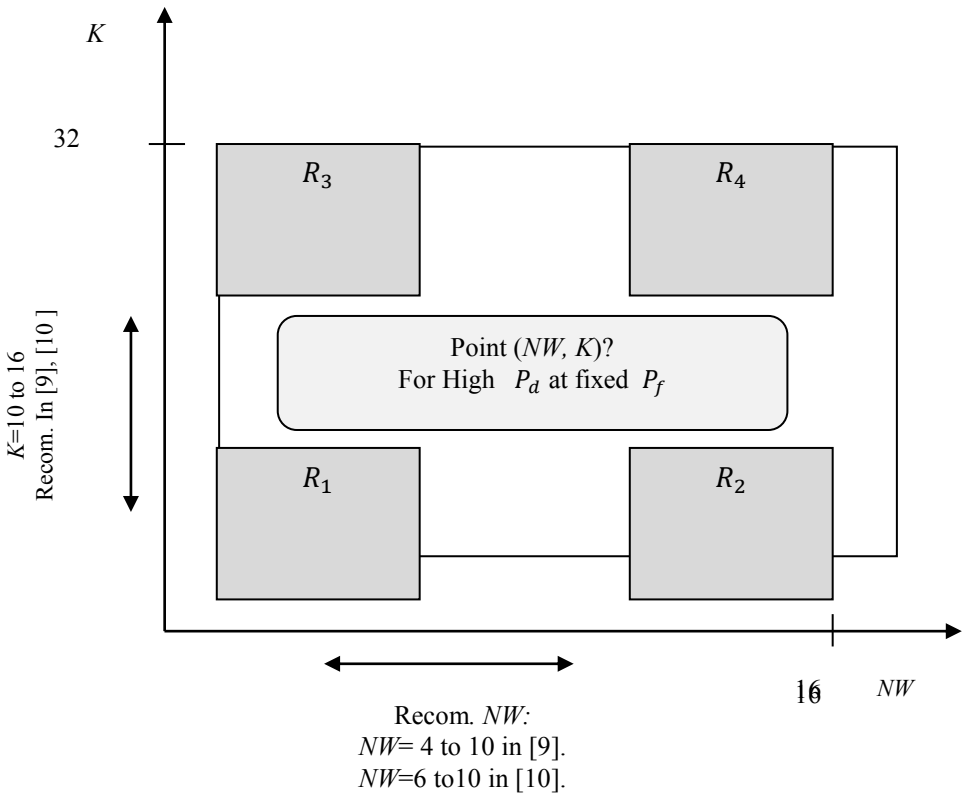

Figure 4.4 Representative diagram of the MTM parameters optimization problem for 64-FFT based CR systems.

4.4 System Model and Problem Formulation

Clearly, optimizing the MTM detector performance requires maximizing the probability of PR signal detection P_d for a predefined probability of false alarm P_f. The optimization process here will be started by defining the basic binary hypothesis test. This hypothesis test will be redeveloped in a way that insures that the effect of choosing optimum MTM parameters is based upon performance evaluation.

Based on (2.3), the binary hypothesis test for MTM spectrum sensing at the lth time can be rewritten to be as follows [87]:

$$\begin{aligned} \mathcal{H}_0: &\quad x_t(l) = w_t(l) \\ \mathcal{H}_1: &\quad x_t(l) = s_t(l) + w_t(l) \end{aligned} \tag{4.2}$$

where l = 0,1,…,L-1 is OFDM block's index, $x_t(l)$, $w_t(l)$, and $s_t(l)$ denote the CR received, noise and PR transmitted samples. The transmitted PR signal is distorted by the zero mean AWGN $w_t(l) \sim \mathcal{CN}(0, \sigma_w^2)$. The signal to noise ratio is SNR $= \frac{E_s}{\sigma_w^2}$.

The time instant l comes from the samples over different OFDM blocks, and time instant t comes from the samples from the same OFDM block (i.e., IFFT/FFT samples). Thus, the spectrum sensing time in second is $(L)(N)(T_s)$, where T_s represents QPSK symbol duration, L represents the number of OFDM blocks used in sensing and N is the number of samples per OFDM block (i.e., FFT size).

The D over time interval L, and at a specific frequency bin using the MTM can be formulated based on (3.4) and (3.5) to be as follows [4, 29]:

$$D_{MTM}(f_i) = \sum_{l=0}^{L-1} \frac{\sum_{k=0}^{K-1} \lambda_k(N,W) \left|\sum_{t=0}^{N-1} v_{(t,k)}(N,W) x_t(l) e^{-j2\pi f_i t}\right|^2}{\sum_{k=0}^{K-1} \lambda_k(N,W)} \tag{4.3}$$

The detection and false alarm probabilities at each frequency bin using MTM are defined as [87]:

$$P_d(f_i) = Pr\{D_{MTM}(f_i) > \gamma | \mathcal{H}_1\}$$

$$P_f(f_i) = Pr\{D_{MTM}(f_i) > \gamma | \mathcal{H}_0\} \tag{4.4}$$

The threshold γ, is defined according to the noise variance σ_w^2. The decision statistic, $D_{MTM}(f_i)$, is calculated at each frequency bin using (4.3), and then the probabilities of detection and false alarm can be evaluated by comparing the decision statistic to the predefined threshold over a number of realizations using (4.4).

In order to include the spectral leakage effect on the MTM performance evaluation, the false alarm should be evaluated in subbands that are vacant and that are neighbours to occupied subbands. Therefore, the leaked power from the occupied to the adjacent vacant subbands can be taken into account in the probability of false alarm evaluation. This allows us to observe the increase and decrease in the false alarm due to using different *NW*, and *K*. At the same time, the increase and decrease in the detection probability due to a using different number of *K* can be observed in the occupied subband. Consequently, the variance effect will be included in the MTM performance evaluation.

By dividing the frequency band under study into three non-overlapped subbands as shown in Figure 4.1, the *NW*, and *K* effects on the MTM performance will be included in the evaluation. The non-overlapped subbands structure consists of a PR signal in the middle subband, and two side adjacent subbands contain noise only.

The binary hypothesis, $\mathcal{H}_0$, will be examined through all frequency bins that do not contain PR signal (i.e., $\{f_i \in ([0, f_a) \cup (f_b, 63])\}$). The binary hypothesis, $\mathcal{H}_1$, will be examined through all frequency bins that contain the PR signal (i.e., $\{f_i \in [f_a, f_b]\}$). Figure 4.5 shows representative diagram of the $\mathcal{H}_0$, and $\mathcal{H}_1$ locations in the developed model.

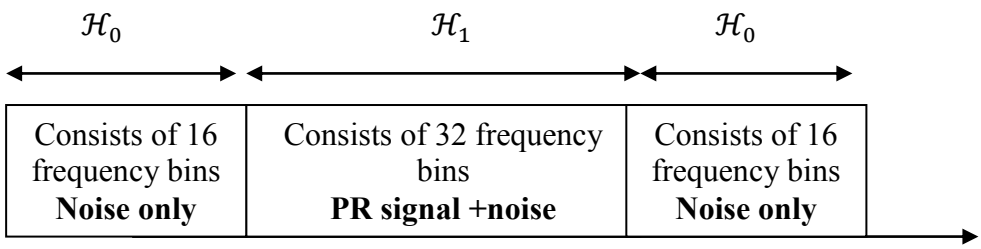

Figure 4.5 Representative diagram of the hypotheses distributions in the optimization model.

The probability of detection P_D over the band under sensing can be achieved from the averaged summation of the individual probability of detection $P_d(f_i)$ of all the bins which lie within the subbands used by the PR user, and can be written as [2]:

$$P_D = \frac{\sum_{f_i=f_a}^{f_i=f_b} P_d(f_i)}{32} \tag{4.5}$$

The probability of false alarm P_F over the band under sensing can be achieved from the averaged summation of the individual probability of false alarm $P_f(f_i)$ of all the bins which lie within the subbands outside the PR's subband, and can be written as follows [2]:

$$P_F = \frac{\sum_{f_i=0}^{f_i=f_a-1} P_f(f_i) + \sum_{f_i=f_b+1}^{63} P_f(f_i)}{32} \tag{4.6}$$

where 32 represents the total number of frequency bins of the hypotheses $\mathcal{H}_0$, and $\mathcal{H}_1$ of the model.

The optimization problem here can be written simply as [2]:

$$find\ (NW^*, K^*)\ \ that\ maximizes\{\ P_D\}\ at\ P_F = \alpha \tag{4.7}$$

where α is a constant false alarm, and is assumed as 10% in this part of our work.

Generally, the performance of the CR spectrum sensing can be evaluated via the ROC (i.e., the pair $(P_d\ , P_f)$) as has been discussed in subsection 2.4.2.1.4. Moreover, the spectrum sensing technique's performance can be evaluated via observing the P_d at a

fixed P_f. Therefore, technique A is better than technique B when it gives higher P_d than technique B at the same fixed false alarm and under the same conditions.

The simulation process of evaluating P_d at each frequency bin, as in (4.4), when the P_f is fixed to a predefined percentage, includes two main stages for a specific SNR. The first is to calculate the threshold that satisfies the predefined P_f when the noise only is exist, and the second is to use the found threshold in P_d calculation. These two stages are shown in the charts in Figures 4.6, and 4.7 respectively. The shown charts can be used for any other energy based spectrum sensing techniques as PE, by using its own equations to calculate the PSD.

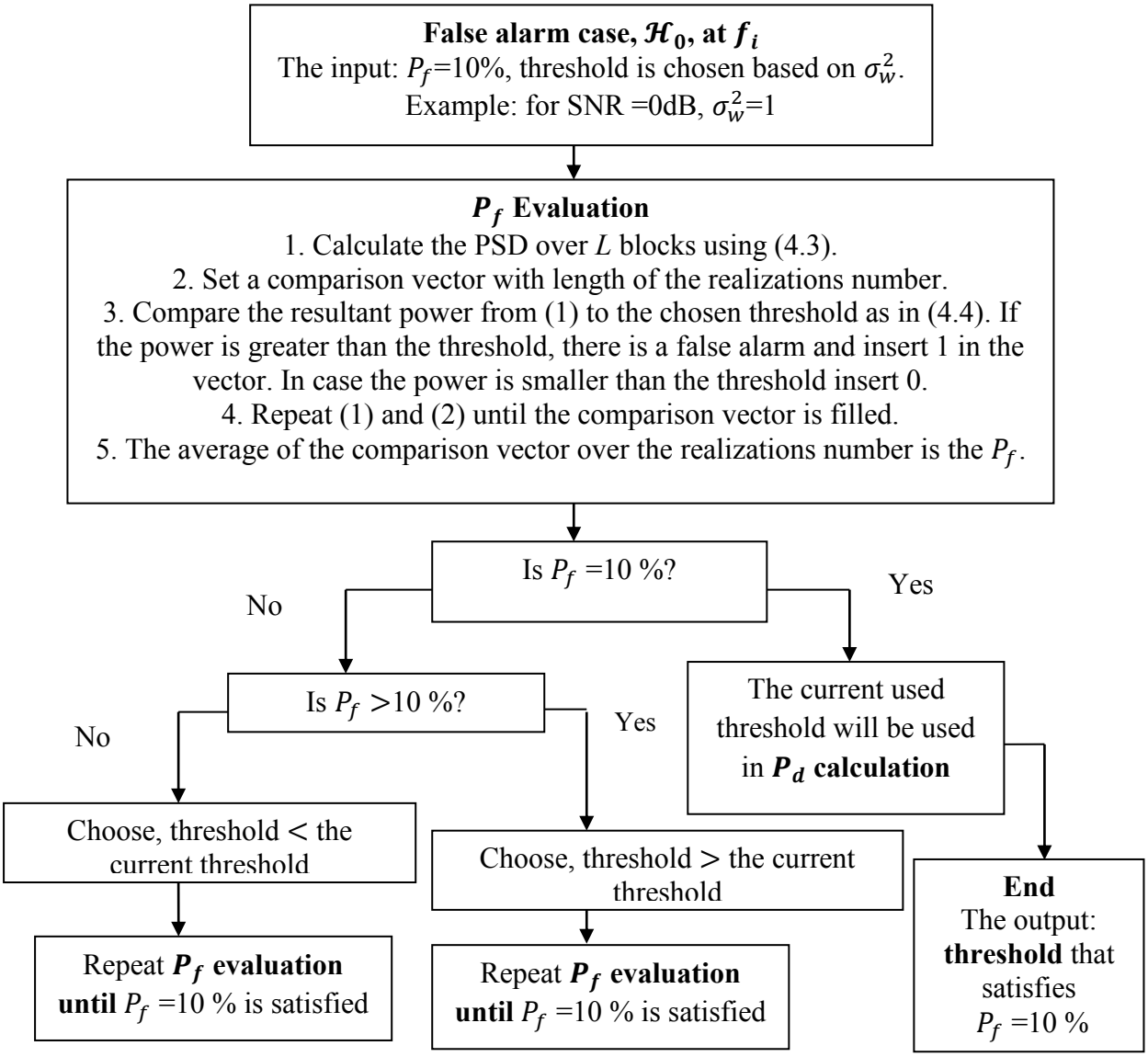

Figure 4.6 Chart of the simulation process of finding the threshold at P_f=10%.

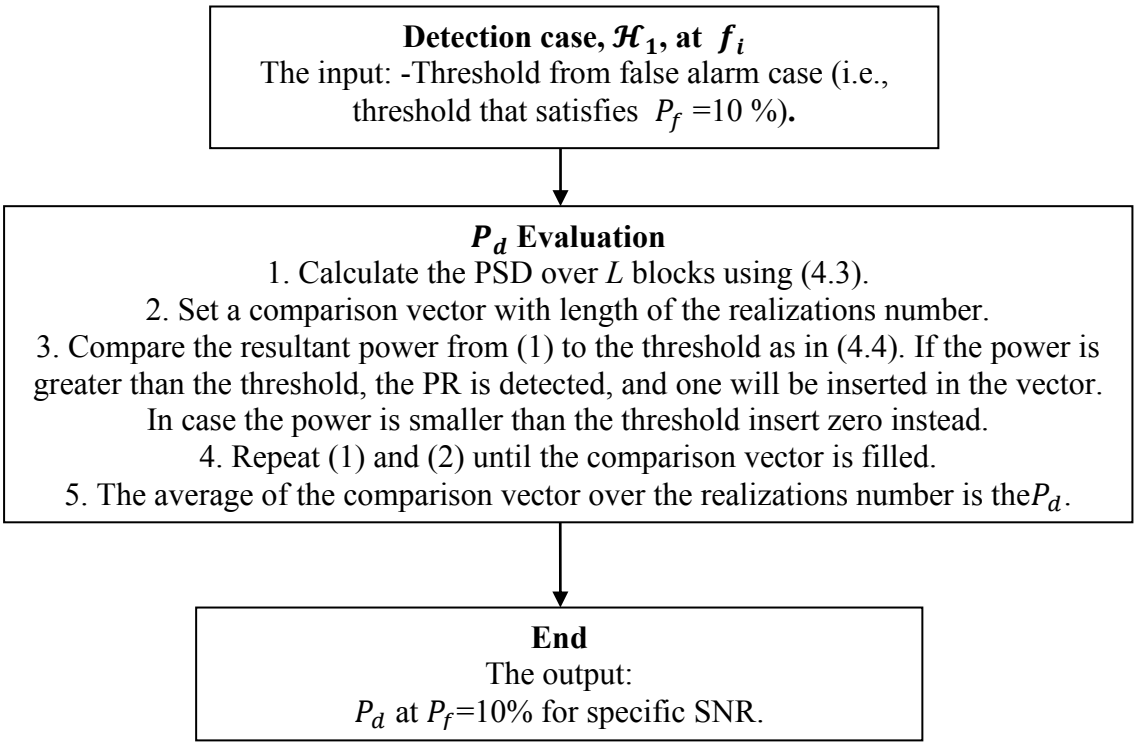

Figure 4.7 Chart of the simulation process for evaluating the P_d using the threshold that satisfies P_f=10%.

Figure 4.8 shows the chart of the simulation process for the MTM parameters optimization in 64-FFT based CR.

4.4.1 Wireless Environment Effect on the Optimal MTM Parameters

As should now be understood, the MTM is based on the use of orthonormal tapers, the DPSS. The way the DPSS work is as a bank of optimal band pass filters. They concentrate the energy within a bandwidth resolution and minimize the spectral leakage outside that resolution. Furthermore, the characteristics of the tapers are independent from the of the PR's power and the noise power. Therefore, the optimization of MTM parameters can be done at any chosen low SNR. Moreover, the fading environment affects the received power level; this is not related to the MTM parameters and their characteristics, and the optimization process can be done at AWGN noise only. Thus, the optimal parameters are also valid in fading environments.

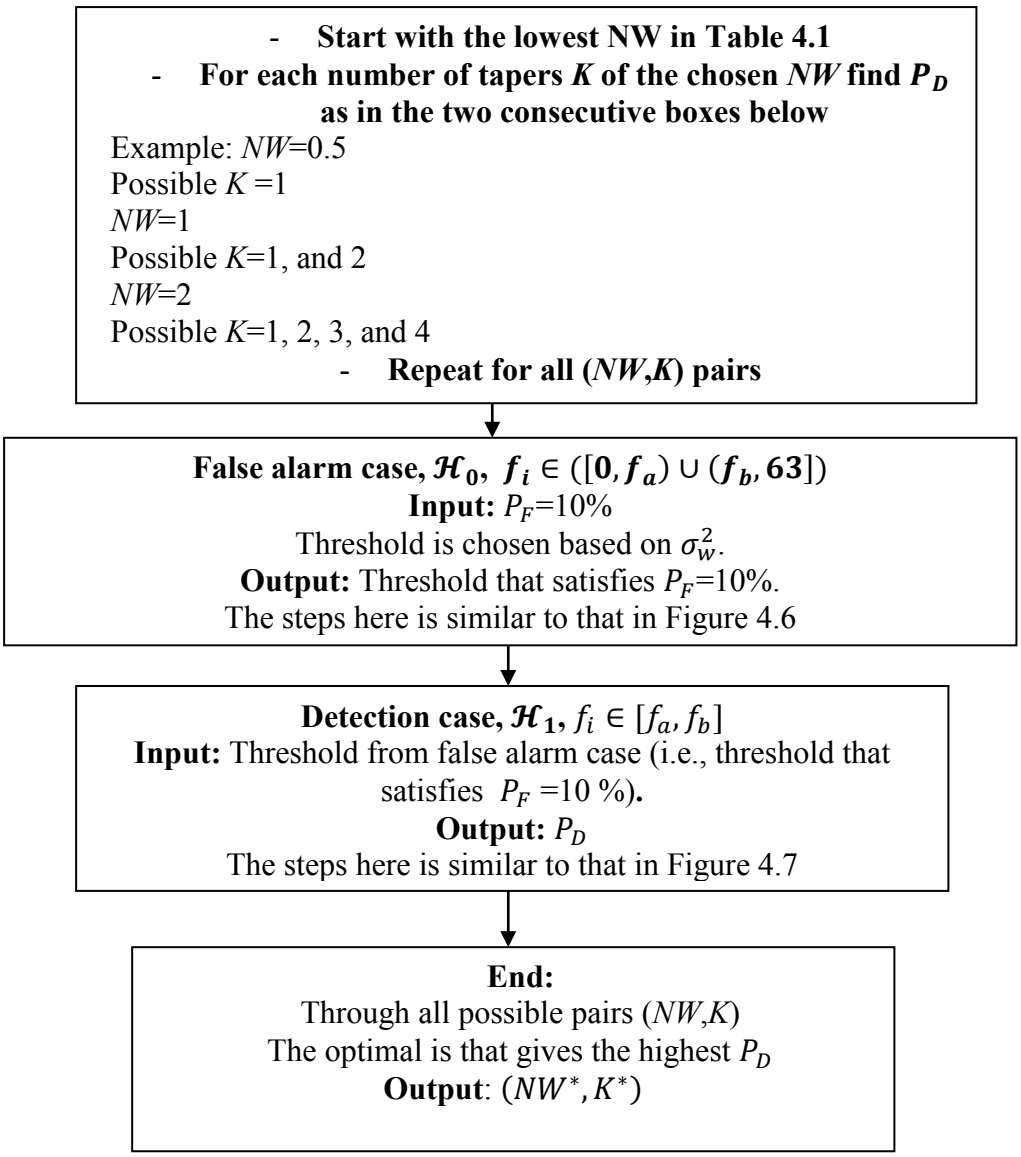

Figure 4.8 Chart of the simulation process for the MTM parameters optimization.

4.4.2 The MTM Complexity

The complexity of MTM detector for producing the spectrum estimate at a specific frequency bin f_i and N-FFT over L OFDM-Blocks, in terms of the number of mathematical operations (i.e., adding, and multiplications) is defined as [2]:

$$com_{MTM} = L[K(3N-1) + 4K - 2] \tag{4.8}$$

Using the PE to produce spectrum estimate at a specific frequency bin f_i, the complexity can be defined as follows [153]:

$$com_{PE} = L(2N) \tag{4.9}$$

4.4.3 Simulation Results

In our simulation, the PR user is transmitting QPSK-OFDM signal using the subband between the frequencies f_a =16 to f_b =48, and with normalized averaged power of 1 over the whole band. The PR's Tx uses 64-IFFT with sampling frequency 20 MHz, where the QPSK symbol duration T_s =0.05µs. The CR's node uses 64-FFT with sampling frequency 20 MHz as well. The performance is evaluated using a number of samples at the CR's node as $N_{samples} = 20(N_{FFT})$ =1280, which corresponds to a sensing time of $64\mu s$; this sensing process is carried out every L =20 OFDM blocks. In all cases of simulations the results are averaged over 10^5 realizations. The channel considered in the simulation is AWGN with zero mean and variance σ_w^2.

The probabilities of detection, P_D, for *NW*= 0.5, 1, and 2 using a different number of tapers are shown in Table 4.3. The wireless channel is assumed to be AWGN with SNR = −5 dB. The threshold γ that gives a probability of false alarm, P_F=10%, was estimated by Monte Carlo simulation using a computer software platform based on Figures 4.6 and 4.8. This threshold is then used in the detection case box that is shown in Figure 4.8 to find optimum *NW* and *K*. The highest probability of detection is P_D=98.8150%, which is achieved using *NW*=2 and *K*=3 tapers in the spectrum sensing.

Figure 4.9 shows the probability of detection, P_D, versus the number of tapers when the half time bandwidth product was as *NW*= 4, 8, and 16, in the same wireless environment applied before. We note that each curve has three different behaviours. It starts from a lower point that represents the minimum probability of detection which is achieved by the first taper. Then it increases sharply to a peak point, and starts to decrease again. The peak point for the different *NW* in this case is at *K*=5 tapers. Table 4.4 summarizes the probability of detection, P_D, for *NW*=4, 8, and 16 for *K*=1, and 5

obtained from Figure 4.9. The highest probability of detection is P_D =99.7138%, which is achieved using NW=4, and K=5. Generally, using 5 tapers is a good compromise between the good bias properties and improved variance. Additionally, NW=4 is the optimal resolution that gives the highest performance.

NW	P_D (%)			
	K=1	K=2	K=3	K=4
0.5	83.233	-	-	-
1	81.2166	87.7376	-	-
2	75.9459	90.7959	98.8150	98.560

Table 4.3 Probability of detection, P_D, for NW=0.5, 1, 2 and different K at AWGN with SNR=−5dB when false alarm is P_F=10%.

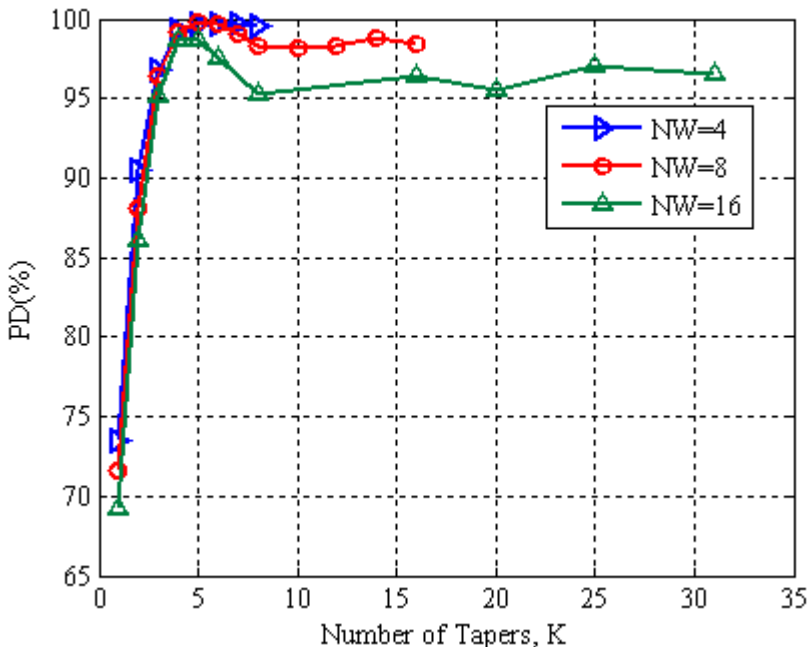

Figure 4.9 Probability of detection, P_D, versus number of tapers, K, using MTM with different half time bandwidth products NW where the probability of false alarm was P_F=10% and at channel AWGN with SNR=−5dB.

NW	P_D (%)	
	K=1	K=5
4	73.4531	99.7138
8	71.6678	99.2422
16	69.1575	98.6350

Table 4.4 Probability of detection, P_D, for NW=4, 8, 16 and different K at AWGN with SNR=−5dB when false alarm is P_F=10%.

In *NW*=16 case, there is an oscillation in the probability of detection levels, which are below the optimal value at *K*=5 tapers, and can be seen beyond the point *K*=5 tapers. In order to understand the source of such oscillating levels, one should refer again to section 4.3 and Figure 4.4 to remember the effect of the change in *NW* and *K* on the terms, spectral leakage and the variance of the estimate. Figure 4.10 shows that the tapers with higher order have poor attenuation and at the same time there are a number of variable nulls that appear. Spectral leakage from these tapers will be added to the band under consideration that would affect the false alarm level in the vacant band (which affects the detection probability by the end). There are two effects to consider, as the number of estimates from different tapers (under the assumptions made) reduces the variance of the estimate (improving performance), increasing the number of tapers can increase the amount of leakage (as there are spectral nulls in the spectrum of the tapers, additional tapers might not produce additional leakage). Since the noise spectrum is assumed white, the distribution of the noise that accrues through leakage will be constant.

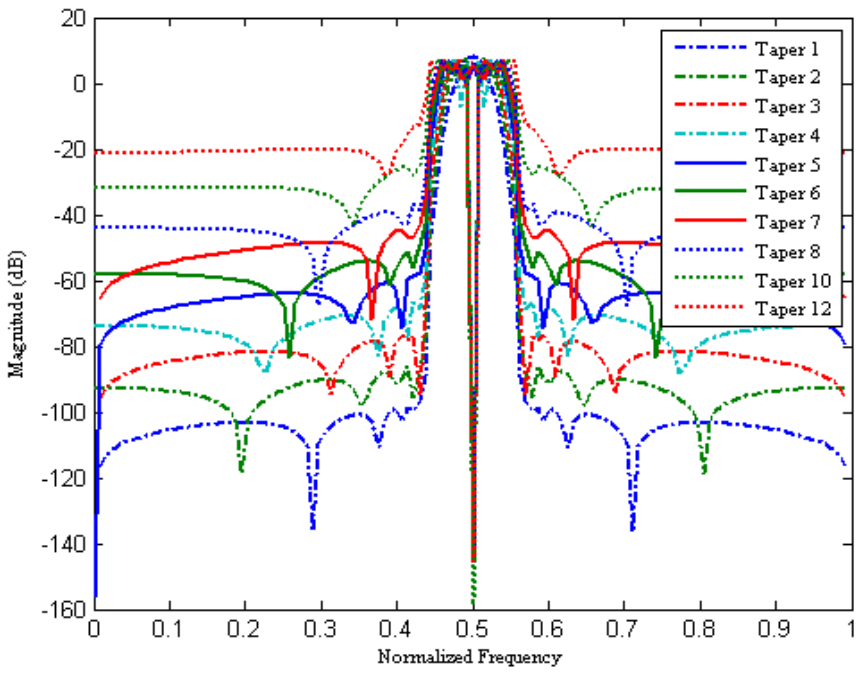

Figure 4.10 DPSS in frequency domain for 10 different tapers.

Table 4.5 shows the complexity of the MTM spectrum sensing based on (4.8) for different numbers of tapers K with length N=64 over one OFDM block (i.e., L=1).

It is clear that, in addition to the high performance achieved by K=5, it requires less mathematical operations computation than that for $K > 5$ cases. The PE complexity is found as 128 operations in the same conditions of MTM using (4.9).

MTM	K=1	K=5	K=10	K=20	K=31
Complexity	193	973	1948	3898	6043

Table 4.5 MTM Complexity evaluation for 64-FFT over L=1 OFDM block using different K.

4.5 The Optimal MTM Based Detector Requirements

The outputs from the last parts of chapter 4 are the optimal NW, and K that can be used in MTM-based spectrum sensing for OFDM-Based CR systems. Those optimal parameters are found as NW=4 and K= 5 tapers. The highest performance in using MTM for OFDM-based CR can be insured by using the mentioned optimal parameters. Furthermore, the complexity is minimized, since the optimal number of tapers has been found, which would finish the possible use of number of tapers more than 5 tapers. In the remaining parts of this thesis, all MTM-based spectrum sensing simulations and analyses will be based on using those optimal MTM parameters.

Based on what has been written in subsection 2.4.2.1 and subsections under, deriving the different probabilities is a very important issue in the design and development of any CR spectrum sensing technique. Although MTM was first studied by Thomson in 1982, statistics and probabilistic theoretical works were still an open research issue. In [152, 154], the authors derived the probabilities of detection and false alarm formulae based on the spectrum estimate characteristic function (CHF) by formulating the MTM spectrum detector as a quadratic function of Gaussian vector. However, their work is based on using the *inverse theory*, which is too complex for our purpuses.

The MTM-based spectrum sensing technique is a powerful. Generally, the choice of threshold level γ can degrade the performance of MTM-based CR system. Unlike methods used to choose γ in classical spectrum sensing techniques such as ED and MF, choosing an appropriate γ in MTM-based system is rather complex and influenced by interdependent system parameters. Consequently, theoretical derivation of the probabilities of detection and false alarm at the optimal *NW*, and *K* is mathematically intractable.

In this part of chapter 4, we present closed-form formulae for the probabilities of detection and false alarm for the MTM-based spectrum detector using Neyman-Pearson criterion. The PDFs of the MTM decision statistic at both hypotheses, $p(D_{MTM}(f_i); \mathcal{H}_0)$, and $p(D_{MTM}(f_i); \mathcal{H}_1)$ are approximated to Gaussian. The *E* and the *Var* of the PDFs have been derived for both hypotheses, and used in the calculation of the probabilities.

Clearly, the chosen value of *NW*, the tapers, number of tapers used (i.e., *K*), the tapers' eigenvalues and the decision threshold level γ have an effect on the probabilities of detection and false alarm. However, in general, the factors that control the probabilities of detection and false alarm and hence optimum threshold level in MTM are: *NW*, *K*, $\lambda_k(N, W)$, $v_{(t,k)}$, noise power σ_w^2 (or SNR), PR signal power, sensing time duration (i.e., *L*) as can be seen later within the remaining subsections of section 4.4. Figure 4.11 shows the possible MTM performance evaluation expressions. Such expressions would lead to the optimal design of MTM-based spectrum sensing that will support the practical design of such a technique in CR systems.

The main steps that have been followed to derive the different MTM performance evaluation expressions are:

1. After defining the system model, the statistical histograms of $|Y_k(f_i)|^2$, and $D_{MTM}(f_i)$ will be examined in AWGN and in different conditions.

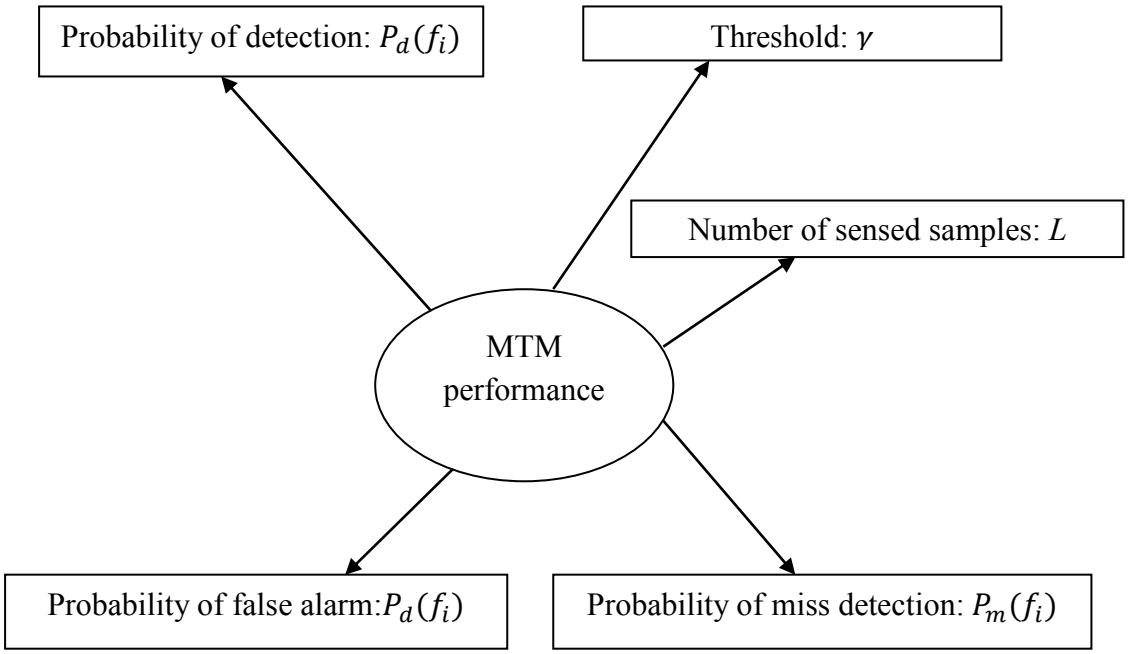

Figure 4.11 MTM performance evaluation expressions.

2. The observations from the examined statistical histograms will be investigated in order to achieve deep understanding of the $p(D_{MTM}(f_i);\mathcal{H}_0)$ and $p(D_{MTM}(f_i);\mathcal{H}_1)$ which are found as Gaussian distributions, as can be seen in the next subsections.
3. The E, and Var of both $p(D_{MTM}(f_i);\mathcal{H}_0)$, and $p(D_{MTM}(f_i);\mathcal{H}_1)$ will be derived.
4. The different probabilities expressions will be defined finally in AWGN.
5. The situation in the multipath fading environment will be discussed including the different statistical parameters as in step (3), and the different probabilities formulae as in step (4).

4.5.1 System Model

The system model here is same as that in section 4.4. The eigenspectrums in MTM are produced using (3.4), and the power is estimated using (3.5). The decision statistic

over L OFDM blocks using MTM is then defined as in (4.3), and for the *PE* the decision statistic over L can be written as follows [100]:

$$D_{PE}(f_i) = \frac{1}{N}\sum_{l=0}^{L-1}\left|\sum_{t=0}^{N-1} x_t(l)\, e^{-j2\pi f_i t}\right|^2 \tag{4.10}$$

In order to evaluate the performance of the MTM spectrum detector we have considered $P_d(f_i)$, $P_f(f_i)$, and $P_m(f_i)$ at any frequency bin f_i based on the *Neyman Pearson* criterion as in subsections 2.4.2.1-2.4.2.3.

4.5.2 The Probability Density Functions of the MTM Decision Statistics

Before focusing on $p(D_{MTM}(f_i);\mathcal{H}_0)$, and $p(D_{MTM}(f_i);\mathcal{H}_1)$, the PDF of the eigenspectrum absolute square, $|Y_k(f_i)|^2$, should be examined via a statistical histogram in order to understand its statistical characteristics. Figure 4.12 shows the statistical histogram of $|Y_k(f_i)|^2$ for $\mathcal{H}_0$ hypothesis using the 5th taper (i.e., k =5 in (4.10)) when SNR=$-$5dB (i.e., σ_w^2=3.1623). The histogram is observed at a specific frequency bin; however, the same result can be generalized for any other frequency bin. It is clear from the figure, the PDF of $|Y_k(f_i)|^2$, is central chi square for $\mathcal{H}_0$. Hence, the PDF of $|Y_k(f_i)|^2$is a non-central chi square for $\mathcal{H}_1$.Therefore, based on *central limit theorem* [88], the PDF of $|Y_k(f_i)|^2$can be approximated to Gaussian for large L, and for both hypotheses. The $D_{MTM}(f_i)$, finally, has PDFs with Gaussian distribution for $\mathcal{H}_1$ and $\mathcal{H}_0$. This is because $D_{MTM}(f_i)$ that in (4.3) and for large L, is a composite of balanced K eigenspectrums absolute squares which are correlated, as shall be demonstrated later. The large L, is defined in [47] as $L\geq 10$. Figure 4.13 shows the statistical histogram of $D_{MTM}(f_i)$ for $\mathcal{H}_1$ hypothesis when SNR=0 dB (i.e., $\sigma_w^2 = 1$). It is clear from the figure, the $p(D_{MTM}(f_i);\mathcal{H}_1)$ is a Gaussian. Figure 4.14 shows the statistical histograms of $D_{MTM}(f_i)$ for both $\mathcal{H}_1$ and $\mathcal{H}_0$ hypotheses when SNR=10 dB (i.e., $\sigma_w^2 = 0.1$). The figures show how both hypotheses have PDFs with Gaussian distribution. Figure 4.15

shows the statistical histogram of $D_{MTM}(f_i)$ for $\mathcal{H}_1$ hypothesis when SNR=10 dB in Rayleigh flat fading environment. The figure shows how also the PDF of the $D_{MTM}(f_i)$ in Rayleigh flat fading can be approximated to Gaussian under the mentioned conditions.

Figure 4.16 summarizes the MTM decision statistic's PDFs defining steps for both $\mathcal{H}_1$, and $\mathcal{H}_0$. In order to derive the theoretical formulae of the different probabilities, number of sensed samples, and threshold that have been shown in Figure 4.11, the different statistical characteristics of those PDFs must be derived. The *E* and *Var*, for both $p(D_{MTM}(f_i); \mathcal{H}_0)$, and $p(D_{MTM}(f_i); \mathcal{H}_1)$ are the required characteristics as shown in Figure 4.17. The derivation of those characteristics will be shown in the next subsections.

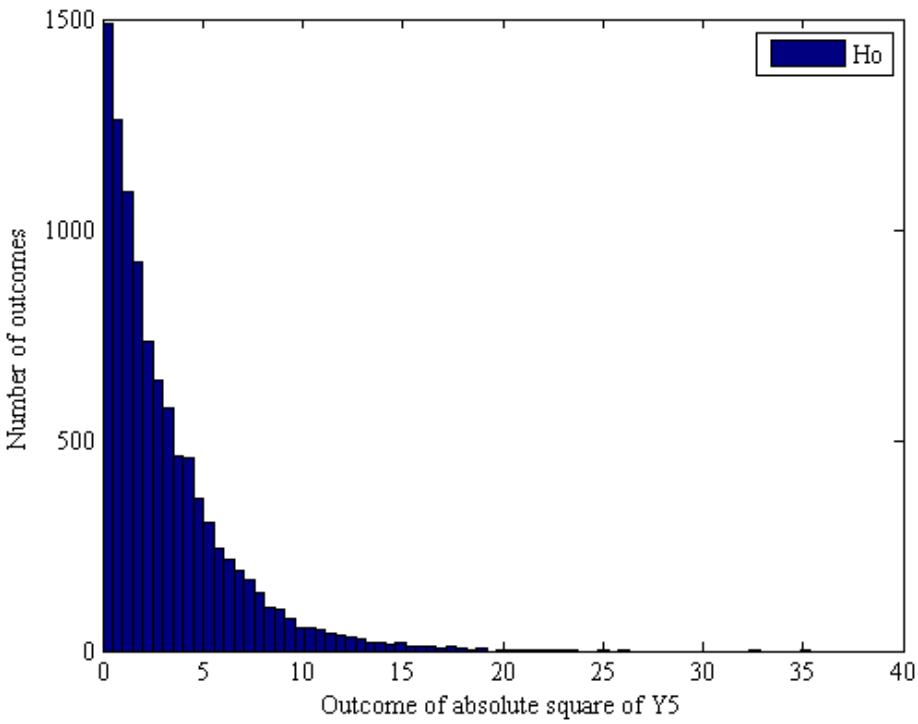

Figure 4.12 The eigenspectrum absolute square histogram for *k*=5 and SNR=-5dB.

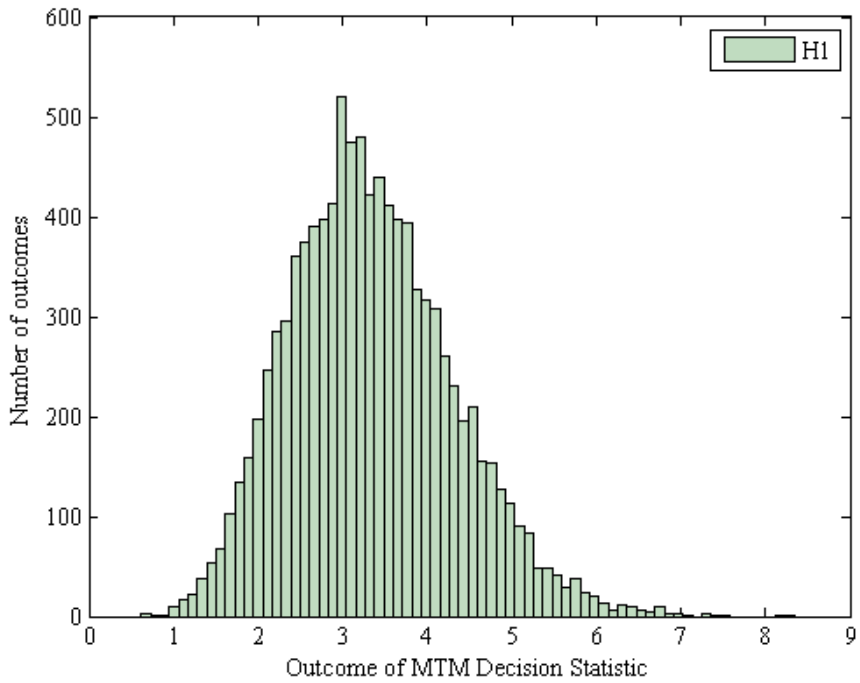

Figure 4.13 The MTM decision statistic histogram for $\mathcal{H}_1$ when SNR=0dB.

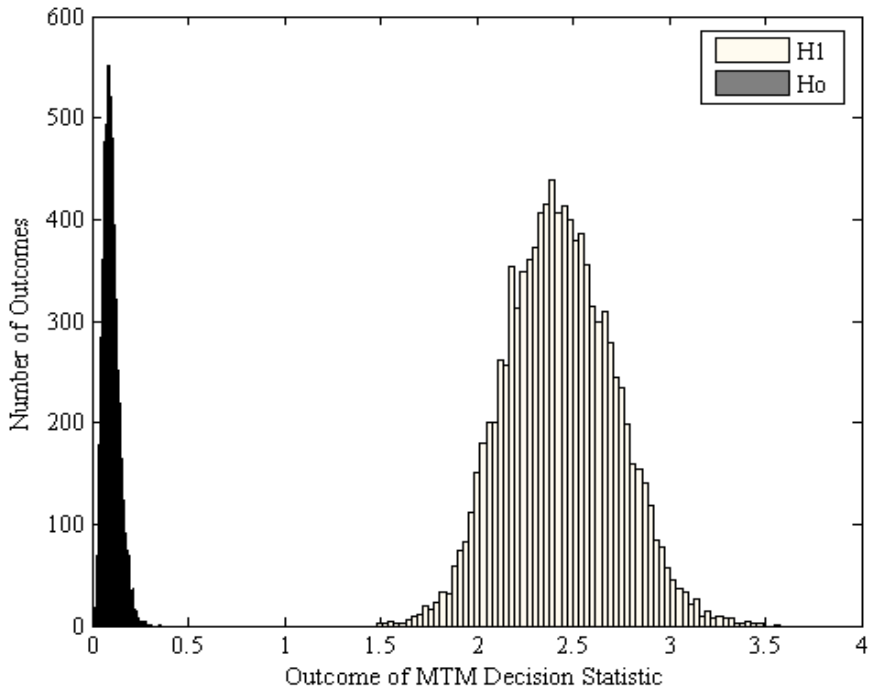

Figure 4.14 The MTM decision statistic histogram for both $\mathcal{H}_1$ and $\mathcal{H}_0$ when SNR=10dB.

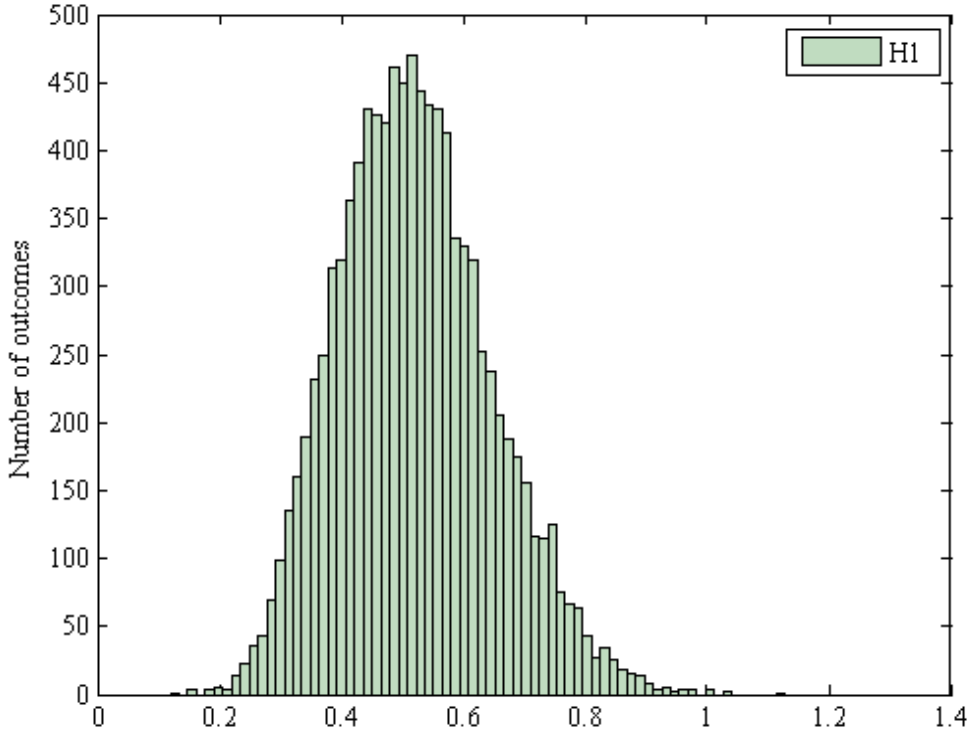

Figure 4.15 The MTM decision statistic histogram for $\mathcal{H}_1$when SNR=10dB in Rayleigh flat fading environment.

4.5.2.1 The Mean of the Decision Statistic in MTM for the Null Hypothesis

When only noise is present at frequency bin f_i, the mean of $p(\ D_{MTM};\mathcal{H}_0)$ over L sensed samples is the mean of (4.3), and can be defined as [4]:

$$E[p(\ D_{MTM}(f_i);\mathcal{H}_0)] = E[(\sum_{l=0}^{L-1} \frac{\sum_{k=0}^{K-1}\lambda_k(N,W)\left|\sum_{t=0}^{N-1} v_{(t,k)}(N,W)w_t(l)e^{-j2\pi f_i t}\right|^2}{\sum_{k=0}^{K-1}\lambda_k(N,W)}\ )\ ] \qquad (4.11)$$

Let us define a constant C [4],

$$C = E[\left(\frac{1}{\sum_{k=0}^{K-1}\lambda_k(N,W)}\right)] = \frac{1}{\sum_{k=0}^{K-1}\lambda_k(N,W)}$$

(4.12)

then (4.11) can be rewritten using (4.12) as:

$$E[p(\ D_{MTM}(f_i);\mathcal{H}_0)] = C.E[\left(\sum_{l=0}^{L-1}\sum_{k=0}^{K-1}(\lambda_k(N,W)\left|\sum_{t=0}^{N-1} v_{(t,k)}(N,W)w_t(l)e^{-j2\pi f_i t}\right|^2\ )\right)]$$

(4.13)

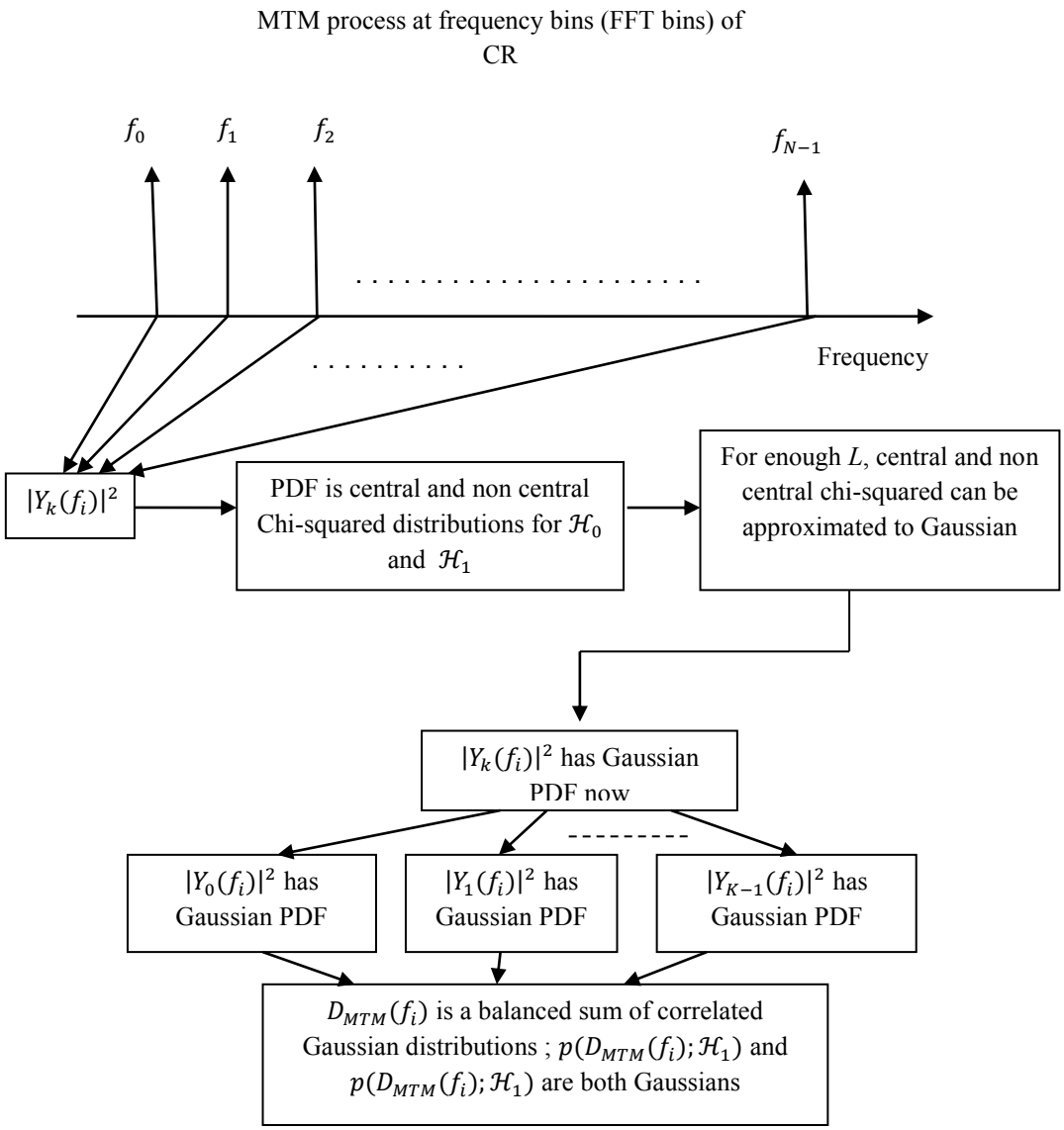

Figure 4.16 Schematic diagram defining the PDFs of MTM decision statistic for the different hypotheses.

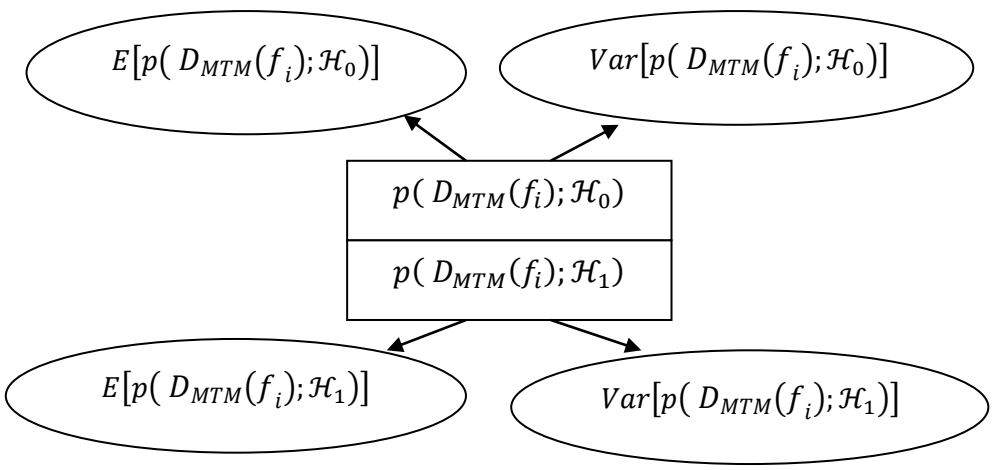

Figure 4.17 The required statistical characteristics for the MTM decision statistics for both $\mathcal{H}_0$ and $\mathcal{H}_1$.

since the FFT process is a linear process, and by distributing the summation over k , (4.13) can be written as [4]:

$$E[p(\, D_{MTM}(f_i); \mathcal{H}_0)]$$

$$= C.\sum_{l=0}^{L-1}(\sum_{t=0}^{N-1}\sum_{t'=0}^{N-1} E[(\lambda_0(N,W)(v_{(t,0)}(N,W)\, v_{(t',0)}(N,W) w_t(l) w_{t'}(l)$$

$$+\ \lambda_1(N,W)(v_{(t,1)}(N,W) v_{(t',1)}(N,W) w_t(l) w_{t'}(l)) + \cdots \tag{4.14}$$

$$+ \lambda_{K-1}(N,W)(v_{(t,K-1)}(N,W) v_{(t',K-1)}(N,W) w_t(l) w_{t'}(l)))]\,)$$

The terms inside the E operator in (4.14) are a sum of K Gaussian distributions, then, (4.14) becomes [4]:

$$E[p(\, DEC_{MTM}(f_i); \mathcal{H}_0)] \ = C.\sum_{l=0}^{L-1}(\sum_{k=0}^{K-1}(\lambda_k(N,W)\,.K\sum_{t=0}^{N-1}\sum_{t'=0}^{N-1} E(v_{(t,k)}(N,W)$$

$$.\, v_{(t',k)}(N,W).\, w_t(l) w_{t'}(l))\,) \tag{4.15}$$

It can be shown that (4.15) can be simplified, when $t = t'$, as follows [4]:

$$E[p(\, DEC_{MTM}(f_i); \mathcal{H}_0)] = \sum_{l=0}^{L-1}\sum_{t=0}^{N-1} v_{(t,k)}^2\,(N,W).K.E\big(w_t(l) w_t(l)\big) \tag{4.16}$$

From the definition of the Discrete Prolate Slepian Sequence (DPSS), we have [30]:

$$\textstyle\sum_{t=0}^{N-1} v_{(t,k)}\,(N,W).\, v_{(t,k')}(N,W) = \begin{cases} 1, & k = k' \\ 0, & k \neq k' \end{cases} \tag{4.17}$$

The orthonormality of the DPSS can be used to simplify (4.16), when $t = t'$as follows [4]:

$$E[p(\, D_{MTM}(f_i); \mathcal{H}_0)] = \sum_{l=0}^{L-1} K.E\left(w_t^2(l)\right)$$

$$= L.K.(\left(E\big(w_t(l)\big)\right)^2 + Var\big(w_t(l)\big)) = LK(0 + \sigma_w^2)$$

$$= LK\sigma_w^2 \tag{4.18}$$

4.5.2.2 The Mean of the Decision Statistic in MTM for the Alternative Hypothesis

When the PR signal is present, for $\mathcal{H}_1$ case, the $E[p(\,D_{MTM}(f_i);\mathcal{H}_1)]$ at frequency bin f_i can be defined as [4]:

$$E[p(\,D_{MTM}(f_i);\mathcal{H}_1)] = E\left[\left(\sum_{l=0}^{L-1}\frac{\sum_{k=0}^{K-1}(\lambda_k(N,W)\left|\sum_{t=0}^{N-1}v_{(t,k)}(N,W)(s_t(l)+w_t(l))e^{-j2\pi f_i t}\right|^2)}{\sum_{k=0}^{K-1}\lambda_k(N,W)}\right)\right] \quad (4.19)$$

Then, (4.19) can be rewritten using (4.12) to be as follows:

$$E[p(\,D_{MTM}(f_i);\mathcal{H}_1)] = C.E[(\sum_{l=0}^{L-1}\sum_{k=0}^{K-1}(\lambda_k(N,W)\left|\sum_{t=0}^{N-1}v_{(t,k)}(N,W)\big(s_t(l) + w_t(l)\big)e^{-j2\pi f_i t}\right|^2))] \quad (4.20)$$

By following the same steps of (4.15) and (4.16), then, (4.20) can be finalized as follows:

$$\begin{aligned}E[p(\,DEC_{MTM}(f_i);\mathcal{H}_1)] &= C.\sum_{l=0}^{L-1}\sum_{t=0}^{N-1}\sum_{t'=0}^{N-1}E[(\lambda_0(N,W)(v_{(t,0)}(N,W)\,v_{(t',0)}(N,W)\big(s_t(l) \\ &+ w_t(l)\big)\left(s_{t'}(l)+w_{t'}(l)\right) \\ &+ \lambda_1(N,W)(v_{(t,1)}\,(N,W)v_{(t',1)}(N,W)\big(s_t(l)+w_t(l)\big)\left(s_{t'}(l)\right. \\ &\left.+ w_{t'}(l)\right)) \\ &+ \cdots\lambda_{K-1}(N,W)(v_{(t,K-1)}\,(N,W)(N,W)v_{(t',K-1)}(N,W)\big(s_t(l) \\ &+ w_t(l)\big)\left(s_{t'}(l)+w_{t'}(l)\right)]\end{aligned}$$

$$= C.\sum_{l=0}^{L-1}\sum_{k=0}^{K-1}(\lambda_k(N,W)\,.K.\sum_{t=0}^{N-1}\sum_{t'=0}^{N-1}E(v_{(t,k)}(N,W)\,v_{(t',k)}(N,W)\big(s_t(l) + w_t(l)\big)\big(s_{t'}(l)+w_{t'}(l)\big))\,) \quad (4.21)$$

Based on the linearity property of the FFT process, the orthonormality of the DPSS, and when $t = t'$, (4.21) can be simplified as [4]:

$$E[p(\, D_{MTM}(f_i); \mathcal{H}_1)] = \sum_{l=0}^{L-1} K.E\big((s_t(l) + w_t(l))(s_t(l) + w_t(l))\big) \tag{4.22}$$

Note that when $t \neq t'$; $E\left(w_t(l)w_{t'}(l)\right) = 0$ since the Gaussian samples are identical and independent. Finally, (4.22) becomes:

$$\begin{aligned} E[p(\, D_{MTM}(f_i); \mathcal{H}_1)] &= L.K.E((s_t(l) + w_t(l))(s_t(l) + w_t(l))) \\ &= L.K.E(s_t^2(l) + 2s_t(l)w_t(l) + w_t^2(l)) \end{aligned} \tag{4.23}$$

Since the mean of $w_t(l)$ is zero, then $E\big(2s_t(l)w_t(l)\big) = 0$. The term $E(s_t^2(l)) = E(E_s) = E_s$ is the energy over each subcarrier, and $E(w_t^2(l)) = VAR(w_t(l)) + (E\big(w_t(l)\big))^2 = \sigma_w^2$. Finally, (4.23) can be written as follows [4]:

$$E[p(\, D_{MTM}(f_i); \mathcal{H}_1)] = L.K.(E_s + \sigma_w^2) \tag{4.24}$$

4.5.2.3 The Variance of the Decision Statistic in MTM for the Null Hypothesis

In order to complete the expressions of the different probabilities, the variances of $p(D_{MTM}(f_i); \mathcal{H}_0)$ and $p(D_{MTM}(f_i); \mathcal{H}_1)$ will be defined in the next stage of our theoretical derivation. Firstly, let us start to define the variance of $p(D_{MTM}(f_i); \mathcal{H}_0)$, $VAR\big[p\big(D_{MTM}(f_i); \mathcal{H}_0\big)\big]$, where the noise only is present. In order to simplify our derivation, (4.3) will be redefined at each frequency bin using decision statistic coefficients α_k , $k = 0,1,2, \dots, K-1$, as follows [4]:

$$D_{MTM}(f_i) = \sum_{l=0}^{L-1} \sum_{k=0}^{K-1} \alpha_k\,(f_i) \tag{4.25}$$

where coefficient α_k is defined as follows:

$$\alpha_k(f_i) = \frac{\lambda_k(N,W)|Y_k(f_i)|^2}{\sum_{k=0}^{K-1} \lambda_k(N,W)},\ k = 0,1,2, \dots, K-1 \tag{4.26}$$

Then, the variance of $\alpha_k(f_i)$ can be defined as follows [4]:

$$Var[\alpha_k(f_i);\mathcal{H}_\Theta] = \frac{\lambda_k^2(N,W).Var[|Y_k(f_i)|^2;\mathcal{H}_\Theta]}{(\sum_{k=0}^{K-1}\lambda_k(N,W))^2}, \Theta = 0,1 \tag{4.27}$$

The variance of $p(\,D_{MTM}(f_i);\mathcal{H}_0)$ where the noise only is present for K correlated Gaussian samples (i.e., eigenspectrum absolute square $|Y_k(f_i)|^2$), $Var[p(\,D_{MTM}(f_i);\mathcal{H}_0)]$, can be defined as follows [4]:

$$Var[p(\,D_{MTM}(f_i);\mathcal{H}_0)] =$$

$$\sum_{l=0}^{L-1}(\sum_{k=0}^{K-1} Var[\alpha_k(f_i);\mathcal{H}_0] + 2\partial_{01}\sqrt{Var[\alpha_0(f_i);\mathcal{H}_0]}\sqrt{Var[\alpha_1(f_i);\mathcal{H}_0]} +$$

$$2\partial_{02}\sqrt{Var[\alpha_0(f_i);\mathcal{H}_0]}\sqrt{Var[\alpha_2(f_i);\mathcal{H}_0]} + \cdots +$$

$$2\partial_{0K-1}\sqrt{Var[\alpha_0(f_i);\mathcal{H}_0]}\sqrt{Var[\alpha_{K-1}(f_i);\mathcal{H}_0]} +$$

$$2\partial_{12}\sqrt{Var[\alpha_1(f_i);\mathcal{H}_0]}\sqrt{Var[\alpha_2(f_i);\mathcal{H}_0]} +$$

$$2\partial_{13}\sqrt{Var[\alpha_1(f_i);\mathcal{H}_0]}\sqrt{Var[\alpha_3(f_i);\mathcal{H}_0]} + \cdots +$$

$$2\partial_{1K-1}\sqrt{Var[\alpha_1(f_i);\mathcal{H}_0]}\sqrt{Var[\alpha_{K-1}(f_i);\mathcal{H}_0]} + \cdots +$$

$$2\partial_{K-2K-1}\sqrt{Var[\alpha_{K-2}(f_i);\mathcal{H}_0]}\sqrt{Var[\alpha_{K-1}(f_i);\mathcal{H}_0]}) \tag{4.28}$$

where $\partial_{iz} \approx 1$, is the correlation coefficient between α_i , and α_z , and since $Var[|Y_k(f_i)|^2;\mathcal{H}_0] = Var[|Y_k(f_i)|^2;\mathcal{H}_0]$, for $k = 0,1,2,\ldots,K-1$ applying the orthonormality in (4.17). Then (4.28) can be rewritten using (4.12) as follows [4]:

$$Var[p(\,D_{MTM}(f_i);\mathcal{H}_0)]$$

$$= C^2.Var[|Y_k(f_i)|^2;\mathcal{H}_0].\sum_{l=0}^{L-1}\left(\sum_{k=0}^{K-1}\lambda_k^2(N,W) + 2\lambda_0(N,W)\lambda_1(N,W)\right.$$

$$+ 2\lambda_0(N,W)\lambda_2(N,W) + \cdots + 2\lambda_0(N,W)\lambda_{K-1}(N,W)$$

$$+ 2\lambda_1(N,W)\lambda_2(N,W) + 2\lambda_1(N,W)\lambda_3(N,W) + \cdots$$

$$+ 2\lambda_1(N,W)\lambda_{K-1}(N,W) + \cdots$$

$$\left.+ 2\lambda_{K-2}(N,W)\lambda_{K-1}(N,W)\right) \tag{4.29}$$

when $t = t'$, and since the variance of the square of Gaussian random variable W, $Var(W^2) = 2(Var(W))^2$, then $Var[|Y_k(f_i)|^2; \mathcal{H}_0]$ can be defined as follows [4]:

$$Var[|Y_k(f_i)|^2; \mathcal{H}_0]$$

$$= \left(\sum_{t=0}^{N-1} v_{(t,k)}^2(N,W)\right)^2 . Var\left[\left(w_t^2(l)\right)\right]$$

$$= (2\sigma_w^4) \tag{4.30}$$

Finally, $Var[p(D_{MTM}(f_i); \mathcal{H}_0)]$ over L can be rewritten using (4.29) and (4.30) as follows [4]:

$$Var[p(D_{MTM}(f_i); \mathcal{H}_0)] = 2C^2 L \lambda_\Sigma \sigma_w^4 \tag{4.31}$$

where λ_Σ, is defined as follows [4]:

$$\lambda_{\Sigma=} \sum_{k=0}^{K-1} \lambda_k^2(N,W) + 2\lambda_0(N,W)\lambda_1(N,W) + 2\lambda_0(N,W)\lambda_2(N,W) + \cdots$$

$$+ 2\lambda_0(N,W)\lambda_{K-1}(N,W) + 2\lambda_1(N,W)\lambda_2(N,W)$$

$$+ 2\lambda_1(N,W)\lambda_3(N,W) + \cdots + 2\lambda_1(N,W)\lambda_{K-1}(N,W) + \cdots$$

$$+ 2\lambda_{K-2}(N,W)\lambda_{K-1}(N,W) \tag{4.32}$$

4.5.2.4 The Variance of the Decision Statistic in MTM for the Alternative Hypothesis

When the PR signal is present for $\mathcal{H}_1$ case at frequency bin f_i, the variance of the $p(D_{MTM}(f_i); \mathcal{H}_1)$, $Var[p(D_{MTM}(f_i); \mathcal{H}_1)]$ is [4]:

$$Var[p(D_{MTM}(f_i); \mathcal{H}_1)] = C^2 . L . \lambda_\Sigma . Var[|Y_k(f_i)|^2; \mathcal{H}_1] \tag{4.33}$$

when $t = t'$, and since $Var[s_t^2(l)] = 0$ in this case, and $Var[2s_t(l)w_t(l)] = 4E_s\sigma_w^2$, then,

$$Var[|Y_k(f_i)|^2; \mathcal{H}_1] = Var\,[s_t^2(l) + 2s_t(l)w_t(l) + w_t^2(l)]$$

$$= (2\sigma_w^4 + 4E_s\sigma_w^2) \tag{4.34}$$

Finally, (4.33) can be written as follows [4]:

$$Var[p(D_{MTM}(f_i);\mathcal{H}_1)] = C^2\, L\lambda_\Sigma(2\sigma_w^4 + 4E_s\sigma_w^2)$$

$$= 2.C^2\,.L.\lambda_\Sigma.\sigma_w^2.(2E_s + \sigma_w^2) \qquad (4.35)$$

4.5.3 The Probabilities Formulae of MTM Based Spectrum Sensing

In the last four subsections, the main statistical characteristics of the MTM decision statistic's PDFs for both $\mathcal{H}_0$ and $\mathcal{H}_1$ have been derived. Consequentially, deriving the MTM probability of detection $P_d^{MTM}(f_i)$, MTM probability of false alarm $P_f^{MTM}(f_i)$, and MTM probability of miss detection$P_m^{MTM}(f_i)$ can be defined using those characteristics in (2.6), (2.8), and (2.10) to be as follow [4]:

$$P_d^{MTM}(f_i\,) = Q(\frac{\gamma - LK(E_s+\sigma_w^2)}{\sqrt{2LC^2\lambda_\Sigma\sigma_w^2(\sigma_w^2+2E_s)}}) \qquad (4.36)$$

$$P_f^{MTM}(f_i\,) = Q(\frac{\gamma - LK\sigma_w^2}{\sqrt{2LC^2\lambda_\Sigma\sigma_w^4}}) \qquad (4.37)$$

$$P_m^{MTM}(f_i\,) = 1 - Q(\frac{\gamma - LK(E_s+\sigma_w^2)}{\sqrt{2LC^2\lambda_\Sigma\sigma_w^2(\sigma_w^2+2E_s)}}) \qquad (4.38)$$

Although the eigenspectrums that build the $D_{MTM}(f_i)$ in (4.3) are considered as correlated. The orthonormality of the DPSS can, in some cases, have an effect on the independence of those eigenspectrums which become independent. In such case, and based on the *central limit theorem*, the means and variances for both hypotheses that have been defined in subsections 4.5.2.1- 4.5.2.4 can be reformulated finally to be:

$$E\big[p\big(D_{MTM}(f_i)\big)\,\big] = \begin{cases} L\sigma_w^2 & \mathcal{H}_0 \\ L(E_s + \sigma_w^2) & \mathcal{H}_1 \end{cases}$$

and *Var*

$$Var[p\big(D_{MTM}(f_i)\big)] = \begin{cases} (1/K)2C^2L\sum_{k=0}^{K-1}\lambda_k^2(N,W)(\sigma_w^4) & \mathcal{H}_0 \\ (1/K)2C^2L\sigma_w^2\sum_{k=0}^{K-1}\lambda_k^2(N,W)(\sigma_w^2 + 2E_s) & \mathcal{H}_1 \end{cases}$$

and then the different probabilities in (4.36)-(4.38) can be redefined to be as follows:

$$P_d^{MTM}(f_i) = Q\left(\frac{\gamma - L(E_s + \sigma_w^2)}{\sqrt{\left(\frac{2}{K}\right) LC^2 \sigma_w^2 \sum_{k=0}^{K-1} \lambda_k^2(N,W)(\sigma_w^2 + 2E_s)}}\right)$$

$$P_f^{MTM}(f_i) = Q\left(\frac{\gamma - L\sigma_w^2}{\sqrt{\left(\frac{2}{K}\right) LC^2 \sum_{k=0}^{K-1} \lambda_k^2(N,W)(\sigma_w^4)}}\right)$$

$$P_m^{MTM}(f_i) = 1 - Q\left(\frac{\gamma - L(E_s + \sigma_w^2)}{\sqrt{\left(\frac{2}{K}\right) LC^2 \sigma_w^2 \sum_{k=0}^{K-1} \lambda_k^2(N,W)(\sigma_w^2 + 2E_s)}}\right)$$

These probabilities equations give exactly the same results as those in (4.36)-(4.38). Note that the $(\frac{1}{K})$ term comes from the fact that the variance of K independent Gaussian samples which have the same variance is the variance of one of them divided by K, as K is large enough, based on the *central limit theorem*. Furthermore, the effect of L and K sizes on the PDF of $D_{MTM}(f_i)$ can be considered jointly (e.g., if L=20 samples, and K=5, total number of independent samples become 50, which is large enough).

4.5.4 The Number of Sensed Samples *L* in MTM Based Spectrum Sensing

By the end of the last subsection, the different MTM based spectrum sensing probabilities formulae were defined. Therefore, the number of sensed samples L, which is needed to achieve predefined probabilities of detection $P_d^{MTM}(f_i)$, and false alarm $P_f^{MTM}(f_i)$ in the MTM technique can be defined by equalizing the threshold, γ, in (4.36) to that in (4.37).

Using (4.36), the threshold, γ, can be defined as follows:

$$Q^{-1}\left(P_d^{MTM}(f_i)\right) = \frac{L(\frac{\gamma}{L} - K(E_s + \sigma_w^2))}{\sqrt{L}.\sqrt{2C^2\lambda_\Sigma \sigma_w^2(\sigma_w^2 + 2E_s)}}$$

$$Q^{-1}\left(P_d^{MTM}(f_i)\right) = \frac{\sqrt{L}(\frac{\gamma}{L} - K(E_s + \sigma_w^2))}{\sqrt{2C^2\lambda_\Sigma \sigma_w^2(\sigma_w^2 + 2E_s)}}$$

$$\mathcal{Q}^{-1}\left(P_d^{MTM}(f_i)\right).\sqrt{2C^2\lambda_\Sigma\sigma_w^2(\sigma_w^2+2E_s)} = \sqrt{L}(\frac{\gamma}{L} - K(E_s+\sigma_w^2))$$

$$\frac{\gamma}{L} - K(E_s+\sigma_w^2) = \frac{\mathcal{Q}^{-1}\left(P_d^{MTM}(f_i)\right)\sqrt{2C^2\lambda_\Sigma\sigma_w^2(\sigma_w^2+2E_s)}}{\sqrt{L}}$$

$$\frac{\gamma}{L} = \frac{\mathcal{Q}^{-1}\left(P_d^{MTM}(f_i)\right)\sqrt{2C^2\lambda_\Sigma\sigma_w^2(\sigma_w^2+2E_s)}}{\sqrt{L}} + K(E_s+\sigma_w^2)$$

$$\gamma = \mathcal{Q}^{-1}\left(P_d^{MTM}(f_i)\right)\sqrt{L}\sqrt{2C^2\lambda_\Sigma\sigma_w^2(\sigma_w^2+2E_s)} + LK(E_s + \sigma_w^2) \tag{4.39}$$

Using (4.37), the threshold γ can be defined as follows:

$$\mathcal{Q}^{-1}\left(P_f^{MTM}(f_i)\right) = \frac{L(\frac{\gamma}{L} - K\sigma_w^2)}{\sqrt{L}.\sqrt{2C^2\lambda_\Sigma\sigma_w^4}}$$

$$\mathcal{Q}^{-1}\left(P_f^{MTM}(f_i)\right) = \frac{\sqrt{L}.(\frac{\gamma}{L} - K\sigma_w^2)}{\sqrt{2C^2\lambda_\Sigma\sigma_w^4}}$$

$$\mathcal{Q}^{-1}\left(P_f^{MTM}(f_i)\right).\sqrt{2C^2\lambda_\Sigma\sigma_w^4} = \sqrt{L}\left(\frac{\gamma}{L} - K\sigma_w^2\right)$$

$$\frac{\gamma}{L} - K\sigma_w^2 = \frac{\mathcal{Q}^{-1}\left(P_f^{MTM}(f_i)\right)\sqrt{2C^2\lambda_\Sigma\sigma_w^4}}{\sqrt{L}}$$

$$\frac{\gamma}{L} = \frac{\mathcal{Q}^{-1}\left(P_f^{MTM}(f_i)\right)\sqrt{2C^2\lambda_\Sigma\sigma_w^4}}{\sqrt{L}} + K\sigma_w^2$$

$$\gamma = Q^{-1}\left(P_f^{MTM}(f_i)\right)\sqrt{L}\sqrt{2C^2\lambda_\Sigma\sigma_w^4} + LK\sigma_w^2 \tag{4.40}$$

It has been said that the threshold in (4.36) is equal to that in (4.37). Therefore, the number of sensed samples L in MTM based spectrum sensing can be defined using this fact as below [4]:

$$Q^{-1}\left(P_f^{MTM}(f_i)\right)\sqrt{L}\sqrt{2C^2\lambda_\Sigma\sigma_w^4} + LK\sigma_w^2 = Q^{-1}\left(P_d^{MTM}(f_i)\right)\sqrt{L}\sqrt{2C^2\lambda_\Sigma\sigma_w^2(\sigma_w^2+2E_s)} + LK(E_s+\sigma_w^2)$$

$$LKE_s = \sqrt{L}Q^{-1}\left(P_f^{MTM}(f_i)\right)\sqrt{2C^2\lambda_\Sigma\sigma_w^4} - \sqrt{L}Q^{-1}\left(P_d^{MTM}(f_i)\right)\sqrt{2C^2\lambda_\Sigma\sigma_w^2(\sigma_w^2+2E_s)}$$

$$\sqrt{L} = \frac{Q^{-1}\left(P_f^{MTM}(f_i)\right)\sqrt{2C^2\lambda_\Sigma\sigma_w^4} - Q^{-1}\left(P_d^{MTM}(f_i)\right)\sqrt{2C^2\lambda_\Sigma\sigma_w^2(\sigma_w^2+2E_s)}}{KE_s}$$

$$L = \left(\frac{\sqrt{2C^2\lambda_\Sigma\sigma_w^4}Q^{-1}\left(P_f^{MTM}(f_i)\right) - \sqrt{2C^2\lambda_\Sigma\sigma_w^2(\sigma_w^2+2E_s)}Q^{-1}\left(P_d^{MTM}(f_i)\right)}{KE_s}\right)^2 \tag{4.41}$$

which can be written in (dB) to be as follows:

$$L_{dB} = 10log_{10}(L)$$

Following the same steps above and using the probabilities equations that have been redefined by the end of subsection 4.5.3, the same result from (4.41) can be achieved using:

$$L = \left(\frac{\sqrt{2F\sigma_w^4}Q^{-1}\left(P_f^{MTM}(f_i)\right) - \sqrt{2F\sigma_w^2(\sigma_w^2+2E_s)}Q^{-1}\left(P_d^{MTM}(f_i)\right)}{E_s}\right)^2$$

where $F = (1/K)(\frac{1}{\sum_{k=0}^{K-1}\lambda_k(N,W)})^2\sum_{k=0}^{K-1}\lambda_k^2(N,W)$.

4.5.5 The Threshold Formulae in MTM Based Spectrum Sensing

The threshold,γ, can be defined in MTM based spectrum sensing as a function of the false alarm probability $P_f^{MTM}(f_i)$ as follows:

$$\gamma = \frac{Q^{-1}\left(P_f^{MTM}(f_i)\right)\sqrt{2C^2\lambda_\Sigma\sigma_w^4}+LK\sigma_w^2}{L} \tag{4.42}$$

and as a function of the probability of detection $P_d^{MTM}(f_i)$ as follows:

$$\gamma = \frac{Q^{-1}\left(P_d^{MTM}(f_i)\right)\sqrt{2C^2\lambda_\Sigma\sigma_w^2(\sigma_w^2+2E_s)}+LK(E_s+\sigma_w^2)}{L} \tag{4.43}$$

Note that, the threshold, γ, choice in MTM spectrum sensing depends on the noise power (i.e., noise variance(σ_w^2)). Therefore, as energy based spectrum sensing technique in CR systems, prior knowledge of the noise power is required; it is similar to the PE, and FB. The noise power can be estimated using different noise estimation methods. Simply, the noise power can be calibrated during the time when the PR user is not active in the licensed frequency subband [108].

4.5.6 The Probabilities Formulae of MTM Based Spectrum Sensing in Multipath Fading Environment

In multipath fading environment, the binary hypothesis test in (4.2) can be redefined for $\mathcal{H}_1$ to be as follows [100]:

$$x_t(l) = \sum_{p=0}^{P-1} h_p s_{t-p}(l) + w_t(l) \tag{4.44}$$

where the discrete channel impulse response between the PR's Tx and CR's Rx is represented by h_p,$p = 0,1,\ldots,P-1$, and P is the total number of resolvable paths. The discrete frequency response of the channel is obtained by taking the N point FFT, with $N \geq P$ as follows [100]:

$$H(f_i) = \sum_{p=0}^{P-1} h_p e^{-j2\pi f_i p} \tag{4.45}$$

In this case, the formulae in (4.36), and (4.37) can be written as follow [3]:

$$P_d^{MTM}(f_i) = Q\left(\frac{\gamma - LK(|H(f_i)|^2 E_s + \sigma_w^2)}{\sqrt{2LC^2\lambda_\Sigma \sigma_w^2(\sigma_w^2 + 2|H(f_i)|^2 E_s)}}\right) \tag{4.46}$$

$$P_m^{MTM}(f_i) = 1 - Q\left(\frac{\gamma - LK(|H(f_i)|^2 E_s + \sigma_w^2)}{\sqrt{2LC^2\lambda_\Sigma \sigma_w^2(\sigma_w^2 + 2|H(f_i)|^2 E_s)}}\right) \tag{4.47}$$

The SNR can be redefined here to be as follows [15]:

$$SNR = \frac{|H(f_i)|^2 E_s}{\sigma_w^2} \tag{4.48}$$

In this thesis, we assume that the channel gain between the PR's Tx and the CR's Rx is constant during the spectrum sensing duration, and $|H(f_i)|^2 = 1$ in AWGN case, and $|H(f_i)|^2 \leq 1$ in the multipath fading case. In practice, $|H(f_i)|^2$ can be estimated priori during the time that PR's transmitter occupies a specific band with specific power [100].

The number of sensed samples in such an environment can be rewritten using (4.37) and (4.46) to be as follows [3]:

$$L = \left(\frac{\sqrt{2C^2\lambda_\Sigma \sigma_w^4} Q^{-1}\left(P_f^{MTM}(f_i)\right) - \sqrt{2C^2\lambda_\Sigma \sigma_w^2(\sigma_w^2 + 2|H(f_i)|^2 E_s)} Q^{-1}\left(P_d^{MTM}(f_i)\right)}{K|H(f_i)|^2 E_s}\right)^2 \tag{4.49}$$

4.5.7 The Performance Evaluation of the Periodogram

It is clear that, the main processing difference between the PE and the MTM detector is simply multiplying the signal by a number of orthonormal tapers, the *DPSS* to produce a single estimate in MTM, while the multiplication in the PE is by a single rectangular taper. Thus, in order to see the effect of this difference, we use the probabilities formulae of the PE which can be for the same system conditions as follow [47, 100]:

$$P_d^{PE}(f_i) = Q\left(\frac{\gamma - L(E_s+\sigma_w^2)}{\sqrt{2L\sigma_w^2(\sigma_w^2+2E_s)}}\right) \tag{4.50}$$

$$P_f^{PE}(f_i) = Q\left(\frac{\gamma - L\sigma_w^2}{\sqrt{(2L\sigma_w^4)}}\right) \tag{4.51}$$

$$P_m^{PE}(f_i) = 1 - Q\left(\frac{\gamma - L(E_s+\sigma_w^2)}{\sqrt{2L\sigma_w^2(\sigma_w^2+2E_s)}}\right) \tag{4.52}$$

The equations above, which represent the probabilities at f_i using PE are rewritten from those representing the ED as in (2.21)-(2.23). Following the same steps in deriving (4.46), the number of sensed samples L^{PE} which is needed to achieve predefined probabilities of detection $P_d^{PE}(f_i)$, and false alarm $P_f^{PE}(f_i)$ in the PE technique can be defined by equalizing the threshold, γ, in (4.50) by that in (4.51). Then,

$$L^{PE} = \left(\frac{\sqrt{2\sigma_w^4}Q^{-1}\left(P_f^{PE}(f_i)\right) - \sqrt{2\sigma_w^2(\sigma_w^2+2E_s)}Q^{-1}\left(P_d^{PE}(f_i)\right)}{E_s}\right)^2 \tag{4.53}$$

In multipath fading environment, (4.50) and (4.52) become:

$$P_d^{PE}(f_i) = Q\left(\frac{\gamma - L(|H(f_i)|^2E_s+\sigma_w^2)}{\sqrt{2L\sigma_w^2(\sigma_w^2+2|H(f_i)|^2E_s)}}\right) \tag{4.54}$$

$$P_m^{PE}(f_i) = 1 - Q\left(\frac{\gamma - L(|H(f_i)|^2E_s+\sigma_w^2)}{\sqrt{2L\sigma_w^2(\sigma_w^2+2|H(f_i)|^2E_s)}}\right) \tag{4.55}$$

4.5.8 The Performance Evaluation of the Autocorrelation Based and SD Spectrum Sensing Techniques for OFDM Based CR Systems

Subsection 2.7.3 describes two of the recent published spectrum sensing techniques for OFDM-based CR systems. In the local autocorrelation based spectrum sensing technique, the CP correlation is exploited [144]. In the SD global cooperative spectrum sensing technique [144], which is classified as SCSS scheme, the CR-BS collects and fuses the decision statistics that resulted when autocorrelation based technique is used at the different CR users and decides, based on this, whether the PR user is active in the frequency subband or not.

The probability of detection, P_d^{AC}, when autocorrelation based spectrum sensing (Auto.Corr) is used for spectrum sensing in OFDM based CR systems is defined as [144]:

$$P_d^{AC} = Q(\sqrt{2L^{AC}}.\frac{\eta_l - \rho_1}{\rho_1^2}) \tag{4.56}$$

and the probability of false alarm is defined as[144]:

$$P_f^{AC} = Q(\sqrt{2L^{AC}}.\eta_l) \tag{4.57}$$

where η_l, is the chosen threshold in this technique, L^{AC} is the total number of sensed samples in Auto.Corr which can be written as function of L , N , and N_{CP} and as follows [144]:

$$L^{AC} = L(N_{CP} + N) \tag{4.58}$$

where L is the number of OFDM blocks, as has been defined before. The ρ_1 in (4.56), is defined as follows [144]:

$$\rho_1 = \left(\frac{N_{CP}}{N_{CP} + N}\right).\left(\frac{E_s}{E_s + \sigma_w^2}\right) \tag{4.59}$$

The SD global cooperative spectrum sensing for OFDM based CR systems has the following probabilities formulae [144]:

$$P_d^{SD} = Q(\frac{\eta_{SD-mf}}{\sigma_{f1}}) \tag{4.60}$$

and

$$P_f^{SD} = Q(\frac{\eta_{SD}}{\sigma_{f0}}) \tag{4.61}$$

where η_{SD} is the threshold for SD spectrum sensing, and mf, σ_{f1}, and σ_{f0} can be defined as follow [144]:

$$mf = 2L^{AC} \sum_{g=1}^{G} \frac{\rho_g^2}{(1 - \rho_g^2)} \tag{4.62}$$

$$\sigma_{f1}{}^2 = 2L^{AC} \sum_{g=1}^{G} \rho_g^2 \tag{4.63}$$

$$\sigma_{f0}{}^2 = 2L^{AC} \sum_{g=1}^{G} \frac{\rho_g^2}{(1-\rho_g^2)^2} \tag{4.64}$$

where g=1, 2, 3,…, G, represents the number of cooperative CR users in SD.

The performance evaluation using simulation and theoretical work of the MTM based spectrum sensing, PE, Auto.Corr, and SD will be discussed in subsection 4.5.9 as can be seen.

4.5.9 Simulation Results

This subsection consists of three parts which deal with:

1. Verification of the derived theoretical formulae of the MTM based detector and examination of the system performance in terms of ROC, number of sensed samples L, and the threshold in AWGN. This part also includes a comparison between the MTM and PE in terms of ROC, L in the same conditions.
2. Comparison between the performance of MTM, Auto Corr., and SD techniques under the same conditions.
3. Examination of the MTM ROC in Rayleigh flat and multipath fading wireless environments. This includes comparison to the PE under the same conditions.

We evaluate our theoretical work by running a simulation program where the PR signal is QPSK with normalized energy equal to 1 over each subcarrier(i.e., E_s). Both CR and PR users employ 64-IFFT/FFT digital signal processing in their communications with sampling frequency 20 MHz/ Ts=0.05μs, where Ts represents the QPSK symbol duration, the MTM parameters used are NW=4, and 5 tapers, and the results obtained over 10^6 realizations. Additionally, we compare the performance of MTM spectrum detector system to that of the PE under the same conditions. We used theoretical and simulation results for a chosen frequency bin at the CR FFT to examine the hypotheses $\mathcal{H}_1$, and $\mathcal{H}_0$.

Figure 4.18 shows the ROC when MTM with *NW*=4 and 5 tapers and PE are used at AWGN with SNR=-10dB and $L = 20$ OFDM blocks. Note that the total number of samples used is $(L = 20) \times (N = 64) = 1280$ approximately corresponds to sensing time$(L = 20) \times (N = 64) \times (Ts = 0.05\mu s) = 64\mu$. By comparing the theoretical to the simulation in the MTM case, we note that the theoretical results match well the simulated one. In the same system conditions, the probability of detection P_d of MTM outperforms that for PE by 40%, when the probability of false alarm is P_f=10%, and the miss detection P_m in MTM is lower than that in PE's case by 40%.

Figure 4.19 shows the results of the number of OFDM blocks, L, required to achieve $P_d = 99\%$, and $P_f = 1\%$ at AWGN environment with different SNR using MTM with *NW*=4 and 5 tapers and compared to the PE. It is clear that the number of OFDM blocks used in the sensing process in the MTM system is lower than that for the PE. For example, at SNR=-15dB, the L required by the MTM is 33dB, and by the PE is 47dB. These two values correspond to 1995 and 50120 OFDM blocks for MTM and the PE, respectively, in the linear scale. Thus, the PE requires 25 times as many samples compared to MTM in order to achieve the same probabilities at the same SNR. Such a large number of the samples for sensing in the CR system might hinder the opportunistic use of the vacant channels, which is the main objective of the developing of CR systems.

Figure 4.20 shows the probabilities of detection P_d that give~~s~~ probabilities of false alarm $P_f = 5\%$, and 10% versus the SNR at AWGN using MTM with *NW*=4 and 5 tapers and $L = 50$. For both predefined probabilities of false alarm the probabilities of detection are almost 100% for SNR=-7dB or higher with unnoticeable change for $P_f = 10\%$ curve, which is reasonable. Both probabilities of detection curves start to decrease with the decrease in the SNR with noticeable outperforming of the $P_f = 10\%$

curve. At SNR=-25dB, $P_d = 11\%$ for $P_f = 10\%$ curve, and $P_d = 6\%$ for $P_f = 5\%$ curve.

Figure 4.20 shows the threshold versus probabilities of false alarm and detection when MTM with *NW*=4 and 5 tapers are used at AWGN with SNR=-7dB (i.e., $\sigma_w^2 = 5.0119$) and $L = 50$. Such a figure presents the range of the threshold that should be chosen in order to meet the specific probability of false alarm and detection at defined SNR level and *L* used in the spectrum sensing. As an example, for threshold=5, the probability of false alarm and detection pair (P_f, P_d) is ($50\%, 100\%$). By increasing the threshold level to 5.3, the pair becomes ($10\%, 100\%$). This figure can be revaluated at different SNR and *L* conditions using (4.42) and (4.43).

The ROC curves for different spectrum sensing techniques will be included and discussed in the next part of this subsection to have more range of comparison to the MTM performance. The Auto.Corr based, and the SD cooperative spectrum sensing techniques are those under comparison to the MTM.

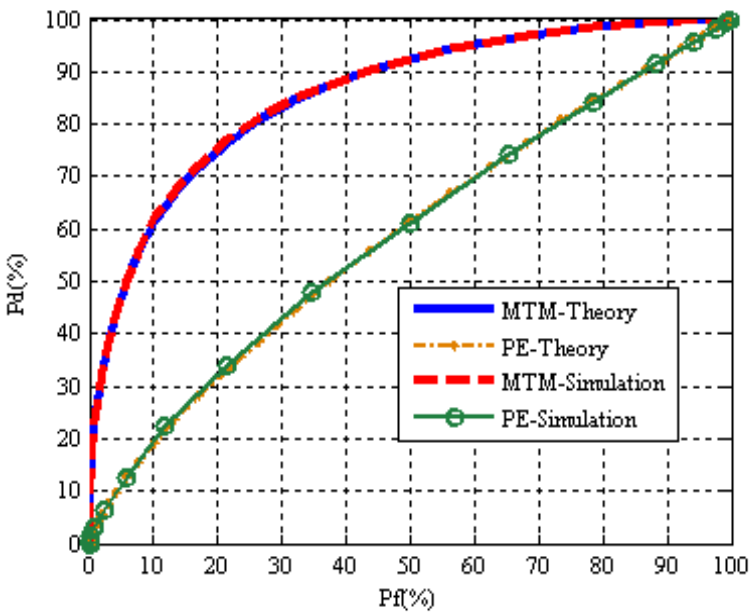

Figure 4.18 The ROC using MTM detector with *NW*=4 and 5 tapers and the PE at AWGN with SNR=-10dB and $L = 20$ OFDM blocks.

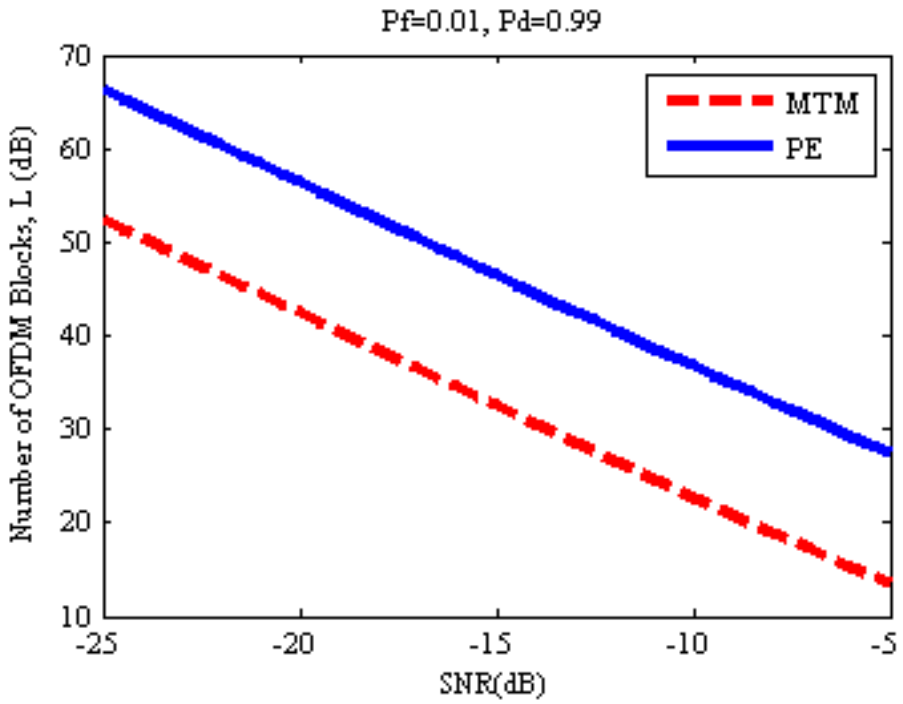

Figure 4.19 Comparison between the MTM with *NW*=4 and 5 tapers and the PE in term of the numbers of OFDM blocks, L, required to achieve $P_d = 99\%$, and $P_f = 1\%$ at AWGN with different SNR using.

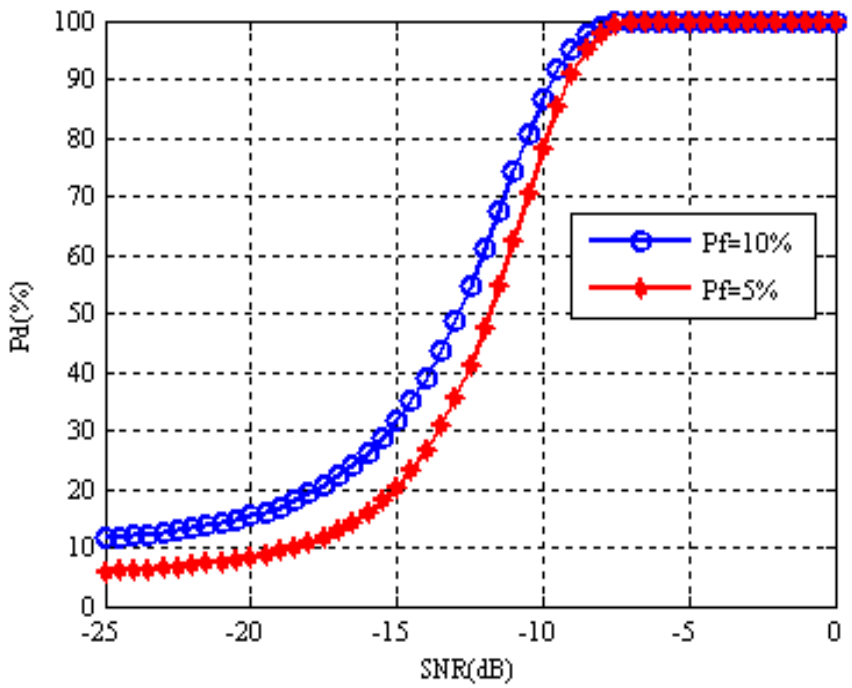

Figure 4.20 Probability of detection, $P_d(\%)$, that meets $P_f = 5$ and 10% versus the SNR at AWGN using MTM with *NW*=4 and 5 taper and $L = 50$ samples for spectrum sensing.

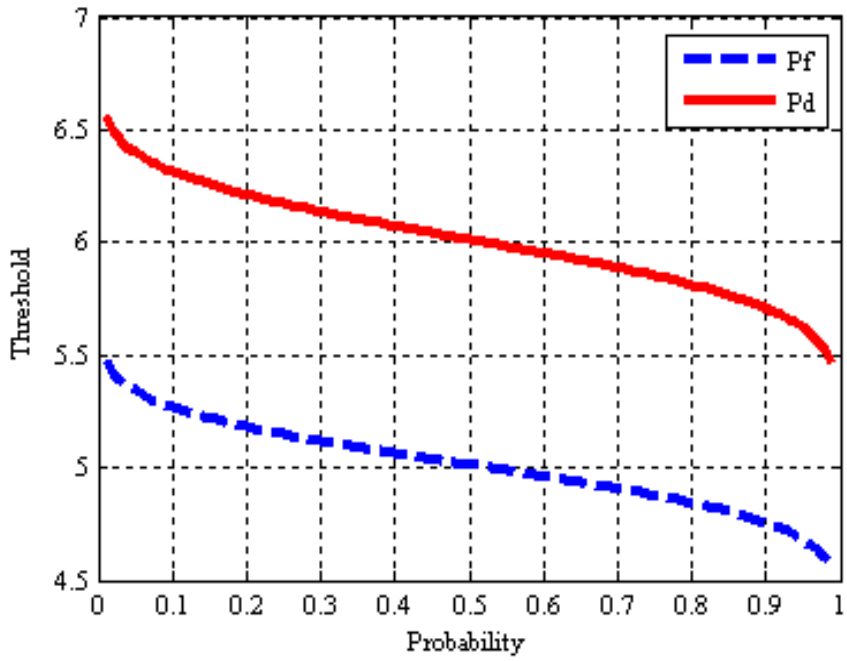

Figure 4.21 Threshold versus P_d and P_f when MTM with NW=4 and 5 tapers is used at AWGN with SNR=-7dB and $L = 50$ samples.

Figure 4.22 Shows the ROC curves for the MTM, Auto.Corr, and cooperative SD with G=2, and 3 CR users based spectrum sensing techniques at AWGN with SNRs= -10dB, and $L = 20$. The Auto.Corr and SD based spectrum sensing techniques are defined here based on the information that has been given under subsection 4.5.8.

The N_{CP} and N are assumed as 8 and 32 respectively following the same work in [144]. It is clear from the figure, the MTM outperforms both techniques in the same conditions. At P_f=10%, the P_d is found as 60% using the MTM for spectrum sensing and 30% using Auto.Corr based spectrum sensing. Furthermore, the MTM using a single CR user gives higher P_d than using 2 or 3 CR users in SD based spectrum sensing techniques. Using 3 CR users in the cooperative SD based spectrum sensing technique gives P_d as 50% at P_f=10%, while using MTM by one CR user gives P_d as 60%. Therefore, MTM gives a better performance compared to the Auto.Corr and outperforms SD which is

based on cooperation. Moreover, the Auto.Corr technique exploits the CP prior knowledge. However, such CP is available only in OFDM based systems which makes this technique useful in such cases and can not be used widely in sensing different PR signals. Meanwhile, the MTM can be used to detect the energy in a wide frequency band with high performance and without need for prior information about the PR signal. The Auto.Corr itself is affected significantly by the length of the CP. Thus, further disadvantage is added to the use of Auto.Corr for OFDM based CR spectrum sensing. Figure 4.23 shows the ROC curves for Auto.Corr with N=64, and N_{CP}=0, 4, 8, and 16 at AWGN with SNR=-10dB and $L = 20$. As can be seen from the figure, as the N_{CP} is increased, the P_d increases and vice versa. The P_d is found as 10%, 15%, 22%, and 40% for N_{CP}=0, 4, 8, and 16 respectively when the P_f is fixed to 10%.

The third part of this subsection deals with Rayleigh flat and multipath fading wireless environments. Let us assume the channel between the PR Tx and CR Rx is flat over the frequency subband. This type of fading is also called non selective slow fading since $|H(f_i)|^2$, the channel response magnitude, is flat over the frequency subband.

In the multipath fading, the channel magnitude response, $|H(f_i)|^2 \leq 1$, varies over the frequency subband producing a frequency selective multipath channel. In our simulation, a Rayleigh channel model consisting of three paths (i.e., P=3) is used. The power delay profile is exponential. Each multipath component is assumed as an independent and identically distributed zero mean Gaussian random variable. A number of six symbols are used as CP by the PR Tx (i.e., N_{CP}=6). At the CR Rx, such CP is removed before implementing MTM for spectrum sensing. Note that the total number of samples used here is $(L) \times (N + N_{CP})$ which approximately corresponds to sensing time $(L) \times (N + N_{CP}) \times (Ts)$.

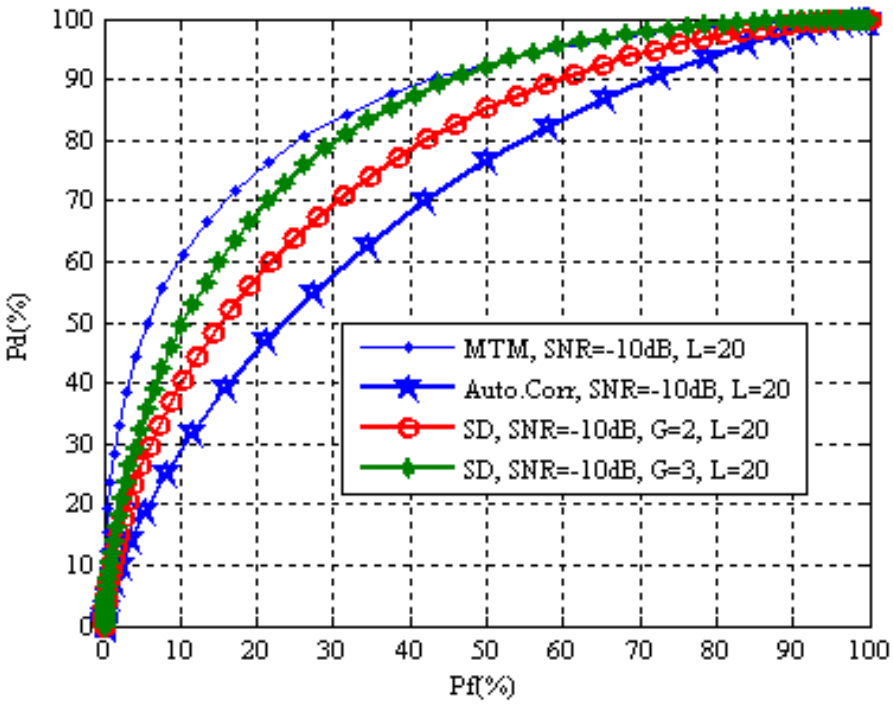

Figure 4.22 The ROC curves when MTM, Auto.Corr, and cooperative SD with G=2, and 3 CR users are used at AWGN with SNRs= -10dB and $L = 20$.

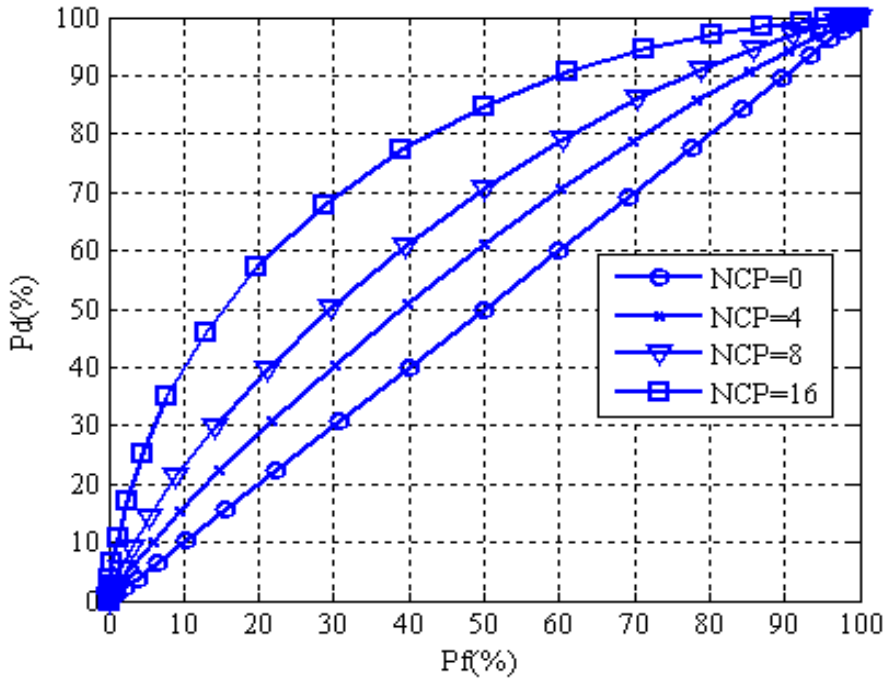

Figure 4.23 The ROC curves when Auto.Corr is used with N=64 and N_{CP}=0, 4, 8, and 16 at AWGN with SNRs= -10dB and $L = 20$.

Figure 4.24 shows the ROC curves when MTM and PE are used for spectrum sensing at Rayleigh flat fading with SNR=-5dB and $L = 20$. The figure shows how the MTM outperforms the PE in such fading environment. MTM gives P_d as 75%, while PE gives 61% when the P_f is fixed to 10% and in the same conditions.

Figure 4.25 shows the ROC curves for both MTM and PE spectrum sensing techniques at multipath fading with P=3 paths and $N_{CP} = 6$ is used as a CP where SNR=0, and -10dB and $L = 20$. It can be seen from the figure how the multipath fading wireless channel degrades the MTM and PE performances. If we compare the results from this figure and that from Figure 4.18 for both techniques at SNR= -10dB, the MTM probability of detection in Figure 4.25 is decreased by 20% at P_f=10% due to the multipath fading effect. The PE probability of detection in Figure 4.25 is decreased by 10% at the same P_f. However, MTM still outperforms the PE in terms of performance. At SNR=0dB and in the same condition, the MTM gives P_d as 90% while PE gives 72% when P_f is fixed to 10% as can be seen from Figure 4.25. The increase in the SNR improves the performance for both techniques.

In order to examine the effect of the increase in the number of sensed OFDM blocks, L, Figure 4.26 shows the ROC curves of the MTM at multipath fading with P=3 paths and $N_{CP} = 6$ is used as a CP where SNR= -10dB and $L = 20$, and 100. The figure shows the improvement that can be achieved by increasing the number of the sensed OFDM blocks L. By increasing the number of OFDM blocks from 20 to 100, the P_d is increased by 22% when P_f is fixed to 10%. Note that, such an improvement comes at the expense of the longer time which is required time to discover the PR frequency subband vacancy. The total number of samples used in the 100 OFDM blocks case is $(L = 100) \times (N + N_{CP} = 64 + 6 = 70) =$ 7000, which approximately corresponds to sensing time$(700) \times (Ts = 0.05\mu s) = 350\mu s$.

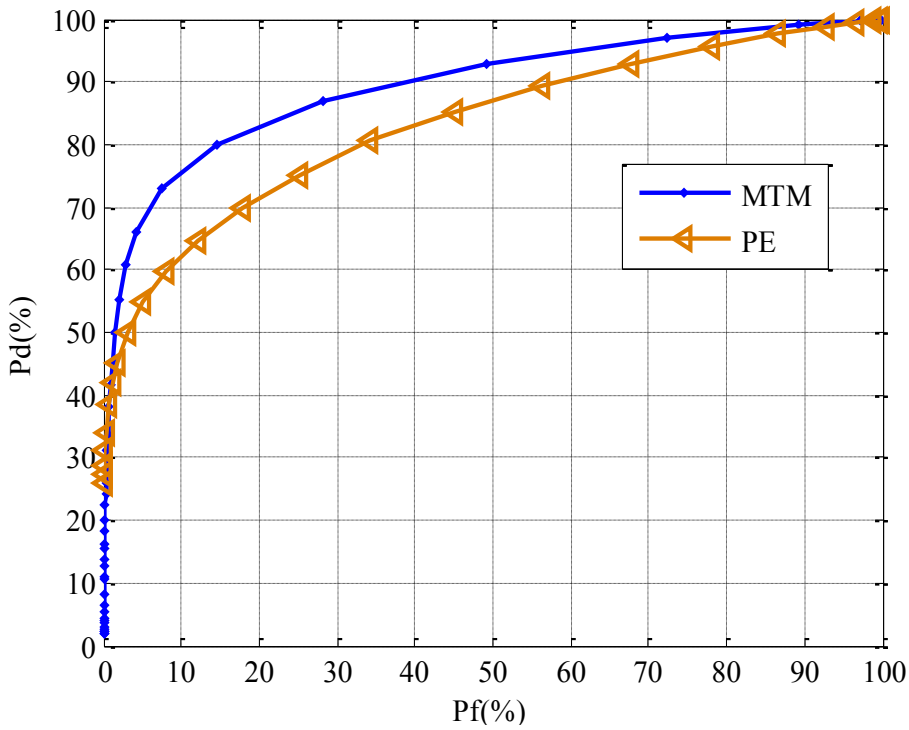

Figure 4.24 The ROC curves when MTM and PE are used at Rayleigh flat fading with SNR=-5dB and $L = 20$.

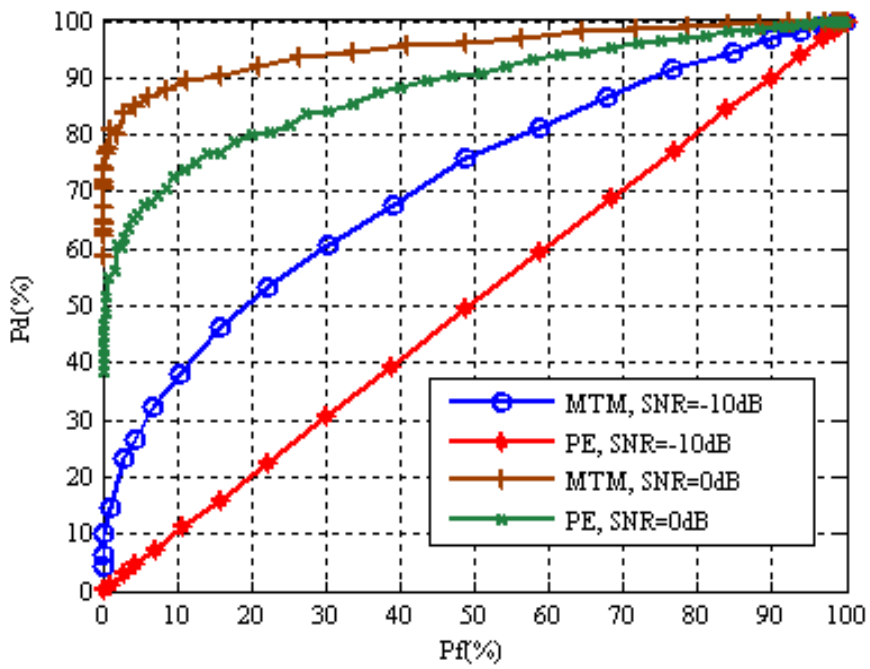

Figure 4.25 The ROC curves when MTM and PE are used at multipath fading with P=3 paths and $N_{CP} = 6$ is used as a CP where SNR=0, and -10dB and $L = 20$.

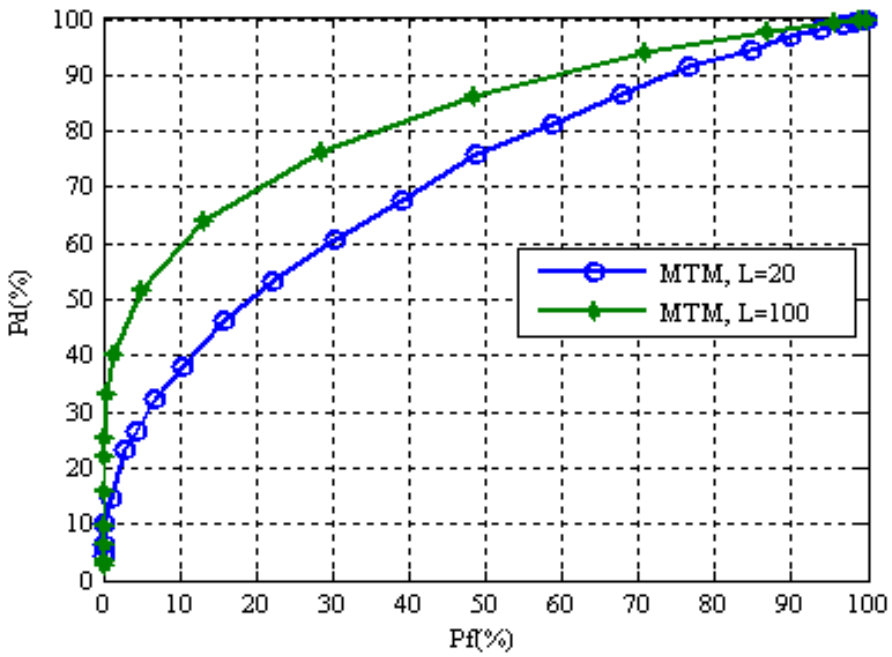

Figure 4.26 The ROC curve when MTM is used at multipath fading with P=3 paths and $N_{CP} = 6$ is used as a CP where SNR= -10dB and $L = 20$, and 100.

As has been mentioned under subsection 2.4.1, the longer the sensing duration, the more accurate sensing decisions can be achieved. However, too long a sensing duration may minimize the CR network throughput, even if it protects the PR frequency band from interference [73, 155]. The trade-off between the sensing duration and the CR network throughput has been tolerated as an optimization problem (as shown in Figure 2.9) in much of the work in the literature as has been mentioned in subsection 2.4.1.

It is interesting now to know the reason behind such improvement in the considered techniques in this thesis. Figure 4.27 shows the averaging over L samples (i.e., L OFDM blocks) process in the MTM systems under consideration which have been applied through all similar techniques in this thesis. Where $l = 1,2, \dots, L$ represents the samples from different L OFDM blocks and $t = 0,1, \dots, N - 1$ represents the samples from each OFDM block (i.e., each FFT).

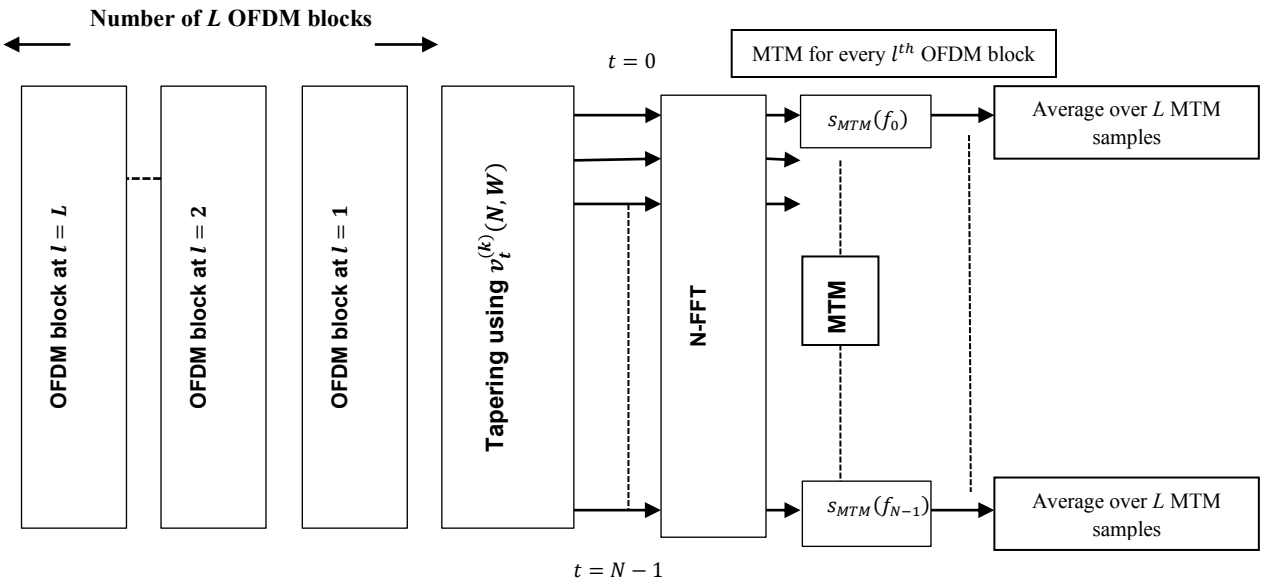

Figure 4. 27 The averaging over L samples (i.e., L OFDM blocks) process in the systems under consideration.

The decrease in the variation in the noise power level is achieved by increasing the averaging over a number of different L samples where the noise samples are independent [156]. Such an increase in L, then, causes an improvement in the spectrum sensing performance by increasing the possibility of distinguishing between the noise and noise added to signal levels. Figures 4.28 and 4.29 show the PDFs versus threshold of noise and noise added to signal cases for L=2, and 100 samples respectively when MTM is used with NW=4 and K =5 tapers at AWGN with SNR=−5dB. This provides an example to understand the reason behind such improvement when L is increased. It is clear from Figure 4.28 that represents L=2, detector faces difficulty in distinguishing between the noise and noise added to signal case along the x-axis due to the small number of sensed samples (i.e., L=2). This can be resolved by increasing the sensed samples to L=100 as in Figure 4.29, where the noise and noise added to signal cases can be distinguished easily and the detection probability will be increased by the end. This is due to the reduction in the variance of the power estimate due to the increase in L.

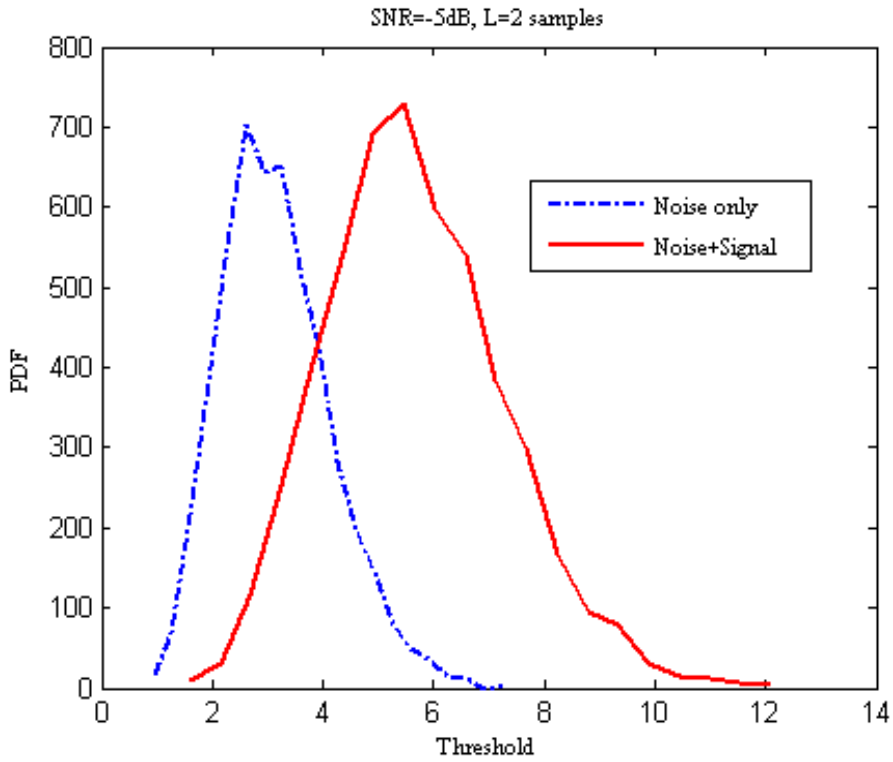

Figure 4.28 PDFs versus threshold of noise and noise added to signal cases for L=2 samples when MTM is used with NW=4 and K =5 tapers at AWGN with SNR=−5dB.

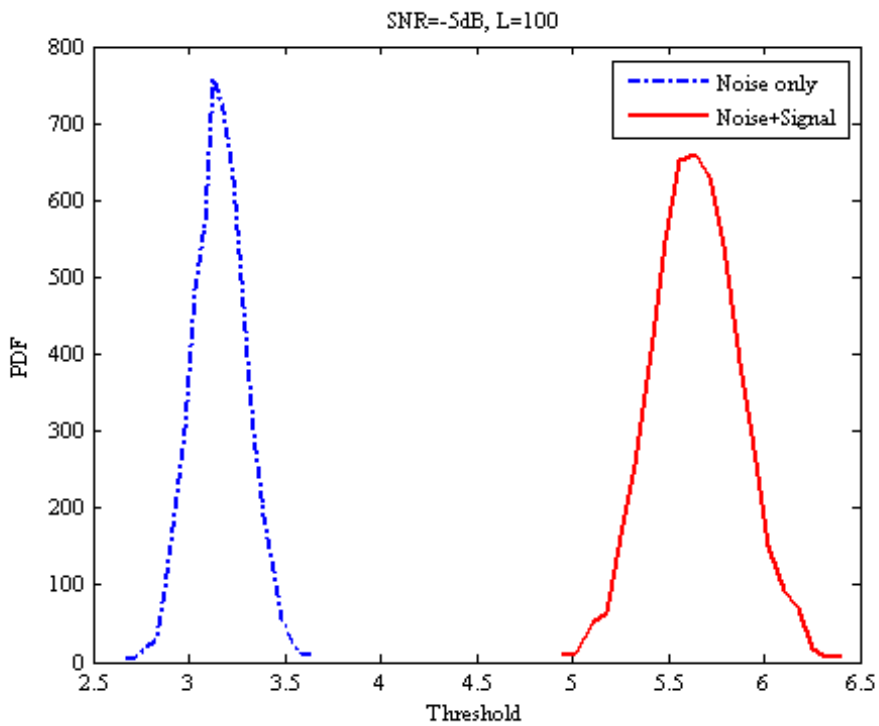

Figure 4.29 PDFs versus threshold of noise and noise added to signal cases for L=100 samples when MTM is used with NW=4 and K =5 tapers at AWGN with SNR=−5dB.

4.6 Conclusion

In the first part of chapter 4 within sections 4.2-4.4, we have investigated the effects of the system parameters, within the ranges suggested in the literature, on the performance of the MTM spectrum sensing for opportunistic use by OFDM-based CR users. We have examined the MTM parameters to find their optimality to give a higher probability of detection at a lower probability of false alarm, and minimal complexity. The MTM technique has been analysed and simulated in AWGN. Our PR and CR users were communicating through OFDM-based systems with 64- IFFT/FFT. This has been published in [2].

Although the first few tapers (i.e., DPSS)) have the best spectral leakage properties, we found that they give the worst performance in terms of detection and false alarm probabilities. We found that an unwise choice of the half time bandwidth NW and number of tapers K from the range suggested in [147] produces catastrophic false alarms in the system. In our chosen 64-IFFT/FFT systems, the optimal number of tapers was 5 for the NW=4, 8, and 16 cases, and the optimal half time bandwidth product is given by NW=4 for 10% false alarm when the system is operating in AWGN channel with SNR= -5 dB. For cases where NW< 4, for example when NW=2, the bad bias properties of the tapers overcome the high resolution in this system. Generally, 5 tapers and half time bandwidth NW=4 can be considered as optimal parameters for different FFT-sizes in OFDM-based CR systems (e.g., 128, 256, 512,.., etc), since the change in FFT affects the resolution only.

In the second part of chapter 4, which lies under section 4.5, we have derived closed-form formulae for the probabilities of false alarm, detection, and miss detection as functions of the parameters of the MTM spectrum detector such as threshold, number of sensed blocks L, number of tapers, eigenvalues of the DPSS, PR signal power and the

noise power. This has been published in [3, 4]. These probabilities control the performance of the MTM-based spectrum sensing detector. Additionally, MTM probabilities can be used to choose the appropriate threshold that maximizes the probability of detection at a fixed probability of false alarm.

In the process of the derivation, we defined the PDF of the MTM decision statistic using simulation and theoretical work. Statistical characteristics, such as the mean, and the variance of the distribution have been derived for different hypotheses.

The simulation and analytical works here included different wireless environments, AWGN, flat Rayleigh and multipath fading. Comparing the performance of the MTM spectrum sensing detector to that of the PE, we found the MTM detector outperforms the performance of the PE by about a 40% increase in the probability of detection at fixed probability of false alarm 10% at AWGN with SNR= -10dB and $L = 20$. Furthermore the PE requires 25 times the number of samples to achieve the same probabilities of detection and false alarm given by the MTM detector operating under the same conditions. Auto.Corr has many disadvantages, since it depends on CP exploitation in OFDM based CR systems. This makes such spectrum sensing technique work only in environments where the PR user is OFDM based. Furthermore, it requires prior information about the PR CP and its frequency subbands. The results show how the MTM outperforms the Auto.Corr significantly. Furthermore, the SD based cooperative spectrum sensing techniques, which are based on Auto.Corr, require cooperation between more than four CRs to outperform the MTM performance.

4.7 Chapter Summary

Two main objectives were studied and investigated in this chapter. Firstly, the MTM parameters that significantly affected the MTM performance and complexity were required to be optimized in order to use the MTM for spectrum sensing in CR

systems in an efficient manner, and with lower complexity. The parameters are known as the half time bandwidth product NW, and the number of used tapers, K. Therefore, the chapter started with a deep technical focus on such parameters and their effect on the MTM performance. This included different examples that showed how different parameter choices can affect the MTM performance in terms of spectral leakage and large variance of estimate.

After understanding the effects of such parameters, the problem was formulated in a way that took into account the spectral leakage and variance of estimate in the evaluation of the MTM performance. A Monte Carlo simulation programme was then developed in order to find the optimal parameters for 64-FFT based CR systems. The optimal NW and K were found as 4 and 5 respectively. The optimization problem was investigated in different conditions and assumptions such as fading environments and the FFT size effects on the OFDM based CR system. The results showed how the use of the optimal parameters can give the highest performance and using K=5tapers limits the complexity of the MTM compared to $K > 5$ cases.

Secondly, the optimal MTM based detector design was the other main objective in this chapter. Such a design was carried out via a number of steps. The first step was the study of the statistical histogram of the MTM decision statistic for different hypotheses using simulation in different wireless environments and conditions. Based on this, the PDF of the MTM decision statistic was found as Gaussian distribution, referring the central limit theorem. The different MTM probabilities formulae were derived using the Neyman Pearson criterion. The number of sensed samples, L, and the chosen threshold were also derived theoretically.

Simulation codes were written in order to examine the MTM optimal detector for OFDM based CR systems. The results showed how our theoretical works match the simulation well. Furthermore, the MTM based spectrum sensing technique was

compared to the PE, Auto.corr, and SD cooperative spectrums sensing. It was found that MTM outperforms all mentioned techniques. The MTM and the PE were examined in Rayleigh flat and multipath fading wireless environments using a simulation. The fading environments degraded the MTM and PE performance; however, MTM still outperformed PE under the same conditions.

Chapter 5: The Proposed Optimal and Suboptimal Multi Antenna Based Spectrum Sensing Techniques for CR Systems

5.1 Introduction

In section 2.4.3.1 of this thesis, local cooperative spectrum sensing using multi antenna at CR Rx is generally reviewed. As has been mentioned, using multi antenna in classical wireless communications allows an increase in the data rate and an improvement in the spatial diversity. Consequently, this chapter aims to improve the local spectrum sensing in CR systems by proposing multi antenna techniques at the CR Rx. This means that the spatial diversity using multi antenna is exploited here in order to improve the local spectrum sensing performance at CR Rx.

MTM based one optimal and two suboptimal multi antenna spectrum sensing techniques are proposed in this chapter. In addition to the achieved spatial diversity when multi antenna are used in spectrum sensing, the MTM features that were discussed in chapters 3 and 4 support the multi antenna based spectrum sensing and improve the performance as well.

Before we start focusing on the proposed multi antenna spectrum sensing techniques, a review about the multi antenna systems and concepts in classical wireless communications will be provided in section 5.2. Then, the use of multi antenna for CR spectrum sensing will be outlined in section 5.3.

After defining the system model of such a case in section 5.4, the different proposed multi antenna based spectrum sensing techniques will be discussed under section 5.5. This includes deep technical descriptions of each technique, defining of the PDFs of two techniques, the different probabilities, and the number of sensed samples formulae derivations. Simulation codes are written to evaluate the different proposed

techniques and compare them to the theoretical works. The simulation environments in the results are AWGN, Rayleigh flat fading and multipath fading wireless environments.

The main content of this chapter has been published in two papers that represent the chapter contributions. The published papers are:

O. A. Alghamdi and M. A. Abu-Rgheff, "Local MTM-SVD based spectrum sensing in SIMO OFDM cognitive radio under bandwidth constraint," in *Proc. 5th IEEE International Conference on Cognitive Radio Oriented Wireless Networks & Communications (CROWNCOM'10)*, 2010, pp. 1-6.

O. A. Alghamdi and M. Z. Ahmed, "Optimal and Suboptimal Multi Antenna Spectrum Sensing Techniques with Master Node Cooperation for Cognitive Radio Systems," *Journal of Communications (JCM),* vol. 6, pp. 512-523, 2011.

5.2 Using Multi Antenna in Classical Wireless Communications

In wireless communications, multi path fading is one of the greatest challenges to overcome, as it degrades the communication performance between two ends (i.e., Tx and Rx ends). This is due to the destructive adding of the reflected signal copies at the Rx end. Diversity techniques can mitigate such channel impairments in wireless communications systems [157]. *Temporal*, *frequency*, and *spatial* diversities are the main diversity techniques [157]. *Temporal* diversity uses channel coding to mitigate the problem of fading. In addition to the loss in the bandwidth efficiency, more delay occurs in this type of diversity. The *frequency* diversity is applicable in broadband communications, where the energy from different paths can be estimated using ML. Such type of diversity can not be used in narrowband communications.

Spatial diversity is based on the use of multi antenna at the Tx and/or the Rx in

order to receive the signal form independent fading paths. This would increase the possibility that at least one of the different paths does not suffer from deep fading [15]. *Spatial* diversity improves the performance and, at the same time, no more bandwidth or transmitted power is required to achieve such improvement [158]. Therefore, the *spatial* diversity, generally, aims to achieve independent fading signal paths using multi antenna. The improvement in performance includes: an increase in the SNR which is called *array* gain, and a change in the slope of the error probability which is called *diversity* gain [15].

The concept of using MIMO systems in wireless communications traces back to 1984, when Winters provided a study of evaluating the performance of the optimal combiner for *spatial* diversity in cellular mobile radio systems [159]. His results show how improvements in performance can be achieved by using MIMO. The achieved improvements are not only by mitigating fading effect in such types of combining techniques; an increase in the SNR is significant. Since that time, more and more advanced studies have contributed to *spatial* diversity using MIMO as in [159-165]. Foschini in [161] proposed an advanced MIMO based communication technique between Tx and Rx in Rayleigh fading environment, where the Tx does not have knowledge about CSI. This technique is called as Bell lab layered space-time (BLSAT). It simply divides the data stream into sub streams and allocates antenna to transmit each sub stream over the same frequency bandwidth. Therefore, the sub streams can be transmitted simultaneously using different antennas without the need for an increase in the bandwidth or the transmitted power. This is called *spatial multiplexing* [157], and it is found that the capacity of such a system is scaled linearly by M when the Tx and Rx have the same number of antennas M [161, 164]. This increase in capacity requires the availability of rich fading environment between Tx and Rx, and perfect knowledge of the channel parameters at Rx [161, 164]. Space time coding (STC) [166], is another

multi antenna based communication technique. It supports the multi antenna based communication system by both *spatial* and *coding* gain diversities. STC has mainly three advantages [157]:1) The down link performance is improved with no need for multi antenna at the terminals' Rxs, 2) the channel coding can be used in STC for *coding gain* diversity achievement, and 3) the CSI is not required at the Tx side. The space time trellis codes (STTC) [166] is one of the two main STC types. In STTC, the information bits are mapped into M symbols using STTC encoder; where M represents the number of transmit antennas. The mapped M symbols are then transmitted simultaneously using the different transmit antennas. The main problem with using STTC is the decoding complexity. The increase in the STTC decoding complexity is found to be exponential, and depends on the transmission rate and the level of diversity. The second type of STC is the space time block codes (STBC). In contrast to STTC, STBC mainly focuses on providing high spatial diversity with low decoding complexity. Alamouti code [167] is one of the well-known STBC that improves the performance using two antennas at the Tx and one antenna at the Rx. In Alamouti code, at the initial time instant, the two data symbols s_1 and s_2 are sent in antenna one and antenna two respectively, at the Tx end. After symbol time duration, the symbols $-s_2^*$ and s_1^* will be transmitted in antenna one and antenna two respectively, at the Tx end. The reception at the Rx consists of combining the different formats, the different times, symbols, and applying ML for detection. However, Alamouti code does not provide *coding gain* diversity, and its decoding simplicity is in Rayleigh flat fading only.

Referring back to the *spatial* diversity concept, *transmit* diversity and *receive* diversity are the main categories under *spatial* diversity. Alamouti code is an example of the *transmit* diversity. *Transmit* diversity is more practical in the down link (e.g., link between BS and terminals) due to the decrease in the cost and complexity; however, it requires an advanced signal processing at the Rxs to efficiently detect the desired

transmitted signal. Another challenge of *transmit* diversity is the generation of correlated signal samples from the main signal without CSI at the Tx [157]. In the *receive* diversity, the transmitted signal is received through a number of antennas at the Rx and then combined, exploiting the positive effect of the independent signal paths. The improvement in the performance or in the SNR becomes lower with the increase in the number of antennas for both *transmit* and *receive* diversities [166].The situation is different in *spatial multiplexing* techniques, where the increase in the capacity increases linearly with the number of antennas [157].

As has been discussed above, *receive spatial* diversity is based on combining independent signal paths at the Rx using a number of antennas. The combining techniques are divided based on the type of combiner into [15, 168]: 1) Linear combiner, 2) Selection combiner, 3) threshold combiner, and 4) squared law combiner [169].

Note that as the Rx surrounding environment contains many scattering objects, a rich fading environment can be achieved at the Rx. Generally, the half wavelength, 0.5λ, separation distance between two adjacent antennas at the Rx or Tx is enough (i.e., $\geq 0.5\lambda$) to achieve independent paths in mobile communications. The wavelength is defined as $\lambda = \frac{C_s}{f_c}$, where C_s=3×10^8 meters/seconds, is the light speed, and f_c is the carrier frequency [159, 161]. Inside buildings sufficient distance separation between two adjacent antennas to achieve independent fading paths would be 0.25λ [170]. This is due to the rich environment of objects and walls that surround the Tx or the Rx inside building.

General reviews about the different combiners can be seen below.

Linear combiner:

In linear combiner (LC), the transmitted signal, *s(l)*, from the Tx arrives at the Rx through different independent paths as different copies of the original one. In this

process, the original signal *s(l)* is affected by the phase, Θ_m, and the amplitude, v_m, of the mth path. Therefore, co-phasing process is necessary to eliminate the effect of the mth branch phase before combining linearly the branches signals. Figure 5.1 shows a schematic diagram of the linear combiner. The signals copies that are received through different antenna branches need to be co-phased by multiplying the mth branch received signal by factor $C_m = c_m e^{-j\Theta_m}$, where c_m is real, and then, the output from this multiplication is $c_m v_m e^{-j\Theta_m + j\Theta_m} s(l) = c_m v_m s(l)$. Therefore, the effect of the mth branch phase has been removed, the signals can be added up constructively. This type of combiner requires channel parameters estimations to complete the co-phasing, which is a wide subject in itself, and there are many types of channel parameters estimation methods in the literature. The way of controlling the number c_m, determines the specific type of the linear combiner. In *equal gain*-LC, the number c_m is assumed as one, and based on this, all antenna branches have the same effect on the performance, in *maximum-ratio*-LC, the c_m is given a weight based on how much the mth branch has suffered from fading. Therefore, the more affected the branch the less weight is given to that branch. The LC does not improve only the *diversity* gain, it also increases the SNR. In AWGN, when each branch has SNR=1 as an example, the resulting SNR from using LC becomes $M \times$SNR=M [15].

Selection combiner:

Selection combiner is distinguished from the LC as it is based on detecting the signal from only one antenna branch. This antenna branch has the highest SNR is being nominated by the combiner. Consequently, only one Rx is required in such cases which should be able to be connect to the different antenna branches based on the highest SNR. Unfortunately, a dedicated Rx for each antenna branch in cases that require continues monitoring of the SNR (i.e., continuous transmission) is needed to keep the

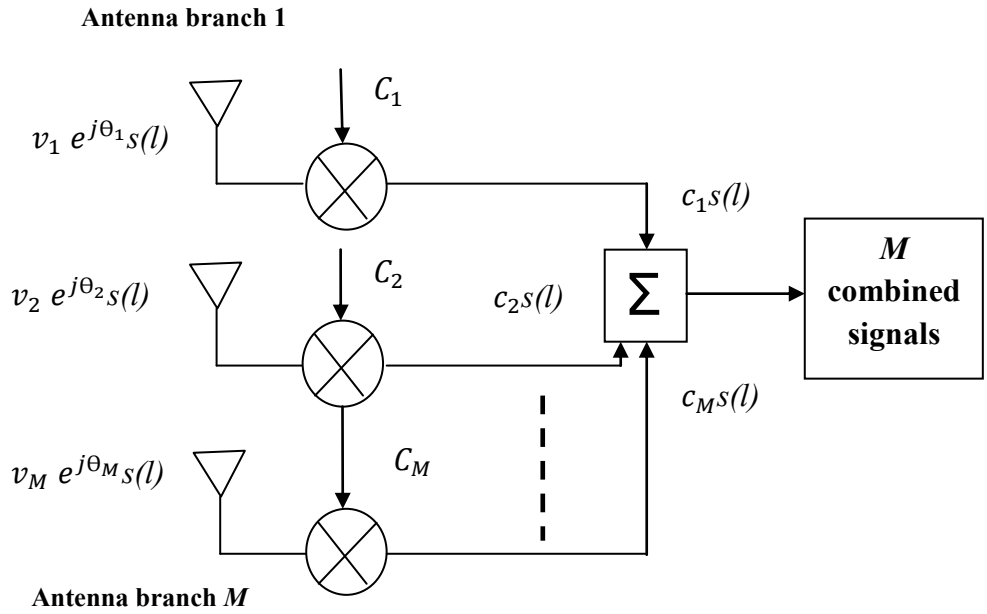

Figure 5.1 Schematic diagram of the linear combiner.

Rx connected to the highest SNR branch [15]. The co-phasing here is required only for the nominated antenna branch. The *threshold* combiner is one of the combiner's types under *selection* combiner. It is also called as *scanning* combiner, since its work is based on the scanning of the different antenna branches' SNR in sequential order until the branch with SNR that is greater than a predefined threshold is found. The Rx can then be switched to that branch finally and there is therefore no need for dedicated Rx in such combiners. In cases when the different antenna branches have the same SNR, the use of such combining techniques gives the same performance when single antenna is used.

Square law combiner:

Figure 5.2 shows a schematic diagram of classical square law combiner (SLC). The transmitted signal that is affected by both channel fading and the Rx noise, which is written as $x_m(l)$ for the mth antenna branch, is squared for each antenna branch output. The squared copies of the original signal are then added finally. The co-phasing process is not required here, and this can be called non coherent detection. The SLC is used

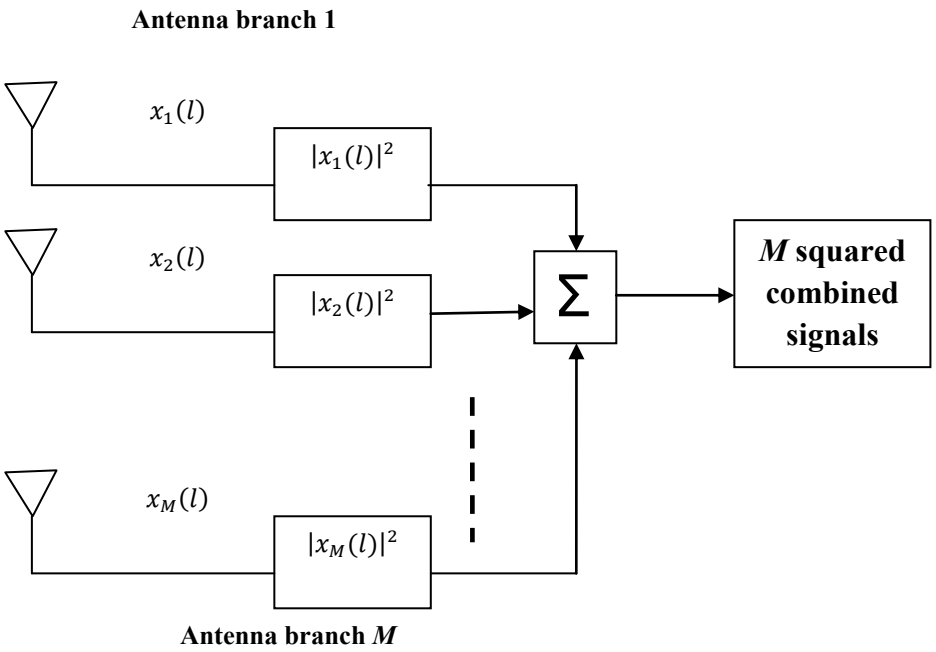

Figure 5.2 Schematic diagram of a classical square law combiner.

widely in radar sonar applications [171], and is preferred due to its simplicity.

Prior to this point, an extensive revision of the use of multi antenna in classical wireless communications has been provided. All that has been discussed illustrates how using multi antenna is very important in wireless communications.

The use of multi antenna became interesting for both research and commercial lines. For example, the use of MIMO is considered as one of the standardization requirements that support the commercial production of long term evolution (LTE) on Evolved universal mobile telecommunications system (UMTS) Terrestrial Radio Access (E-UTRA) [172]. In OFDM based wireless standards, the MIMO is useful in practice, since the CP insertion in OFDM based systems simplifies the equalization [28]. The IEEE802 standardization group considered the use of MIMO in IEEE802.16 to improve the system performance [56, 158].

5.3 Using Multi Antenna in Cognitive Radio Systems

As a summary of section 5.2, the use of multi antenna in wireless communications,

generally, supports the communication process by the following advantages:

1. Increases the data rate.
2. Increases the capacity.
3. Mitigates the channel fading effect.
4. Increases the SNR.

Moreover, using multi antenna can improve the user position estimation (i.e., geo location purposes) such as in emergency and security based wireless systems, by estimating the angle of arrival (AOR) of the signal from the Tx [173]. Consequentially, all these advantages of using multi antenna are still useful in CR communications. The use of multi antenna in CR systems improves the performance of:

1. Communications between CR users.
2. Spectrum sensing of the PR signal existence within frequency subband.

In terms of communication performance improvement (e.g., capacity increase, data rate increase, channel effect mitigation…etc), the use of multi antenna for such purposes in CR systems has been studied in a number of academic researches. In [174], the authors proposed an opportunistic spectrum sharing scheme to maximize the throughput of the downlink between the CR-BS and the CR users while keeping the interference to the PR user limited. This was achieved by implementing a multi antenna system at the CR-BS. Their work is extended to examine employing multi antenna at the Rxs of CR users. It is found that the Rx multi antenna at CR users maximizes the throughput and minimizes the feedback complexity. The work in [175], aimed to maximize the throughput in MIMO based CR systems under constraint of interference to the PR user. The work included the study of three different scenarios about the degree of the CR Tx knowledge about the channel parameters to the CR Rx. They are called, complete, partial, or no knowledge scenarios.

As has been provided in subsection 2.4.3.1, different multi antenna based spectrum sensing techniques are proposed in the literature to improve the spectrum sensing performance in CR systems. We call these types of techniques local cooperative spectrum sensing techniques since the cooperation is based on a number of antennas cooperate sensing the PR signal at the same CR Rx. Before we start focusing on the system model and the proposed multi antenna spectrum sensing techniques, a review about the available multi antenna spectrum sensing techniques in the literature will be provided (see also section 2.4.3.1). These techniques fall, mainly, under two categories as:

1. Multi antenna PE based spectrum sensing techniques:

   The proposed PE- based multi antenna spectrum sensing techniques, generally, use one of the Rx combiner techniques discussed in section 5.2; *linear*, s*election*, and s*quare* law combiners to combine the PR independent paths received signals at the CR Rx. The PE, which is based on estimating the energy over L time samples by summing the square absolute of those samples, can be done after linearly combining the PR signal copies at the CR Rx, or by combining the resultant estimated energy over all antenna branches. In *selection* combiner based, the PE is applied to the antenna branch with the highest SNR. Note that the PE is the ED but in multi band (i.e., ED of the FFT frequency bins). Another PE multi antenna based CR spectrum sensing technique applies the PE at each antenna branch and decides about the existence of the PR if the majority of the antenna branches decide that. Subsection 2.4.3.1 contains more information about the publications of such techniques.

2. Multi antenna GLRD based spectrum sensing techniques:

   GLRD is a well known detection technique in signal detection theory [87]. It is based on estimating the unknown parameters of the LRT in (2.12) using ML. The

unknown parameters are signal variance and/or noise variance, and/or channel gains. Consequently, the GLRD requires the ML estimation for any unknown parameters of the PDFs in the LRT that makes it blind or semi blind in its main philosophy. The multi antenna GLRD based spectrum sensing techniques that have been reviewed in subsection 2.4.3.1, generally, receive the transmitted PR signal copies under different assumptions and conditions through M antennas at the CR Rx. Then, the LRT (refer to (2.12) sub section 2.4.2.1.4) test is constructed assuming that the PDFs have Gaussian distributions for the different hypothesis, but with different unknown parameters which will be estimated using ML, as has been said. The use of ML in GLRD increases the computational complexity, and the GLRD's performance is based on estimating the unknown parameters.

5.4 The Proposed Multi Antenna Based Spectrum Sensing Techniques

In order to support the research in this field, two sub optimal and one optimal multi antenna spectrum sensing techniques are proposed in this chapter. The proposed techniques are mainly based on using the MTM to estimate the power over a wide frequency band (i.e., through the frequency bins of the CR Rx). Consequently, in addition to the performance improvement that can be achieved by exploiting *spatial* diversity using multi antenna, the *bias-variance dilemma* can also be mitigated due to the use of the MTM.

In the remaining parts of this chapter, we consider CR spectrum sensing using multi antenna to detect an IFFT/FFT PR's transmitted signal (e.g., OFDM). Our CR user is assumed to be an IFFT/FFT based signal processing. This will allow for the practical use of MTM in spectrum sensing.

We propose the use of linear combiner-MTM based (MTM-LC) spectrum sensing,

which is optimal when the channel coefficients can be known by CR, and this is possible when the PR's signaling is known. The linear combining here increases the SNR [15], and using MTM minimizes the spectral leakage, and improves the variance of the estimate. Two suboptimal multi antenna spectrum sensing techniques have also been proposed; square low combining-MTM based (MTM-SLC) and Local-MTM-SVD (LMS). In MTM-SLC, the MTM is performed through each antenna separately, and then the final spectrum estimate can be averaged over all the antennas' estimates. MTM-SLC improves the performance at low SNR, and does not require coherent detection. The LMS combines the received signals from the different antenna branches of the CR Rx and then constructs the spatio temporal matrix, which contains the different eigenspectrums from different tapers and different antenna branches. By applying SVD to the spatio temporal matrix, the PR's transmitted signal power, over the frequency bins, can be isolated from the noise.

Our proposed techniques have been derived theoretically and compared to simulation. The same techniques have been derived as well for PE and comparison between different techniques is presented in the results. Decision statistics' PDFs of the proposed LC and SLC based techniques have been defined for different hypothesis in different cases for both MTM, and PE.

5.5 System Model

The system model here is similar to that in section 4.4 and subsection 4.5.1 but with the existing of number of antennas at the CR Rx. However, we find that rewriting the equations and the system information for multi antenna case in this section is important to maintain seamless understanding. In our system model, number of antennas M is added to the CR for both spectrum sensing and communications as well. Figure 2.16 shows a representative diagram of multi antenna based spectrum sensing in

CR's systems.

The received PR signal, at the CR receiver, is sampled to generate a finite discrete time samples series $\{x_t^m; t = 0,1,\dots,N-1, m = 1,\dots,M\}$, where m denotes the antenna number, and t is time index. The discrete time samples are dot multiplied with different tapers $v_{(t,k)}(N,W)$ (tapers are DPSS). The associated eigenvalue of the kth taper is $\lambda_k(N,W)$.

The binary hypothesis test for CR spectrum sensing at the lth time, and using the mth antenna branch is given by [87]:

$$\mathcal{H}_0: \quad x_{t,m}(l) = w_{t,m}(l)$$

$$\mathcal{H}_1: \quad x_{t,m}(l) = s_t(l) + w_{t,m}(l) \tag{5.1}$$

where l = 0,1,…,L-1 is OFDM block's index, $x_{t,m}(l)$, $w_{t,m}(l)$, and $s_t(l)$ denote the CR received, noise at the branch m, and PR's transmitted samples. The transmitted PR signal is distorted by the zero mean AWGN, $w_{t,m}(l) \sim \mathcal{CN}(0,\sigma_w^2)$, at the output from the different antenna branches, which are independent and with identical σ_w^2. Note that at each frequency bin of CR FFT, $\mathcal{H}_0$ indicates no PR signal present while $\mathcal{H}_1$ means there is a PR signal occupying that frequency bin.

Following the same model assumption in sections 4.4 and (section 4.4.1), the time instant l comes from the samples over different OFDM blocks; and time instant t comes from the samples from the same OFDM block (i.e., IFFT/FFT samples). Thus, the spectrum sensing time in seconds is $(L)(N)(T_s)$, where T_s represents symbol duration, L represents the number of OFDM blocks used in sensing, and N is the number of samples per OFDM block (i.e., FFT size).

For K orthonormal tapers used in the MTM, there will be K different eigenspectrums produced from the mth antenna rewritten from (3.4) to be as [29]:

$$Y_{k,m}(f_i) = \sum_{t=0}^{N-1} v_{(t,k)}(N,W)(x_{t,m}(l))e^{-j2\pi f_i t} \tag{5.2}$$

where, $f_i = 0, \frac{1}{N}, \frac{2}{N}, \ldots, \frac{N-1}{N}$ are the normalized frequency bins.

The decision statistic over L using MTM in (4.3) can be redefined for the m^{th}antenna as follows [6]:

$$D_{MTM}^{m}(f_i) = \sum_{l=0}^{L-1} \frac{\sum_{k=0}^{K-1} \lambda_k(N,W) \left|\sum_{t=0}^{N-1} v_{(t,k)}(N,W) x_{t,m}(l) e^{-j2\pi f_i t}\right|^2}{\sum_{k=0}^{K-1} \lambda_k(N,W)} \tag{5.3}$$

where $S_{MTM}^{m}(f_i) = \frac{\sum_{k=0}^{K-1} \lambda_k(N,W) \left|Y_{k,m}(f_i)\right|^2}{\sum_{k=0}^{K-1} \lambda_k(N,W)}$ [29], is the power spectrum estimate using the mth antenna.

Using the PE; the decision statistic over L in (4.10)is redefined for the mth antenna as follows [100]:

$$D_{PE}^{m}(f_i) = \frac{1}{N} \sum_{l=0}^{L-1} \left| \sum_{t=0}^{N-1} x_{t,m}(l) e^{-j2\pi f_i t} \right|^2 \tag{5.4}$$

As has been provided in chapter 4 (subsection 4.5.2), for single antenna MTM-based spectrum sensing, and according to the central limit theorem, if the number of samples L is large (i.e., $L \geq 10$), the decision statistic, $D_{MTM}^{m}(f_i)$, has asymptotically normally distributed PDF, $p\left(D_{MTM}^{m}(f_i)\right)$, with E for the mth antenna as [4]:

$$E\left[p\left(D_{MTM}^{m}(f_i)\right)\right] = \begin{cases} LK\sigma_w^2 & \mathcal{H}_0 \\ LK(E_s + \sigma_w^2) & \mathcal{H}_1 \end{cases} \tag{5.5}$$

and Var

$$Var[p\left(D_{MTM}^{m}(f_i)\right)] = \begin{cases} 2LC^2\lambda_\Sigma\sigma_w^4 & \mathcal{H}_0 \\ 2LC^2\lambda_\Sigma\sigma_w^2(\sigma_w^2 + 2E_s) & \mathcal{H}_1 \end{cases} \tag{5.6}$$

where C and λ_Σ were defined in (4.12) and (4.32) respectively.

On the other hand for the PE, and at the same assumption, the decision statistic $D_{PE}^{m}(f_i)$ using the mth antenna has E [47]:

$$E[p(D_{PE}^{m}(f_i))] = \begin{cases} L\sigma_w^2 & \mathcal{H}_0 \\ L(E_s + \sigma_w^2) & \mathcal{H}_1 \end{cases} \tag{5.7}$$

and Var

$$Var[p(D_{PE}^{m}(f_i))] = \begin{cases} 2L\sigma_w^4 & \mathcal{H}_0 \\ 2L\sigma_w^2(\sigma_w^2 + 2E_s) & \mathcal{H}_1 \end{cases} \tag{5.8}$$

The different probabilities formulae for MTM based spectrum sensing were derived in (4.36)-(4.38), and the number of sensed samples was derived in (4.41). The PE based spectrum sensing probabilities formulae for single antenna case are shown in (4.50)-(4.52), and the number of sensed samples when PE is used is shown in (4.53).

5.6 The Local-MTM-SVD (LMS) Based Multi Antenna Spectrum Sensing

In the LMS, the PR's signal power estimation at CR Rx is based on the following steps:

1. Producing different eigenspectrums, using different tapers, and different antennas based on MTM technique at each frequency binf_i.
2. The related statistical information about the transmitted PR signal that have been built from step 1 can be exploited using SVD which isolates the required information from noise and fading components and produces a near optimal power estimate at each frequency binf_i.

Figure 5.3 shows a schematic diagram of the proposed LMS.

For the binary hypothesis test in (5.1), when a number of M antennas are used, the complex eigenspectrums row vector $\boldsymbol{r}^m(f_i)$, which resulted from the mth antenna using the different tapers, is defined as [5]:

$$\boldsymbol{r}^m(f_i) = \left[Y_{0,m}(f_i)\ \ Y_{1,m}(f_i)\ Y_{2,m}(f_i) \ldots . Y_{K-1,m}(f_i)\right] \tag{5.9}$$

where $Y_{k,m}(f_i)$ denotes the eigenspectrum which is produced from the mth antenna using the kth taper. The complex eigenspectrums column vector $\boldsymbol{c}^k(f)$, which is resulted from the kth taper using different antennas, is defined as [5]:

$$\boldsymbol{c}^k(f_i) = \left[Y_{k,0}(f_i)\ \ Y_{k,1}(f_i)\ Y_{k,2}(f_i) \ldots . Y_{k,M-1}(f_i)\right]^{\mathrm{T}} \tag{5.10}$$

where Ŧ, is the vector transpose. Now, the local spatio-temporal complex matrix $\boldsymbol{A}(f_i)$ can be constructed using either complex eigenspectrums row vectors $\boldsymbol{r}^m(f_i)$, or column vectors $\boldsymbol{c}^k(f_i)$ as follows [5]:

$$\boldsymbol{A}(f_i) = \begin{bmatrix} \boldsymbol{r^0}(f_i) \\ \boldsymbol{r^1}(f_i) \\ \boldsymbol{r^2}(f_i) \\ . \\ . \\ . \\ \boldsymbol{r^{M-1}}(f_i) \end{bmatrix} \tag{5.11}$$

$$\boldsymbol{A}(f_i) = [\boldsymbol{c^0}(f_i)\ \ \boldsymbol{c^1}(f_i)\ \boldsymbol{c^2}(f_i) \ldots . \boldsymbol{c}^{K-1}(f_i)] \tag{5.12}$$

The row complex vector $\boldsymbol{r}^m(f_i) \in \mathbb{C}^{1\times K}$, and the column complex vector $\boldsymbol{c}^k(f_i) \in \mathbb{C}^{M\times 1}$; thus based on (5.11), and (5.12) the spatio-temporal complex matrix $\boldsymbol{A}(f_i) \in \mathbb{C}^{M\times K}$,which represents the collected eigenspectrums from different antennas using different tapers.

The SVD of the matrix $\boldsymbol{A}(f_i)$, produces three different matrices representing the decomposition process as [151]:

$$\boldsymbol{A}(f_i) = \boldsymbol{U}(f_i)\boldsymbol{\sigma}(f_i)\boldsymbol{V}(f_i)^{\mathfrak{h}} \tag{5.13}$$

where $\boldsymbol{\sigma}(f_i) \in \mathbb{R}^{M\times K}$, is a diagonal real positive matrix consisting of singular values of matrix $\boldsymbol{A}(f_i)$. If $R = min\{M,K\}$, there will be exactly R nonzero singular values. These singular values are represented by the R nonzero diagonal elements of the top left $R \times R$ block of $\boldsymbol{\sigma}(f_i)$, where $\sigma_1(f_i) \geq \sigma_2(f_i) \geq \cdots \geq \sigma_R(f_i) > 0$. Complex matrix $\boldsymbol{U}\,(f) \in$

$\mathbb{C}^{M\times M}$ consists of the associated left vectors. Complex matrix $\boldsymbol{V}\ (f_i) \in \mathbb{C}^{K\times K}$ consists of the associated right vectors; the subscript $\mathfrak{h}$ denotes the Hermitian transpose. The eigenvalues of the matrix produced from $\boldsymbol{A}(f_i)^{\mathfrak{h}}\boldsymbol{A}(f_i)$ are $|\sigma_1(f_i)|^2 \geq |\sigma_2(f_i)|^2 \geq \cdots \geq |\sigma_R(f_i)|^2 > 0$.

The spectrum estimation using LMS can be defined based on the singular value squares $|\sigma_1(f_i)|^2$, $|\sigma_2(f_i)|^2$,..., $|\sigma_R(f_i)|^2$, the number of tapers *K*, and the number of used antennas *M* as follows [5]:

$$S_{LMS}(f_i) = \frac{1}{MK}\left(\sum_{v=1}^{V}|\sigma_v(f_i)|^2\right) \tag{5.14}$$

where *MK*, is found as the scaling factor of the resulted summation of the different singular value squares, and *V* represents the number of the singular value squares which should be used in the LMS spectrum estimation, where $1 \leq V \leq R$. The number of singular values that should be used in LMS will be discussed through our simulation results section. The term $S_{LMS}(f_i)$ represents the spectrum estimation at frequency f_i using *K* tapers, and *M* antennas, while the term $S_{MTM}^{m}(f_i)$ in (3.5) represents the spectrum estimation that is achieved using MTM from single antenna using *K* tapers.

The *D* when number of *M* antennas are used in the LMS spectrum sensing can be redefined using (5.14) as [5]:

$$D_{LMS}(f_i) = \frac{1}{MK}\sum_{l=0}^{L-1}\left(\sum_{v=1}^{V}|\sigma_v(f_i)|^2\right) \tag{5.15}$$

The detection and false alarm probabilities at each frequency bin using the decision statistic $D_{LMS}(f_i)$ are defined as:

$$P_d^{LMS}(f_i) = Pr\{D_{LMS}(f_i) > \gamma|\mathcal{H}_1\}$$

$$P_f^{LMS}(f_i) = Pr\{D_{LMS}(f_i) > \gamma|\mathcal{H}_0\}$$

The threshold γ, is defined according to the noise variance σ_w^2 when single antenna is used. When a number of antennas are used as in the LMS, the overall system noise

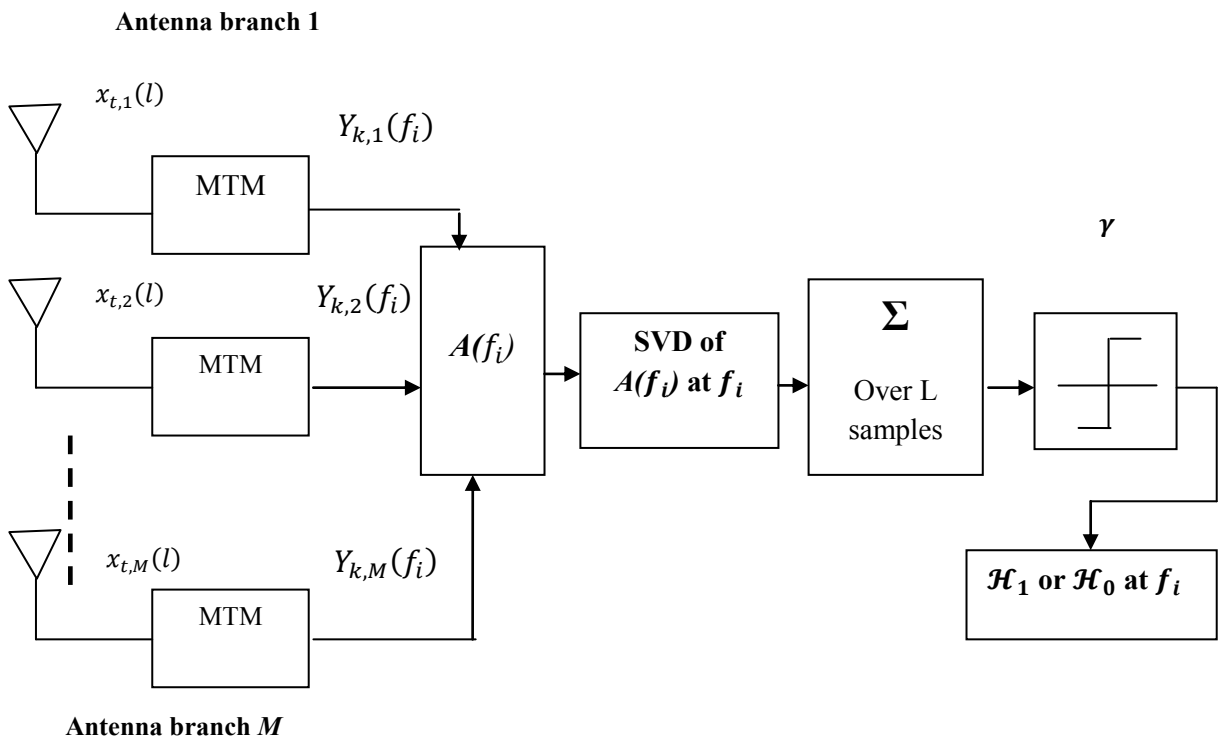

Figure 5.3 Schematic diagram of the proposed LMS.

variance σ_{com}^2 in AWGN can be defined using the noise variances for the different antennas branches, σ_w^2, as [5]:

$$\sigma_{com}^2 = \frac{1}{M}\sum_{m=0}^{M-1}\sigma_w^2 \tag{5.16}$$

Thus from (5.16), the LMS as a combining technique averages the noise variance over number of antennas output branches. If the different antennas output have the same receiver noise variance σ_w^2; the resulting combined noise variance will be σ_w^2 as well.

5.7 Square Law Combining–MTM Based Multi Antenna Spectrum Sensing

The second proposed sub optimal technique is the MTM-SLC, which can be

developed by using number of antennas M at the CR Rx for spectrum sensing based on MTM and SLC. The decision statistic is performed via each antenna branch separately using MTM over L samples, and then the overall decision statistic is calculated by summing the outputs decision statistics from the different antennas branches as square law combining. MTM-SLC is compared theoretically and analytically to the PE -square law combining (PE-SLC) as can be seen below.

5.7.1 Mean and Variance of MTM-SLC and PE-SLC

The decision statistics in (5.3), and (5.4) can be redefined for square law combining using M antennas for both techniques MTM, and PE respectively as follow [6]:

$$D_{MTM-SLC}(f_i) = \sum_{m=0}^{M-1}\sum_{l=0}^{L-1} \frac{\sum_{k=0}^{K-1}\lambda_k(N,W)\left|\sum_{t=0}^{N-1} v_{(t,k)}(N,W)x_{t,m}(l)e^{-j2\pi f_i t}\right|^2}{\sum_{k=0}^{K-1}\lambda_k(N,W)} \tag{5.17}$$

and,

$$D_{PE-SLC}(f_i) = \sum_{m=0}^{M-1}\sum_{l=0}^{L-1}\left|\sum_{t=0}^{N-1} x_{t,m}(l)e^{-j2\pi f_i t}\right|^2 . \tag{5.18}$$

Figure 5.4 shows a schematic diagram of the proposed MTM-SLC.

From (5.17), and (5.18) the decision statistic using square law combining is a sum of identical and independent normally distributed M antennas decision statistics. Thus, the E of the $D_{MTM-SLC}(f_i)$'s PDF, $E[p(D_{MTM-SLC}(f_i))]$, using M antennas can be defined as follows [6]:

$$E\left[p\left(D_{MTM-SLC}(f_i)\right)\right] = \begin{cases} MLK\sigma_w^2 & \mathcal{H}_0 \\ MLK(E_s + \sigma_w^2) & \mathcal{H}_1 \end{cases} \tag{5.19}$$

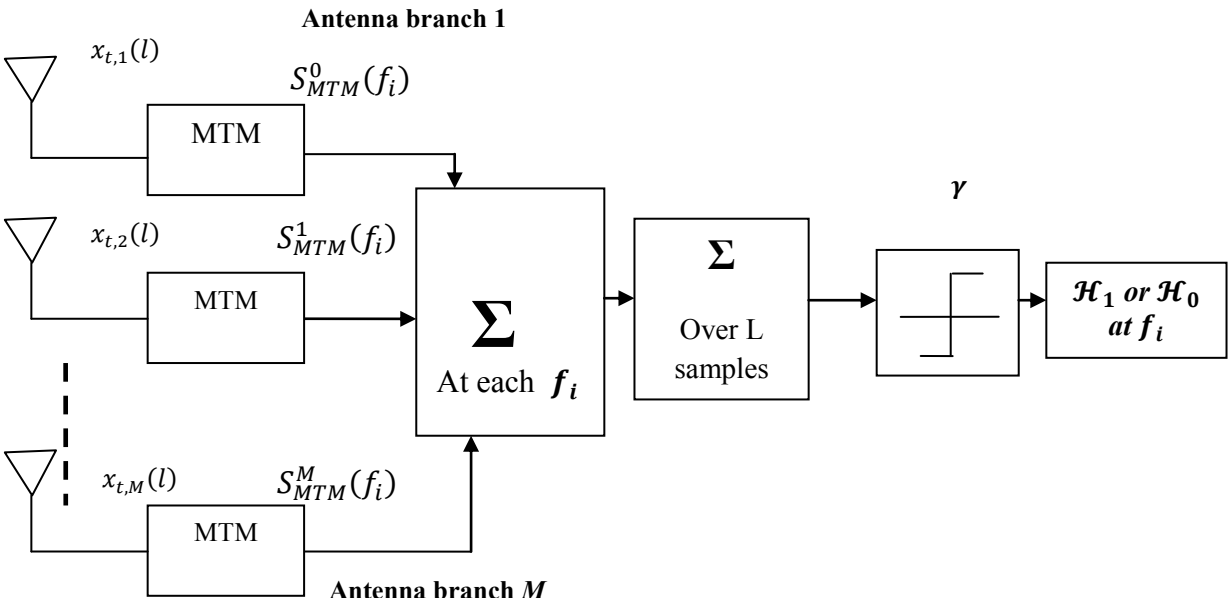

Figure 5.4 Schematic diagram of the proposed MTM-SLC.

and the *Var* can be defined as follows [6]:

$$Var[p(D_{MTM-SLC}(f_i))] = \begin{cases} 2MLC^2\lambda_\Sigma\sigma_w^4 & \mathcal{H}_0 \\ 2MLC^2\lambda_\Sigma\sigma_w^2(\sigma_w^2 + 2E_s) & \mathcal{H}_1 \end{cases}. \tag{5.20}$$

In the PE case, the E of the decision statistic $D_{PE-SLC}(f_i)$'s PDF, $E[\,p(D_{PE-SLC}(f_i))]$, using square law combining through M antennas can be defined as follows [6]:

$$E[p(D_{PE-SLC}(f_i))\,] = \begin{cases} ML\sigma_w^2 & \mathcal{H}_0 \\ ML(E_s + \sigma_w^2) & \mathcal{H}_1 \end{cases} \tag{5.21}$$

and the *Var* is defined as follows:

$$Var[p(D_{PE-SLC}(f_i))] = \begin{cases} 2ML\sigma_w^4 & \mathcal{H}_0 \\ 2ML\sigma_w^2(\sigma_w^2 + 2E_s) & \mathcal{H}_1 \end{cases}. \tag{5.22}$$

5.7.2 MTM-SLC and PE-SLC Probabilities Formulae

The different probabilities can be redefined for the square law combining technique using *M* antennas for both MTM, and PE cases by substituting the means and variances defined in (5.19), (5.20), (5.21), and (5.22) in (2.6), (2.8), and (2.10).Thus, the different probabilities for MTM-SLC can be defined as follows [6]:

$$P_d^{MTM-SLC}(f_i) = Q\left(\frac{\gamma - MLK(E_s+\sigma_w^2)}{\sqrt{2MLC^2\lambda_\Sigma\sigma_w^2(\sigma_w^2+2E_s)}}\right) \tag{5.23}$$

$$P_f^{MTM-SLC}(f_i) = Q\left(\frac{\gamma - MLK\sigma_w^2}{\sqrt{2MLC^2\lambda_\Sigma\sigma_w^4}}\right) \tag{5.24}$$

$$P_{mi}^{MTM-SLC}(f_i) = 1 - Q\left(\frac{\gamma - MLK(E_s+\sigma_w^2)}{\sqrt{2MLC^2\lambda_\Sigma\sigma_w^2(\sigma_w^2+2E_s)}}\right) \tag{5.25}$$

When the effect of the DPSS orthonormality on the eigenspectrums' independence is considered as in the end of subsection 4.5.3, the means and variances in (5.19) and (5.20) can be redefined to be as follows:

$$E\left[p\left(D_{MTM-SLC}(f_i)\right)\right] = \begin{cases} ML\sigma_w^2 & \mathcal{H}_0 \\ ML(E_s+\sigma_w^2) & \mathcal{H}_1 \end{cases}$$

and *Var*

$$Var[p\left(D_{MTM-SLC}(f_i)\right)] = \begin{cases} (1/K)2MC^2L\sum_{k=0}^{K-1}\lambda_k^2(N,W)(\sigma_w^4) & \mathcal{H}_0 \\ (1/K)2MC^2L\sigma_w^2\sum_{k=0}^{K-1}\lambda_k^2(N,W)(\sigma_w^2+2E_s) & \mathcal{H}_1 \end{cases}$$

and then the different probabilities in (5.23)-(5.25) can be redefined to be as follows:

$$P_d^{MTM-SLC}(f_i) = Q\left(\frac{\gamma - ML(E_s+\sigma_w^2)}{\sqrt{\left(\frac{2}{K}\right)MC^2L\sigma_w^2\sum_{k=0}^{K-1}\lambda_k^2(N,W)(\sigma_w^2+2E_s)}}\right)$$

$$P_f^{MTM-SLC}(f_i) = Q\left(\frac{\gamma - ML\sigma_w^2}{\sqrt{\left(\frac{2}{K}\right)MC^2L\sum_{k=0}^{K-1}\lambda_k^2(N,W)(\sigma_w^4)}}\right)$$

$$P_{mi}^{MTM-SLC}(f_i) = 1 - Q\left(\frac{\gamma - ML(E_s+\sigma_w^2)}{\sqrt{\left(\frac{2}{K}\right)MC^2L\sigma_w^2\sum_{k=0}^{K-1}\lambda_k^2(N,W)(\sigma_w^2+2E_s)}}\right)$$

These probabilities equations give exactly the same results as those in (5.23)-(5.25). When PE-SLC is used with M antennas, the different probabilities can be written as follows [6]:

$$P_d^{PE-SLC}(f_i) = Q\left(\frac{\gamma - ML(E_s+\sigma_w^2)}{\sqrt{2ML\sigma_w^2(\sigma_w^2+2E_s)}}\right) \tag{5.26}$$

$$P_f^{PE-SLC}(f_i) = Q\left(\frac{\gamma - ML\sigma_w^2}{\sqrt{2ML\sigma_w^4}}\right) \tag{5.27}$$

$$P_{mi}^{PE-SLC}(f_i) = 1 - Q\left(\frac{\gamma - ML(E_s+\sigma_w^2)}{\sqrt{2ML\sigma_w^2(\sigma_w^2+2E_s)}}\right) \tag{5.28}$$

The threshold, γ in this case, is controlled by the term $LM\sigma_w^2$.

5.7.3 MTM-SLC and PE-SLC Number of Sensed Samples

The MTM-SLC's mean is K times PE-SLC's mean for both hypotheses, and the difference in the variance is defined as the variance factor (VF), which can be written as follows [6]:

$$VF = C^2\,\lambda_\Sigma = \beta \tag{5.29}$$

The number of samples, $L^{MTM-SLC}$ (i.e., OFDM blocks) needed to achieve predefined probabilities of detection, $P_d^{MTM-SLC}$, and false alarm, $P_f^{MTM-SLC}$ in the MTM-SLC technique can be written using the resulting MTM-SLC probabilities of detection and false alarm formulae in (5.23) and (5.24) as follows [6]:

$$L^{MTM-SLC} = \left(\frac{a^{MTM-SLC} - b^{MTM-SLC}}{MKE_s}\right)^2 \tag{5.30}$$

where

$$a^{MTM-SLC} = \sqrt{2VFM\sigma_w^4}\,Q^{-1}\left(P_f^{MTM-SLC}(f_i)\right)$$

and

$$b^{MTM-SLC} = \sqrt{2VFM\sigma_w^2(\sigma_w^2+2E_s)}\,Q^{-1}\left(P_d^{MTM-SLC}(f_i)\right)$$

This can be written in (dB) as follows:

$$L^{MTM-SLC}{}_{dB} = 10log_{10}(L^{MTM-SLC})$$

The derivation of $L^{MTM-SLC}$ is achieved by redefining the probabilities of detection and false alarm, $P_d^{MTM-SLC}(f_i)$, and $P_f^{MTM-SLC}(f_i)$ that in (5.23) and (5.24) in terms of number of sensed samples, $L^{MTM-SLC}$, to be as:

$$P_d^{MTM-SLC}(f_i) = Q\left(\frac{\gamma - L^{MTM-SLC}KM(E_s+\sigma_w^2)}{\sqrt{2L^{MTM-SLC}MC^2\lambda_\Sigma\sigma_w^2(\sigma_w^2+2E_s)}}\right) \tag{5.31}$$

$$P_f^{MTM-SLC}(f_i) = Q\left(\frac{\gamma - L^{MTM-SLC}KM\sigma_w^2}{\sqrt{2L^{MTM-SLC}MC^2\lambda_\Sigma\sigma_w^4}}\right) \tag{5.32}$$

In order to calculate the number of samples, $L^{MTM-SLC}$, which are required to achieve specific probabilities of detection and false alarm, the threshold, γ, used in both (5.31), and (5.32) are the same. Thus, after mathematical manipulation, the threshold form (5.31) can be defined as follows [6]:

$$\gamma = Q^{-1}\left(P_d^{MTM-SLC}(f_i)\right)\sqrt{2L^{MTM-SLC}MC^2\lambda_\Sigma\sigma_w^2(\sigma_w^2+2E_s)} + L^{MTM-SLC}KM(E_s+\sigma_w^2) \tag{5.33}$$

using (5.32), the threshold can be defined as [6]:

$$\gamma = Q^{-1}\left(P_f^{MTM-SLC}(f_i)\right)\sqrt{2L^{MTM-SLC}MC^2\lambda_\Sigma\sigma_w^4} + L^{MTM-SLC}KM\sigma_w^2 \tag{5.34}$$

Therefore, based on the thresholds equality in (5.33) and (5.34), the $L^{MTM-SLC}$ can be defined as in (5.30).

Using the same steps in deriving L and referring to the probabilities equations of MTM-SLC that have been redefined within subsection 5.7.2, the same result from (5.30) can be achieved using:

$$L^{MTM-SLC} = \left(\frac{\sqrt{2FM\sigma_w^4}Q^{-1}\left(P_f^{MTM-SLC}(f_i)\right) - \sqrt{2FM\sigma_w^2(\sigma_w^2+2E_s)}Q^{-1}\left(P_d^{MTM-SLC}(f_i)\right)}{ME_s}\right)^2$$

where F is defined in subsection 4.5.4.

Substituting $VF = 1$ and K=1in (5.30), produces the number of samples, L for PE-SLC which can be written as follows [6]:

$$L^{PE-SLC} = \left(\frac{\sqrt{2M\sigma_w^4}Q^{-1}\left(P_f^{PE-SLC}(f_i)\right) - \sqrt{2M\sigma_w^2(\sigma_w^2 + 2E_s)}Q^{-1}\left(P_d^{PE-SLC}(f_i)\right)}{ME_s} \right)^2 \tag{5.35}$$

5.8 Linear Combining–MTM Based Multi Antenna Spectrum Sensing

The third proposed technique is MTM-LC of the received samples from different M antennas at the CR receiver. The received data samples at the CR receiver are summed from the different M antennas branches in the time domain to be as follows [6]:

$$x_t(l) = \sum_{m=0}^{M-1} x_{t,m}(l). \tag{5.36}$$

Then the eigenspectrums of the resulted new received samples $x_t(l)$ can be written using (3.4) and (5.36) as follow:

$$Y_k(f_i) = \sum_{t=0}^{N-1} v_t^{(k)}(N,W)x_t(l)e^{-j2\pi f_i t}. \tag{5.37}$$

The MTM-LC decision statistic over L samples of (5.36) can be defined as follows:

$$D_{MTM-LC}(f_i) = \sum_{l=0}^{L-1} \frac{\sum_{k=0}^{K-1}\lambda_k(N,W)\left|\sum_{t=0}^{N-1} v_{(t,k)}(N,W)x_t(l)e^{-j2\pi f_i t}\right|^2}{\sum_{k=0}^{K-1}\lambda_k(N,W)}. \tag{5.38}$$

Note that (5.37) and (5.38) represents the case in MTM-LC where the received signal at CR Rx is the sum of the signals from different M antennas as in (5.36), while the case of using one antenna branch is shown in (5.2) and (5.3).

Figure 5.5 shows a schematic diagram of the proposed MTM-LC.

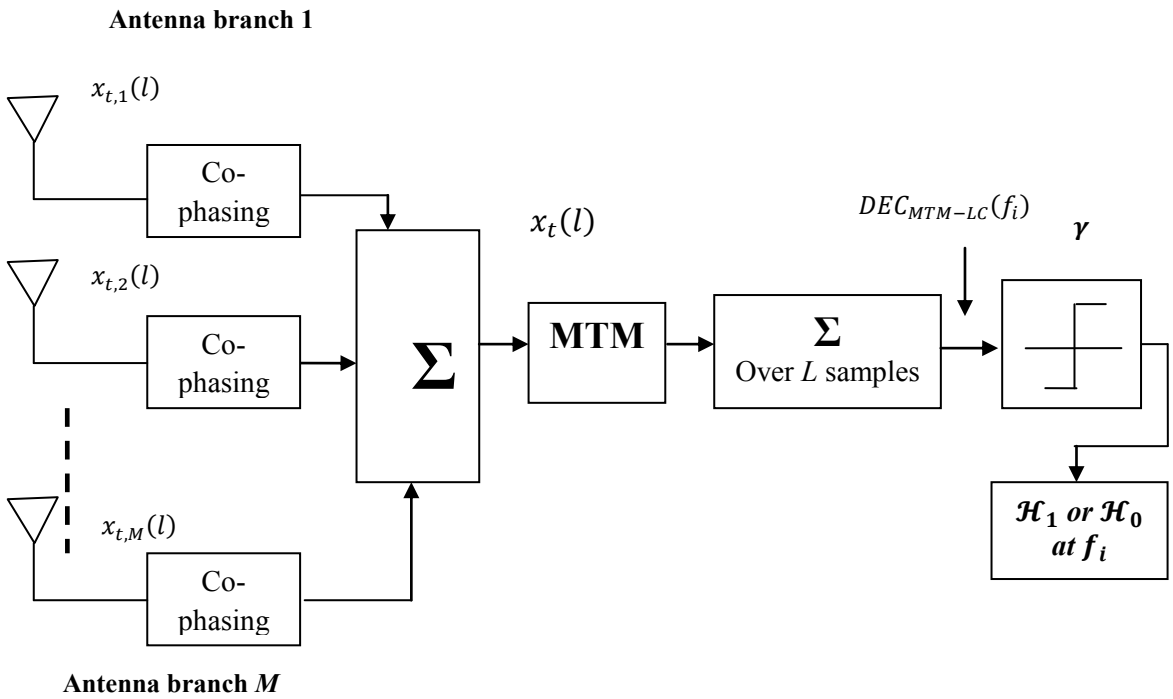

Figure 5.5 Schematic diagram of the proposed MTM-LC.

5.8.1 Mean and Variance of MTM-LC and PE-LC

In order to derive the different probabilities expressions of $D_{MTM-LC}(f_i)$, we need to derive the E and the Var of its PDF, $p(D_{MTM-LC}(f_i))$, for the different hypotheses. We follow our theoretical derivation of the MTM-single based as in sub section 4.5.2. The linear combiner binary hypothesis can be defined as follows [6]:

$$\mathcal{H}_0: \quad x_t(l) = w_{t,1}(l) + w_{t,2}(l) + \cdots \; w_{t,M}(l)$$

$$\mathcal{H}_1: \; x_t(l) = s_t(l) + w_{t,1}(l) + \cdots + s_t(l) + \; w_{t,M}(l) \tag{5.39}$$

The main different in $\mathcal{H}_0$ between MTM, and MTM-LC is the effect of the combined noise signals from different antennas. Thus, the mean for K correlated Gaussian samples of the decision statistic in (5.38); $E[p(D_{MTM-LC}(f_i);\, \mathcal{H}_0)]$ can be defined as follows [6]:

$$E[p(D_{MTM-LC}(f_i);\ \mathcal{H}_0)] = C.\sum_{l=0}^{L-1}(\sum_{k=0}^{K-1}(\lambda_k(N,W).K\sum_{t=0}^{N-1}\sum_{t'=0}^{N-1}E[v_{(t,k)}(N,W)$$

$$.v_{(t',k)}(N,W).x_t(l)x_{t'}(l)] \tag{5.40}$$

It can be shown that (5.40) can be simplified as:

$$E[p(D_{MTM-LC}(f_i);\ \mathcal{H}_0)] =$$

$$\sum_{l=0}^{L-1}\sum_{t=0}^{N-1}(v_{(t,k)}(N,W).v_{(t',k)}(N,W)).K.E[x_t(l)x_{t'}(l)] \tag{5.41}$$

In the remaining parts of this chapter, the terms $w_{t,m}(l)$, and $s_t(l)$ will be written as $w_m(l)$, and $s(l)$ respectively for expressions simplification.

The orthonormality of the sequences in (4.17) can be used to simplify (5.41), over L (L here is for MTM-LC technique which is different from that for MTM-SLC or that for MTM) sensed samples, when $t = t'$as follows [6]:

$$E[p(D_{MTM-LC}(f_i);\ \mathcal{H}_0)] = \sum_{l=0}^{L-1}K.E[x_t^2(l)]$$

$$= LK.E[\big(w_1(l) + w_2(l) + \cdots + w_M(l)\big)\big(w_1(l) + w_2(l) + \cdots + w_M(l)\big)]$$

$$= LK.E[w_1^2(l) + w_1(l)w_2(l) + w_1(l)w_3(l) + \cdots + w_1(l)w_M(l)$$

$$+ w_2^2(l) + w_2(l)w_1(l) + w_2(l)w_3(l) + \cdots + w_2(l)w_M(l) + \cdots + w_M^2(l)$$

$$+ w_M(l)w_1(l) + w_M(l)w_2(l) + \cdots$$

$$+ w_M(l)w_{M-1}(l)] \tag{5.42}$$

since $E[w_i(l)w_j(l)] = 0$, for $i \neq j$, and $i, j = 1,2, \ldots M$; then (5.42) can be rewritten as follows [6]:

$$E[p(D_{MTM-LC}(f_i);\ \mathcal{H}_0)] = LK.(E[w_1^2(l)] + E[w_2^2(l)] + \cdots + E[w_M^2(l)])$$

$$= LK.((E[w_1(l)])^2 + Var(w_1(l)) + (E[w_2(l)])^2 + Var(w_2(l)) + \cdots + (E[w_M(l)])^2$$

$$+ Var(w_M(l))) \tag{5.43}$$

finally, $E[w_m(l)] = 0$, and $Var\big(w_m(l)\big) = \sigma_w^2$, then (5.44) can be written as follows [6]:

$$E[p(D_{MTM-LC}(f_i);\ \mathcal{H}_0)] = MLK\sigma_w^2\,. \tag{5.44}$$

The variance of K correlated Gaussian samples in (5.38); $Var[p(D_{MTM-LC}(f_i);\ \mathcal{H}_0)]$ over L sensed samples when $t = t'$, can be defined as follows [6]:

$$Var[p(D_{MTM-LC}(f_i);\ \mathcal{H}_0)] = \beta L.\left(\sum_{t=0}^{N-1} v_{(t,k)}^2(N,W)\right)^2 .Var\big(x_t^2(l)\big)$$

$$\begin{aligned}
= \beta L\,.Var(&w_1^2(l) + w_1(l)w_2(l) + w_1(l)w_3(l) + \cdots + w_1(l)w_M(l) + w_2^2(l)\\
&+ w_2(l)w_1(l) + w_2(l)w_3(l) + \cdots + w_2(l)w_M(l) + \cdots + w_M^2(l)\\
&+ w_M(l)w_1(l) + w_M(l)w_2(l)\\
&+ \cdots w_M(l)w_{M-1}(l)\ )
\end{aligned} \tag{5.45}$$

Where β is defined in (5.29), then, (5.45) can be simplified to be as follows [6]:

$$\begin{aligned}
&Var[p(D_{MTM-LC}(f_i);\ \mathcal{H}_0)]\\
&\quad= \beta L\ (Var\big(w_1^2(l)\big) + Var\big(w_2^2(l)\big) + \cdots +\ Var\big(w_M^2(l)\big)\\
&\quad+ Var\big(2w_1(l)w_2(l)\big) + Var\big(2w_1(l)w_3(l)\big) + \cdots + Var(2w_1(l)w_M(l))\\
&\quad+ Var\big(2w_2(l)w_3(l)\big) + Var\big(2w_2(l)w_4(l)\big) + \cdots\\
&\quad+ Var\Big(2w_2(l)w_M(l)) + \cdots + Var\big(2w_M(l)w_{M-1}(l)\big)\Big)\\
&= \beta L\ \Bigg(Var\big(w_1^2(l)\big) + Var\big(w_2^2(l)\big) + \cdots +\ Var\big(w_M^2(l)\big)\\
&\quad+ \binom{M}{2}\ Var\Big(2w_i(l)w_j(l)\Big)\Bigg)\ ,\forall\ i \neq j, and\ i,j\\
&\quad= 1,2,\ldots M
\end{aligned} \tag{5.46}$$

where $Var\left(w_m^2(l)\right) = 2\sigma_w^4$, and $Var\left(2w_i(l)w_j(l)\right) = 4\sigma_w^4, \forall\ i \neq j, and\ i,j = 1,2,\ldots M$. Finally, (5.46) can be written as follows [6]:

$$Var[p(D_{MTM-LC}(f_i);\ \mathcal{H}_0)] = \beta L\ (M(2\sigma_w^4) + 2\binom{M}{2}\ (2\sigma_w^4))$$

$$= \beta L\ \left(M(2\sigma_w^4) + 2\left(\frac{M!}{(M-2)!\,2!}\right)(2\sigma_w^4)\right)$$

$$= \beta L\ M^2(2\sigma_w^4). \tag{5.47}$$

When the PR's signal is present, the $E[p(D_{MTM-LC}(f_i);\ \mathcal{H}_1)]$ over L sensed samples when $t = t'$, can be defined as follows [6]:

$$E[p(D_{MTM-LC}(f_i);\ \mathcal{H}_1)]$$

$$= LK.E[\big(s(l) + w_1(l) + s(l) + w_2(l) + \cdots + s(l) + w_M(l)\big)\big(s(l) + w_1(l) + s(l) + w_2(l) + \cdots + s(l) + w_M(l)\big)]$$

$$= LK.E[M^2s^2(l) + w_1^2(l) + w_2^2(l) + \cdots + w_M^2(l) + s(l)w_1(l) + s(l)w_2(l) + \cdots + s(l)w_M(l) + \cdots + w_M(l)s(l)]$$

$$= LK(E[M^2s^2(l)] + 2ME[s(l)]E[w_m(l)] + E[w_1^2(l)] + E[w_2^2(l)] + \cdots + E[w_M^2(l)]) \tag{5.48}$$

where $E[M^2s^2(l)] = M^2E_s$, $E[w_m(l)] = 0$, and $E[w_m^2(l)] = ((E[w_m(l)])^2 + Var(w_m(l))) = 0 + \sigma_w^2$; then (5.48) can be simplified to be as follows [6]:

$$E[p(D_{MTM-LC}(f_i);\ \mathcal{H}_1)] = LK(M^2E_s + M\sigma_w^2)$$

$$= MLK(ME_s + \sigma_w^2) \tag{5.49}$$

The variance; $Var[p(D_{MTM-LC}(f_i);\ \mathcal{H}_1)]$ can be defined as follows [6]:

$$Var[p(D_{MTM-LC}(f_i);\ \mathcal{H}_1)]$$

$$= \beta L.Var\big(M^2 s^2(l) + w_1^2(l) + w_2^2(l) + \cdots + w_M^2(l) + s(l)w_1(l)$$

$$+ s(l)w_2(l) + \cdots + s(l)w_M(l) + \cdots + w_M(l)s(l)\big)$$

$$= \beta L\Bigg(Var\big(2Ms(l)w_1(l)\big) + Var\big(2Ms(l)w_2(l)\big) + \cdots + Var\big(2Ms(l)w_M(l)\big)$$

$$+ Var\big(w_1^2(l)\big) + Var\big(w_2^2(l)\big) + \cdots + Var\big(w_M^2(l)\big)$$

$$+ \binom{M}{2}\ Var\left(2w_i(l)w_j(l)\right)\Bigg)\ ,\forall\ \ i \neq j, and\ i,j = 1,2,\ldots M$$

$$= \beta L(M(4M^2)E_s\sigma_w^2 + M(2\sigma_w^4) + 2\left(\frac{M!}{(M-2)!\,2!}\right)(2\sigma_w^4)\ )$$

$$= \beta L\big(M(4M^2)E_s\sigma_w^2 + M^2(2\sigma_w^4)\big)$$

$$= 2\beta LM^2\sigma_w^2\ (\sigma_w^2 + 2ME_s) \tag{5.50}$$

Finally, the different MTM-LC hypotheses' mean is summarized as follows [6]:

$$E[p(D_{MTM-LC}(f_i))] = \begin{cases} MLK\sigma_w^2 & \mathcal{H}_0 \\ MLK(ME_s + \sigma_w^2) & \mathcal{H}_1 \end{cases} \tag{5.51}$$

and the *Var* [6]:

$$Var[p(D_{MTM-LC}(f_i))] = \begin{cases} 2\beta L\ M^2\sigma_w^4 & \mathcal{H}_0 \\ 2\beta LM^2\sigma_w^2\ (\sigma_w^2 + 2ME_s) & \mathcal{H}_1 \end{cases} \tag{5.52}$$

The same derivation steps can be followed for $p\big(DEC_{PE-LC}(f_i)\big)$, then the different hypotheses' mean, and variance can be written as follows [6]:

$$E[D_{PE-LC}(f_i)] = \begin{cases} ML\sigma_w^2 & \mathcal{H}_0 \\ ML(ME_s + \sigma_w^2) & \mathcal{H}_1 \end{cases} \tag{5.53}$$

$$Var\big(D_{PE-LC}(f_i)\big) = \begin{cases} 2M^2L\sigma_w^4 & \mathcal{H}_0 \\ 2M^2L\sigma_w^2(\sigma_w^2 + 2ME_s) & \mathcal{H}_1 \end{cases} \tag{5.54}$$

5.8.2 MTM-LC and PE-LC Probabilities Formulae

The different probabilities can be redefined for the linear combining technique using M antennas for both MTM, and PE cases by substituting the means and variances defined in (5.51), (5.52), (5.53), and (5.54) into (2.6), (2.8), and (2.10). Thus, the different probabilities for MTM-LC can be defined as follow [6]:

$$P_d^{MTM-LC}(f_i) = Q\left(\frac{\gamma - MLK(ME_s+\sigma_w^2)}{\sqrt{2\beta LM^2\sigma_w^2\,(\sigma_w^2+2ME_s)}}\right) \tag{5.55}$$

$$P_f^{MTM-LC}(f_i) = Q\left(\frac{\gamma - MLK\sigma_w^2}{\sqrt{2\beta L\,M^2\sigma_w^4}}\right) \tag{5.56}$$

$$P_{mi}^{MTM-LC}(f_i) = 1 - Q\left(\frac{\gamma - MLK(ME_s+\sigma_w^2)}{\sqrt{2\beta LM^2\sigma_w^2\,(\sigma_w^2+2ME_s)}}\right) \tag{5.57}$$

When the effect of the DPSS orthonormality on the eigenspectrums' independence is considered as in the end of subsection 4.5.3 and subsection 5.7.2, the means and variances in (5.51) and (5.52) can be redefined to be as follows:

$$E\left[p\left(D_{MTM-LC}(f_i)\right)\right] = \begin{cases} ML\sigma_w^2 & \mathcal{H}_0 \\ ML(ME_s + \sigma_w^2) & \mathcal{H}_1 \end{cases}$$

and Var

$$Var[p\left(D_{MTM-LC}(f_i)\right)] = \begin{cases} (1/K)2M^2C^2L\sum_{k=0}^{K-1}\lambda_k^2(N,W)(\sigma_w^4) & \mathcal{H}_0 \\ (1/K)2M^2C^2L\sigma_w^2\sum_{k=0}^{K-1}\lambda_k^2(N,W)(\sigma_w^2+2ME_s) & \mathcal{H}_1 \end{cases}$$

and then the different probabilities in (5.55)-(5.57) can be redefined to be as follow:

$$P_d^{MTM-LC}(f_i) = Q\left(\frac{\gamma - ML(ME_s+\sigma_w^2)}{\sqrt{(\frac{2}{K})M^2C^2L\sigma_w^2\sum_{k=0}^{K-1}\lambda_k^2(N,W)(\sigma_w^2+2ME_s)}}\right)$$

$$P_f^{MTM-LC}(f_i) = Q\left(\frac{\gamma - ML\sigma_w^2}{\sqrt{(\frac{2}{K})M^2C^2L\sum_{k=0}^{K-1}\lambda_k^2(N,W)(\sigma_w^4)}}\right)$$

$$P_{mi}^{MTM-LC}(f_i) = 1 - Q\left(\frac{\gamma - ML(ME_s+\sigma_w^2)}{\sqrt{\left(\frac{2}{K}\right)M^2C^2L\sigma_w^2\sum_{k=0}^{K-1}\lambda_k^2(N,W)(\sigma_w^2+2ME_s)}}\right)$$

These probabilities equations give exactly the same results as same as those in (5.55)-(5.57).

When PE-LC is used with M antennas, the different probabilities can be written as follow [6]:

$$P_d^{PE-LC}(f_i) = Q\left(\frac{\gamma - ML(ME_s + \sigma_w^2)}{\sqrt{2M^2L\sigma_w^2(\sigma_w^2 + 2ME_s)}}\right) \tag{5.58}$$

$$P_f^{PE-LC}(f_i) = Q\left(\frac{\gamma - ML\sigma_w^2}{\sqrt{(2M^2L\sigma_w^4)}}\right) \tag{5.59}$$

$$P_{mi}^{PE-LC}(f_i) = 1 - Q\left(\frac{\gamma - ML(ME_s + \sigma_w^2)}{\sqrt{2M^2L\sigma_w^2(\sigma_w^2 + 2ME_s)}}\right) \tag{5.60}$$

The threshold, γ in this case, is controlled by the term $LM\sigma_w^2$.

5.8.3 MTM-LC and PE-LC Number of Sensed Samples

The number of samples L^{MTM-LC} (i.e., number of OFDM blocks) which are needed to achieve predefined probabilities of detection P_d^{MTM-LC}, and false alarm P_f^{MTM-LC} can be written using the resulting MTM-LC probabilities of detection and false alarm formulae in (5.55) and (5.56) to be as follows [6]:

$$L^{MTM-LC} = \left(\frac{a^{MTM-LC} - b^{MTM-LC}}{M^2KE_s}\right)^2 \tag{5.61}$$

where

$$a^{MTM-LC} = \sqrt{2VFM^2\sigma_w^4}\,Q^{-1}\left(P_f^{MTM-LC}(f_i)\right)$$

and

$$b^{MTM-LC} = \sqrt{2VFM^2\sigma_w^2(\sigma_w^2 + 2ME_s)}\,Q^{-1}\left(P_d^{MTM-LC}(f_i)\right)$$

Using the same steps in deriving L and referring to the probabilities equations of MTM-LC that have been redefined within subsection 5.8.2, the same result from (5.61) can be achieved using:

$$L = \left(\frac{\sqrt{2FM^2\sigma_w^4}Q^{-1}\left(P_f^{MTM-LC}(f_i)\right) - \sqrt{2FM^2\sigma_w^2(\sigma_w^2 + 2ME_s)}Q^{-1}\left(P_d^{MTM-LC}(f_i)\right)}{M^2E_s} \right)^2$$

where F is defined in subsection 4.5.4.

Note that, in order to calculate the L^{MTM-LC}, which is required to achieve specific probabilities of detection and false alarm, the threshold, γ that used in both (5.55), and (5.56) are the same. Substituting $VF = 1$ and K=1 in (5.61) produces the number of samples L for PE-LC, which can be written as follows:

$$L^{PE-LC} = \left(\frac{\sqrt{2M^2\sigma_w^4}Q^{-1}\left(P_f^{PE-LC}(f_i)\right) - \sqrt{2M^2\sigma_w^2(\sigma_w^2+2ME_s)}Q^{-1}\left(P_d^{PE-LC}(f_i)\right)}{M^2E_s} \right)^2 \quad (5.62)$$

5.9 Multi Path Fading Environment

The channel model that is assumed in this chapter is similar to that in [176], where an AWGN is added to the PR's signal at the CR's receiver. In the multipath fading environment, (5.1) can be rewritten as follows [100]:

$$\mathcal{H}_0: \quad x_{t,m}(l) = w_{t,m}(l)$$

$$\mathcal{H}_1: \quad x_{t,m}(l) = \sum_{p=0}^{P-1} h_{p,m} s_{t-p}(l) + w_{t,m}(l) \quad (5.63)$$

where the discrete channel impulse response between the PR's transmitter and CR's m^{th} branch is represented by $h_{p,m}, p = 0,1,\ldots,P-1$, and P is the total number of resolvable paths. The discrete frequency response of the channel through the mth branch is obtained by taking the N point FFT, with $N \geq P$ as follows [100]:

$$H_m(f_i) = \sum_{p=0}^{P-1} h_{p,m} e^{-j2\pi f_i p} \quad (5.64)$$

In such an environment, using MTM-SLC ,and PE-SLC does not need co-phasing to cancel the effect of the channel of each antenna branch. Since the decision statistic

will be performed via each CR's antenna branch independently, the MTM-SLC's decision statistic can be approximated to Gaussian, and then (5.19) and (5.20) can be rewritten as [6]:

$$E[p(D_{MTM-SLC}(f_i))] = \begin{cases} MLK\sigma_w^2 & \mathcal{H}_0 \\ LK(E_s(\sum_{m=0}^{M-1}|H_m(f_i)|^2) + M\sigma_w^2) & \mathcal{H}_1 \end{cases} \quad (5.65)$$

$$Var(D_{MTM-SLC}(f_i)) = \begin{cases} 2MLC^2\lambda_\Sigma\sigma_w^4 & \mathcal{H}_0 \\ 2LC^2\lambda_\Sigma\sigma_w^2(M\sigma_w^2 + 2E_s(\sum_{m=0}^{M-1}|H_m(f_i)|^2)) & \mathcal{H}_1 \end{cases} \quad (5.66)$$

In practice, $|H_m(f_i)|^2$ can be estimated a priori during the time that PR's transmitter occupies a specific band with specific power [100]. In this thesis, we assume that the channel gain between the PR's transmitter and the CR's receiver is constant during the spectrum sensing duration, and this is useful for application like in IEEE802.22.

When applying MTM-LC and PE-LC, the CR wants to coherently add up the signals from different branches by co-phasing, which requires knowing the channel coefficients a priori via training sequences or pilot signals. This means that under such conditions, the CR requires to perform coherent detection of the PR's transmitted signal. An alternative method to identify the channel coefficients is the use of blind equalization (i.e., co-phasing) methods [177, 178]. Consequently, CR does not need coherent detection to estimate the channel coefficients in spectrum sensing mission when blind estimation techniques are used. The blind estimation techniques are based on the statistical properties of the PR's transmitted signal. Such techniques are, mainly, classified into two categories; second order and higher order statistics [178]. In the higher order statistics based techniques, the channel phase information is retained, whereas second order statistics cannot distinguish between minimum and non minimum phase channels [179]. However, the higher order statistics based techniques require large number of sensed samples to achieve a more accurate estimation of the channel

coefficients [180]. In multi antenna based communication systems, the cyclostationary property of the transmitted signal can be exploited to find the non minimum phase channel estimation through the second order statistics [181]. In a CR spectrum sensing technique such as that proposed in this chapter, which is based on using multi antenna at the CR Rx (i.e., MTM-LC), such estimation techniques are very useful for fast and more reliable estimations. However, the subject of blind channel equalization is a major subject itself in wireless communications, and more research is required in the direction of blind channel equalization for CR spectrum sensing purposes. For example, the thesis in [179], deals only with blind equalization techniques for MIMO-OFDM systems.

5.10 The Complexity of the Proposed Multi Antenna Based Spectrum Sensing Techniques

The complexity of the proposed LMS spectrum sensing technique for producing the spectrum estimate at a specific frequency bin f_i, using M antennas and N-FFT over L sensed samples (i.e., OFDM-Blocks), in terms of the number of mathematical operations (i.e., adding, and multiplication), is defined as follows:

$$com_{LMS} = L[KM(3N-1) + com_{SVD}] \tag{5.67}$$

where com_{SVD} represents the SVD process complexity which is defined for $\boldsymbol{A}(f_i) \in \mathbb{C}^{M\times K}$ as follows [151]:

$$com_{SVD} = 4M^2K + 8MK^2 + 9K^3 \tag{5.68}$$

The MTM-SLC complexity under the same conditions can be defined as follows:

$$com_{MTM-SLC} = L[M(K(3N-1) + 4K - 2) + M] \tag{5.69}$$

The proposed optimal multi antenna spectrum sensing techniques, MTM-LC, in the absence of co-phasing, have a complexity as:

$$com_{MTM-LC} = L[K(3N-1) + 4K - 2 + M] \tag{5.70}$$

Similarly, the other PE based multi antenna spectrum sensing techniques, PE-SLC, and PE-LC have complexities as:

$$com_{PE-SLC} = L[M(2N) + M] \tag{5.71}$$

$$com_{PE-LC} = L[M + 2N] \tag{5.72}$$

5.11 Simulation Results

In our system, CR node uses 64-FFT with sampling frequency 20 MHz. The PR user's Tx uses 64-IFFT with symbol duration T_s =0.05μs, and transmits QPSK signal with normalized energy equal to 1 over each subcarrier (i.e., $E_s = 1$). The results here start with focusing, firstly, on using LMS for spectrum sensing in CR systems, to discuss the proper number of singular values squares, *V*, which should be used in the LMS spectrum estimation as in (5.14). The work, in this part, includes evaluating the performance using *M*=1, 2, 3, and 4 antennas in AWGN and Rayleigh flat fading channels, and *L*=20 for spectrum sensing. Then, secondly, the multi antenna based spectrum sensing techniques considered in this chapter; MTM-SLC, MTM-LC, PE-SLC, PE-LC, and LMS are examined with different number of antennas *M*=2, and 4.

In MTM techniques, the used half time bandwidth product is *NW*=4, and the number of tapers is *K*=5 [2]. In all cases of simulations, the results are averaged over 10^6 realizations. The channels considered in the simulation are AWGN with zero mean and variance σ_w^2, Rayleigh flat fading, and multipath fading. The performance is evaluated over a chosen frequency bin, when it is assumed that the whole band under sensing is occupied by PR's signal. Finally, a comparison between the different considered spectrum sensing techniques in terms of complexity will be discussed.

Figure 5.6 shows the ROC curves for the LMS technique with *M*=1,2,3 and 4 antennas, *V*=1 in *M*=1 case, and 2 in *M*=2, 3, and 4 cases. The channel is assumed as AWGN with SNR=−10dB per single antenna, and therefore SNR=−10dB using LMS as well. The number of sensed samples (i.e., OFDM blocks) is *L*=20. The performance

is compared with the MTM, and the PE using single antenna for both techniques in the same conditions as shown in Figure 5.6 and Table 5.1.

Firstly, we note that both LMS and MTM spectrum estimation when single antenna is used have the same performance in the same system conditions. Secondly, the number of singular values squares, V, used in the LMS should be smaller than or equal to two ($V \leq 2$) because the improvement in the performance using more than two singular values is not noticeable. Thus, using$V \leq 2$, achieves good enough performance, and at the same time minimizes the complexity of the processing by using enough singular values squares.

The percentage of improvement using multi antenna compared to single antenna for the MTM is as follows: 20% using two antennas with V=2; 30% using three antennas with $V > 1$; and 37% using four antennas with $V > 1$.

The PE gives the probability of detection as 20% under the same conditions, thus the LMS outperforms the PE by 40% using single antenna, 60% using two antennas and V=2, 70% using three antennas with $V > 1$, and finally 77% using four antennas with $V > 1$. Although, there is an improvement in the performance with the increase in the number of antennas, such improvement becomes less as M increases that satisfies what has been mention in section 5.2. From Table 5.1, as an example, the difference between the probabilities of detection for M=1, and 2 cases is 20 %. This difference becomes 10% between M=2, and 3 cases. Finally, for M=3, and 4 cases, the difference becomes 7%.

Figure 5.7 Shows the ROC curves for LMS with M=1, V=1, and M=2, 3, 4 where V=2, and the MTM and PE with M=1 when the wireless channel is Rayleigh flat fading with average signal to noise ratio SNR=-5dB and L=20. The performance is compared with the MTM, and the PE using single antenna for both techniques in the same conditions as shown in Table 5.2. As can be seen from the table, the use of M=2 in LMS

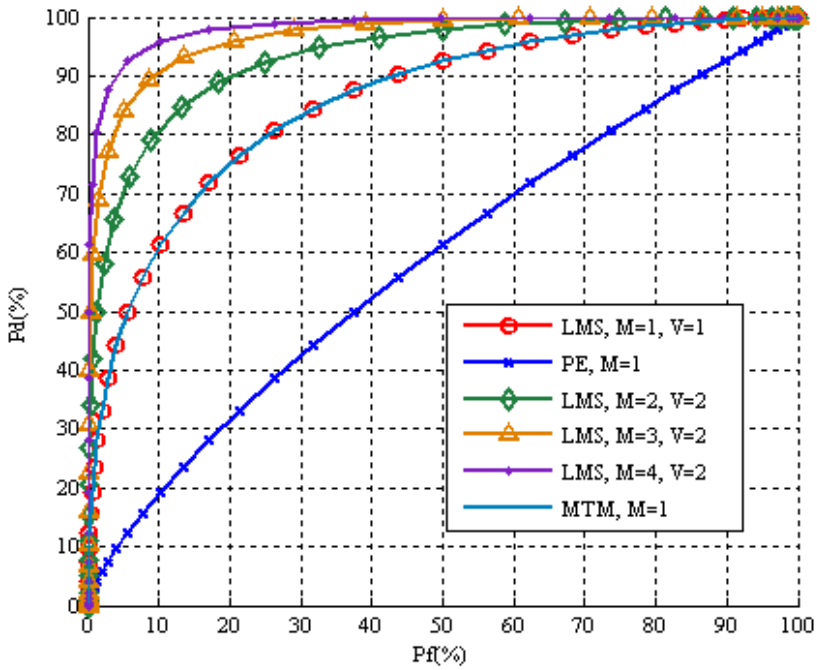

Figure 5.6 The ROC curves for LMS, MTM, and the PE at AWGN with SNR=−10dB and L=20.

No. of antennas, *M*	LMS				**MTM**	**PE**
	***V*=1**	***V*=2**	***V*=3**	***V*=4**		
1	60%	-	-	-	60%	20%
2	78%	80%	-	-	-	-
3	89%	90%	90%	-	-	-
4	96%	97%	97%	97%	-	-

Table 5.1 Probability of detection for local-MTM-SVD, MTM, and PE at AWGN with SNR=−10dB when false alarm is 10%.

gives probability of detection 17% higher than that when single antenna is used for MTM under the same conditions. The M=3, and 4 cases improve the probability of detection by 22 and 24% respectively compared to the M=1 case. The PE with single antenna case gives probability of detection below LMS technique with M=1 by 13% in the same conditions. When the number of antennas is increased to M=2,3, and 4, the probability of detection is increased by 30, 35, and 37%, respectively, compared to the PE.

Figure 5.8, and Figure 5.9 show ROC curves when the different spectrum sensing techniques are used with different number of antennas at AWGN with SNR=−10dB and 20 OFDM blocks (i.e., $L = 20$) used in sensing. Note that the number of samples used is $(L = 20) \times (N = 64) = 1280$, which approximately corresponds to sensing time64μs. Both figures show significant improvement in the performance using the proposed MTM with multi antenna techniques. Additionally, we can see how the LMS technique has the same performance that is achieved by MTM-SLC under the same conditions. This suggests, MTM-SLC is more practical for spectrum sensing since it does not need SVD process and gives the same performance with lower complexity, which will be discussed numerically by the end of this chapter.

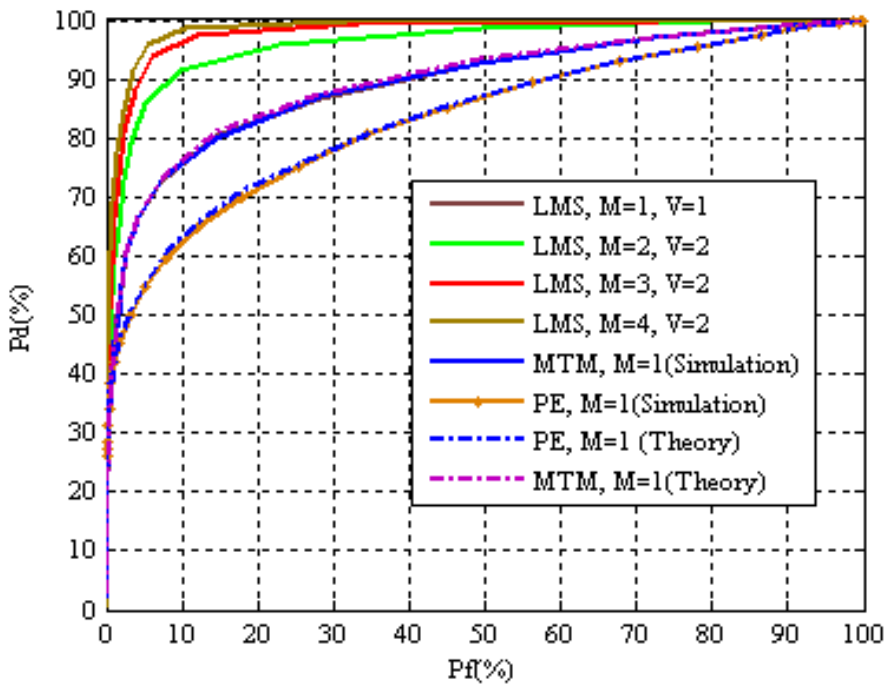

Figure 5.7 The ROC curves for LMS, the MTM, and the PE at Rayleigh flat fading with average SNR=−5dB.

No. of antennas, *M*	LMS		MTM	PE
	***V*=1**	***V*=2**		
1	75%	-	75%	62%
2	-	92%	-	-
3	-	97%	-	-
4	-	99%	-	-

Table 5.2 Probability of detection for LMS, MTM, and PE at Rayleigh flat fading with SNR=−5dB when false alarm is 10%.

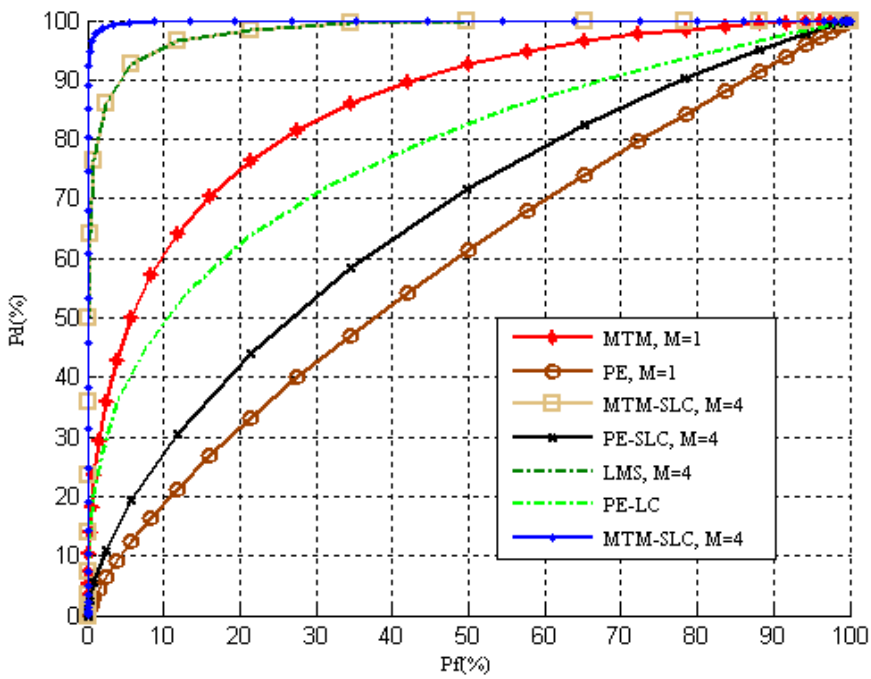

Figure 5.8 ROC curves for MTM and PE with *M*=1, and LMS, MTM-SLC, MTM-LC, PE-SLC, and PE-LC with *M*=4 antennas at AWGN with SNR=−10dB and $L = 20$.

Using *M*=2 antennas, when $P_f = 10\%$, MTM-SLC, MTM-LC, PE-SLC, and PE-LC techniques have P_d =80, 95, 21, and 29% respectively. The MTM-LC outperforms MTM-SLC in terms of P_d by 5% for *M*=4 case, and by 14% for *M*=2 case, when $P_f = 10\%$ under the same conditions. PE techniques have the poorer performance compared to the others in the same conditions.

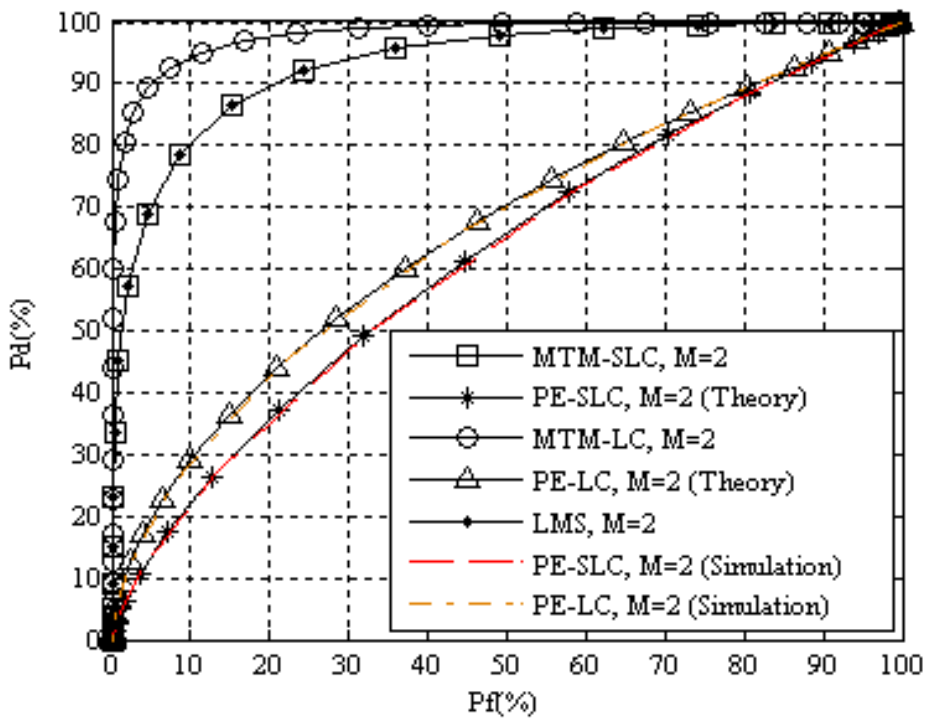

Figure 5.9 ROC curves for LMS, MTM-SLC, MTM-LC, PE-SLC, and PE-LC with M=2 antennas at AWGN with SNR=−10dB and $L = 20$.

The improvement in detection probability is significant when LC based is used as it multiples the SNR in AWGN by the number of antennas M [15], as has been mentioned in section 5.2 under the LC definition. Therefore, for signals with SNR=−10dB each arrive at different M=4 antenna branches at the CR Rx, and the resulting SNR from adding these signals using LC will be SNR=−3.98dB for both MTM-LC and PE-LC. Then, MTM will then be applied finally. Add to this, the improvement that can be achieved by averaging over L samples as has been discussed in subsection 4.5.9 (Figures 4.27-4.29) and the advantages when MTM is used in MTM-LC. Although the assumed conditions and the considered systems here are different from those in Zhang's work in [154]. Figures 3 and 4 in his work show that the probability of detection when MTM was used is 100% at false alarm was fixed to 0.1% and the SNR=−18dB.

The improvement in detection probability curves when SLC based with M antennas is used is achieved by averaging the estimated power that contains independent

Gaussian samples of noise from different M antennas and over L samples. Therefore, the performance using M antennas in MTM-SLC with L samples over each antenna is equal to the performance when MTM with one antenna is used under the same conditions but with samples equal to $L \times M$. Figure 5.10 shows the PDFs of noise and noise added to signal cases when MTM with M=1 and L=80 samples and MTM-SLC with M=4 and L=20 samples are used where NW=4 and K =5 tapers at AWGN with SNR=-10dB. The figure shows how the use of MTM-SLC with M=4 antennas and L=20 samples over each antenna produces the same PDFs for MTM with M=1 but with L=80 samples.

Figure 5.11 shows the ROC curves for the different considered multi antenna based spectrum sensing techniques with number of antennas M=2 at Rayleigh flat fading with average SNR=-5dB and $L = 20$. It is clear that the MTM-LC and PE-LC' performance

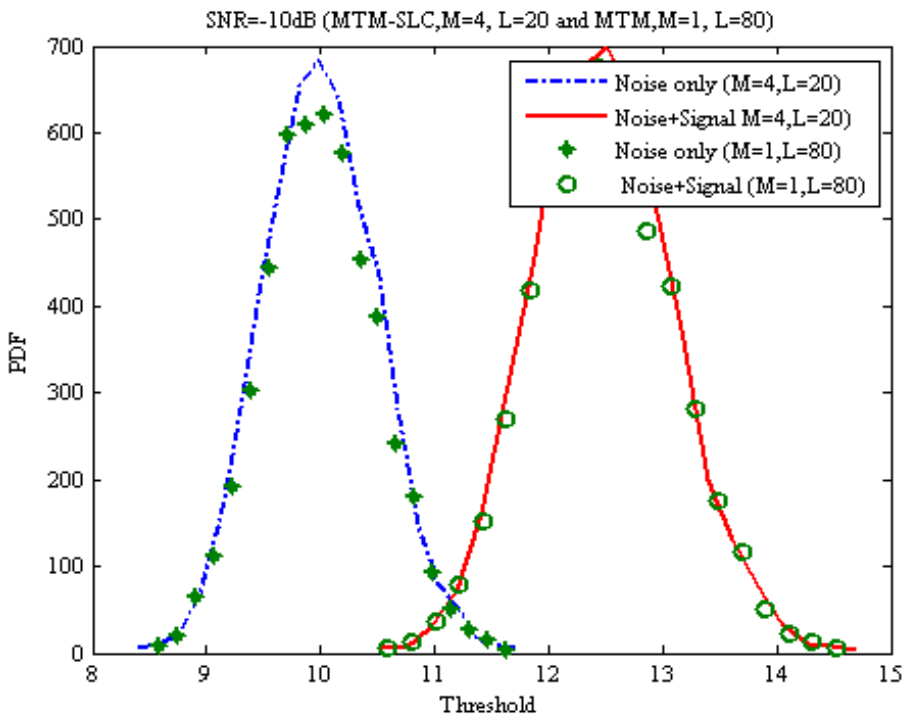

Figure 5.10 PDFs versus threshold of noise and noise added to signal cases when MTM with M=1 and L=80 samples and MTM-SLC with M=4 and L=20 samples are used where NW=4 and K =5 tapers at AWGN with SNR=-10dB.

are affected by fading more than that in MTM-SLC and PE-SLC. This is due to the destructive adding of the received signals from different antennas without co-phasing the channels coefficients. There is a significant outperforming of MTM against PE even in fading environment, and the LMS still has the same performance when using MTM-SLC under the same conditions. The probability of detection P_d's percentages when false alarm fixed to P_f =10% using MTM-LC, MTM-SLC, PE-LC, PE-SLC, and LMS are 77, 93, 62, 81, and 93 % respectively.

Figure 5.12 shows the probabilities of detection P_d that meet the probability of false alarm P_f =10% versus the SNR at AWGN using MTM with single antenna, MTM-SLC, and MTM-LC with *M*=4 antennas, and $L = 50$ is used for spectrum sensing. We can see the noticeable improvement in the performance using both proposed techniques

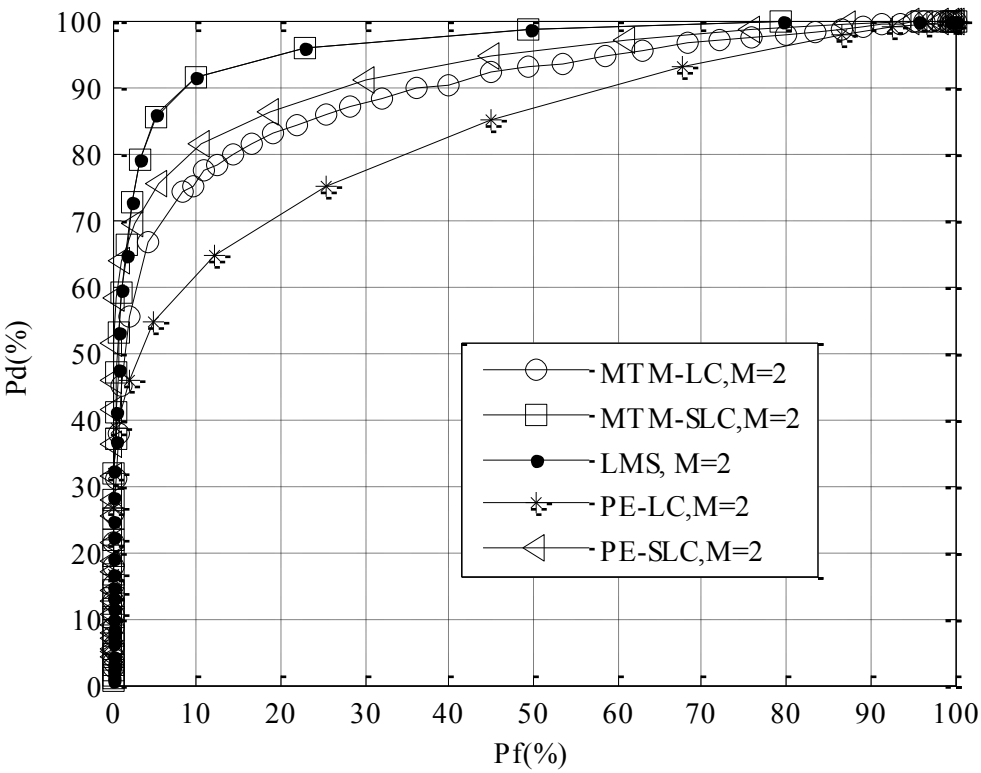

Figure 5.11 The ROC curves for LMS, MTM-SLC, MTM-LC, PE-SLC, and PE-LC with *M*=2 antennas at Rayleigh flat fading with SNR=−5dB and $L = 20$.

compared to MTM with single antenna. At SNR=−15dB, MTM-SLC outperforms MTM with single antenna in terms of probability of detection P_d by 30%. On the other hand, MTM-LC outperforms MTM with single antenna by 66%. It can be seen from the figure that our simulations match the theory.

Figure 5.13 shows a comparison between the number of OFDM blocks L required to achieve $P_d = 99\%$, and $P_f = 1\%$ at AWGN environment with different SNR using the different considered techniques with M=1, and 4 antennas.

It is clear that the number of OFDM blocks used in the sensing process in the MTM system is lower than that for PE in all cases. Additionally, LC techniques require a lower number of OFDM blocks compared to SLC for both MTM, and PE cases under the same conditions. For example, from the figure at SNR=−15dB the number of OFDM blocks L in dB that are required by PE only, PE-SLC, PE-LC, MTM only, MTM-SLC, and MTM-LC are 50, 42, 35, 32, 27, and 20 , or in *seconds* as 0.32, 0.0507,

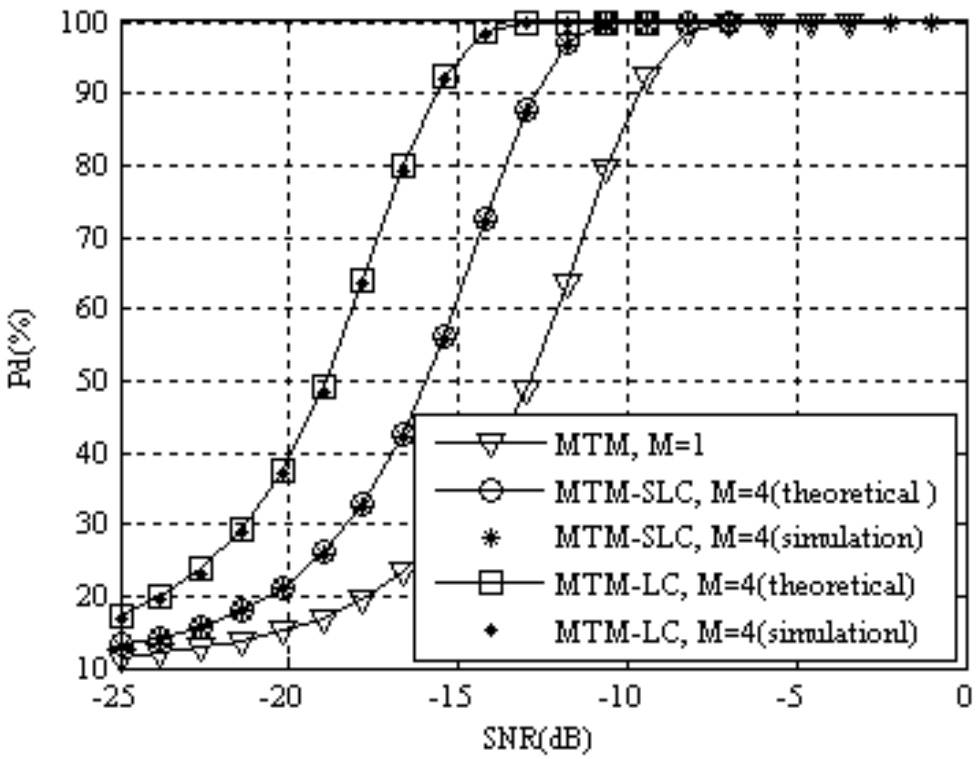

Figure 5.12 Probability of detection curves that meet $P_f = 10\%$ versus the SNR at AWGN using MTM, MTM-SLC, and MTM-LC spectrum sensing techniques with number of antennas M=4 and $L = 50$.

0.0101, 0.0051, 0.0016, and 3.2×10^{-4} respectively. It is clear the MTM multi antenna based spectrum sensing techniques proposed in this chapter are faster than the others. For example, MTM-LC is faster than MTM only by 93.75% (i.e., faster by 0.0048 $m\ seconds$) and than PE-LC by 96.85%. Figure 5.14 shows the ROC curves when MTM, MTM-SLC, LMS with *M*=2, and 3 for MTM multi antenna based techniques are used at multipath fading with *P*=3 paths and $N_{CP} = 6$ symbols is used as a CP where SNR $= -10$dB and $L = 20$.

In the multipath fading, the channel magnitude response, $|H_m(f_i)|^2$, varies over the frequency subband producing frequency selective multipath channel. In our simulation, the multipath fading channel over each antenna is independent from the other antennas and is produced, similarly, as in subsection 4.5.9, where Rayleigh channel model consists of three paths (i.e., *P*=3) is used for each antenna.

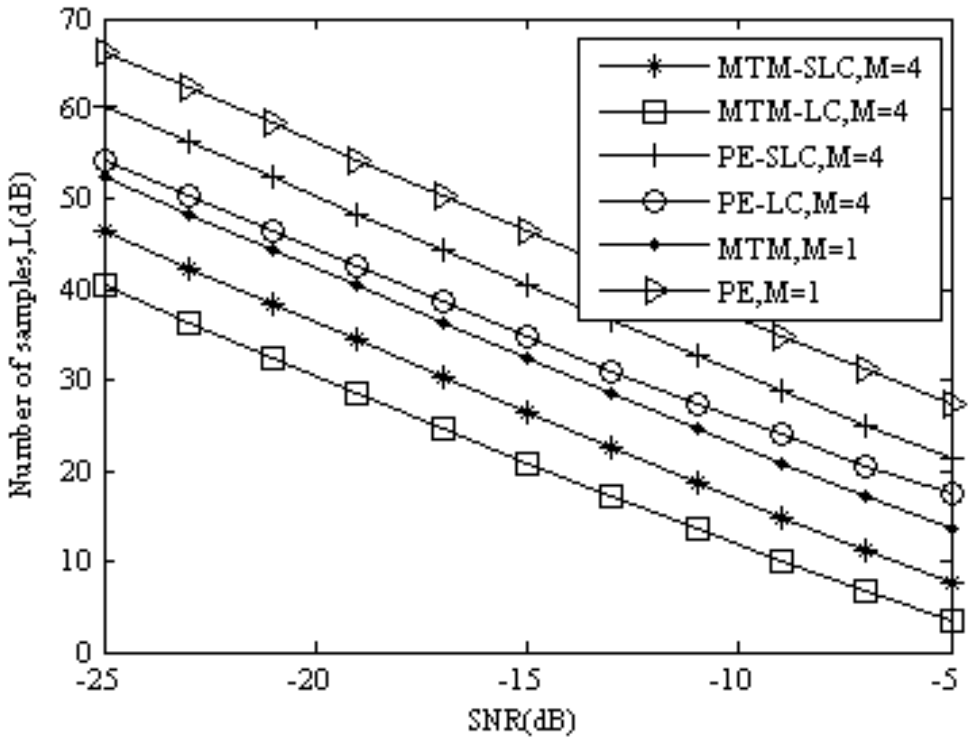

Figure 5.13 Numbers of samples, *L*, required to achieve $P_d = 99\%$, and $P_f = 1\%$ at AWGN with different SNR using MTM, MTM-SLC, MTM-LC, PE, PE-SLC, and PE-LC spectrum sensing techniques with number of antennas *M*=1, and 4.

The power delay profile is exponential. Each multipath component per each antenna is assumed as an independent and identically distributed zero mean Gaussian random variable. A number of six symbols are used as CP by the PR Tx (i.e., N_{CP}=6). At the CR Rx, such CP is removed before implementing MTM multi antenna based spectrum sensing. Note that, the total number of samples used here is $(L) \times (N + N_{CP})$ which approximately corresponds to sensing time$(L) \times (N + N_{CP}) \times (Ts)$.

The figure shows how the multipath fading wireless channel degrades the MTM-SLC and LMS with *M*=2 performances compared to the AWGN case in Figure 5.9. As a comparison, the MTM-SLC, and LMS's P_d is decreased by 29% at P_f=10% in the multipath fading model considered here compared to that in Figure 5.9 for *M*=2 case. However, the use of MTM-SLC and LMS improves the P_d compared to use MTM with single antenna in multipath fading. From Figure 5.14, using MTM-SLC, and LMS with *M*=2 increases the P_d by 12% compared to using MTM only with single antenna in the same fading conditions. When *M* is increased to three antennas, the improvement in P_d is increased by 22% compared to MTM only with single antenna under the same conditions. The MTM-SLC and LMS still have the same performance even in multipath fading environment.

The required SNRs in (dB) for MTM-SLC, MTM-LC, PE-SLC, PE-LC to achieve probability of detection 99.99%, using *M*=4 antennas at AWGN when the false alarm is 1% and *L*=16 sensed samples, can be summarized as follow:

- The MTM-SLC and MTM-LC give the same probability of detection, when the SNR for them is -7.5, and -12dB respectively.
- The PE-SLC and PE-LC achieve the same probability of detection under the same conditions, when their SNRs are 5, and 0 dB respectively.

It's clear that the MTM-LC has a 12dB SNR's gain compared to PE-LC, and 17dB compared to PE-SLC.

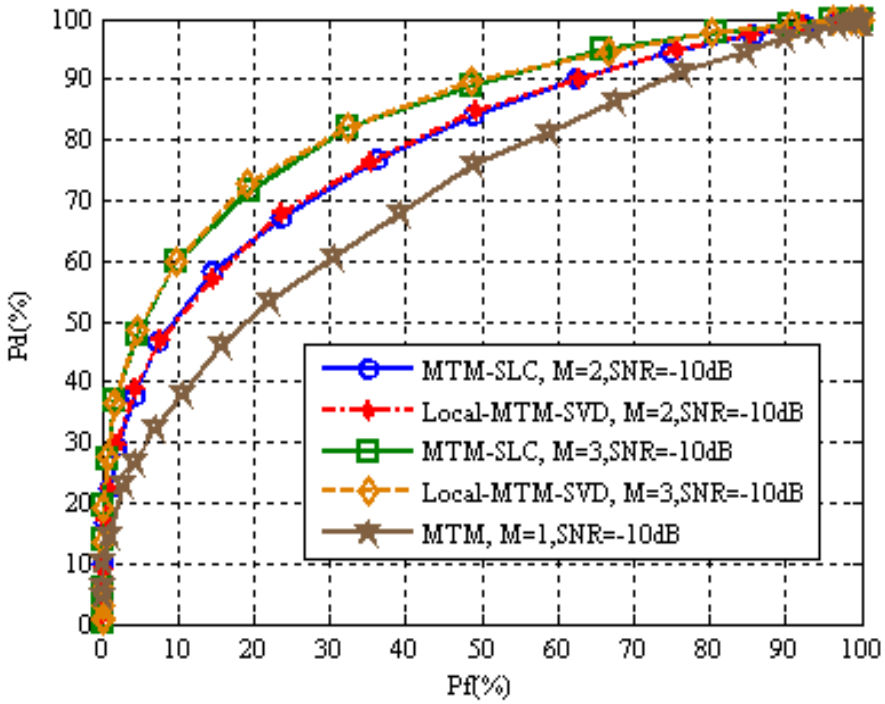

Figure 5.14 The ROC curves when MTM, MTM-SLC, and Local-MTM-SVD are used at multipath fading with P=3 paths and $N_{CP} = 6$ is used as a CP where SNR= -10dB, $L = 20$, and M=2, and 3 antennas for MTM multi antenna based techniques.

Table 5.3 shows the complexity of the different considered techniques, MTM, LMS, MTM-SLC, MTM-LC, PE, PE-SLC, and PE-LC based on (4.8), (4.9), and (5.68)-(5.73) for K =5 in MTM based cases with length N=64, and L=1 (i.e., over one OFDM block).

It is clear that MTM based techniques are more complex than the PE based in all cases. However, such simplicity in PE based spectrum sensing techniques comes at the expense of the performance, as has been shown in chapter 4 and in this section. The LC based multi antenna based spectrum sensing techniques, when the equalization process is neglected, have computation complexity lower than that for the SLC based ones. The LMS is more complex than the MTM-SLC; however, they have the same sensing performance. This similarity in performance makes the MTM-SLC more promising in

Technique	Complexity			
	M=1	M=2	M=3	M=4
MTM	973	-	-	-
PE	128	-	-	-
LMS	-	3515	4770	6065
MTM-SLC	-	1948	2922	3896
MTM-LC	-	975	976	977
PE-SLC	-	258	387	516
PE-LC	-	130	131	132

Table 5.3 The complexity evaluation of the different considered techniques for K=5, 64-FFT, and over L=1 OFDM block.

terms of simplicity compared to the LMS. The increase in M causes an increase in the complexity for all multi antenna based techniques. In LC based techniques, as M increases by one, the complexity increases only by one. In contrast, the increase in complexity becomes significantly higher when M increases by one in the other cases.

As examples, when M=2, the MTM-SLC's complexity is lower than that for LMS by 55.4196%. At the same M, the PE-SLC's complexity is lower than that for MTM-SLC by 13.2444%. By increasing M to 4, the LMS's complexity increases by 57.9555% compared to the same technique when M=2.

5.12 Conclusion

In this chapter, different MTM-multi antenna based techniques are studied as efficient CR spectrum sensing techniques. Theoretical work has been derived for the proposed techniques in AWGN, and multipath fading wireless environments. The PE-multi antenna based spectrum sensing techniques have also been derived and compared to that of MTM, and the LMS. This has been published in [5, 6]

Using multi antenna in MTM-LC, and MTM-SLC gives more improvement in performance compared to that for PE-LC, PE-SLC. The LMS spectrum sensing technique has the same performance of MTM-SLC under the same conditions. Therefore, we can say that the MTM-SLC is more practical for spectrum sensing than

LMS as it does not need SVD processors, and this minimizes the complexity and the cost of the system. In MTM-LC, and MTM-SLC techniques, the required SNRs are found as -12 and -7.5 dB, respectively to achieve a probability of detection of 99.99% at false alarm 1% with AWGN using 4 antennas and L=16 samples for sensing. The proposed techniques represent local cooperation using multi antenna. The different hard and soft cooperation algorithms in the literature can be used here to improve the overall performance in the CR network.

5.13 Chapter Summary

This chapter has explored the area of multi antenna systems in wireless communication. Different technical concepts relevant to multi antenna based systems were defined and discussed. The use of multi antenna in classical wireless communication was reviewed, and then the benefits from using multi antenna in CR systems were introduced.

One optimal, MTM-LC, and two suboptimal, MTM-SLC, and LMS multi antenna based spectrum sensing techniques were proposed in this chapter. The work here included deriving the statistical parameters of the D PDFs for MTM-LC and MTM-SLC for different hypotheses. The statistical work of the PE multi antenna based was also presented. The different probabilities and number of sensed samples formulae were derived for MTM-LC, MTM-SLC. Similarly, the PE based multi antenna spectrum sensing techniques theoretical work was presented as well. The singular values squares use for the power spectrum estimation in LMS techniques was discussed and the computational complexity of the different considered spectrum sensing techniques was investigated.

Finally, simulation codes were written in order to examine the proposed multi antenna based spectrum sensing techniques for OFDM based CR systems. For the

MTM-LC, and MTM-SLC, the results showed how our theoretical works match well the simulation. The MTM-LC increases the SNR and then improves the performance, however, such techniques requires co-phasing to eliminate the channel coefficients. This is possible, when prior information about the PR signal is known to the CR (i.e., training sequence and pilot signal). The blind equalization techniques [177, 178] are promising in such cases. The LMS gives the performance as MTM-SLC, but with higher complexity. Therefore, MTM-SLC is more promising since it has less complexity, which would make the spectrum sensing process much faster than if LMS were to be used. However, the SVD process itself is useful in eliminating multi user interference (MUI) in the downlink and uplink paths in mobile communications systems as in [182]. The different considered techniques here are examined in different environments including AWGN, Rayleigh flat fading and multipath fading. The proposed techniques outperform all other discussed techniques in term of performance.

Chapter 6: New Optimization Method for Cooperative Spectrum Sensing in Cognitive Radio Networks

6.1 Introduction

Subsection 2.4.3.2 reviews the concepts and literature works relevant to CSS and its two main types SCSS, and HCSS. As has been mentioned in subsection 2.4.3.2.1, the work in this thesis concentrates on HCSS, due to the narrow bandwidth CC that is required in such types of cooperation. Furthermore, HCCS is able to deliver a higher level performance than its counterparts when large numbers of CRs share the cooperation in the CR network [77].

HCSS optimization is an important issue in CR systems. Different numbers of CRs, in the CR network, share their binary local decisions about the PR signal at a CR-BS, which fuses this information and decides finally the state of the frequency subband under sensing. The global performance at CR-BS (i.e., overall/or global probability of detection, or overall/or global probability of false alarm), generally, is affected by the type of fusion rule, the local chosen threshold at each CR, and the total number of cooperated CRs when a specific spectrum sensing technique like PE is used locally at each CR. Therefore, some works in the literature had optimized the overall performance by optimizing such factors. However, we believe that the global performance can be taken to the optimum point by optimizing the locally sensed samples at each CR. Thus, two strategies have been proposed in this chapter to achieve our aim. Additionally, the effects of spectrum sensing technique type used locally at each CR, the number of locally sensed samples, the local SNR, and the total number of cooperated CRs on the optimal fusion rule are investigated. A PE and MTM spectrum sensing techniques are examined as local spectrum sensing techniques.

In this chapter we also introduce a new cooperation concept, the master node (MN) cooperation. In MN, a single CR node can be supported by advanced hardware components, and advanced signal processing. This improves the detection's probability, minimizes the overall CR network complexity, minimizes the overhead that is required when all CR's nodes share sensing and accelerates the decision process.

The main content of this chapter has been published in two papers that represent the chapter contributions. The published papers are:

O. A. Alghamdi and M. Z. Ahmed, "Optimal and Suboptimal Multi Antenna Spectrum Sensing Techniques with Master Node Cooperation for Cognitive Radio Systems," *Journal of Communications (JCM),* vol. 6, pp. 512-523, 2011.

O. A. Alghamdi and M. Z. Ahmed, "New optimization method for cooperative spectrum sensing in cognitive radio networks," in *Proc. 7th IEEE Wireless Advanced Conference (WiAd 2011)*, 2011, pp. 54-59.

6.2 HCSS Optimization Techniques

Numbers of strategies and factors have been investigated to optimize the HCSS performance by minimizing the total error probability, or maximizing the global probability of detection [51, 132, 133]. This was achieved by optimizing the number of cooperated CRs and the threshold as in [132]. In [51], the authors maximized the global probability of detection in "OR'' and "AND'' fusion rules by fixing the global false alarm probability and maximizing the local probability of detection. Optimal strategies to minimize the total error probability under Neyman Pearson and Bayesian criterions have been considered in [133].

In this chapter, we contribute to the HCSS optimization area by adding an important factor: the number of locally sensed samples *L,* which can be controlled in time to minimize the total error probability in the cooperative spectrum sensing. The

work here can be applied to all mentioned optimization strategies to take them to the optimum point. All optimization published works focused only on PE as a local spectrum sensing. In this thesis, PE and MTM are studied in optimization. Additionally, the effects of using different numbers of CRs and different SNR on the optimal fusion rule have been investigated.

The next section, describes the HCSS system model, the effect of using different local spectrum sensing techniques on optimization, the proposed optimization strategies and then the effect of different numbers of cooperated CRs on the optimization.

6.3 HCSS System Model and Optimization

The local spectrum sensing at each CR has been described theoretically, as in sections 4.4 and 4.5, when PE or MTM are used. In general, the cooperation in spectrum sensing is achieved when a number G of CRs in the CR's network send their local decisions to the CR-BS via CC. After this, CR-BS combines these decisions and decides finally about the presence of PR's signal in frequency bin f_i. Note that, in our work here, we are interested in examining the performance when the power spectrum is sensed at f_i when the whole band under sensing is occupied by PR's signal in $\mathcal{H}_1$ case. The HCSS starts by performing local spectrum sensing using PE or MTM. The rth CR decides, $\mathcal{H}_1$ as represented by binary digit b_r="1'', or $\mathcal{H}_0$ represented by binary digit b_r ="0'', based on its own local decision statistic. Finally, the CR-BS combines the received digits from different CRs to declare the final decision about the presence of the PR user. The representative diagram of centralized CSS can be seen in Figure 2.18.

The received binary digits at the CR-BS from the different CRs in the CR network, are fused together to declare the final decision using the following logic rule [132]:

$$D_{COP}(f_i) = \sum_{r=1}^{G} b_r \begin{cases} \geq g, & H_1, \\ < g, & H_0, \end{cases} \tag{6.1}$$

where $D_{COP}(f_i)$ is the cooperative decision at CR-BS, and H_1 represents the final decision that has been made by the CR-BS, stating that the PR's signal is present in f_i, and H_0 represents that the PR's signal is absent. The number of CRs g that decide the presence of the PR's signal in f_i, determines the type of fusion rule at CR-BS. When $g = 1$ out of total G CRs; the fusion rule is "OR''. The fusion rule is "AND'', if only and if all $g = G$ CRs decide $\mathcal{H}_1$, and then the final decision will be H_1. Finally, when $1 < g < G$, the fusion rule is "VOTING''. This process can be written as follows:

$$g = \begin{cases} 1, & ''OR'' \\ G, & ''AND'' \\ 1 < g < G, & ''VOTING'' \end{cases} \tag{6.2}$$

In order to evaluate the cooperative spectrum sensing performance, we define three joint probabilities; the joint probability of detection $Q_d(f_i)$, the joint probability of false alarm $Q_f(f_i)$, and the joint probability of missed detection $Q_m(f_i)$. The joint probability of detection $Q_d(f_i)$ can be written as follows [132]:

$$Q_d(f_i) = P(D_{COP}(f_i) \geq g / \mathcal{H}_1)$$

$$= \sum_{r=g}^{G} \binom{G}{r} [P(D(f_i) > \gamma / \mathcal{H}_1)]^r [P(D(f_i) < \gamma / \mathcal{H}_1)]^{G-r}$$

$$= \sum_{r=g}^{G} \binom{G}{r} P_d(f_i)^r \left(1 - P_d(f_i)\right)^{G-r} \tag{6.3}$$

and the joint probability of false alarm $Q_f(f_i)$ can be written as follows [132]:

$$Q_f(f_i) = P(D_{COP}(f_i) \geq g / \mathcal{H}_0)$$

$$= \sum_{r=g}^{G} \binom{G}{r} [P((f_i) > \gamma / \mathcal{H}_0)]^r [P(D(f_i) < \gamma / \mathcal{H}_0)]^{G-r}$$

$$= \sum_{r=g}^{G} \binom{G}{r} P_f(f_i)^r \left(1 - P_f(f_i)\right)^{G-r} \tag{6.4}$$

Note that $D(f_i)$ here means that the decision statistic of the used local sensing technique at each CR (i.e., $D_{MTM}(f_i)$ or $D_{PE}(f_i)$ that defined in (4.3) and (4.10) respectively). Finally, the joint probability of missed detection can be written as follows:

$$Q_m(f_i) = P(DEC_{COP}(f_i) < g / \mathcal{H}_1)$$

$$= 1 - Q_d(f_i). \tag{6.5}$$

$Q_d(f_i)$ is defined as the probability that CR-BS decides correctly the presence of the PR signal in the sensed frequency subband (i.e., at f_i here in this case), while $Q_f(f_i)$ is defined as the probability of declaring the presence of the PR signal by CR-BS when it is absent. The joint probabilities would be called overall or global probabilities.

The total error probability of the cooperative CR spectrum sensing is defined as follows [132]:

$$Q_{error}(f_i) = Q_f(f_i) + Q_m(f_i). \tag{6.6}$$

The joint probability of detection, $Q_d(f_i)$, and the joint probability of false alarm, $Q_f(f_i)$, of the "OR'' rule combining at the CR-BS using G CR with identical probabilities of detection and false alarm, and perfect CC, are given by [48]:

$$Q_d(f_i) = 1 - \prod_{r=1}^{G}(1 - P_{d,r}(f_i)) \tag{6.7}$$

$$Q_f(f_i) = 1 - \prod_{r=1}^{G}(1 - P_{f,r}(f_i)) \tag{6.8}$$

where $P_{d,r}(f_i)$, $P_{f,r}(f_i)$ represent the probabilities of detection and false alarm achieved by the rth CR. Such probabilities are defined in (4.36) –(4.37) for MTM and in (4.50)-(4.51) for PE.

The different joint probabilities formulae can be defined for “AND’’ rule case, in the same conditions, as follow [130]:

$$Q_d(f_i) = \prod_{r=1}^{G} P_{d,r}(f_i) \tag{6.9}$$

$$Q_f(f_i) = \prod_{r=1}^{G} P_{f,r}(f_i) \tag{6.10}$$

Figure 6.1 shows the joint probabilities of detection versus joint probabilities of false alarm when “OR’’ and “AND’’ fusion rules are used at CR-BS with G=5 CRs where the PE and MTM with NW=4and K=5 tapers are used locally at each CR in AWGN channel with SNR=− 10dB and L=20 OFDM blocks. By comparing this figure to Figure 4.18 which shows the ROC when only one CR uses MTM and PE under the same conditions, it is clear that sharing the decisions of number of CRs in the CR network improves the performance. When the joint false alarm is fixed to 10%, fusing the decisions at CR-BS using “OR’’ rule when MTM is used locally at the five CRs increases the joint probability of detection by 28%, compared to that when one CR is used (i.e., Figure 4.18 case). The use of “AND’’ fusion rule increases the joint probability of detection by 20% compared to using one single CR. Generally, HCCS improves the spectrum sensing probability of detection. However, as it can be seen from the results, the use of “OR’’ gives more opportunity to access the frequency subband, while “AND’’ minimizes the interference possibility to the PR’s frequency subband by ensuring that all CRs agree the presence or absence of PR signal in a specific frequency subband under sensing. In the same case, and compared to the PE use for single CR as in Figure 4.18 when PE is used locally at each CR for the five CRs, the “OR’’HCSS increases the joint probability of detection by 7%, while “AND’’ increases the joint probability of detection by 2%. The HCSS based on local MTM outperforms that based on PE by 60% under the same conditions when “OR’’ fusion rule is used at CR-BS.

Additionally, The HCSS-based on local MTM also outperforms that based on PE by 60% under the same conditions when "AND'' fusion rule is used at CR-BS.

The proposed multi antenna based spectrum sensing techniques in chapter 5 can be used in all types of CSS. This would improve the overall performance of the CSS by exploiting both local (i.e., when multi antenna are used at each CR) and global spatial diversities. Figures 6.2 and 6.3 show the "OR'' rule joint probability of detection versus the joint probability of false alarm for MTM and PE with a single antenna, and MTM-SLC, MTM-LC, PE-SLC, and PE-LC with *M*=3 antennas, and *G*=5 CR users in AWGN with SNR=-12dB and *L*=20 OFDM blocks. At joint probability of false alarm, Q_f =10%, the joint probability of detection is Q_d =100% using the MTM-LC, 92% using MTM-SLC, 45% using PE-LC, and 25% using PE-SLC. When MTM-LC with *M*=3 antennas is used locally at each CR in the HCSS, the joint probability of detection is increased by 40% compared to using MTM with a single antenna under the HCSS in the same conditions when Q_f =10%. Such a high improvement in the performance comes from: firstly, the increase in the SNR when LC is used as it multiplies the SNR by factor *M* at the CR Rx [15] as has been discussed in Figures 5.8 and the results under section 5.11. Secondly, the decrease in the noise power variation by increasing the number of locally sensed samples at each CR Rx (i.e., *L*=20 OFDM blocks), as has been verified in the results discussion of Figures 4.28 and 4.29 under subsection 4.5.9. Thirdly, Figure 5.10 verifies that the performance of using 4 antennas with *L*=20 in MTM-SLC is same as when a single antenna is used in MTM with *L*=80 samples. Thirdly, exploiting the "OR'' rule HCSS [48] and finally, the advantages of using MTM locally at each CR. For locally used MTM-SLC, the joint probability of detection of the HCSS is increased by 32% compared to using MTM with a single antenna in the HCSS under the same conditions. For local PE cases, the increase in the joint probability of detection of HCSS when PE-LC with *M*=3 antennas is used locally is 21% compared to

using PE locally with single antenna under the same conditions. The PE-SLC increases the HCSS's joint probability of detection by 4% under the same conditions. The conclusions here is that using multi-antenna based spectrum sensing techniques locally at each CR improves the overall probability of detection of the HCSS by exploiting more spatial diversity via a number of antennas. The HCSS that is based on using MTM spectrum sensing techniques outperforms significantly the one based on PE in terms of performance under the same conditions.

Up to this point in this section, the concept of HCSS has been analyzed using "OR'' and "AND'' fusion rules at the CR-BS when the MTM and PE are used locally at each CR and G=5 CRs send their binary decisions to that CR-BS. The HCSS has been studied using a single antenna at each CR in AWGN environment. Furthermore, the use of M=3 antennas locally for the proposed techniques in chapter 5 has been investigated to achieve more spatial diversity (i.e., local cooperation via a number of antennas at each CR).

In "OR'' fusion rule, as has been mentioned earlier in this chapter, the CR-BS needs only one CR (i.e., g=1 in (6.1)) out of G CRs decides that the PR signal is present in the frequency subband to declare, finally, its presence to the CR network users. In "AND'' fusion rule, the all cooperative CRs (i.e., g=G in (6.1)) are required to decide the PR's presence in the frequency subband in order for CR-BS to declare this, finally, to the CR network users.

Although, the "OR'' outperforms the "AND'' fusion rule in terms of giving higher joint probability of detection, allowing more spectrum opportunity be achieved, the "OR'' rule is not the optimal rule. The results from [132] shows that the optimal fusion rule that minimizes the total error probability in (6.6), when PE is used locally at each CR, is the half-voting rule for G=10 CRs and SNR=10 dB. This means if G=10 CRs in the

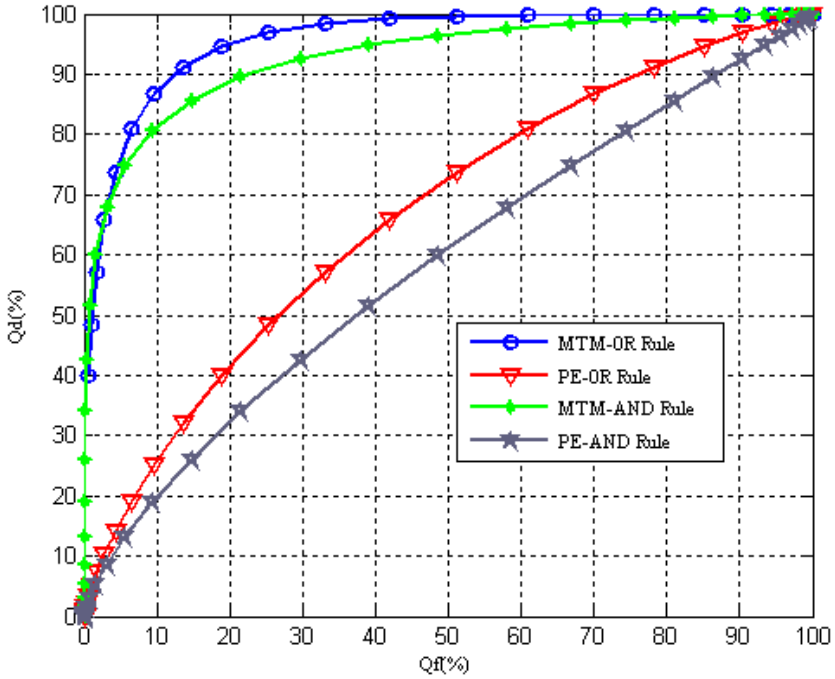

Figure 6.1 Joint probabilities of detection versus joint probabilities of false alarm when "OR'' and "AND'' fusion rules are used at CR-BS with *G*=5 CRs where the PE and MTM with NW=4and *K*=5 tapers are used locally at each CR in AWGN with SNR=− 10dB and *L*=20 OFDM blocks.

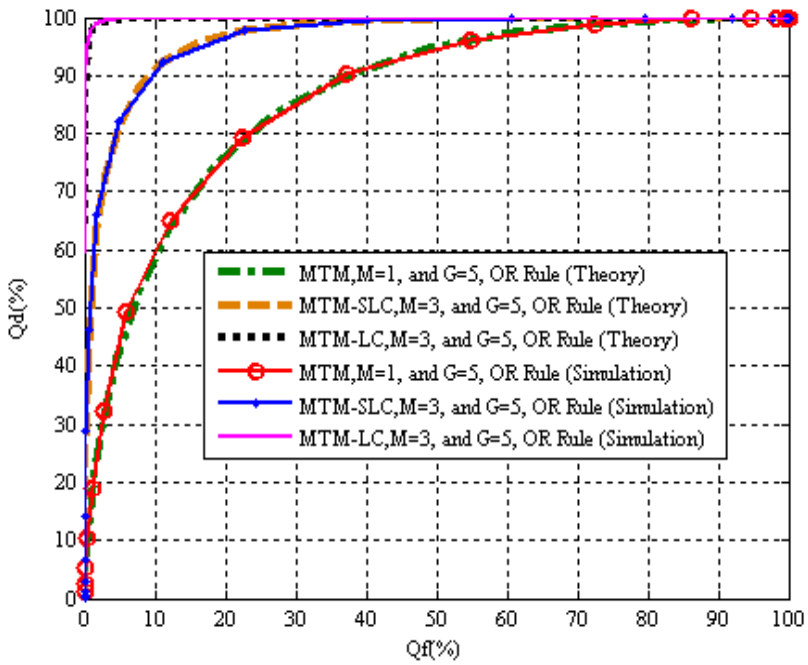

Figure 6.2 Joint probability of detection versus joint probability of false alarm when "OR'' fusion rule is used at CR-BS with *G*=5CRs where the MTM with NW=4 and *K*=5 tapers and single antenna, and MTM-SLC, MTM-LC with *M*=3 antennas are used locally at each CR in AWGN with SNR=− 12dB and *L*=20 OFDM blocks.

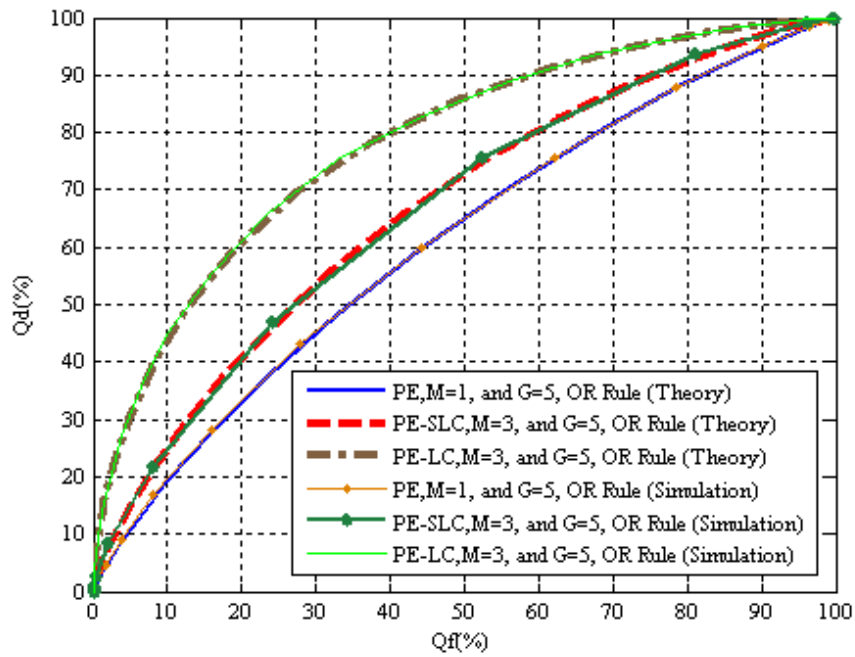

Figure 6.3 Joint probability of detection versus joint probability of false alarm when "OR'' fusion rule is used at CR-BS with *G*=5CRs where the PE with a single antenna, PE-SLC, and PE- LC with *M*=3 antennas are used locally at each CR in AWGN with SNR=− 12dB and *L*=20 OFDM blocks.

HCSS, the optimal *g* is 5. However, we find that this result can not be generalized for the following reasons:

- The used local spectrum sensing technique at each CR plays a crucial role on the optimal fusion rule since different techniques have different local performances under the same conditions.
- The different local SNR at each CR might affect the optimal fusion rule.
- The number of sensed samples at each CR has an important affect, as well, on the optimal fusion rule since it controls the local performance at each CR and, therefore, affects the optimal fusion rule.
- The optimal fusion rule would be changed with the change in the total number of cooperative CRs in the CR network.

Based on this, these factors are considered and analysed in the next subsections to achieve deeper understanding of the fusion rule optimization process in HCSS as can be seen later.

As has been mentioned before in section 6.2, the HCSS optimization methods and strategies in the literature aimed to maximize the overall or global probability of detection (i.e., joint probability of detection), or to minimize the total error probability in (6.6). The optimal fusion rule that minimizes the total error probability is found as half voting in [132], when PE is used locally at each CR, and the total number of cooperated CRs is G=10. The local chosen threshold at each CR that minimizes the total error probability is found in [132] as well, when PE is used locally at each CR. the authors in [51], maximized the global probability of detection in "OR'' and "AND'' fusion rules by fixing the overall or global false alarm probability and maximizing the local probability of detection when PE is used locally at each CR. All these methods ignored the effect of the locally sensed samples in the optimization process. The number of locally sensed samples increases the local probability of detection when it is increased; and the total error probability will then be minimized. Therefore, optimizing the number of locally sensed samples is required to optimize the HCSS by minimizing the total error probability. This type of optimization can be added to all the optimization methods mentioned above to take their performance to the optimist point. Two strategies are proposed here to achieve this objective as can be seen in subsection 6.3.2. Figure 6.4 shows HCSS optimization methods and the proposed method.

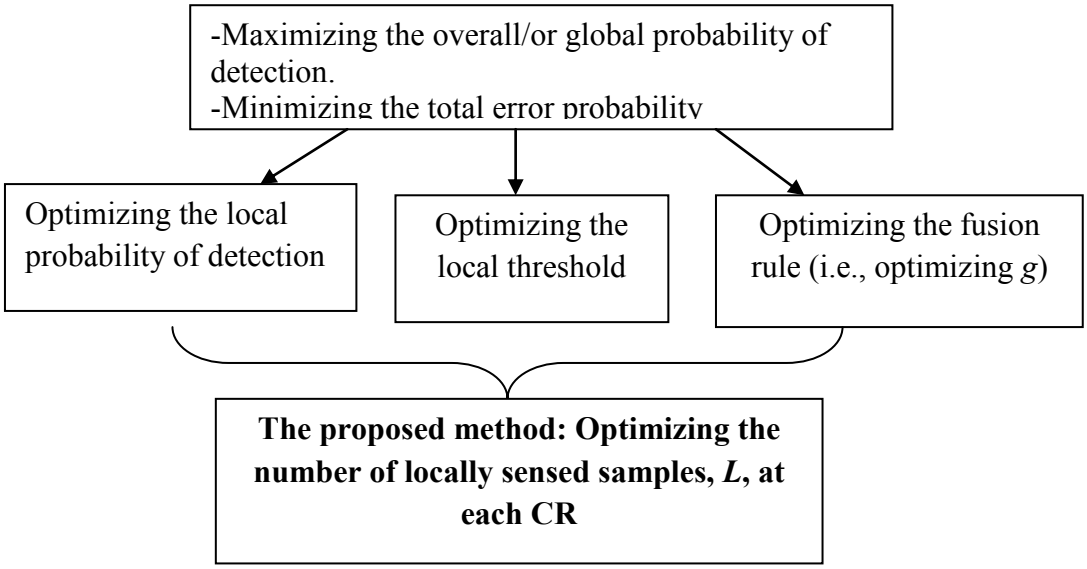

Figure 6.4 The HCSS optimization methods and the proposed method.

6.3.1 Effect of Different Local Spectrum Sensing Techniques on HCSS

In order to examine the performance optimization of the HCSS when different local spectrum sensing techniques are used, the total error probability (Q_{error}) is evaluated at frequency bin f_i, using both PE and MTM. Note that, as we mentioned earlier in this chapter, the different probabilities will be computed at a specific frequency bin f_i. Thus, they will be written in the reminder of the chapter without f_i. There are $G = 10$CRs cooperating the spectrum sensing decisions, at a CR-BS, in the CR network. The local spectrum sensing techniques are PE and MTM. The local SNR $= -5dB$, and $L = 10$ samples (i.e., $L = 10$ OFDM blocks) are used locally for sensing.

Figure 6.5 and Figure 6.6 show the total error probability (Q_{error}) versus the chosen local threshold for different number g out of G CRs that controls the fusion rule in (6.1) using PE, and MTM respectively. Note that the threshold here is based on the noise variance at each CR, as has been in discussed in section 4.4. When we compare the different curves that represent the total error for different numbers of g in Figure 6.5, we note that there are noticeable differences in the performance through using $g =$

1,2, … ,10 as a fusion rule of $G = 10$. While, $g = 10$ which represent "AND" fusion rule, gives a high total error compared to the other curves, it is found that $g = 2$ gives the minimum total error (min Q_{error}) at the mentioned conditions. Thus, $g = 2$ is the optimal fusion rule here (i.e.,$g_{optimal} = 2$). It is clear from Figure 6.6 that all numbers of g out of G have similar min Q_{error} values which are very small compared to the PE case. The optimal fusion is found as $g_{optimal} = 5$ as it gives the minimum total error.

Figure 6.7 shows the minimum total error probability (min Q_{error}) versus g out $G = 10$ CRs for PE and MTM with SNR $= -5$dB , and $L = 10$ sensed samples. Generally, the MTM has minimum total error probabilities (min Q_{error}), lower than that when PE is used through all values of g.

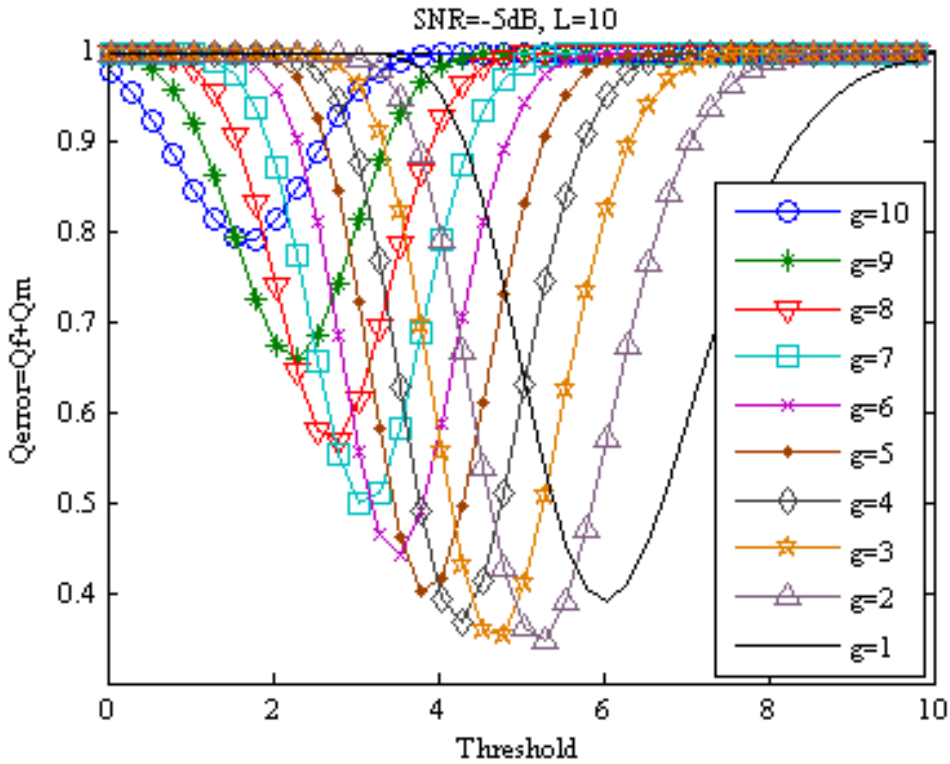

Figure 6.5 Total error probability (Q_{error}) of g out of $G = 10$ CRs versus local threshold when PE is used locally with SNR $= -5dB$ and $L = 10$ sensed samples used at each CR.

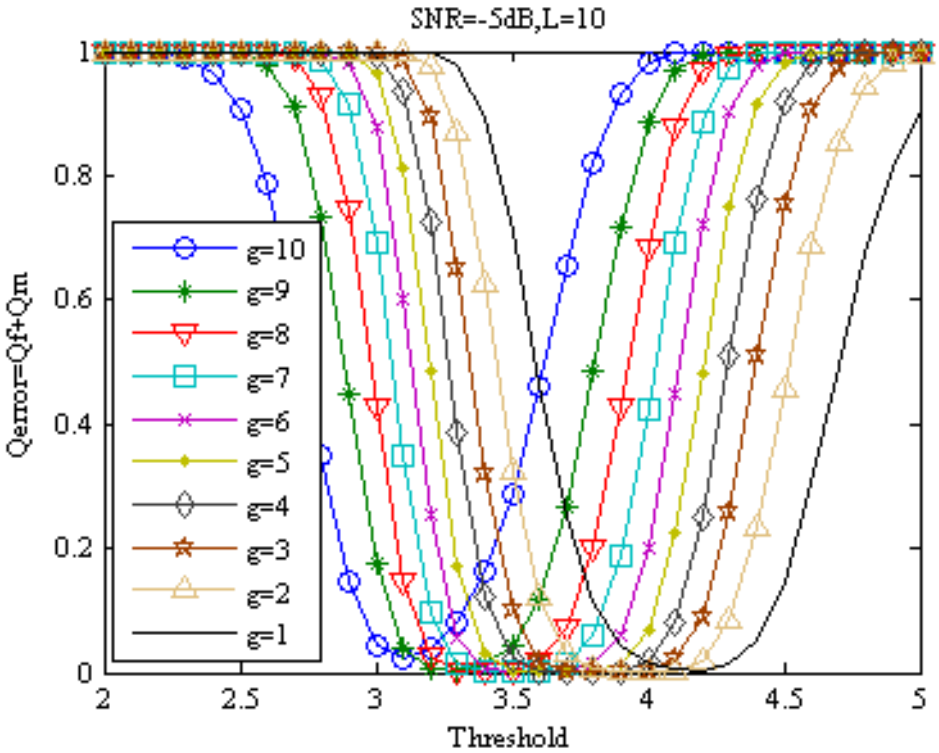

Figure 6.6 Total error probability (Q_{error}) of g out of $G = 10$ CRs versus local threshold when MTM is used locally with $\text{SNR} = -5dB$ and $L = 10$ sensed samples.

In MTM, the optimal total error probability is found as min $Q_{error} = 6.483 \times 10^{-5}$ when $g = 5$, which is the optimal, or $g_{optimal}$ =5. The optimal total error probability is found as, min $Q_{error} = 0.3463$ when $g = 2$ for PE case. This means that the optimization of total error probability shall be done for every type of local spectrum sensing technique. This can be achieved by using the local probabilities of any technique in (6.3)-(6.6). Figure 6.8 shows the log version of Figure 6.7, and the optimality of MTM is clear compared to that case when PE is used locally at each CR. Furthermore, powerful spectrum sensing techniques such as MTM here have approximately similar and very low minimum total error over the different combinations of g.

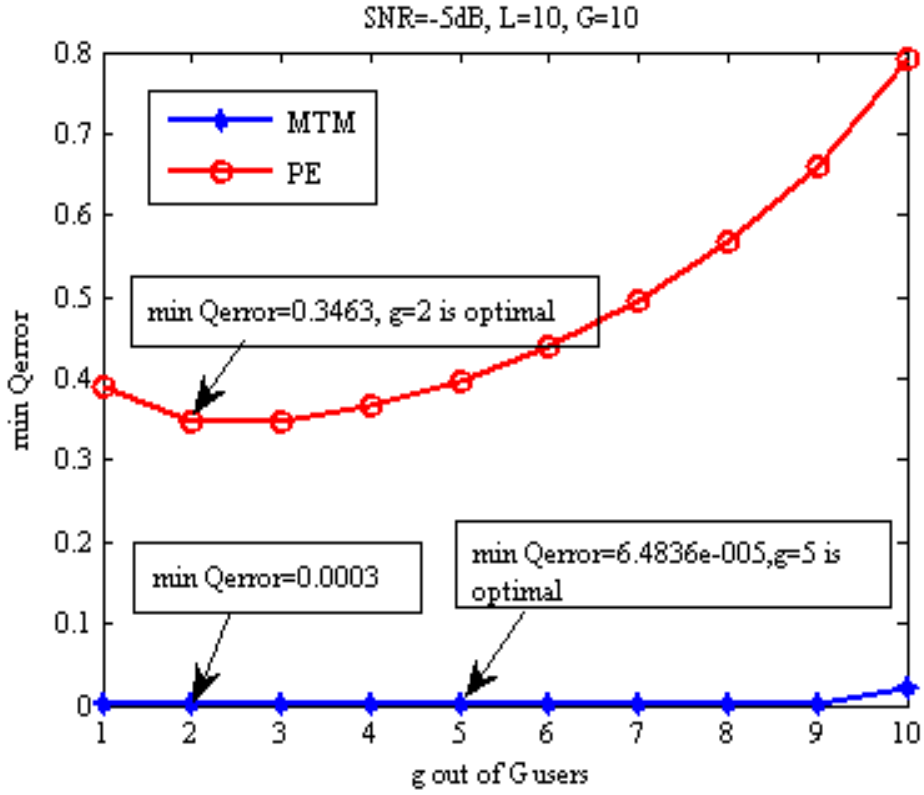

Figure 6.7 Minimum total error probability (min Q_{error}) versus g out of $G = 10$ CRs for PE and MTM with local SNR $= -5dB$ and $L = 10$ sensed samples.

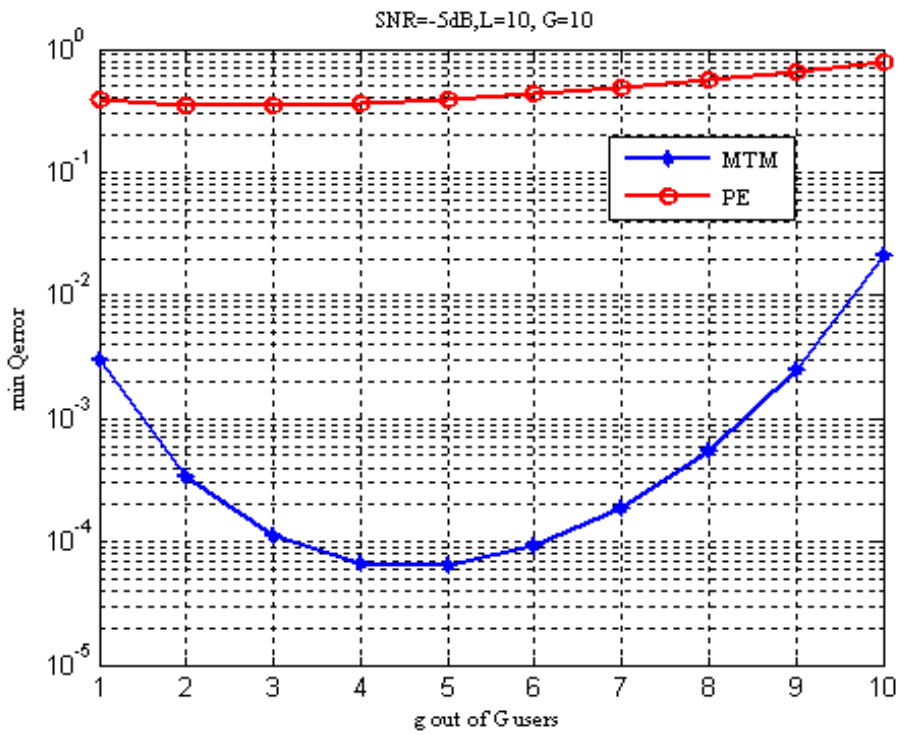

Figure 6. 8 Minimum total error probability (min Q_{error}) versus g out of $G = 10$ CRs for PE and MTM with local SNR $= -5dB$ and $L = 10$ sensed samples in Log scale.

Figure 6.9 shows the minimum total error probability ($min\ Q_{error}$) versus g out $G = 20$ CRs for PE and MTM with SNR $= -5$dB, and $L = 10$ sensed samples. In this case of G=20 and using MTM, the optimal total error probability is found as min $\mathrm{Q_{error}} = 7.6729 \times 10^{-7}$ when $g = 9$, which is the optimal, or $g_{optimal}$ =9. Optimal total error probability is found as, $min\ Q_{error} = 0.1885$ when $g = 5$ for PE case. Figure 6.10 shows the log version of Figure 6.9.

Table 6.1 shows the optimal fusion rule ($g_{optimal}$) for total CRs G =10, and L=10 local sensed samples when PE and MTM are used with different local SNRs. Generally, $g_{optimal}$ in MTM has a value higher than that in PE. For SNR $= -5, -10, -15,$ and $-20dB$, the $g_{optimal}$ is found as 5 in MTM's case, and 2 in PE's case. It is known that, in low SNR conditions, adding more CRs with low SNR does not improve the performance due to the low local SNR [51, 52]. Furthermore, it's clear that the MTM can include more CRs in the cooperation than PE at these low SNR, and gives a much better performance

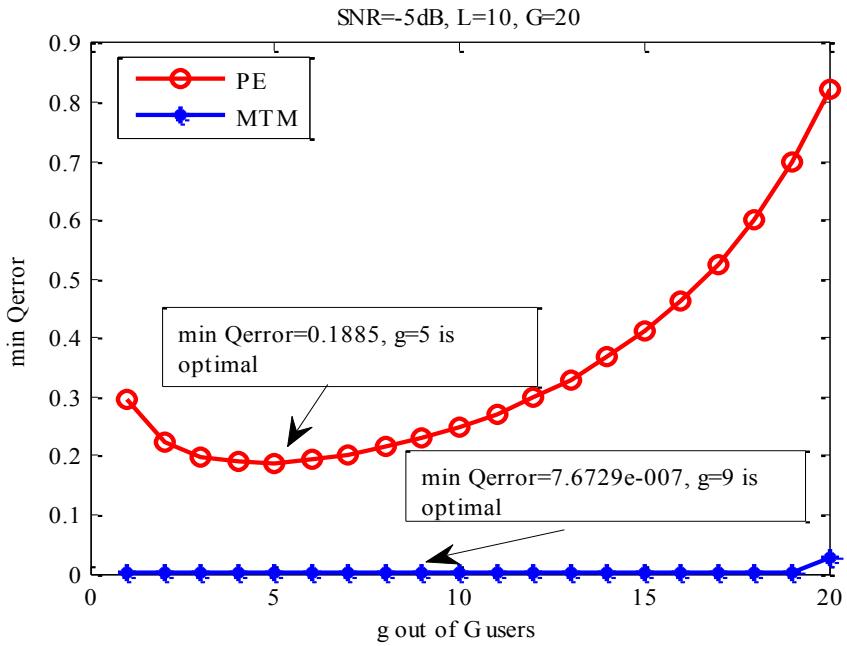

Figure 6.9 Minimum total error probability (min Q_{error}) versus g out of $G = 20$ CRs for PE and MTM with local SNR $= -5dB$ and $L = 10$ sensed samples.

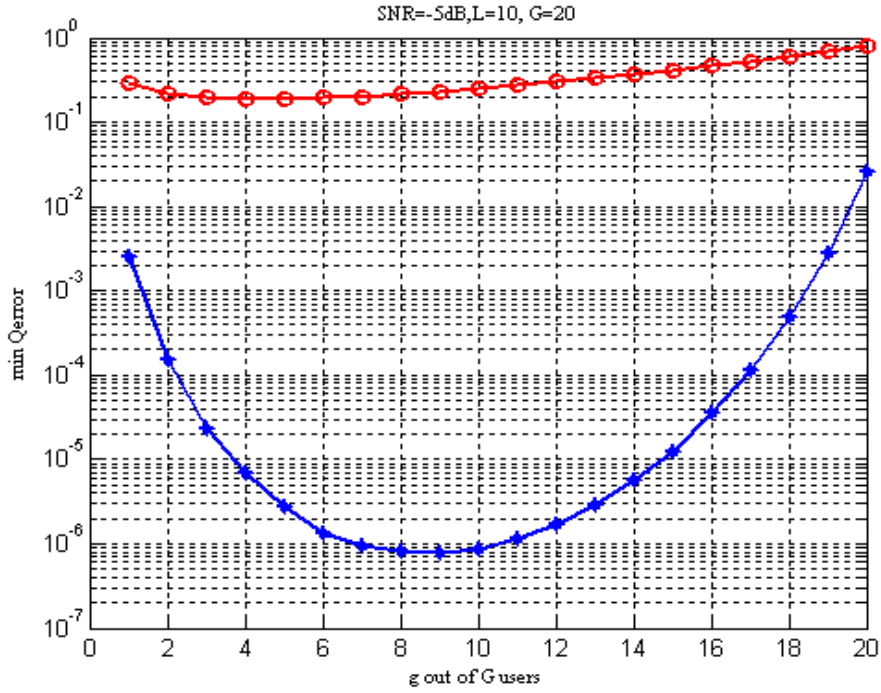

Figure 6.10 Minimum total error probability ($min\ \ Q_{error}$) versus g out of $G = 20$ CRs for PE and MTM with local SNR $= -5$dB and $L = 10$ sensed samples in Log scale.

SNR(dB)	**−20**	**−15**	**−10**	**−5**	**0**	**5**	**10**
	$g_{optimal}$						
PE	2	2	2	2	3	3	3
MTM	5	5	5	5	2-7	1-8	1-8

Table 6.1 Optimal fusion rule for *G*=10 and *L*=10 when PE and MTM are used locally with different SNRs.

at the same time. At SNR $= 5$ and 10 dB, there are more than one $g_{optimal}$ that minimize the total error to 0 in MTM; $g_{optimal}$=1, 2, 3, 4, 5, 6, 7 and 8. In PE, $g_{optimal}$=3 at the same case. This means that efficient spectrum sensing techniques such as MTM might not need cooperation in such cases if SNR is priori known to CR-BS.

6.3.2 The Proposed HCSS Optimization Strategies

One of the most important factors that has an effect on the optimization of the total error, in HCSS, is the number of sensed samples (i.e., *L* at each CR).It is known that the

increase in L, improves the local spectrum sensing performance. However, it should be taken into account that as long as the performance improvement is achieved by increasing L, as the sensing time becomes longer.

The last might decreases the capacity of the CR network, since the vacant PR's spectrum is not being quickly exploited by the CR network. Furthermore, as the local spectrum sensing is performed quickly, the probability of interfering with the PR's frequency subband becomes large. Therefore, optimizing the HCSS performance in terms of L is one of the most important factors that affects the performance. Two optimization strategies will be investigated below.

The first *L* optimization strategy:

The optimization problem when G, $g = 1,2,\dots,G$, and SNR are known, can be defined by [7]:

Find optimal L (L'), that minimizes the total error probability (Q_{error}).

or;

$$L' = arg\min_{L}(Q_{error})$$

The optimal L (L'), can be found by [132] [7]:

$$\frac{\partial Q_{error}}{\partial L} = \frac{\partial Q_f}{\partial L} + \frac{\partial Q_m}{\partial L} = 0, \tag{6.12}$$

where $\frac{\partial Q_f}{\partial L} = \sum_{r=g}^{G}\binom{G}{r} r.{P_f}^{r-1}.\frac{\partial P_f}{\partial L}\left(1 - P_f\right)^{G-r}$

$$-\sum_{r=g}^{G}\binom{G}{r}\,{P_f}^{r}.\frac{\partial P_f}{\partial L}.(G-r)\left(1 - P_f(f_i)\right)^{G-r-1}.\frac{\partial P_f}{\partial L}$$

$$= \frac{\partial P_f}{\partial L}\left[\sum_{r=g}^{G}\binom{G}{r}\,{P_f}^{r-1}.\left(1 - P_f\right)^{G-r}\left(\left(r - (G - r)\right)\frac{P_f}{1 - P_f}\right)\right] \tag{6.13}$$

Let us consider the local probability of false alarm P_f at frequency f_i, when PE is used; $\frac{\partial P_f}{\partial L}$ can be defined, using $\frac{\partial}{\partial x}\left(\int_{b(x)}^{a(x)} f(x)dx\right) = f\left(a(x)\right)\frac{\partial a(x)}{\partial x} - f(b(x))\frac{\partial b(x)}{\partial x}$ and referring to (4.51), as follows [87]:

$P_f = Q\left(\frac{\gamma - L\sigma_w^2}{\sqrt{(2L\sigma_w^4)}}\right) = \frac{1}{\sqrt{2\pi}}\int_{\left(\frac{\gamma - L\sigma_w^2}{\sqrt{(2L\sigma_w^4)}}\right)}^{\infty} e^{-\frac{t^2}{2}}\, dt$, and then [7],

$$\frac{\partial\, P_f(f_i)}{\partial L} = \frac{1}{\sqrt{2\pi}}\left[e^{-\infty} - e^{-\frac{\left(\frac{\gamma - L\sigma_w^2}{\sqrt{(2L\sigma_w^4)}}\right)^2}{2}}\ \frac{\partial\left(\frac{\gamma - L\sigma_w^2}{\sqrt{(2L\sigma_w^4)}}\right)}{\partial L}\right]$$

$$= \frac{1}{\sqrt{2\pi}}\left[e^{-\infty} - e^{-\frac{\left(\frac{\gamma - L\sigma_w^2}{\sqrt{(2L\sigma_w^4)}}\right)^2}{2}}\ \frac{\partial\left(\frac{(\zeta)(L) - L\sigma_w^2}{\sqrt{(2L\sigma_w^4)}}\right)}{\partial L}\right]$$

$$= \frac{1}{\sqrt{2\pi}}\left[e^{-\infty} - e^{-\frac{\left(\frac{\gamma - L\sigma_w^2}{\sqrt{(2L\sigma_w^4)}}\right)^2}{2}}\ \frac{\partial\left(\sqrt{L}\,\frac{\zeta - \sigma_w^2}{\sqrt{(2\sigma_w^4)}}\right)}{\partial L}\right]$$

$$= \frac{1}{\sqrt{2\pi}}\left[0 - e^{-\frac{\left(\frac{\gamma - L\sigma_w^2}{\sqrt{(2L\sigma_w^4)}}\right)^2}{2}}\ \frac{1}{2\sqrt{L}}\frac{\zeta - \sigma_w^2}{\sqrt{(2\sigma_w^4)}}\right]$$

$$= -\frac{1}{2\sqrt{2\pi L}}e^{-\frac{\left(\frac{\gamma - L\sigma_w^2}{\sqrt{(2L\sigma_w^4)}}\right)^2}{2}}\ \frac{\zeta - \sigma_w^2}{\sqrt{(2\sigma_w^4)}} \tag{6.14}$$

Similarly, the term $\frac{\partial Q_m}{\partial L}$ can be defined as follows[132] [7]:

$$\frac{\partial Q_m}{\partial L} = \frac{\partial}{\partial L}(1 - Q_d)$$

$$= -\sum_{r=g}^{G}\binom{G}{r} r.{P_d}^{r-1}.\frac{\partial\, P_d}{\partial L}(1 - \ P_d)^{G-r}$$

$$+\sum_{r=g}^{G}\binom{G}{r}\,{P_d}^{r}.\frac{\partial\,P_d}{\partial L}.(G-r)(1-\,P_d)^{G-r-1}.\frac{\partial\,P_d}{\partial L}$$

$$=-\frac{\partial\,P_d}{\partial L}\left[\sum_{r=g}^{G}\binom{G}{r}\,{P_d}^{r-1}(1-\,P_d)^{G-r}\left(\left(r-(G-r)\right)\frac{P_d}{1-P_d}\right)\right]. \qquad (6.15)$$

The term $\frac{\partial\,P_d}{\partial L}$ can be defined, for PE based, by following the same steps above and referring to (4.50), as follows [100]:

$$P_d=Q\left(\frac{\gamma-L(|H(f_i)|^2E_s+\sigma_w^2)}{\sqrt{2L\sigma_w^2(\sigma_w^2+2|H(f_i)|^2E_s)}}\right)=\frac{1}{\sqrt{2\pi}}\int_{\left(\frac{\gamma-L(|H(f_i)|^2E_s+\sigma_w^2)}{\sqrt{2L\sigma_w^2(\sigma_w^2+2|H(f_i)|^2E_s)}}\right)}^{\infty}e^{-\frac{t^2}{2}}\,dt$$

and then [7],

$$\frac{\partial\,P_d}{\partial L}=\frac{1}{\sqrt{2\pi}}\left[e^{-\infty}-e^{-\frac{\left(\frac{\gamma-L(|H(f_i)|^2E_s+\sigma_w^2)}{\sqrt{2L\sigma_w^2(\sigma_w^2+2|H(f_i)|^2E_s)}}\right)^2}{2}}\;\frac{\partial\left(\frac{\gamma-L(|H(f_i)|^2E_s+\sigma_w^2)}{\sqrt{2L\sigma_w^2(\sigma_w^2+2|H(f_i)|^2E_s)}}\right)}{\partial L}\right]$$

$$=\frac{1}{\sqrt{2\pi}}\left[0-e^{-\frac{\left(\frac{\gamma-L(|H(f_i)|^2E_s+\sigma_w^2)}{\sqrt{2L\sigma_w^2(\sigma_w^2+2|H(f_i)|^2E_s)}}\right)^2}{2}}\;\frac{\partial\left(\frac{(\zeta)(L)-L(|H(f_i)|^2E_s+\sigma_w^2)}{\sqrt{2L\sigma_w^2(\sigma_w^2+2|H(f_i)|^2E_s)}}\right)}{\partial L}\right]$$

$$=\frac{1}{\sqrt{2\pi}}\left[0-e^{-\frac{\left(\frac{\gamma-L(|H(f_i)|^2E_s+\sigma_w^2)}{\sqrt{2L\sigma_w^2(\sigma_w^2+2|H(f_i)|^2E_s)}}\right)^2}{2}}\;\frac{\partial\left(\sqrt{L}\,\frac{\zeta-(|H(f_i)|^2E_s+\sigma_w^2)}{\sqrt{2\sigma_w^2(\sigma_w^2+2|H(f_i)|^2E_s)}}\right)}{\partial L}\right]$$

$$=\frac{1}{\sqrt{2\pi}}\left[0-e^{-\frac{\left(\frac{\gamma-L(|H(f_i)|^2E_s+\sigma_w^2)}{\sqrt{2L\sigma_w^2(\sigma_w^2+2|H(f_i)|^2E_s)}}\right)^2}{2}}\;\frac{1}{2\sqrt{L}}\,\frac{\zeta-(|H(f_i)|^2E_s+\sigma_w^2)}{\sqrt{2\sigma_w^2(\sigma_w^2+2|H(f_i)|^2E_s)}}\right]$$

$$= -\frac{1}{2\sqrt{2\pi L}} e^{-\frac{\left(\frac{\gamma - L(|H(f_i)|^2 E_s + \sigma_w^2)}{\sqrt{2L\sigma_w^2(\sigma_w^2 + 2|H(f_i)|^2 E_s)}}\right)^2}{2}} \frac{\zeta - (|H(f_i)|^2 E_s + \sigma_w^2)}{\sqrt{2\sigma_w^2(\sigma_w^2 + 2|H(f_i)|^2 E_s)}} \tag{6.16}$$

Note that, the ζ is based directly on σ_w^2, while γ is a function of $L\sigma_w^2$. Similarly, (6.14) and (6.16) can be redefined for MTM referring to (4.37) and (4.46), and can be written, respectively, as follow:

$$\frac{\partial P_f}{\partial L} = -\frac{1}{2\sqrt{2\pi L}} e^{-\frac{\left(\frac{\gamma - LK\sigma_w^2}{\sqrt{2LC^2\lambda_\Sigma \sigma_w^4}}\right)^2}{2}} \frac{\zeta - K\sigma_w^2}{\sqrt{2LC^2\lambda_\Sigma \sigma_w^4}} \tag{6.17}$$

$$\frac{\partial P_d}{\partial L}$$

$$= -\frac{1}{2\sqrt{2\pi L}} e^{-\frac{\left(\frac{\gamma - LK(|H(f_i)|^2 E_s + \sigma_w^2)}{\sqrt{2LC^2\lambda_\Sigma \sigma_w^2(\sigma_w^2 + 2|H(f_i)|^2 E_s)}}\right)^2}{2}} \frac{\zeta - K(|H(f_i)|^2 E_s + \sigma_w^2)}{\sqrt{2LC^2\lambda_\Sigma \sigma_w^2(\sigma_w^2 + 2|H(f_i)|^2 E_s)}} \tag{6.18}$$

Using (6.13)-(6.18) into (6.12) with g=1,2,..,G, the solution of L' can be computed numerically for PE and MTM. The fusion rule that satisfies L' here is $g_{optimal}$.

Table 6.2 shows the optimal numbers of sensed samples and fusion rules for G=10, when PE and MTM are used with different SNR. We conclude that the decrease in SNR causes an increase in L', and with the increase in L' there is an increase in the optimal fusion rule$g_{optimal}$. The optimal fusion rules are equal for both techniques, only at L'. Note that L' can be written in seconds as, $L'(seconds) = L'NT_s$.

The second *L* optimization strategy:

Until here we have found the optimal L (i.e., L') that minimizes Q_{error} to zero. However, L' might be too large. Of course, that would minimize the spectrum opportunity as it is mentioned earlier in this sub section.

The optimization here can be modified in a different way, where the CR's network optimization is subject to a predefined L, which satisfies CR's network requirements with respect to the capacity and the acceptable interference to the PR's spectrum.

Suppose that G, $g = 1,2,\ldots,G$, *and* SNR, *are known; find the minimum total error probability (* Q_{error}*) that subject to* $L \leq s$ [7].

Note that, the g satisfies the minimum Q_{error} when $L = s$, is $g_{optimal}$ at $L = s$. Figure 6.11 shows the minimum total error probability (min Q_{error}) versus L when $G = 10$ CRs and PE is used with local SNR $= -5$, and $0dB$. Generally, It is clear that min Q_{error}, decreases with the increase in L. The min $Q_{error}$of $0dB$ curve, has a significant decrease with the increase in L, more than that in $-5dB$. It is found that $g_{optimal}$=3 for L=10 to 30 for both SNRs, and $g_{optimal}$=4 for L=31 to 165.

	PE		MTM	
SNR(dB)	L'	$g_{optimal}$	L'	$g_{optimal}$
5	28	3	1	3
0	167	4	6	4
-5	1188	5	47	5
-10	10060	5	417	5

Table 6.2 The Optimal number of sensed samples and fusion rules for G=10 when PE and MTM are used with different local SNRs.

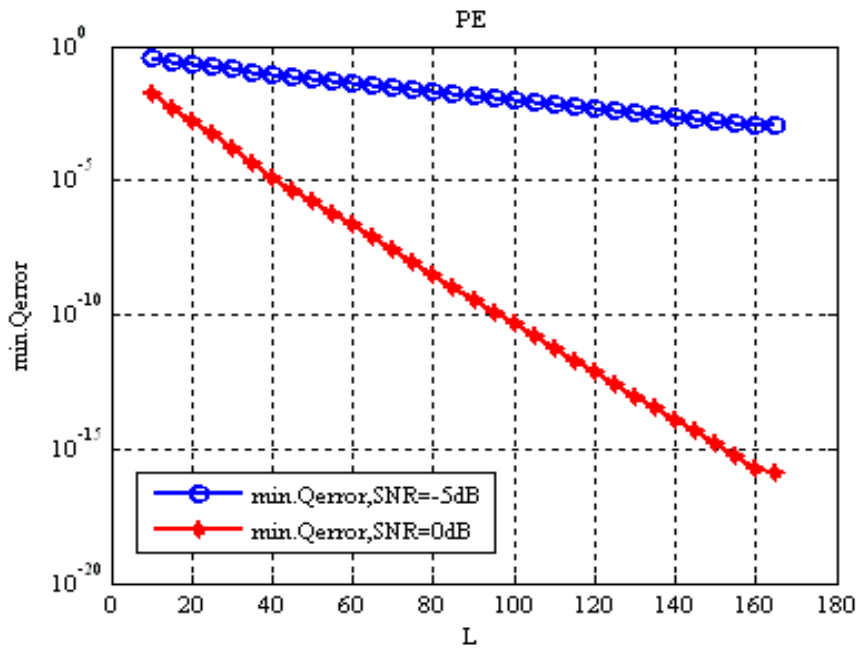

Figure 6.11 Min Q_{error} versus L when $G = 10$ CRs and PE is used with local SNR $= -5$ and 0dB.

6.3.3 Effect of Different Number of Total CRs, G, on HCSS

An interesting question now: Is the $g_{optimal}$ that achieves min Q_{error} the same when the total number of CRs is different? Table 6.3 shows the optimal fusion rule and min $Q_{error}$when G=10 and 30, and the PE is used locally, with SNR $= -5dB$, and a different number of the sensed samples L. The improvement in the performance by increasing the total number G of CRs at fixed L, is noticeable. For example, the min Q_{error} =0.1380 when G=10 CRs with L=30, and min Q_{error} =0.0128 when G is increased to 30 at the same L. The increase in the number of sensed samples L causes a decrease in the $min\ Q_{error}$. Furthermore, as the number of the total cooperated CRs, G, is increased, the $g_{optimal}$ is increased. For example, at $L = 40$, $g_{optimal}$=4 for G=10 case, and $g_{optimal}$=10 for G=30 case. The increase in L, causes an increase in $g_{optimal}$ as well. For example, in G=10 case, the $g_{optimal}$ is increased from 3 to 5 as L increased from 30 to 210, and for G=30, $g_{optimal}$ is increased from 8 to 12.

Table 6.4 shows the optimal fusion rule and min $Q_{error}$when G=10 and 30, and the MTM is used locally, with SNR $= -5dB$, and a different number of the sensed samples L. It can be noticed that the increase in the total cooperative CRs, G, decreases the min Q_{error} as will in MTM's case. The $g_{optimal}$ is, also, increased as in PE's case. The MTM, has min Q_{error} lower than that for PE in the same conditions.

L	$g_{optimal}$		$min.Q_{error}$	
	G=10	**G=30**	**G=10**	**G=30**
30	3	8	0.1380	0.0128
35	3	9	0.1127	0.0069
40	4	10	0.0924	0.0041
45	4	11	0.0756	0.0025
120	4	11	0.0049	1.77×10^{-6}
208	5	12	0.00026	7544×10^{-10}
210	5	12	0.00024	6.439×10^{-10}

Table 6.3 Optimal fusion rule and min total error for G=10 and 30 when PE is used with SNR= $-5dB$ and different L.

L	$g_{optimal}$		$min.Q_{error}$	
	G=10	**G=30**	**G=10**	**G=30**
30	5	11	$1.8153\times\ 10^{-9}$	$4.8036\times\ 10^{-14}$
35	5	11	$1.0468\times\ 10^{-10}$	$2.617\times\ 10^{-15}$
40	5	13	$6.3845\times\ 10^{-12}$	$1.532\times\ 10^{-15}$
45	6	13	$5.3845\times\ 10^{-12}$	$1.088\times\ 10^{-15}$
120	6	14	$4.2111\times\ 10^{-17}$	$6.770\times\ 10^{-21}$
208	6	14	$1.7354\times\ 10^{-17}$	$4.445\times\ 10^{-21}$
210	7	14	$1.5284\times\ 10^{-17}$	$4.939\times\ 10^{-21}$

Table 6.4 Optimal fusion rule and min total error for G=10 and 30 when MTM is used with SNR= $-5dB$ and different L.

6.4 Master Node Cooperation Concept

The works in [51, 52] show that, including the decision from a CR user with a low SNR in the cooperation at the CR-BS degrades the probability of detection.

Thus, the authors in [52] propose a fusion rule at the CR-BS that uses only the reliable decisions, which come from the CR users with a high SNR. The main drawbacks here are the requirements for SNR estimation, and in addition to sending decisions from different CR users to the CR-BS, each CR has to send its own estimated SNR to the CR-BS. Different hard cooperation optimization algorithms have been proposed in [49, 132, 183-185]. The common objective of this work is the minimizing of the number of binary bits sent to the CR-BS that require a wideband control channel, or the choosing of CRs with reliable decisions to cooperate at the main station, while at the same time keeping the probability of opportunity high.

Generally, implementing spectrum sensing at each CR in the cooperative CR network, decoding or amplifying the sensed signals and then sending the results to a main CR-BS, have the following main challenges:

1) The need for sensing units at each CR that will increase the hardware cost, the system complexity, the sensing delay and power consumption.

2) The need for sending the sensed information or decisions to a main CR-

BS, which requires more signal processing at both sides, the CR's terminals and CR-BS.

3) The need for control channels and huge overhead feedback to send the sensed information from all CRs to the CR-BS. Additionally, algorithms for information sharing and coordination are required in such cases [72].

4) Additional information such as the SNRs at different CRs has to be sent to the main CR-BS in optimized cooperative sensing.

5) The availability of some CRs in the network with reliable decisions is not guaranteed at all times. Thus, cooperating the sensed information produces more errors.

In order to face such challenges, the CR system needs to minimize the spectrum sensing processing in the CR network and ensure that the performance is kept high. Supporting the CR network with an ideal CR node can satisfy the two above conditions. Adding highly advanced hardware and software components to a single CR node in the CR network and excluding the other CRs is a good solution. In this solution, the spectrum sensing using advanced high performance techniques such as those considered in this thesis is performed at this ideal CR, and the final decision can be sent to the main CR-BS. The hardware components here should allow the ideal CR node to sense different frequency bands at the same time. Prior information about the different PR's signals must be known at this ideal node in order to resolve multipath fading. Training sequences and pilot signals are examples of this information. Blind equalizations, is also a good candidate in estimating the channel coefficients in such cases.

Figure 6.12 shows the MN cooperative spectrum sensing scenario in a centralized CR networks. The work in [186] proposes implementing spectrum sensing using devices that are separate from the CR network and can be provided by the CR's service

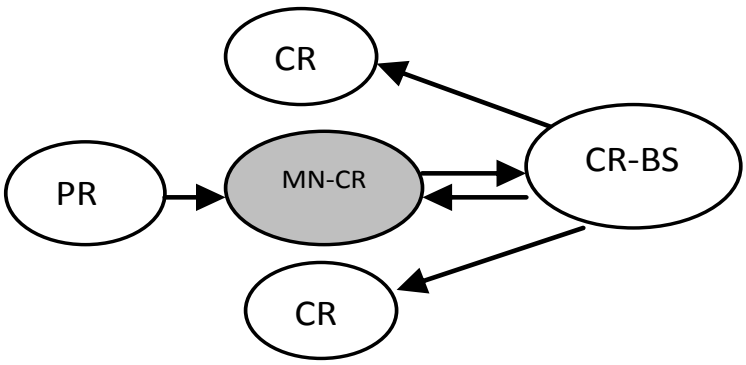

Figure 6.12 MN cooperative spectrum sensing scenario in a centralized CR network.

provider. In addition to the PR's and CR's system, a separate sensing system appears in their work. Of course, this would increase the overall system complexity, require more technical and management coordination protocols and sensing devices can not be used in the CR's cycle.

6.5 Conclusion

This chapter contributes to the HCSS optimization area by introducing an efficient optimization factor; the number of locally sensed samples; L. Proper controlling of L will take all optimization strategies and conditions to the optimum performance. Therefore, two strategies have been proposed to control L. This has been published in [7]. Based on the simulation results, the optimal number of sensed samples that minimizes the total error to zero is found as 417 and 10060 samples when MTM and PE are used respectively in AWGN with local SNR=−10dB and 10 CRs cooperate sensing. Thus, using MTM in cooperative sensing is much faster than using PE. The optimal fusion rule is found as 5 out of 10 in this case. Additionally, we investigate how the optimization output can be changed based on the used local spectrum sensing technique (i.e., PE and MTM), the different SNR, the different number of sensed samples and the

total number of cooperated CRs. Therefore, the optimization process depends on these different factors.

The MN concept has been introduced in this chapter, where a MN, in the CR network, can be supported by advanced hardware and software components. MN sends its sensing decisions to the CR-BS to announce it finally to the CRs. This part has been published in [6].

6.6 Chapter Summary

This chapter has focused on contributing to the HCSS optimization field, and, generally, to the CSS in CR systems. A revision about the HCSS was covered, including the optimization methods that exist in the literature. The system model of the HCSS was defined, and different simulation results were shown for "OR'' and "AND'' fusion rules in AWGN environment for perfect CC case.

The number of locally sensed samples optimization was proposed through two different strategies under different assumptions to optimize the HCSS. Such types of optimization take the reviewed optimization methods performances to the optimum performances. Different factors that might affect the HCSS optimization results were analyzed. This included, the effect of using different local spectrum sensing techniques, the local SNR and the total number of cooperated CRs in the CR network.

The MN cooperation concept was defined. Such a type of cooperation might resolve many challenges in practical CSS development. The huge feedback, the CRs hardware complexity, the power consumptions, the sensing delay and the coordination protocols, for example, would not be needed any more in such types of cooperation. However, more study toward this definition is required.

Chapter 7: Conclusion and Future Work

7.1 Thesis Main Contributions and Conclusion

Nowadays, the increasing demand for more radio spectrums, and the noticeable growth in the number of wireless services and applications, shows how the allocation and assignment of new frequencies for new wireless services is a big challenge nationally and globally. The inefficient use of the already assigned frequencies has promoted research centres and governments to develop different techniques to exploit such unused frequencies, at specific times and locations, without interfering with the PR user. This exploitation provides communication anywhere at any time and offers radio frequencies for the new wireless services.

CR is an intelligent radio system that was proposed to enhance the concept of using unlicensed or licensed frequencies when they are unoccupied by their licensed users (i.e., PR users). The CR can be distinguished from the classical radio systems mainly by its awareness about its surrounding RF environment. The spectrum sensing task is the main key for such awareness. Therefore, academic and industrial research centres, in addition to international and national spectrum agencies, have focused on spectrum sensing and management issues. The reasons behind this are the lower interference to the PR frequency subbands and the fact that higher spectrum opportunity can be achieved via robust and reliable spectrum sensing techniques. Chapter 2 shows how the spectrum sensing is a complicated issue in CR systems. At the PHY layer, different techniques were proposed to enhance the spectrum sensing in CR systems. Such techniques operate under different assumptions and conditions to deal with the decision about the presences or absence of the PR signal in a specific frequency subband. The performance of the used spectrum sensing technique can be described analytically by probabilities formulae, which are based on the way such techniques work locally at each CR Rx. They are

necessary to control the different parameters at the CR Rx such as threshold and number of sensed samples to a achieve specific performance. Cooperative spectrum sensing either locally among different numbers of antennas or globally among a number of CR users in the CR network improves the spectrum sensing performance by exploiting spatial diversity. These two types of cooperation are hot topics in CR spectrum sensing research.

OFDM system is a promising candidate for CR systems due to the many advantages that are discussed in chapter 2. Chapter 2 discusses the OFDM transceiver for CR applications based on the literature information. Furthermore, the challenges that might meet the practical implementation of OFDM-Based CR are reviewed.

MTM is promising in OFDM-Based CR systems, since it is based on FFT processing. However, this method required a lot of work to be useful in CR application.

In this thesis, we have focused on spectrum sensing and cooperation techniques for CR systems. Our work has started, mainly, by an extensive review and study of the CR and its relevant technical issues. The work, then, has focused on spectrum sensing and cooperation algorithms for CR systems. The following points have been investigated in the study in chapter 2:

- Revision of the general definitions and concepts relevant to the CR.
- Revision of the CR cognition cycle and its differences from classical radio.
- Focusing on spectrum sensing technical issues as a key functional factor in CR systems, including, the performance evaluation of spectrum sensing and the problem formulation, exploring different local spectrum sensing techniques, multi antenna based and cooperation spectrum sensing techniques and spectrum management issues.
- Revision of the OFDM system including its structure and advantages to be used for CR applications, the OFDM-Based CR, the IEEE802.22 standard and the

other OFDM based wireless standards and the spectrum sensing in OFDM-Based CR.

Based on the study in chapter 2, MTM has been chosen as a local spectrum sensing technique in our study, as discussed in subsection 2.4.2.5 and in chapter 3. The use of MTM-SVD (which is classified as SCSS) in a CR application required an evaluation of its performance and practical requirements. A simulation code was written in order to evaluate the MTM-SVD for spectrum sensing in CR as in [1]. A number of CR users in the CR network forward their measurements using different tapers (i.e., DPSS) about the PR to a CR-BS that uses SVD to fuse such received measurements in AWGN environment. It has high performance, but requires huge overhead to transmit a number of measurements from different CR users using different tapers.

The optimal use of MTM in CR systems was investigated in chapter 4. The following work has been done:

- Optimizing the MTM parameters in OFDM-based CR systems using Monte Carlo simulation [2].
    - The work included finding the optimal half time bandwidth product, NW, and the optimal number of tapers, K, which are found as 4 and 5 respectively.
    - The hypothesis problem is reformulated to include the effect of the spectral leakage and variance of the estimate on the spectrum sensing decisions. The high performance and low complexity are achieved using such optimal parameters.
- The optimal use of MTM as a spectrum sensing technique requires developing the theoretical based formulae for such a technique. The optimal MTM detector is developed [3, 4] and closed theoretical expressions are derived theoretically including:

- Decision statistics' Probability Density Functions (PDFs) for the different hypotheses.
- Probability of false alarm.
- Probability of detection.
- Probability of miss detection.
- Number of required sensed samples to achieve a specific performance.
- The chosen threshold to achieve a specific performance.
- Analytical expressions to evaluate the MTM complexity and compare it to the PE.

Simulation codes are written to evaluate the performance in AWGN, Rayleigh flat fading, and multipath fading environments. The theoretical results match well the analytical results. MTM-based spectrum sensing technique has the highest performance compared to classical and recently proposed spectrum sensing techniques.

In terms of supporting CR spectrum sensing by using efficient multi antenna based spectrum sensing techniques, the following work has been done [5, 6]:

- One optimal MTM based spectrum sensing technique is proposed using LC. The work here includes deriving the PDFs for different hypotheses, the probabilities formulae, and the number of sensed samples.
- One suboptimal, MTM based spectrum sensing technique is proposed using SLC. The work here includes deriving the PDFs for different hypotheses, the probabilities formulae, and the number of sensed samples.
- One suboptimal, MTM based spectrum sensing technique, is proposed using SVD.

- Analytical expressions to evaluate the proposed techniques' complexities and compare them to the PE based techniques.
- Simulation codes are written to evaluate the proposed techniques and compare them to the PE based in AWGN, Rayleigh flat, and multi path fading environments. The proposed techniques outperform those based on PE.
- The proposed techniques are found more efficient in terms of performance compared to the GLRD based multi antenna spectrum sensing techniques.
- The proposed SVD based suboptimal technique has a higher level of complexity than SLC suboptimal technique, but is found to give the same performance. However, SVD still have advantages when used for communications.

The HCSS improves the spectrum sensing performance by fusing the different binary digits received from different CR users at the CR-BS. The HCSS optimization is an important subject in CR systems since the overall performance is affected by different factors. In order to support such a point, the following work has been done [7]:

- The effect of using different local spectrum sensing techniques on the total minimum error in HCSS performance is examined when MTM and PE are used locally at each CR. It is found that the HCSS when MTM is used locally gives the total minimum error faster than that when PE is used. Furthermore, the different local spectrum sensing techniques give different fusion rules.
- Two strategies are proposed in order to optimize the number of locally sensed samples at each CR which take all HCSS optimization strategies and methods to the optimum performance. These two strategies optimize the HCSS's minimum total error in two different ways based on the CR network capacity

requirements and the allowed amount of interference to the PR frequency subband.

- The effect of use a different number of locally sensed samples at each CR, on the optimal fusion rule, is examined. The optimal fusion rule is affected by the number of sensed samples.
- The effect of the local SNR at CRs, on the optimal fusion rule, is examined. The optimal fusion rule is, also, affected by the number of sensed samples.
- The effect of the total number of cooperated CRs in the CR network, on the optimal fusion rule, is examined. The optimal fusion rule is, also, affected by the total number of cooperated CRs.

There are number of challenges that meet the practical implementation of CSS in centralized CR networks, which are discussed in section 6.5. Based on this, an introduction to a new concept of cooperation is provided. The following work has been done [6]:

- The CSS challenges are defined, and the master node cooperation concept (MN) is proposed. This includes listing the main requirements of such new concept of cooperation.

7.2 Suggested Future Work

The research into CR systems and networks has increased more and more since 1999 and such innovative wireless communications systems are thus becoming more and more practical. The work is not restricted only to technical issues, however, regulations and rules that manage the practical implementation of such systems have been considered by different national and international agencies.

CR is still an open research area, and a lot of work is required at PHY, MAC, and upper layers. The spectrum sensing mission is the key to a successful, practical CR

system. Through this thesis, a number of contributions have been achieved that will support the CR development. However, the work here can also be extended in a number of ways. Below, a number of suggested future work aspects are listed.

- The study in this thesis focuses, mainly, on non-parametric spectrum estimation methods such as MTM and PE. However, the parametric methods of spectrum estimation, which are based on modelling the stochastic process under measurement, are interesting. Therefore, a part of my future study would include exploring different non-parametric methods such as autoregressive (AR), moving average (MA), and autoregressive moving average (ARMA) for CR spectrum sensing. This would include performance evaluation for different PR signals assumptions in different wireless environments.
- The use of multi antenna for both spectrum sensing and communication in CR systems can be considered as a joint optimization problem. Achieving high performance for spectrum sensing and high capacity for communications should be studied jointly. Using similar techniques in the CR Rx for spectrum sensing and communications would minimize the system complexity; however, this might come at the expense of the performance of one of the two tasks. Consequently, focusing on this joint problem is necessary to achieve high performance with low complexity for both tasks.
- The wideband and continuous spectrum sensing topics are still open areas for more research. CR is expected to operate in different frequency subbands in the future. However, such an expectation requires more work at both sides of software and hardware components. Furthermore, spectrum sensing, mostly, is assumed to be performed periodically. However, the exact time of PR user reappearance in its licensed frequency subband is unknown, this requires further

study of such cases, with a view to keeping PR frequency subbands free from interference.

- Although cooperation in CR spectrum sensing improves the overall probability of detection, many practical challenges operate against such cooperation, such as complexity, overhead and coordination protocols and sensing delays. This thesis introduced a new concept of cooperation, the mater node cooperation (MN), where a single node in the CR network is responsible for the spectrum sensing task. This idea still needs some study in order to evaluate the hardware and software requirements for different CR systems.
- In OFDM-based CR systems, there are a number of problems which have not been given full consideration and final solutions under different conditions. The resource allocation is an important topic in such systems. Finding optimal assignments of subcarriers, bits and power among a number of users in the CR network is interesting, since there are new factors that affect the optimization problem here such as mutual interference between CR and PR adjacent frequency subbands. Although a number of studies have been provided to solve the problem, more studies from the angle of minimizing the interference is called for. Furthermore, the provided studies have not taken into account the change in the frequency subbands distributions (i.e., available bandwidths) that are free to be used by CR. The problem needs more research for MIMO OFDM-Based CR systems, and Ad Hoc CR networks which do not depend on CR-BS in their communications. The hardware components and spectrum sensing algorithms that might be added to the CR Rx in OFDM-Based CR systems need more studies to minimize the cost and computation complexity.

References

[1] O. A. Alghamdi and M. A. Abu-Rgheff, "Performance evaluation of cognitive radio spectrum sensing using multitaper-singular value decomposition," in *Proc. 4th IEEE International Conference on Cognitive Radio Oriented Wireless Networks and Communications (CROWNCOM '09)*, 2009, pp. 1-6.

[2] O. A. Alghamdi, M. A. Abu-Rgheff and M. Z. Ahmed, "MTM Parameters Optimization for 64-FFT Cognitive Radio Spectrum Sensing using Monte Carlo Simulation," in *Proc. The Second International Conference on Emerging Network Intelligence (EMERGING 2010)*, 2010, pp. 107-113.

[3] O. A. Alghamdi, M. A. Abu-Rgheff and M. Z. Ahmed, "Probabilities of Detection and False Alarm in MTM- Based Spectrum Sensing for Cognitive Radio Systems," in *Proc. The Second International Conference on Emerging Network Intelligence (EMERGING 2010)*, 2010, pp. 114-119.

[4] O. A. Alghamdi, M. Z. Ahmed and M. A. Abu-Rgheff, "Probabilities of detection and false alarm in multitaper based spectrum sensing for cognitive radio systems in AWGN," in *Proc. 12th IEEE International Conference on Communication Systems (ICCS'10)*, 2010, pp. 579-584.

[5] O. A. Alghamdi and M. A. Abu-Rgheff, "Local MTM-SVD based spectrum sensing in SIMO OFDM cognitive radio under bandwidth constraint," in *Proc. 5th IEEE International Conference on Cognitive Radio Oriented Wireless Networks & Communications (CROWNCOM'10)*, 2010, pp. 1-6.

[6] O. A. Alghamdi and M. Z. Ahmed, "Optimal and Suboptimal Multi Antenna Spectrum Sensing Techniques with Master Node Cooperation for Cognitive Radio Systems," *Journal of Communications (JCM),* vol. 6, pp. 512-523, 2011.

[7] O. A. Alghamdi and M. Z. Ahmed, "New optimization method for cooperative spectrum sensing in cognitive radio networks," in *Proc. 7th IEEE Wireless Advanced Conference (WiAd 2011)*, 2011, pp. 54-59.

[8] "The FCC official web site, avaliable [online]:," http://www.fcc.gov/.

[9] "The NTIA official web site, avaliable [online]:," http://www.ntia.doc.gov/

[10] "The ofcom official web site, avaliable[online]:," http://www.ofcom.org.uk/.

[11] "The OFCOM official web site; radio spectrum allocation chart of the UK, avaliable [online]:

," http://www.ofcom.org.uk/radiocomms/isu/ukfat/.

[12] "The ITU official web site, avaliable[online]:," http://www.itu.int/net/home/index.aspx.

[13] "The ITU-R official web site, avaliable[online]:," http://www.itu.int/ITU-R/index.asp?category=information&rlink=rhome&lang=en.

[14] "ITU article No.5, avaliable[online]:," http://life.itu.int/radioclub/rr/art05.htm#Alloc.

[15] A. Goldsmith, *Wireless communications*: Cambridge Univ Pr, 2005.

[16] "The ICT regulation toolkit web site(in cooperation with ITU), avaliable[online]:," http://www.ictregulationtoolkit.org/en/Section.2843.html.

[17] QinetiQ, "Cognitive Radio Technology - A Study for Ofcom – Summary Report," *QINETIQ/06/00420, Issue 1.1, February 2007*.

[18] FCC, "Spectrum Policy Task Force," *FCC, ET Docket No 03-135, November 2002*.

[19] Z. Qing and B. M. Sadler, "A survey of Dynamic Spectrum Access," *IEEE Signal Processing Magazine,* vol. 24, pp. 79-89, 2007.

[20] X. Lin, R. Tonjes, T. Paila, W. Hansmann, M. Frank and M. Albrecht, "DRiVE-ing to the Internet: Dynamic Radio for IP services in Vehicular Environments," in *Proc. 25th Annual IEEE Conference on Local Computer Networks (LCN 2000)*, 2000, pp. 281-289.

[21] Y. Benkler, "Overcoming agoraphobia: Building the commons of the digitally networked environment," *Harvard Journal of Law & Technology,* vol. 11, pp. 287-871, 1998.

[22] W. Lehr and J. Crowcroft, "Managing shared access to a spectrum commons," in *Proc. First IEEE International Symposium on New Frontiers in Dynamic Spectrum Access Networks (DySPAN 2005)*, 2005, pp. 420-444.

[23] O. Ileri, D. Samardzija and N. B. Mandayam, "Demand responsive pricing and competitive spectrum allocation via a spectrum server," in *Proc. First IEEE International Symposium on New Frontiers in Dynamic Spectrum Access Networks (DySPAN 2005)*, 2005, pp. 194-202.

[24] M. Z. Win and R. A. Scholtz, "Impulse radio: How it works," *IEEE Communications letters,* vol. 2, pp. 36-38, 1998.

[25] J. Mitola and G. Q. Maguire, "Cognitive radio: making software radios more personal," *IEEE personal communications,* vol. 6, pp. 13-18, 1999.

[26] S. Haykin, "Cognitive radio: brain-empowered wireless communications," *IEEE journal on selected areas in communications,* vol. 23, pp. 201-220, 2005.

[27] T. A. Weiss and F. K. Jondral, "Spectrum pooling: an innovative strategy for the enhancement of spectrum efficiency," *IEEE Communications Magazine,* vol. 42, pp. S8-14, 2004.

[28] H. Mahmoud, T. Yucek and H. Arslan, "OFDM for cognitive radio: merits and challenges," *IEEE Wireless Communications Magazine,* vol. 16, pp. 6-15, 2009.

[29] D. J. Thomson, "Spectrum estimation and harmonic analysis," *Proceedings of the IEEE,* vol. 70, pp. 1055-1096, 1982.

[30] D. Slepian, "Prolate spheroidal wave functions, Fourier analysis, and uncertainty. V- The discrete case," *Bell System Technical Journal,* vol. 57, pp. 1371–1430, 1978.

[31] P. Stoica and T. Sundin, "On nonparametric spectral estimation," *Journal of Circuits, Systems, and Signal Processing,* vol. 18, pp. 169-181, 1999.

[32] D. J. Thomson, "Jackknifing multitaper spectrum estimates," *IEEE Signal Processing Magazine,* vol. 24, pp. 20-30, 2007.

[33] X. Wu, Y. Chan, H. Preissl, H. Eswaran, J. Wilson, P. Murphy and C. L. Lowery, "Time-frequency and coherence analysis of fMEG signals," *Journal of Neurology & clinical neurophysiology (NCN),* vol. 2004, p. 11, 2004.

[34] M. K. van Vugt, P. B. Sederberg and M. J. Kahana, "Comparison of spectral analysis methods for characterizing brain oscillations," *Journal of neuroscience methods,* vol. 162, pp. 49-63, 2007.

[35] D. J. Thomson, "Quadratic-inverse spectrum estimates: applications to palaeoclimatology," *Philosophical Transactions: Physical Sciences and Engineering,* vol. 332, pp. 539-597, 1990.

[36] M. Ghil, M. R. Allen, M. D. Dettinger, K. Ide, D. Kondrashov, M. E. Mann, A. W. Robertson, A. Saunders, Y. Tian and F. Varadi, "Advanced spectral methods for climatic time series," *Reviews of Geophysics Journal,* vol. 40, pp. 1-41, 2002.

[37] J. Park, C. R. Lindberg and F. L. Vernon, "Multitaper spectral analysis of high-frequency seismograms," *Reviews of Geophysics Journal,* vol. 92, pp. 675–12, 1987.

[38] G. A. Prieto, P. M. Shearer, F. L. Vernon and D. Kilb, "Earthquake source scaling and self-similarity estimation from stacking P and S spectra," *Journal of Geophysical Research,* vol. 109, pp. 1-13, 2004.

[39] K. E. Wage, "Multitaper Array Processing," in *Proc. Forty-First Asilomar Conference on Signals, Systems and Computers (ACSSC 2007)*, 2007, pp. 1242-1246.

[40] A. Moghtaderi, "Multitaper Methods for Time-Frequency Spectrum Estimation and Unaliasing of Harmonic Frequencies," *Ph. D. Thesis, Queen's University, Kingston Ontario, 2008*.

[41] H. Huixia, "Multitaper higher-order spectral analysis of nonlinear multivariate random processes," *Ph. D. Thesis, Queen's University, Kingston Ontario, 2008*.

[42] G. A. Prieto, "Improving earthquake source spectrum estimation using multitaper techniques," *Ph. D. Thesis, University of California, San Diego, 2007*.

[43] K. Q. Lepage, "Some Advances in the Multitaper Method of Spectrum Estimation," *Ph.D thesis,Queen's University, Kingston Ontario,* 2009.

[44] M. E. Mann and J. Park, "Global-scale modes of surface temperature variability on interannual to century timescales," *Journal of Geophysical Research,* vol. 99, pp. 25819-25833, 1994.

[45] M. E. Mann and J. Park, "Oscillatory spatiotemporal signal detection in climate studies: A multiple-taper spectral domain approach," *Advances in Geophysics,* vol. 41, pp. 1-132, 1999.

[46] D. Cabric, S. M. Mishra and R. W. Brodersen, "Implementation issues in spectrum sensing for cognitive radios," in *Proc. Thirty-Eighth Asilomar Conference on Signals, Systems and Computers*, 2004, pp. 772-776.

[47] Q. Zhi, C. Shuguang and A. H. Sayed, "Optimal Linear Cooperation for Spectrum Sensing in Cognitive Radio Networks," *IEEE Journal of Selected Topics in Signal Processing,* vol. 2, pp. 28-40, 2008.

[48] A. Ghasemi and E. S. Sousa, "Collaborative spectrum sensing for opportunistic access in fading environments," in *Proc. First IEEE International Symposium on New Frontiers in Dynamic Spectrum Access Networks (DySPAN '05)*, 2005, pp. 131-136.

[49] S. Chunhua, Z. Wei and K. B. Letaief, "Cooperative Spectrum Sensing for Cognitive Radios under Bandwidth Constraints," in *Proc. IEEE Wireless Communications and Networking Conference (WCNC 2007)*, 2007, pp. 1-5.

[50] L. Hong, J. Ma, F. Xu, S. Li and Z. Zhou, "Optimization of Collaborative Spectrum Sensing for Cognitive Radio," in *Proc. IEEE International Conference on Networking, Sensing and Control (ICNSC 2008)*, 2008, pp. 1730-1733.

[51] E. Peh and L. Ying-Chang, "Optimization for Cooperative Sensing in Cognitive Radio Networks," in *Proc. IEEE Wireless Communications and Networking Conference (WCNC 2007)*, 2007, pp. 27-32.

[52] Z. Yi, X. Xianzhong and Y. Lili, "Cooperative Spectrum Sensing Based on SNR Comparison in Fusion Center for Cognitive Radio," in *Proc. First IEEE International Conference on Advanced Computer Control (ICACC '09)*, 2009, pp. 212-216.

[53] ITU-R, "Software defined radio in the land mobile, amateur and amateur satellite services," *ITU-R, Report M.2117 ,2007*.

[54] ITU-R, "2012 World Radiocommunication Conference: Agenda and References," *ITU-Radiocommunication sector, World Radiocommunication Conference 2012 (WRC-12) document,2010*.

[55] C. Cordeiro, K. Challapali, D. Birru and N. Sai Shankar, "IEEE 802.22: the first worldwide wireless standard based on cognitive radios," in *Proc. First IEEE International Symposium on New Frontiers in Dynamic Spectrum Access Networks (DySPAN 2005)*, 2005, pp. 328-337.

[56] C. Stevenson, G. Chouinard, L. Zhongding, H. Wendong, S. Shellhammer and W. Caldwell, "IEEE 802.22: The first cognitive radio wireless regional area network standard," *IEEE Communications Magazine,* vol. 47, pp. 130-138, 2009.

[57] J. Mitola, "The software radio architecture," *IEEE Communications Magazine,* vol. 33, pp. 26-38, 1995.

[58] J. Mitola, III, "Software radios-survey, critical evaluation and future directions," *IEEE Aerospace and Electronic Systems Magazine,* vol. 8, pp. 25-36, 1992.

[59] F. K. Jondral, "Software-defined radio: basics and evolution to cognitive radio," *EURASIP Journal on Wireless Communications and Networking,* vol. 3, pp. 275-283, 2005.

[60] W.-Y. L. I. F. Akyildiz, M. C. Vuran, and S. Mohantly, "Next Generation/dynamic spectrum access /cognitive radiowireless network: A survey," *Elsevier Computer Networks Journal,* vol. 50, pp. 2127-2159, 2006.

[61] T. C. Clancy, "Dynamic Spectrum Access in Cognitive Radio Networks " *Ph.D Thesis , University of Maryland, 2006*.

[62] C. X. Wang, H. Chen, X. Hong and M. Guizani, "Cognitive radio network management," *IEEE Vehicular Technology Magazine,* vol. 3, pp. 28-35, 2008.

[63] W. Beibei and K. J. R. Liu, "Advances in Cognitive Radio Networks: A Survey," *IEEE Journal of Selected Topics in Signal Processing,* vol. 5, pp. 5-23, 2011.

[64] J. Mitola III, "Cognitive Radio: An integrated agent architecture for software radio architecture," *Ph. D Dissertation, Royal Institute of Technology (KTH),* 2000.

[65] T. C. Clancy, "Formalizing the interference temperature model," *Journal of Wireless Communications and Mobile Computing,* vol. 7, pp. 1077-1086, 2007.

[66] S. Haykin, K. Huber and C. Zhe, "Bayesian sequential state estimation for MIMO wireless communications," *Proceedings of the IEEE,* vol. 92, pp. 439-454, 2004.

[67] I. F. Akyildiz, L. Won-Yeol, M. C. Vuran and S. Mohanty, "A survey on spectrum management in cognitive radio networks," *IEEE Communications Magazine,* vol. 46, pp. 40-48, 2008.

[68] C. Raman, R. D. Yates and N. B. Mandayam, "Scheduling variable rate links via a spectrum server," in *Proc. First IEEE International Symposium on New Frontiers in Dynamic Spectrum Access Networks (DySPAN 2005)*, 2005, pp. 110-118.

[69] I. Akyildiz, L. Won-Yeol and K. Chowdhury, "Spectrum management in cognitive radio ad hoc networks," *IEEE Network Magazine,* vol. 23, pp. 6-12, 2009.

[70] I. F. Akyildiz, W. Y. Lee and K. R. Chowdhury, "CRAHNs: Cognitive radio ad hoc networks," *Elsevier Ad Hoc Networks Journal,* vol. 7, pp. 810-836, 2009.

[71] B. Wild and K. Ramchandran, "Detecting primary receivers for cognitive radio applications," in *Proc. First IEEE International Symposium on New Frontiers in Dynamic Spectrum Access Networks (DySPAN 2005)*, 2005, pp. 124-130.

[72] S. Hussain and X. Fernando, "Spectrum sensing in cognitive radio networks: Up-to-date techniques and future challenges," in *Proc. IEEE Toronto International Conference of Science and Technology for Humanity (TIC-STH)*, 2009, pp. 736-741.

[73] T. Yucek and H. Arslan, "A survey of spectrum sensing algorithms for cognitive radio applications," *IEEE Communications Surveys & Tutorials,* vol. 11, pp. 116-130, 2009.

[74] M. Jun, G. Y. Li and J. Biing Hwang, "Signal Processing in Cognitive Radio," *Proceedings of the IEEE,* vol. 97, pp. 805-823, 2009.

[75] Z. Guodong, M. Jun, L. Ye, W. Tao, Y. H. Kwon, A. Soong and Y. Chenyang, "Spatial Spectrum Holes for Cognitive Radio with Directional Transmission," in *Proc. IEEE Global Telecommunications Conference (GLOBECOM 2008)*, 2008, pp. 1-5.

[76] Z. Guodong, M. Jun, G. Y. Li, W. Tao, K. Young, A. Soong and Y. Chenyang, "Spatial spectrum holes for cognitive radio with relay-assisted directional transmission," *IEEE Transactions on Wireless Communications,* vol. 8, pp. 5270-5279, 2009.

[77] S. M. Mishra, A. Sahai and R. W. Brodersen, "Cooperative Sensing among Cognitive Radios," in *Proc. IEEE International Conference on Communications (ICC '06)*, 2006, pp. 1658-1663.

[78] N. S. Shankar, C. Cordeiro and K. Challapali, "Spectrum agile radios: utilization and sensing architectures," in *Proc. First IEEE International Symposium on New Frontiers in Dynamic Spectrum Access Networks (DySPAN 2005)*, 2005, pp. 160-169.

[79] Y. Hur, J. Park, W. Woo, K. Lim, C. H. Lee, H. S. Kim and J. Laskar, "A wideband analog multi-resolution spectrum sensing (MRSS) technique for cognitive radio (CR) systems," in *Proc. IEEE International Symposium on Circuits and Systems (ISCAS '06)*, 2006, pp. 4090-4093.

[80] Y. Yuan, P. Bahl, R. Chandra, P. A. Chou, J. I. Ferrell, T. Moscibroda, S. Narlanka and W. Yunnan, "KNOWS: Cognitive Radio Networks Over White Spaces," in *Proc. 2nd IEEE International Symposium on New Frontiers in Dynamic Spectrum Access Networks (DySPAN '07)*, 2007, pp. 416-427.

[81] P. Wang, L. Xiao, S. Zhou and J. Wang, "Optimization of detection time for channel efficiency in cognitive radio systems," in *Proc. IEEE Wireless Communications and Networking Conference (WCNC '07)*, 2007, pp. 111-115.

[82] A. Ghasemi and E. S. Sousa, "Optimization of Spectrum Sensing for Opportunistic Spectrum Access in Cognitive Radio Networks," in *Proc. 4th IEEE Consumer Communications and Networking Conference (CCNC2007)*, 2007, pp. 1022-1026.

[83] Z. Qianchuan, S. Geirhofer, T. Lang and B. M. Sadler, "Optimal Dynamic Spectrum Access via Periodic Channel Sensing," in *Proc. IEEE Wireless Communications and Networking Conference (WCNC '07)*, 2007, pp. 33-37.

[84] L. Won-Yeol and I. F. Akyildiz, "Optimal spectrum sensing framework for cognitive radio networks," *IEEE Transactions on Wireless Communications,* vol. 7, pp. 3845-3857, 2008.

[85] C. Cordeiro, K. Challapali, D. Birru and S. Shankar, "IEEE 802.22: an introduction to the first wireless standard based on cognitive radios," *Journal of communications (JCM),* vol. 1, pp. 38-47, 2006.

[86] H. V. Poor, *An introduction to signal detection and estimation*: Springer, 1994.

[87] S. M. Kay, *Fundamentals of statistical signal processing: detection theory*: Prentice-Hall, 1998.

[88] A. Papoulis, S. U. Pillai and S. Unnikrishna, *Probability, random variables, and stochastic processes* vol. 196: McGraw-hill New York, 1965.

[89] E. Hossain, D. Niyato and Z. Han, *Dynamic spectrum access and management in cognitive radio networks*: Cambridge University Press, 2009.

[90] H. Urkowitz, "Energy detection of unknown deterministic signals," *Proceedings of the IEEE,* vol. 55, pp. 523-531, 1967.

[91] D. B. Percival and A. T. Walden, *Spectral analysis for physical applications: multitaper and conventional univariate techniques*: Cambridge Univ Press, 1993.

[92] D. Cabric, A. Tkachenko and R. W. Brodersen, "Spectrum Sensing Measurements of Pilot, Energy, and Collaborative Detection," in *Proc. IEEE Military Communications Conference (MILCOM '06)*, 2006, pp. 1-7.

[93] F. F. Digham, M. S. Alouini and M. K. Simon, "On the energy detection of unknown signals over fading channels," in *Proc. IEEE International Conference on Communications (ICC '03)*, 2003, pp. 3575-3579

[94] H. Tang, "Some physical layer issues of wide-band cognitive radio systems," in *Proc. First IEEE International Symposium on New Frontiers in Dynamic Spectrum Access Networks (DySPAN '05)*, 2005, pp. 151-159.

[95] D.-C. Oh and Y.-H. Lee, "Cooperative spectrum sensing with imperfect feedback channel in the cognitive radio systems," *International Journal of Communication Systems,* vol. 23, pp. 763-779.

[96] Y. H. Lee and D. C. Oh, "Energy detection based spectrum sensing for sensing error minimization in cognitive radio networks," *International Journal of Communication Networks and Information Security (IJCNIS),* vol. 1, 2011.

[97] D. Cabric, A. Tkachenko and R. W. Brodersen, "Experimental study of spectrum sensing based on energy detection and network cooperation," in *Proc. The First International Workshop on Technology and Policy for Accessing Spectrum (TAPAS '06)*, 2006, pp. 1-8.

[98] J. Hillenbrand, T. A. Weiss and F. K. Jondral, "Calculation of detection and false alarm probabilities in spectrum pooling systems," *IEEE Communications letters,* vol. 9, pp. 349-351, 2005.

[99] W. Pu, F. Jun, H. Ning and L. Hongbin, "Multiantenna-Assisted Spectrum Sensing for Cognitive Radio," *IEEE Transactions on Vehicular Technology,* vol. 59, pp. 1791-1800, 2010.

[100] Q. Zhi, C. Shuguang, A. H. Sayed and H. V. Poor, "Optimal Multiband Joint Detection for Spectrum Sensing in Cognitive Radio Networks," *IEEE Transactions on Signal Processing,* vol. 57, pp. 1128-1140, 2009.

[101] M. P. Wylie-Green, "Dynamic spectrum sensing by multiband OFDM radio for interference mitigation," in *Proc. First IEEE International Symposium on New Frontiers in Dynamic Spectrum Access Networks (DySPAN '05)*, 2005, pp. 619-625.

[102] H. Di, L. Yingpei, H. Chen and J. Lingge, "A Novel Spectrum-Sensing Technique in Cognitive Radio Based on Stochastic Resonance," *IEEE Transactions on Vehicular Technology,* vol. 59, pp. 1680-1688, 2010.

[103] S. Geirhofer, T. Lang and B. M. Sadler, "A Measurement-Based Model for Dynamic Spectrum Access in WLAN Channels," in *Proc. IEEE Military Communications Conference (MILCOM '06)*, 2006, pp. 1-7.

[104] R. Tandra and A. Sahai, "Fundamental limits on detection in low SNR under noise uncertainty," in *Proc. International Conference on Wireless Networks, Communications and Mobile Computing*, 2005, pp. 464-469

[105] R. Tandra and A. Sahai, "SNR Walls for Signal Detection," *IEEE Journal of Selected Topics in Signal Processing,* vol. 2, pp. 4-17, 2008.

[106] M. P. Olivieri, G. Barnett, A. Lackpour, A. Davis and P. Ngo, "A scalable dynamic spectrum allocation system with interference mitigation for teams of spectrally agile software defined radios," in *Proc. First IEEE International Symposium on New Frontiers in Dynamic Spectrum Access Networks (DySPAN '05)*, 2005, pp. 170-179.

[107] J. J. Lehtomaki, J. Vartiainen, M. Juntti and H. Saarnisaari, "Spectrum Sensing with Forward Methods," in *Proc. IEEE Military Communications Conference (MILCOM '06)*, 2006, pp. 1-7.

[108] Z. Quan, S. Cui, H. V. Poor and A. H. Sayed, "Collaborative wideband sensing for cognitive radios," *IEEE Signal Processing Magazine,* vol. 25, pp. 60-73, 2008.

[109] S. Enserink and D. Cochran, "A cyclostationary feature detector," in *Proc. The Twenty-Eighth Asilomar Conference on Signals, Systems and Computers*, 1994, pp. 806-810

[110] D. Cabric and R. W. Brodersen, "Physical layer design issues unique to cognitive radio systems," in *Proc. IEEE 16th International Symposium onPersonal, Indoor and Mobile Radio Communications (PIMRC'05).* 2005, pp. 759-763.

[111] J. Lunden, V. Koivunen, A. Huttunen and H. V. Poor, "Spectrum Sensing in Cognitive Radios Based on Multiple Cyclic Frequencies," in *Proc. 2nd IEEE International Conference on Cognitive Radio Oriented Wireless Networks and Communications (CROWNCOM '07)*, 2007, pp. 37-43.

[112] K. Maeda, A. Benjebbour, T. Asai, T. Furuno and T. Ohya, "Recognition Among OFDM-Based Systems Utilizing Cyclostationarity-Inducing Transmission," in *Proc. 2nd IEEE International Symposium on New Frontiers in Dynamic Spectrum Access Networks (DySPAN '07)*, 2007, pp. 516-523.

[113] P. D. Sutton, K. E. Nolan and L. E. Doyle, "Cyclostationary Signatures for Rendezvous in OFDM-Based Dynamic Spectrum Access Networks," in *Proc. 2nd IEEE International Symposium on New Frontiers in Dynamic Spectrum Access Networks (DySPAN '07)*, 2007, pp. 220-231.

[114] W. A. Gardner, "Exploitation of spectral redundancy in cyclostationary signals," *IEEE Signal Processing Magazine,* vol. 8, pp. 14-36, 1991.

[115] P. D. Sutton, J. Lotze, K. E. Nolan and L. E. Doyle, "Cyclostationary Signature Detection in Multipath Rayleigh Fading Environments," in *Proc. 2nd IEEE International Conference on Cognitive Radio Oriented Wireless Networks and Communications (CROWNCOM '07)*, 2007, pp. 408-413.

[116] A. Tkachenko, A. D. Cabric and R. W. Brodersen, "Cyclostationary Feature Detector Experiments Using Reconfigurable BEE2," in *Proc. 2nd IEEE International Symposium on New Frontiers in Dynamic Spectrum Access Networks (DySPAN2007)*, 2007, pp. 216-219.

[117] B. Farhang-Boroujeny, "Filter bank spectrum sensing for cognitive radios," *IEEE Transactions on Signal Processing,* vol. 56, pp. 1801-1811, 2008.

[118] B. Farhang-Boroujeny and R. Kempter, "Multicarrier communication techniques for spectrum sensing and communication in cognitive radios," *IEEE Communications Magazine,* vol. 46, pp. 80-85, 2008.

[119] A. Pandharipande and J. P. M. G. Linnartz, "Performance Analysis of Primary User Detection in a Multiple Antenna Cognitive Radio," in *Proc. EEE International Conference on Communications (ICC '07)*, 2007, pp. 6482-6486.

[120] L. Jong-Hwan, B. Jun-Ho and H. Seung-Hoon, "Collaborative Spectrum Sensing using Energy Detector in Multiple Antenna System," in *Proc. 10th International Conference on Advanced Communication Technology (ICACT '08)*, 2008, pp. 427-430.

[121] V. Kuppusamy and R. Mahapatra, "Primary user detection in OFDM based MIMO Cognitive Radio," in *Proc. 3rd IEEE International Conference on Cognitive Radio Oriented Wireless Networks and Communications (CROWNCOM'08)*, 2008, pp. 1-5.

[122] M. Wei, W. Mu Qing, L. Dong and W. Meng Ling, "User sensing based on MIMO cognitive radio sensor networks," in *Proc. 2nd IEEE International Conference on Computer Science and Information Technology (ICCSIT '09)*, 2009, pp. 205-208.

[123] A. Taherpour, M. Nasiri-Kenari and S. Gazor, "Multiple antenna spectrum sensing in cognitive radios," *IEEE Transactions on Wireless Communications,* vol. 9, pp. 814-823, 2010.

[124] Z. Rui, L. Teng, L. Ying-Chang and Z. Yonghong, "Multi-antenna based spectrum sensing for cognitive radios: A GLRT approach," *IEEE Transactions on Communications,* vol. 58, pp. 84-88, 2010.

[125] G. Ganesan and L. Ye, "Cooperative Spectrum Sensing in Cognitive Radio, Part I: Two User Networks," *IEEE Transactions on Wireless Communications,* vol. 6, pp. 2204-2213, 2007.

[126] J. N. Laneman, D. N. C. Tse and G. W. Wornell, "Cooperative diversity in wireless networks: Efficient protocols and outage behavior," *IEEE Transactions on Information Theory,* vol. 50, pp. 3062-3080, 2004.

[127] G. Ganesan and Y. Li, "Cooperative Spectrum Sensing in Cognitive Radio, Part II: Multiuser Networks," *IEEE Transactions on Wireless Communications,* vol. 6, pp. 2214-2222, 2007.

[128] K. Ben Letaief and Z. Wei, "Cooperative Communications for Cognitive Radio Networks," *Proceedings of the IEEE,* vol. 97, pp. 878-893, 2009.

[129] B. Shen, S. Ullah and K. Kwak, "Deflection coefficient maximization criterion based optimal cooperative spectrum sensing," *AEU - International Journal of Electronics and Communications,* vol. 64, pp. 819-827, 2009.

[130] E. Visotsky, S. Kuffner and R. Peterson, "On collaborative detection of TV transmissions in support of dynamic spectrum sharing," in *Proc. First IEEE International Symposium on New Frontiers in Dynamic Spectrum Access Networks (DySPAN '05)*, 2005, pp. 338-345.

[131] V. Aalo and R. Viswanathan, "Asymptotic performance of a distributed detection system in correlated Gaussian noise," *IEEE Transactions on Signal Processing,* vol. 40, pp. 211-213, 1992.

[132] Z. Wei, R. K. Mallik and K. Ben Letaief, "Cooperative Spectrum Sensing Optimization in Cognitive Radio Networks," in *Proc. IEEE International Conference on Communications (ICC '08)*, 2008, pp. 3411-3415.

[133] J. Shen, S. Liu, L. Zeng, G. Xie, J. Gao and Y. Liu, "Optimisation of cooperative spectrum sensing in cognitive radio network," *IET Journal of Communications,* vol. 3, pp. 1170-1178, 2009.

[134] Z. Xiaorong, S. Lianfeng and T. S. P. Yum, "Analysis of Cognitive Radio Spectrum Access with Optimal Channel Reservation," *IEEE Communications Letters,* vol. 11, pp. 304-306, 2007.

[135] H. Celebi and H. Arslan, "Utilization of Location Information in Cognitive Wireless Networks," *IEEE Wireless Communications Magazine,* vol. 14, pp. 6-13, 2007.

[136] S. Hang and Z. Xi, "Cross-Layer Based Opportunistic MAC Protocols for QoS Provisionings Over Cognitive Radio Wireless Networks," *IEEE Journal on Selected Areas in Communications,* vol. 26, pp. 118-129, 2008.

[137] Z. Qing, T. Lang, S. Ananthram and C. Yunxia, "Decentralized cognitive MAC for opportunistic spectrum access in ad hoc networks: A POMDP framework," *IEEE Journal on Selected Areas in Communications,* vol. 25, pp. 589-600, 2007.

[138] J. Hai, L. Lifeng, F. Rongfei and H. V. Poor, "Optimal selection of channel sensing order in cognitive radio," *IEEE Transactions on Wireless Communications,* vol. 8, pp. 297-307, 2009.

[139] J. Zhu and K. J. R. Liu, "Cognitive Radios for Dynamic Spectrum Access - Dynamic Spectrum Sharing: A Game Theoretical Overview," *IEEE Communications Magazine,* vol. 45, pp. 88-94, 2007.

[140] D. Niyato and E. Hossain, "Market-Equilibrium, Competitive, and Cooperative Pricing for Spectrum Sharing in Cognitive Radio Networks: Analysis and Comparison," *IEEE Transactions on Wireless Communications,* vol. 7, pp. 4273-4283, 2008.

[141] W. Fan, M. Krunz and C. Shuguang, "Price-Based Spectrum Management in Cognitive Radio Networks," *IEEE Journal of Selected Topics in Signal Processing,* vol. 2, pp. 74-87, 2008.

[142] R. Rajbanshi, A. M. Wyglinski and G. J. Minden, "An Efficient Implementation of NC-OFDM Transceivers for Cognitive Radios," in *Proc. IEEE 1st International Conference on Cognitive Radio Oriented Wireless Networks and Communications (CROWNCOM'06)*, 2006, pp. 1-5.

[143] C. Cordeiro, K. Challapali and M. Ghosh, "Cognitive PHY and MAC layers for dynamic spectrum access and sharing of TV bands," in *Proc. First International Workshop on Technology and Policy for Accessing Spectrum (TAPAS '06)*, 2006, pp. 1-11.

[144] S. Chaudhari, V. Koivunen and H. V. Poor, "Autocorrelation-Based Decentralized Sequential Detection of OFDM Signals in Cognitive Radios," *IEEE Transactions on Signal Processing,* vol. 57, pp. 2690-2700, 2009.

[145] L. Zhongding and F. P. S. Chin, "Sensing OFDM Systems Under Frequency-Selective Fading Channels," *IEEE Transactions on Vehicular Technology,* vol. 59, pp. 1960-1968, 2010.

[146] P. Welch, "The use of fast Fourier transform for the estimation of power spectra: A method based on time averaging over short, modified periodograms," *IEEE Transactions on Audio and Electroacoustics,* vol. 15, pp. 70-73, 1967.

[147] S. Haykin, D. J. Thomson and J. H. Reed, "Spectrum Sensing for Cognitive Radio," *Proceedings of the IEEE,* vol. 97, pp. 849-877, 2009.

[148] F. J. Harris, "On the use of windows for harmonic analysis with the discrete Fourier transform," *Proceedings of the IEEE,* vol. 66, pp. 51–83, 1978.

[149] "FFT Windows Function: Limits on FFT Analysis," *Bores Signal Processing (Online: http://bores.com)*.

[150] T. Erpek, A. Leu and B. L. Mark, "Spectrum Sensing Performance in TV Bands using the Multitaper Method," in *Proc. 15th IEEE Signal Processing and Communications Applications Conference(SIU'07)*, 2007, pp. 1-4.

[151] G. H. Golub and C. F. Van Loan, *Matrix computations*: Johns Hopkins Univ Press, 1996.

[152] W. Jun and Q. T. Zhang, "A Multitaper Spectrum Based Detector for Cognitive Radio," in *Proc. IEEE Wireless Communications and Networking Conference (WCNC '09)*, 2009, pp. 1-5.

[153] Z. Yonghong and L. Ying-Chang, "Covariance Based Signal Detections for Cognitive Radio," in *Proc. 2nd IEEE International Symposium on New Frontiers in Dynamic Spectrum Access Networks (DySPAN '07)*, 2007, pp. 202-207.

[154] Q. T. Zhang, "Theoretical Performance and Thresholds of the Multitaper Method for Spectrum Sensing," *IEEE Transactions on Vehicular Technology,* vol. 60, pp. 2128-2138, 2011.

[155] E. Hossain, D. Niyato and Z. Han, *Dynamic spectrum access and management in cognitive radio networks*: Cambridge University Press, 2009.

[156] N. Benvenuto, G. Cherubini and J. Wiley, *Algorithms for communications systems and their applications*: Wiley Online Library, 2002.

[157] S. N. Diggavi, N. Al-Dhahir, A. Stamoulis and A. R. Calderbank, "Great expectations: the value of spatial diversity in wireless networks," *Proceedings of the IEEE,* vol. 92, pp. 219-270, 2004.

[158] R. D. Murch and K. B. Letaief, "Antenna systems for broadband wireless access," *IEEE Communications Magazine,* vol. 40, pp. 76-83, 2002.

[159] J. Winters, "Optimum Combining in Digital Mobile Radio with Cochannel Interference," *IEEE Journal on Selected Areas in Communications,* vol. 2, pp. 528-539, 1984.

[160] J. H. Winters, "The diversity gain of transmit diversity in wireless systems with Rayleigh fading," *IEEE Transactions on Vehicular Technology,* vol. 47, pp. 119-123, 1998.

[161] G. J. Foschini, "Layered space time architecture for wireless communication in a fading environment when using multi element antennas," *Bell labs technical journal,* vol. 1, pp. 41-59, 1996.

[162] G. J. Foschini and M. J. Gans, "On limits of wireless communications in a fading environment when using multiple antennas," *Journal of Wireless personal communications,* vol. 6, pp. 311-335, 1998.

[163] G. D. Golden, C. J. Foschini, R. A. Valenzuela and P. W. Wolniansky, "Detection algorithm and initial laboratory results using V-BLAST space-time communication architecture," *IEE Electronics Letters,* vol. 35, pp. 14-16, 1999.

[164] A. Goldsmith, S. A. Jafar, N. Jindal and S. Vishwanath, "Capacity limits of MIMO channels," *IEEE Journal on Selected Areas in Communications,* vol. 21, pp. 684-702, 2003.

[165] D. Gesbert, M. Shafi, S. Da-shan, P. J. Smith and A. Naguib, "From theory to practice: an overview of MIMO space-time coded wireless systems," *IEEE Journal on Selected Areas in Communications,* vol. 21, pp. 281-302, 2003.

[166] V. Tarokh, N. Seshadri and A. R. Calderbank, "Space-time codes for high data rate wireless communication: performance criterion and code construction," *IEEE Transactions on Information Theory,* vol. 44, pp. 744-765, 1998.

[167] S. M. Alamouti, "A simple transmit diversity technique for wireless communications," *IEEE Journal on Selected Areas in Communications,* vol. 16, pp. 1451-1458, 1998.

[168] D. G. Brennan, "Linear diversity combining techniques," *Proceedings of the IEEE,* vol. 91, pp. 331-356, 2003.

[169] B. R. Tomiuk, N. C. Beaulieu and A. A. Abu-Dayya, "Maximal ratio combining with channel estimation errors," in *Proc. IEEE Pacific Rim Conference on Communications, Computers, and Signal Processing*, 1995, pp. 363-366.

[170] J. Winters, "On the Capacity of Radio Communication Systems with Diversity in a Rayleigh Fading Environment," *IEEE Journal on Selected Areas in Communications,* vol. 5, pp. 871-878, 1987.

[171] J. S. Bird, "Calculating the performance of linear and square-law detectors," *IEEE Transactions on Aerospace and Electronic Systems,* vol. 31, pp. 39-51, 1995.

[172] A. Ghosh and R. Ratasuk, "Multi-Antenna Systems for LTE eNodeB," in *Proc. 70th IEEE Vehicular Technology Conference*, 2009, pp. 1-4.

[173] M. Steinbauer, A. F. Molisch and E. Bonek, "The double-directional radio channel," *IEEE Antennas and Propagation Magazine,* vol. 43, pp. 51-63, 2001.

[174] K. Hamdi, Z. Wei and K. Letaief, "Opportunistic spectrum sharing in cognitive MIMO wireless networks," *IEEE Transactions on Wireless Communications* vol. 8, pp. 4098-4109, 2009.

[175] Z. Ying Jun and A. M. So, "Optimal Spectrum Sharing in MIMO Cognitive Radio Networks via Semidefinite Programming," *IEEE Journal on Selected Areas in Communications,* vol. 29, pp. 362-373, 2011.

[176] F. Sheikh, S. Masud and B. Bing, "Harmonic power detection in wideband cognitive radios," *IET Journal of Signal Processing,* vol. 3, pp. 40-50, 2009.

[177] T. Lang and S. Perreau, "Multichannel blind identification: from subspace to maximum likelihood methods," *Proceedings of the IEEE,* vol. 86, pp. 1951-1968, 1998.

[178] T. Lang, X. Guanghan and T. Kailath, "Blind identification and equalization based on second-order statistics: a time domain approach," *IEEE Transactions on Information Theory,* vol. 40, pp. 340-349, 1994.

[179] C. Xi, "Blind channel estimation for MIMO OFDM communication systems," *Ph. D. Thesis, National University of Singapore, Singapore,* 2009.

[180] J. K. Tugnait, T. Lang and D. Zhi, "Single-user channel estimation and equalization," *IEEE Signal Processing Magazine,* vol. 17, pp. 16-28, 2000.

[181] W. Gardner and L. Franks, "Characterization of cyclostationary random signal processes," *IEEE Transactions on Information Theory,* vol. 21, pp. 4-14, 1975.

[182] W. Liu, Y. Lie-Liang and L. Hanzo, "SVD Assisted Joint Transmitter and Receiver Design for the Downlink of MIMO Systems," in *Proc. 68th IEEE Vehicular Technology Conference (VTC '08)*, 2008, pp. 1-5.

[183] L. Wang, "Novel scheme for cooperation spectrum sensing in cognitive radio networks," in *Proc. The 2nd International Conference on Computer and Automation Engineering (ICCAE '10)*, 2010, pp. 371-375.

[184] A. Jamshidi, "Performance analysis of low average reporting bits cognitive radio schemes in bandwidth constraint control channels," *IET Journal of Communications,* vol. 3, pp. 1544-1556, 2009.

[185] S. Chunhua, Z. Wei and K. Ben, "Cluster-Based Cooperative Spectrum Sensing in Cognitive Radio Systems," in *Proc. IEEE International Conference on Communications (ICC '07)*, 2007, pp. 2511-2515.

[186] H. Zhu, F. Rongfei and J. Hai, "Replacement of spectrum sensing in cognitive radio," *IEEE Transactions on Wireless Communications,* vol. 8, pp. 2819-2826, 2009.